

# **Molecular analysis of zDHHc9 and its links to physiology and pathophysiology**

by

**Mohammad Al-Mhadeen**

In fulfilment of the requirement for the degree of

**Doctor of Philosophy**

**2025**

**University of Strathclyde**


Strathclyde Institute of Pharmacy and Biomedical  
Sciences

## **Declaration of authenticity and authors rights**

*This thesis is the result of the author's original research. It has been composed by the author and has not been previously submitted for examination which has led to the award of a degree.*

*The copyright of this thesis belongs to the author under the terms of the United Kingdom Copyright Acts as qualified by University of Strathclyde Regulation 3.50. Due acknowledgement must always be made of the use of any material contained in, or derived from, this thesis.*

**Signed:**

A handwritten signature in black ink, consisting of a series of loops and a long horizontal stroke, is centered on a light blue rectangular background.

**Date:**

30/04/2025

## Acknowledgements

Professor Luke Chamberlain, I don't think my words would be enough to express my deep appreciation and gratitude for your unwavering support, mentorship, cheerful face despite every downfall, and your humanity on a personal level. It was an honor to be mentored by you. Your mentorship reflected on my personal life, making me a better person. Thank you, sir. Without you, this would not be possible.

The pillars of my life, my father, Dr.Ahmad Almhadeen, my mother, brothers and sisters, your unconditional love and support gave me the strength to carry on, so thank you.

To my wife, Hadeel, your presence in my life made this journey a pretty one. Thank you.

To the University of Petra and my supervisors, Dr Luay Abu Qatoseh and Dr. Qasem Mahmoud. Thank you for granting me this opportunity and your support through this journey; I sincerely appreciate your efforts.

Lastly, Dr Christine Salaün, you always picked me up before falling. Your knowledge, generosity, and your nature as a mentor and teacher are exceptional. I was fortunate to work next to you, Liam and Debbie, guys working next to you, saving me all the time; you were my family, so thank you guys, it was a privilege.

I would like to extend my appreciation to Lee Wheeler for taking the time to help us in the PBU during our long, daunting experiment.

Without you all, I wouldn't have been able to make it, so thank you all.

Yours sincerely

Mohammad

<b>Table of contents</b>	
Declaration of authenticity and authors rights	ii
Acknowledgements	iii
Table of Contents	iv
List of figures	viii
List of tables	xi
Abbreviations	xii
Abstract	xiv
<b>Chapter 1</b> <b>Introduction</b>	1
1.1 Post-translational modifications (PTMs)	2
1.2 Protein S-Acylation	4
1.3 Enzymatic regulation of S-acylation	9
1.3.1 The zDHHc Family	9
1.3.2 Protein Deacylases	14
1.4 Subcellular Localisation of Acylation Enzymes	19
1.5 Accessory proteins / Co-factors	21
1.5.1 GCP16 and zDHHc9	21
1.5.2 Golga7b, GCP16 and ZDHHc5	22
1.5.3 HTT and zDHHc17/13	23
1.5.4 SelK and zDHHc6	24
1.6 S-acylation and disease	25
1.6.1 S-acylation and cancer	25
1.6.2 S-acylation and inflammasome function	28
1.6.3 S-acylation and neurological disorders	29
1.7 zDHHc9	31
1.7.1 zDHHc9 Structure and function	31
1.7.2 The <i>ZDHHc9</i> gene and its transcripts	33
1.7.3 Regulation of <i>ZDHHc9</i> transcription	34

1.8 GCP16 (Golgi Complex-Associated Protein of 16 kDa)	35
1.8.1 Expression and localization	35
1.8.2 The zDHHC9-GCP16 complex	36
1.8.3 Golga7 interactions with zDHHC5 and other zDHHC enzymes	38
1.9 zDHHC9 Substrates	39
1.10 <i>ZDHHC9</i> mutations in humans linked to brain abnormalities	43
1.10.1 <i>ZDHHC9</i> mutations and their effect on the nervous system	44
1.11 Aims	46
<b>Chapter 2</b> <b>Materials and Methods</b>	48
2.1 <i>Zdhhc9</i> knock-out mice	49
2.1.1 Breeding, genotyping, and analysis of mutant mice	49
2.1.2 Diet protocol for liver stress and ketosis analysis	50
2.1.3 Cardiac puncture	51
2.1.4 Blood preparation for chemistry and hematology tests	51
2.2 Cellular biology	52
2.2.1 Mammalian cell culture	52
2.2.2 Plasmids	53
2.2.3 Transfection of HEK293T cells	54
2.2.4 Cycloheximide chase experiments to assess protein stability	54
2.3 Molecular biology	55
2.3.1 mRNA extraction from mouse brain tissue	55
2.3.2 Site-directed mutagenesis	58
2.3.3 Subcloning	60
2.3.4 Transformation of <i>Escherichia coli</i>	62
2.3.5 Isolation of plasmid DNA	63
2.3.6 DNA sequencing	64
2.4 Protein Biochemistry	64
2.4.1 Click Chemistry	64
2.4.2 Co-Immunoprecipitation Assay (Co-IP)	66
2.4.3 Sodium dodecyl sulphate (SDS) polyacrylamide gel electrophoresis (PAGE)	67

2.4.4 Immunoblotting	68
2.5 Bioinformatic tools	69
2.5.1 AlphaFold2 CoLab	69
2.5.2 mRNA-Seq analysis	69
2.6 Data analysis	70
2.7 illustrations tools	72
<b>Chapter 3</b> <b>General analysis of GCP16 interactions with zDHHC enzymes</b>	73
3.1 Introduction	74
3.2 Results	76
3.2.1 Analysis of the effects of GCP16-zDHHC5/zDHHC9 interactions on protein stability	76
3.2.2 Analysis of the interaction of GCP16 with other (Golgi) zDHHC Enzymes	79
3.2.3 Analysis of the interactions of GCP16 and Golga7b With zDHHC5 and zDHHC9	85
3.2.4 Implementation of a computational model predicting the 3D structure of zDHHC9 interactions and subsequent experimental validation	89
3.3 The effect of GCP16 S-acylation on its interactions with zDHHC5 and zDHHC9	92
3.4 Discussion	104
3.4.1 GCP16 and zDHHC5/zDHHC9 show reciprocal stabilization	104
3.4.2 GCP16 interactions with different zDHHC enzymes	106
3.4.3 Comparison of the interactions of Golga7b and GCP16 with zDHHC enzymes	107
3.4.4 Predicting GCP16 interactions using the AlphaFold 3D protein prediction tool	109
3.4.5 Overall effect of GCP16 S-acylation on its interaction with zDHHC5 and zDHHC9	110
<b>Chapter 4</b> <b>Molecular analysis of ZDHHC9 mutants (R96W and R148W) linked to pathophysiology</b>	114

4.1 Introduction	115
4.2 Results	117
4.2.1 Sub-cloning of human zDHHc9 and mutants into the pEFBOS-HA vector	117
4.2.2 Analysis of the effects of R96W and R148W substitutions on the reciprocal stabilization and interaction with EGFP-GCP16	118
4.2.3 Analysis of the interaction of R96W and R148W zDHHc9 mutants with the substrate protein EGFP-H-Ras	123
4.2.4 Analysis of the effects of R96W and R148W substitutions on S-acylation of HA-zDHHc9 and EGFP-GCP16	124
4.2.5 AlphaFold analysis of wild-type and mutant zDHHc9	127
4.3 Discussion	129
<b>Chapter 5</b> <b>Effects of ZDHHc9 Mutations: Molecular, Genomic, and Clinical Perspective</b>	135
5.1 Introduction	136
5.2 Results	139
5.2.1 Molecular analysis of GLUT1 interaction with zDHHc9	139
5.2.2 Analysis of changes in mRNA expression in <i>Zdhhc9</i> knockout mouse brain	144
5.2.3 Inducing liver stress in knockout mice using a high-calorie diet to assess physiological adaptation that has been associated with GLUT1 deficiency syndrome	146
5.3 Discussion	148
5.3.1 Molecular and mRNA expression analyses	150
5.3.2 Inducing liver stress to assess adaptive responses in <i>Zdhhc9</i> knockout mice	154
<b>Chapter six</b> <b>General Discussion</b>	157
General Discussion	158
<b>Chapter seven</b>	168

<b>References</b>	
References	169



<b>List of figures</b>		
<b>Chapter 1</b>		
Figure 1.1	The amino acid relationships between zDHHc enzymes and their subcellular localization	11
Figure 1.2	Reversible S-acylation and the enzyme components	17
Figure 1.3	Cryo-electron microscopy structures of the human zDHHc9–GCP16 complex	32
Figure 1.4	GCP16 and Golga7b interaction with zDHHc5 and zDHHc9 enzymes, and the localisation of each enzyme	37
Figure 1.5	zDHHc9 substrates and their functions	39
Figure 1.6	Depiction of the zDHHc9 protein amino acid substitutions	45
<b>Chapter 3</b>		
Figure 3.1	Cycloheximide assay to assess the stability of GCP16 in the absence or presence of zDHHc5/zDHHc9	77
Figure 3.2	Cycloheximide chase assay to assess the stability of zDHHc5 and zDHHc9 in the absence and presence of GCP16	78
Figure 3.3	Analysis of the steady-state levels of zDHHc5 and zDHHc9 in the absence and presence of GCP16	79
Figure 3.4	Co-immunoprecipitation analysis of EGFP-GCP16 interaction with zDHHc enzymes	80
Figure 3.5	Co-immunoprecipitation analysis of EGFP-GCP16 interaction with HA-zDHHc13 and HA-zDHHc17	81

Figure 3.6	S-acylation of EGFP-GCP16 by Golgi-localised zDHHC enzymes	83
Figure 3.7	Amino acid alignment of Golga7b and GCP16	85
Figure 3.8	Analysis of the binding of HA-zDHHC5, HA-zDHHC9, and HA-GCP16 to EGFP-GCP16 and EGFP-Golga7b	86
Figure 3.9	Comparison of the expression levels of EGFP-Golga7b and EGFP-GCP16 when co-expressed with either HA-zDHHC5 or HA-zDHHC9	87
Figure 3.10	Effect of HA-zDHHC5 and HA-zDHHC9 on the S-acylation of EGFP-Golga7b and EGFP-GCP16	88
Figure 3.11	3D protein structure and interaction predictions for GCP16, zDHHC5, and zDHHC9 using AlphaFold2 CoLab software	90
Figure 3.12	Analysis of EGFP-GCP16 mutant (R118A, R121A) to HA-zDHHC5 and HA-zDHHC9	91
Figure 3.13	Effect of mutating the major S-acylation sites in GCP16 on zDHHC interactions	93
Figure 3.14	Effect of mutating EGFP-GCP16 S-acylated cysteines on the stability of HA-zDHHC5 and HA-zDHHC9	95
Figure 3.15	Effect of wild-type and C69,72A mutant GCP16 on S-acylation of zDHHC5 and zDHHC9	97
Figure 3.16	Cycloheximide chase assays to assess the stability of EGFP-GCP16 wild-type and the C69,72A mutant when co-expressed with either HA-zDHHC5 or HA-zDHHC9	99
Figure 3.17	Comparison of the S-acylation of EGFP-GCP16 (C69,72A) mutant when co-expressed with HA-zDHHC5 or HA-zDHHC9	100

Figure 3.18	Analysis of S-acylation of EGFP-GCP16 cysteine mutants by HA-zDHHC5 and HA-zDHHC9	102
<b>Chapter 4</b>		
Figure 4.1	Sub-cloning of zDHHC9 and mutants into the pEFBOS-HA vector	118
Figure 4.2	Cycloheximide chase assays to assess the effect of EGFP-GCP16 on the stability of HA-zDHHC9 wild-type and the R96W and R148W mutants	120
Figure 4.3	Cycloheximide chase assays to assess the effect of HA-zDHHC9 wild-type and mutant proteins on the stability of EGFP-GCP16	121
Figure 4.4	Co-immunoprecipitation of HA-zDHHC9 wild-type and R148W/R96W mutants with EGFP-GCP16	122
Figure 4.5	Analysis of the interaction of HA-zDHHC9 wild-type and R148W/R96W mutants with EGFP-H-Ras	124
Figure 4.6	Analysis of S-acylation of EGFP-GCP16 by HA-zDHHC9 wild-type and R148W and R96W mutants	125
Figure 4.7	Effect of EGFP-GCP16 on the S-acylation of HA-zDHHC9 (R148W) and zDHHC9 (R96W) mutants	126
Figure 4.8	AlphaFold analysis of the effects of the R96W substitution in zDHHC9	128
<b>Chapter 5</b>		
Figure 5.1	Analysis of GLUT1 binding to zDHHC9 wild-type, R148W, and R96W variants	140

Figure 5.2	Co-immunoprecipitation analysis of the interaction of EGFP-GLUT1 with different zDHHC enzymes and GCP16	141
Figure 5.3	Analysis of EGFP-GLUT1 S-acylation by HA-zDHHC9 and HA-GCP16	143
Figure 5.4	Liver function biomarkers and BHB levels in wild-type and <i>Zdhhc9</i> knock-out mice after six months of a high-calorie diet	147

## List of tables

<b>Chapter 2</b>		
Table 2.1	The Nutritional Composition of the used Breeding Diet compared to the Maintenance Diet (taken from the product sheet, Special Diet Services, Rosenberg Germany)	50
Table 2.2	Details of plasmids used in this thesis alongside the origin of these plasmids.	53
Table 2.3	Details of the brain samples used for the total mRNA analysis	56
Table 2.4	The sequences of the primers used in the site-directed mutagenesis of the GCP16 plasmid	59
Table 2.5	Sequences of the primers used in subcloning zDHHC9 R148W and R96W mutants from the pcDNA3.1 vector into pEF-BOS-HA	60
<b>Chapter 3</b>		
Table 3.1	List of zDHHC5/zDHHC9 residues forming bonds with GCP16 Arginine-118/121	91
<b>Chapter 5</b>		
Table 5.1	Differentially expressed genes in <i>Zdhhc9</i> knockout mice	145

## Abbreviations

ABHD	$\alpha/\beta$ -hydrolase domain
Akr1p	Ankyrin-repeat containing protein 1
AlkPhos	Alkaline phosphatase
ALT	Alanine transaminase
APP	Amyloid precursor protein
APT	Acyl protein thioesterase
APT1/2	Acyl protein thioesterase 1 and 2
APTs	Acyl protein thioesterases
AR	Ankyrin repeat domain
AST	Aspartate aminotransferase
BHB	Beta-hydroxybutyrate
CBC	Complete blood count
CCM	C-terminal cysteine motif
CFD	Complement factor D
CRD	Cysteine-rich domain
CSP	Cysteine-string protein
DHHC	Aspartate-histidine-histidine-cysteine
DMEM	Dulbecco's modified eagle medium
DR4	Death receptor 4
Efr4	Effector on Ras function 4
FBS	Fetal bovine serum
FSEC chromatography	Fluorescence-detection size-exclusion
GGT	Gamma-glutamyl transferase
GPCR	G protein-coupled receptor
Hb	Haemoglobin
Hct	Haematocrit
HD	Huntington's disease

INCL	Infantile Neuronal Ceroid Lipofuscinosis
KO	Knock-out
Limk1	LIM-domain-containing protein kinase 1
LRP6	Low-density lipoprotein receptor-related protein 6
LRR	Leucine-rich repeat
MAC	Membrane attack complex
MBP	Myelin basic protein
MC1R	Melanocortin-1 receptor
MCH	Mean corpuscular haemoglobin
MCHC	Mean corpuscular haemoglobin concentration
MCV	Mean corpuscular volume
OCD	Obsessive-compulsive disorder
PIL	Personal license
PPT1	Protein palmitoyl thioesterase 1
PRRs	Pattern recognition receptors
RBC	Red blood cells
RDW	Red cell distribution width
REAM	Reduced expression associated with metastasis
RISC	RNA-induced silencing complex
SOCE	Store-operated Ca <sup>2+</sup> entry regulation
TMD	Transmembrane domain
TP	Total protein
TRAIL	Tumour necrosis factor-related apoptosis-inducing ligand
WBC	White blood count
Yck2p	Yeast casein kinase 2
zDABM	zDHHC AR binding motif

## Abstract

S-Acylation is a reversible protein modification that is mediated by a family of 23 “zDHHc” enzymes. zDHHc9 is important for brain physiology, and mutations in the gene encoding this enzyme cause intellectual disability and epilepsy. This thesis aimed to shine new light on the interaction of zDHHc9 with its accessory protein, GCP16, to explore how mutations in *ZDHHc9* that cause brain dysfunction affect the zDHHc9-GCP16 interaction, and to further investigate how *ZDHHc9* loss-of-function might lead to clinical phenotypes.

Cycloheximide chase experiments revealed that the zDHHc9-GCP16 interaction promotes stabilisation of each protein. The stabilisation of zDHHc9 was dependent on GCP16 being S-acylated. Click chemistry assays revealed that zDHHc9 catalysed the S-acylation of GCP16, and that GCP16 also stabilised the S-acylated state of zDHHc9. Thus, both the protein stability and S-acylation of zDHHc9 and GCP16 are modulated by the zDHHc9-GCP16 interaction.

The R96W substitution in zDHHc9 causes intellectual disability, and work in this thesis showed that this change perturbed both the catalytic activity against GCP16 and the S-acylated state of zDHHc9. AlphaFold predictions suggested that R96W disrupts hydrogen bonding between this region of zDHHc9 and the active site of the enzyme, providing a potential molecular explanation for its loss of activity.

Finally, providing *Zdhhc9* knockout mice with a ketogenic diet to mimic GLUT1 deficiency treatment led to metabolic profiles that aligned with GLUT1 deficiency models. This suggests that *Zdhhc9* loss may impair GLUT1 function, which could underlie some of the symptoms seen in patients with *ZDHHc9* mutations, and that this might be possible to manage through dietary intervention.

Overall, these findings establish GCP16 as a critical regulator of zDHHc9 stability and activity, provide new insight into molecular perturbations of disease-causing *ZDHHc9* mutants, and uncover a novel phenotype following dietary intervention with *Zdhhc9* knockout mice.

[Word count: 294]



# **CHAPTER 1**

## **GENERAL INTRODUCTION**

# Chapter 1

## Introduction

### 1.1 Post-translational modifications (PTMs)

Cellular proteins usually undergo some form of chemical modification after being synthesised in the cell; these modifications can be crucial for controlling the protein's attributes, such as function, location, and stability. A recent review by Suskiewicz (2024) traced post-translational modifications (PTMs) back to work of Carl and Gerti Cori in the 1940s, who demonstrated the two interconvertible states of glycogen phosphorylase when phosphorylated and dephosphorylated (e.g. Cori and Green, 1943), thus laying the foundation for the identification of phosphorylation as a widespread PTM (Cori and Green, 1943). Nowadays, a large and growing body of research has emphasised the essential role played by a large number of different PTMs in diversifying the functional properties of proteins, and highlighted that many of these modifications are implicated in the pathophysiology of disease. For instance, Hermann *et al.* (2022) have examined the use of PTM identification and quantification as a novel clinical diagnostic tool for detecting the onset and progression of many diseases, such as cancer, cardiovascular, renal, neurological, and metabolic disorders. PTMs often involve the covalent attachment of molecules such as sugars or lipids to amino acid side chains, changing protein attributes such as hydrophobicity, and subsequently impacting the localisation, half-life, and other crucial characteristics that affect protein function (Chamberlain and Shipston, 2015).

A vast array of PTMs occur on cellular proteins, and some of the most common types include phosphorylation, ubiquitination, glycosylation, and lipidation. Phosphorylation is the addition of phosphate groups onto serine, threonine, or tyrosine residues and is mediated by enzymes known as kinases, and the removal of these phosphates is catalysed by phosphatases. Dynamic phosphorylation plays a pivotal role as a

regulatory switch in essentially all cell signalling pathways (Cheng *et al.*, 2023), and indeed, this is the most common PTM based on the number of experimentally validated sites (Ramazi *et al.*, 2021). Ubiquitination typically involves the addition of a chain of ubiquitin molecules onto lysine residues on target proteins. This controls protein degradation in a process called ubiquitin-dependent degradation. In addition to its role in regulating protein turnover, ubiquitination can also modulate processes such as endocytic trafficking (Desai *et al.*, 2018). Ubiquitination is the 3<sup>rd</sup> most common PTM (Ramazi *et al.*, 2021). Glycosylation involves the attachment of carbohydrate chains to either the nitrogen atom of asparagine side chains, referred to as N-linked glycosylation (7<sup>th</sup> most common PTM; Ramazi *et al.*, 2021), which starts in the endoplasmic reticulum and is completed in the Golgi apparatus, or to the oxygen atom of serine or threonine side chains known as O-linked glycosylation (8<sup>th</sup> most common PTM; Ramazi *et al.*, 2021), which occurs in the Golgi apparatus. Glycosylation impacts protein folding and stability and is important for cell-cell recognition (Cheng *et al.*, 2023).

Lipidation is a diverse process involving the attachment of lipid or lipid-like groups, and thus typically increasing protein hydrophobicity and changing protein structure and affinity for cellular membranes or membrane sub-domains (Chamberlain and Shipston, 2015). Lipid modifications can be classified into two main categories; the first type occurs in the cytoplasm or at the cytoplasmic surface of membranes, whereas the second category represents those taking place in the lumen of the secretory pathway. Proteins that are lipidated in the secretory pathway include Wnt, Hedgehog, and Ghrelin (Chamberlain and Shipston, 2015). The lipid modifications that occur in the cytoplasm include N-myristoylation, S-acylation, and prenylation (Nadolski and Linder, 2007). N-myristoylation can occur both co-translationally and post-translationally. The co-translational reaction involves the attachment of myristate to a glycine residue in the consensus sequence MGXXXS/T; the initiating methionine

residue (M) is first removed, and then myristoyl chains are added to the amine group of the glycine (Aitken *et al.*, 1982; Chamberlain and Shipston, 2015). To a lesser extent, post-translational N-myristoylation occurs following protein cleavage during apoptosis, which can expose the NH<sub>2</sub>-terminal of internal glycine residues (Udenwobele *et al.*, 2017). Prenylation involves the post-translational addition of either farnesyl or geranylgeranyl chains onto the C-terminal end of a protein *via* thioether linkage to a cysteine residue; in this case, the consensus motif is typically CAAX, in which A is an aliphatic or hydrophobic amino acid, and X is any amino acid. In contrast to N-myristoylation and prenylation, S-acylation is distinct due to its unique dynamic and reversible nature. This modification involves the attachment of fatty acids to cysteine residues through a labile thioester linkage. The fatty acids typically associated with S-acylation include palmitate, stearate, and oleate. However, due to the frequent occurrence of the lipid palmitate at these sites, this modification is often referred to as palmitoylation (Chamberlain and Shipston, 2015). It is now recognised that S-acylation is widespread, and indeed, it was suggested to rank as the 14<sup>th</sup> most common PTM based on the number of experimentally validated sites (Ramazi *et al.*, 2021).

## **1.2 Protein S-Acylation**

Protein S-acylation involves the enzymatic addition of fatty acyl chains onto cysteine residues *via* a labile thioester linkage, and is the only fully reversible post-translational lipid modification of proteins (Chamberlain and Shipston, 2015). S-acylation is frequently referred to as palmitoylation and many authors have suggested that palmitate (C16:0) is the major lipid group attached to S-acylated proteins. However, a recent analysis of the acyl chains released from cellular proteins following hydroxylamine treatment to cleave thioesters showed that in HEK293 cells, 37% of S-acylated proteins contained C18 acyl chains and only 22% contained C16 chains

(Busquets-Hernández *et al.*, 2024). The C18 chains were composed of roughly similar amounts of stearate (C18:0) and oleate (C18:1) (Busquets-Hernández *et al.*, 2024).

S-acylation controls protein attributes such as function, localisation and stability (Linder and Deschenes, 2007; Anwar and van der Goot, 2023). The first report on S-acylation was made by Schmidt and Schlesinger (1979), who detected this modification in a glycoprotein from the vesicular stomatitis virus. The researchers used chicken embryo fibroblast cultures labelled with [<sup>3</sup>H] palmitic acid. These were then infected with the vesicular stomatitis virus, and this resulted in the observation of covalent attachment of the radiolabelled palmitate to the glycoprotein polypeptide chain during protein maturation. Indeed, this observation, together with the widespread use of radiolabeled palmitate to study this modification, is why the term "palmitoylation" is still widely used despite mass spectrometry analysis showing a far greater diversity in the acyl chain identity on S-acylated proteins (Busquets-Hernández *et al.*, 2024). In the following years, S-acylation was reported to occur on many mammalian proteins, such as heterotrimeric and monomeric G proteins, G-coupled protein receptors, and other signalling molecules (Milligan *et al.*, 1995). Furthermore, the first demonstration that S-acylation is reversible came from a study focused on N- and H-Ras, which reported different turnover rates for the acyl chains on these proteins (Magee *et al.*, 1987). Since these early seminal studies, breakthroughs in proteomic analyses have facilitated proteome-level analysis, suggesting that around 20% of human proteins are prone to S-acylation (Blanc *et al.*, 2019).

Although S-acylation occurs on a broad range of cellular proteins, there is no obvious consensus recognition motif (Anwar and van der Goot, 2023). The only essential requirement for S-acylation seems to be the presence of a free and suitable reactive cysteine residue positioned at the cytoplasmic side of cell membranes. Despite this, there are some reports of other requirements for S-acylation, which are linked to

specific interactions with S-acyltransferase enzymes (discussed later). For example, the enzyme zDHHC17 recruits specific substrate proteins through an interaction with the N-terminal Ankyrin Repeat domain of this enzyme. This domain recognises a short, unstructured peptide motif present in multiple substrates (Lemonidis *et al.*, 2015).

S-acylated proteins can be broadly divided into two categories: those that associate peripherally with membranes and integral membrane proteins containing a transmembrane domain(s) (TMD) (Nadolski and Linder, 2007). For the first category of proteins, S-acylation is often essential to mediate stable membrane attachment (Vogel and Roche, 1990), and in many cases, S-acylation occurs together with either N-myristoylation or prenylation. Here, the attachment of myristoyl or prenyl chains by cytoplasmic enzymes provides sufficient hydrophobicity to allow transient membrane interaction of the soluble protein, thus enabling S-acylation of the protein by membrane-localised S-acyltransferases – and thereby leading to a stable membrane attachment (Shahinian and Silviu, 1995; Chamberlain and Shipston, 2015). For TMD proteins, representing the second category of S-acylated proteins, Rodenburg *et al.* (2017) reported that a key determinant for cysteine acylation is also proximity to the membrane interface, and modified cysteines are often found adjacent to TMDs. Indeed, the S-acylation of transmembrane proteins was also suggested to be stochastic in this study and determined by the accessibility of cysteines to membrane-bound S-acylation enzymes. It is worth noting that the term "stochastic" is probably not correct, as there is specificity in the S-acylation system, in this case, dictated by cysteine position with respect to the membrane interface. Instead, the loose substrate specificity of S-acylation enzymes may facilitate the modification of a large and diverse pool of cellular proteins (Lemonidis *et al.*, 2014). As many different transmembrane proteins are modified by S-acylation, the importance of this modification goes beyond anchoring soluble proteins to membranes. Instead, the

dynamic nature of S-acylation plays a significant role in shuttling modified proteins between cell compartments, re-localising proteins in the cell or within different regions of the membrane (Guan and Fierke, 2011). For example, S-acylation is a pivotal modification for the specific localisation and signalling events carried out by H- and N-Ras proteins. These proteins are S-acylated at the endoplasmic reticulum and/or Golgi membrane and then transported to the plasma membrane, where they function in the signalling processes taking place at the inner surface of the cell membrane (Goodwin *et al.*, 2005; Rocks *et al.*, 2005; Rocks *et al.*, 2010). Furthermore, H- and N-Ras are also deacylated at the plasma membrane and/or Golgi, which results in release into the cytosol and subsequent reacylation at the ER/Golgi (Rocks *et al.*, 2005). The dynamic nature of S-acylation is essential to bring about the precise localization of these proteins at the plasma membrane and Golgi, and blocking S-acylation leads to an inappropriate accumulation of the proteins on endosomal membranes (Rocks *et al.*, 2005; Rocks *et al.*, 2010).

The role of S-acylation in mediating protein trafficking and localization is also seen with transmembrane proteins. For example, LRP6 (Low-density lipoprotein receptor-related protein 6), a co-receptor for Wnt, requires S-acylation for trafficking to the plasma membrane (Abrami *et al.*, 2008). When the S-acylation sites in this protein are substituted for alanine, LRP6 becomes trapped at the ER and is degraded by the ER-associated degradation pathway. In this case, S-acylation is proposed to facilitate hydrophobic matching of the long TMD of LRP6 with the ER membrane, promoting its stability and enabling subsequent trafficking to the cell surface (Abrami *et al.*, 2008). Indeed, Ernst *et al.* (2018) proposed that S-acylation is a more general signal for protein trafficking through the secretory pathway by mediating the lateral segregation of modified proteins to the rims of Golgi cisternae, from where vesicle budding occurs. There is also a substantial literature describing the role of S-acylation in regulating many aspects of G protein-coupled receptor (GPCR) biology.

Approximately 70% of GPCRs have cysteine(s) residues, typically 10-14 residues downstream of the seventh TMD, which in several cases have been demonstrated to undergo S-acylation (Patwardhan *et al.*, 2021). For many of these GPCRs, it has been shown that cysteine substitution to prevent S-acylation leads to a loss of plasma membrane targeting, and this is the case for CCR5, PAR2, and dopamine receptors, to name a few (Blanpain *et al.*, 2001; Adams *et al.*, 2011; Ebersole *et al.*, 2015; Patwardhan *et al.*, 2021). Conversely, S-acylation can also regulate GPCR internalization; for example, loss of S-acylation of the Luteinizing hormone receptor results in rapid ligand-induced internalization, leading to faster degradation of the ligand (Kawate and Menon, 1994). It has also been shown that S-acylation can regulate protein-protein interactions through a variety of mechanisms, including S-acylation-dependent membrane binding of interaction domains. S-acylation of cysteine-34 in the  $\beta$ 2-adrenoreceptors was proposed to interact with membrane cholesterol and thereby modulate receptor dimerization (Cherezov *et al.*, 2007). In addition to the effects discussed above on protein trafficking and protein-protein interactions, S-acylation can also affect membrane micro-localization and is suggested to play a crucial role in targeting modified proteins to cholesterol-rich rafts; for example, S-acylation of the SNARE protein SNAP25 seems to control its association with rafts, thus regulating its function in exocytosis and endocytosis in neuroendocrine cells (Salaün *et al.*, 2005; Greaves *et al.*, 2011). A further topical example is the S-acylation of the spike protein of SARS-CoV-2. This protein is extensively modified on ten cysteine residues, and this density of saturated lipid chains was suggested to drive the formation of cholesterol-rich domains at the Golgi complex and form platforms for virus budding (Mesquita *et al.*, 2021).

In summary, dynamic S-acylation can impact proteins in a variety of ways, including: (i) membrane association, as seen for Ras proteins; (ii) protein trafficking, as discussed for LRP6 and Luteinizing hormone receptor; (iii) protein interactions, as



described for dimerization of  $\beta$ 2-adrenoreceptor; and (iv) membrane microlocalization as seen for SNAP25. Finally, another important role for S-acylation is in stabilizing proteins. One of the first examples of this came from a study examining the yeast SNARE protein Tlg1, which requires S-acylation of a membrane-proximal cysteine to be protected from ubiquitination (Valdez-Taubas and Pelham, 2005). In this case, S-acylation was suggested to prevent acidic amino acids from coming into contact with the membrane bilayer, which is a signal for recognition by the ubiquitin ligase Tul1. Similar roles of S-acylation in preventing premature protein degradation have also been reported for a variety of mammalian proteins, including the tumour suppressor Sprouty-2 (Locatelli *et al.*, 2020).

### **1.3 Enzymatic regulation of S-acylation**

S-acylation is the only reversible lipid modification of cellular proteins, and its dynamic nature is dependent on the opposing actions of S-acyltransferase enzymes, which belong to the zDHHC family, and acyl protein thioesterase (APT) enzymes.

#### **1.3.1 The zDHHC family**

The human genome contains twenty-three *ZDHHC* genes, which encode a family of polytopic membrane proteins. These proteins contain four to six predicted transmembrane domains and a conserved catalytic DHHC cysteine-rich domain (Fukata *et al.*, 2004). The identification of these S-acyltransferases in the early 2000s represented a major breakthrough almost 25 years after the discovery of this PTM. The first main breakthrough in the search for S-acyltransferase enzymes came from work undertaken in the yeast *Saccharomyces cerevisiae*. Two concurrent studies identified a protein complex consisting of Erf2 and Efr4 (ERF = effector of Ras function) with acylation activity against Ras (Lobo *et al.*, 2002), and Akr1p (ankyrin-repeat containing protein 1), which was shown to catalyse the S-acylation of Yck2p (yeast casein kinase 2) (Roth *et al.*, 2002). Although Akr1p acted in isolation as an S-

acyltransferase, both Erf2 and Erf4 subunits were required for activity, as deletion of either gene led to decreased S-acylation and mislocalization of Ras (Lobo *et al.*, 2002). Analysis of the Erf2 and Akr1p amino acid sequences revealed a conserved 51-amino acid zinc finger DHHC (aspartate-histidine-histidine-cysteine)-cysteine-rich domain (Figure 1.1). Indeed, it was shown that this domain accounted for their S-acylation activity (Roth *et al.*, 2002; Lobo *et al.*, 2002). This DHHC domain was then used to identify potential S-acylation enzymes encoded in mammalian genomes, leading to the identification of 23 zDHHC enzymes, which were cloned from mouse cDNA (Fukata *et al.*, 2004). Topology analysis showed that all the zDHHC family members are predicted to have their catalytic domain facing the cytosol (Politis *et al.*, 2005; Chamberlain and Shipston, 2015), which was later confirmed by X-ray crystallography analysis of human zDHHC20 and zDHHC15 (Rana *et al.*, 2018). Thus, zDHHC enzymes are expected to exclusively modify cysteines present at the cytosolic side of cellular membranes.

The catalytic mechanism of zDHHC enzymes was uncovered by work studying the activity of purified zDHHC2 and zDHHC3 against model peptides using radiolabelled palmitoyl-CoA (Jennings and Linder, 2012). This study showed that S-acylation proceeds through a two-step ping-pong mechanism where the cysteine in the DHHC motif undergoes autoacylation and the acyl group is then transferred to a cysteine in the target protein. Furthermore, the work of Rana *et al.* (2018) managed to provide a step-by-step structural analysis of the activity carried out through the DHHC catalytic domain; this work involved a series of structure-guided mutagenesis experiments, enabling the authors to shed light on the exact role of each residue in catalytic DHHC domains. The researchers found that the catalytic DHHC domain acts by forming a triad-like formation.

A)



Alignment across the human genome identified ZDHC genes, encoding enzymes with a similar DHHC domain

B)

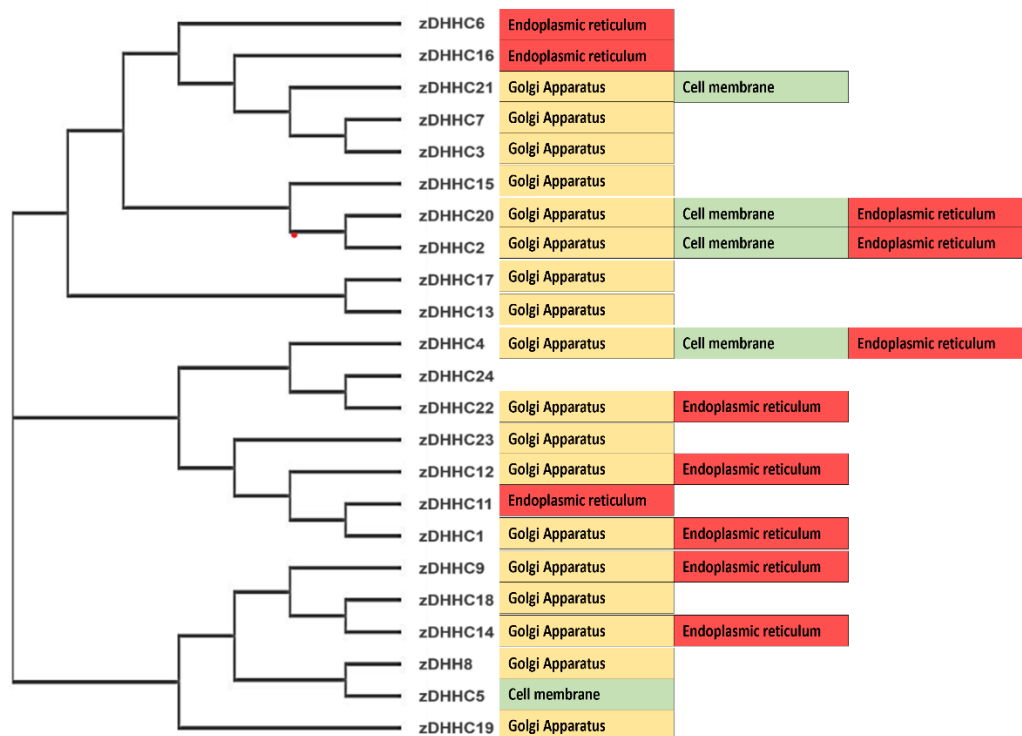


**Figure 1.1 The amino acid relationships between zDHC enzymes and their subcellular localization**

(A) shows the alignment of the DHHC-CRD domains of AKR1 and ERF. (B) shows a phylogenetic cladogram tree of the 23 human zDHC acyltransferases generated using EMBL-EBI website tools, with the subcellular localization of each enzyme also shown.

The mechanism of this formation in zDHHC20 was proposed to be Asp-153 polarising His-154, which then deprotonates the Cys-156 residue. The cysteine proton extraction results in the formation of an active thiolate. This cascade subsequently facilitates the positioning of the active cysteine thiolate for nucleophilic attack toward the fatty acyl-CoA, resulting in the formation of the autoacylation intermediate, and the final step is the transfer of the acyl group to the target protein. It is worth noting that Rana *et al.* (2018) also emphasized the stabilizing role of zinc ions proposed by Mitchell *et al.* (2010); it is assumed that two zinc ions bind to two C<sub>3</sub>H zinc finger domains, reinforcing the structural stability of the enzyme rather than playing a direct role in catalysis.

The study of Rana *et al.* (2018) also reported that the four transmembrane helices of zDHHC20 form a tepee-like structure, with the narrow end facing the membrane luminal side and widening towards the cytoplasmic interface, forming a cavity. The cavity acts like a pocket in which the acyl chain is inserted. Interestingly, the residues lining this cavity play a key role in acyl-CoA specificities. As discussed previously (Busquettes-Hernandez *et al.*, 2024), S-acylated proteins contain diverse lipid species, including palmitate, palmitoleate, stearate, and oleate. Rana *et al.* (2018) reported that zDHHC20 prefers shorter fatty acyl chains and prefers C14/C16 fatty acids over C18 fatty acids. A key residue determining this acyl chain specificity is Tyrosine-181 within TMD3, and substituting this amino acid with a smaller alanine allowed the enzyme to more efficiently use the longer chain stearyl CoA (C18:0) (Rana *et al.*, 2018). This analysis by Rana *et al.* (2018) of the fatty acid specificity of zDHHC20 also validated previous work by Greaves *et al.* (2017), which had shown that isoleucine-182, residing in the third transmembrane domain, limits the ability of zDHHC3 to utilize longer chain fatty acids, and that replacing this residue with a less bulky serine, allowed it to better use C18 fatty acids as substrates. Isoleucine-182 of zDHHC3 is in exactly the same position as Tyrosine-181 in zDHHC20.

As discussed previously, no strict consensus sequence is required for S-acylation. The only requirement is the presence of cysteine residues, which are usually located at the cytoplasmic-membrane interface beside either transmembrane domains or prenylation or N-myristoylation sites. Nevertheless, some zDHHC enzymes have been shown to recognize specific features of proteins, which contributes to their substrate specificity. This is exemplified by studies showing the importance of the Ankyrin Repeat (AR) domain present in zDHHC17 and zDHHC13 for their substrate recognition. The ankyrin domain is a protein-protein binding motif forming a structural unit composed of 33 amino acids (Kohl *et al.*, 2003), and there are seven of these ankyrin units in the AR domain of zDHHC17 (Verardi *et al.*, 2017). The AR domain of zDHHC17 was previously shown to interact with huntingtin, and appending this domain onto zDHHC3 allowed this enzyme also to recruit and S-acylate the huntingtin protein (Huang *et al.*, 2009). In 2015, work by Lemonidis *et al.* showed that the AR domain of zDHHC17 also interacts with other substrates, including SNAP25, SNAP23, CLIP3, and cysteine-string protein (CSP). Furthermore, this study also identified a conserved recognition motif in these proteins with the consensus [VIAP][VIT]XXQP sequence (where X is any amino acid). A subsequent study showed that this so-called zDABM (zDHHC AR Binding Motif) is present in many different proteins, and peptide screening validated 95 of these novel zDABM sequences, including in the Sprouty protein family (Lemonidis *et al.*, 2017). The zDABM sequence of SNAP25 is essential for its S-acylation and plasma membrane targeting in PC12 cells (Greaves *et al.*, 2010), whereas although this sequence is the major zDHHC17 interaction site in Sprouty-2, it is not essential for the S-acylation of this protein by zDHHC17 or its localization in PC12 cells (Locatelli *et al.*, 2020). Furthermore, the Sprouty-related protein SPRED3 is effectively S-acylated by zDHHC17 despite lacking a zDABM sequence. Thus, zDHHC17 S-acylates proteins through both zDABM-dependent and -independent mechanisms.

Other than the AR-zDABM recognition mechanism employed by zDHHC17 and zDHHC13, other zDHHC enzymes contain PDZ ligands that bind to PDZ binding motifs, which usually consist of approximately 90 amino acids (Castro-Cruz *et al.*, 2023); these PDZ ligands are present in nine zDHHC enzymes, including zDHHC3, zDHHC5, zDHHC7, zDHHC8, zDHHC14, zDHHC16, zDHHC17, zDHHC20 and zDHHC21 (Malgapo and Linder, 2021), and it has been shown that these sequences in zDHHC5 and zDHHC8 are important for the recognition and S-acylation of Grip1b in neurons, and thereby contribute to the role of this protein in regulating AMPA receptor dynamics at synapses (Thomas *et al.*, 2012).

In addition to these recognized mechanisms of zDHHC enzyme-substrate interactions, there are many reported enzyme-substrate pairs for which the underlying recognition mechanism is unknown. This is especially true for enzymes such as zDHHC3 and zDHHC7, which modify a broad and diverse pool of proteins in co-expression experiments without any obvious mechanism of substrate selectivity. Indeed, these enzymes were shown to S-acylate SNAP25 in the absence of any detectable interaction, and it was proposed that zDHHC3 and zDHHC7 may be able to modify any membrane-exposed cysteine, thus accounting for their activity against substrates with no obvious similarities (Lemonidis *et al.*, 2014). For other zDHHC enzymes, substrate specificity might also be determined through their association with different accessory proteins, such as GCP16 for zDHHC9, Golga7b for zDHHC5, and selenoprotein K for zDHHC6 (Salaün *et al.*, 2020), and this is an area that requires more detailed investigation.

### **1.3.2 Protein Deacylases**

Acyl protein thioesterase (APTs) catalyse the removal of acyl chains from S-acylated proteins. Interestingly, deacylation enzymes were discovered in the late 1990s before the discovery of the zDHHC family. The first breakthrough in this area came with the purification of protein palmitoyl thioesterase 1 (PPT1) from bovine brain and the

demonstration of deacylation activity against H-Ras (Camp *et al.*, 1994). However, later work showed that this enzyme is localised to lysosomes, where it is believed to play a role in deacylation during protein degradation (Hellsten *et al.*, 1996). However, later work Duncan and Gilman (1998) reported the isolation of a cytoplasmic acyl protein thioesterase enzyme (APT1) activity from rat liver homogenates and subsequently purified the protein from *E. coli* through recombinant DNA technology. This enzyme was shown to be active against H-Ras and G $\alpha$  subunits, and had a cytosolic localisation, and thus could contribute to dynamic S-acylation in cells. Later work identified a related cytosolic enzyme, APT2 (Toyoda *et al.*, 1999), which shares 81% amino acid similarity with APT1. These two enzymes do have some common substrates, but they are not functionally interchangeable; for instance, only APT1 can deacylate  $\beta$ 2-adrenergic receptors (Adachi *et al.*, 2016), and only APT2 is active against GAP43 and zDHH6 (Abrami *et al.*, 2017; Tomatis *et al.*, 2010). In addition, the tumour suppressor protein Scribble was reported to undergo very rapid deacylation kinetics, and it was shown conclusively that this is mediated by APT2. To show this, the authors used highly selective, isoform-specific inhibitors, ML348 and ML349, which target APT1 and APT2, respectively (Hernandez *et al.*, 2017). They showed that APT2 action led to the release of Scribble from cell-cell junctions, leading to enhanced growth and malignancy, and that this could be restored by APT2 inhibition with ML349, but not by APT1 inhibition with ML348. This emphasizes the S-acylation reversibility potential in cancer therapeutics.

A study by Amara *et al.* (2019) used a chemical biology approach to investigate how deacylase specificity is determined. To do this, they generated model peptides with a fluorophore at the N-terminus, which was quenched by a neighbouring S-acyl chain with a quencher group. This tool compound provided an increased fluorescence signal when the S-acyl chain was cleaved (by a thioesterase). By analyzing the effects of different amino acids around the S-acylated cysteine on the specificity of cleavage

by APT1 and APT2, they uncovered clear sequence preferences. Indeed, their analysis was able to potentially explain why Scribble is a substrate for APT2 but not APT1, as isoleucine and asparagine, when present immediately downstream of the modified cysteine, as seen in Scribble, lead to preferential deacylation by APT2.

In addition to APT and PPT enzymes, subsequent studies reported that  $\alpha/\beta$ -hydrolase domain-containing (ABHD) proteins also have deacylase activity. This was first reported by the Conibear group, who showed that ABHD17 has activity against both PSD95 and N-Ras. In this study, they showed that knockdown or overexpression of APT1 or APT2 did not affect the deacylation of these substrates, whereas the expression of ABHD17 enzymes enhanced their acylation turnover (Lin and Conibear, 2015). A subsequent study explored the actions of ABHD17 in neurons, showing that ABHD17A/B/C localized at various subcellular compartments within neurons, including endosomes, the dendritic plasma membrane, and the synaptic fraction (Yokoi *et al.*, 2016). Over-expression of ABHD17 in hippocampal neurons led to a decreased S-acylation status of PSD95, resulting in its decreased accumulation at synapses and consequently affecting AMPA receptor clustering at synapses (Yokoi *et al.*, 2016). ABHD and APT enzymes likely work in concert to regulate neuronal dynamics, as it is also established that APT1 has important functional roles in neurons. For example, one study reported that the microRNA mi138 reduces the expression of APT1, and that mimicking this by shRNA-mediated depletion of APT1 led to an increase in the S-acylation and membrane binding of G $\alpha$ 13, resulting in a decrease in dendritic spine volume (Siegel *et al.*, 2009).

All identified deacylation enzymes have a conserved Ser-His-Asp catalytic triad that is essential for their activity. However, because S-acylated proteins are membrane-associated, deacylation enzymes require a mechanism to interact with membranes to bring them into proximity with their substrates. A study by Abrami *et al.* (2021) presented a model for how this occurs for APT2. This model suggests that this protein



associates with membranes through the insertion of a hydrophobic loop and that this is followed by S-acylation of neighbouring cysteines by either zDHHC3 or zDHHC7 to enable tighter membrane binding. Molecular dynamics simulations suggested that APT2 can then deform the membrane to facilitate access of the active site to the S-acyl chain, which is then sequestered within a hydrophobic pocket of APT2 after its cleavage.

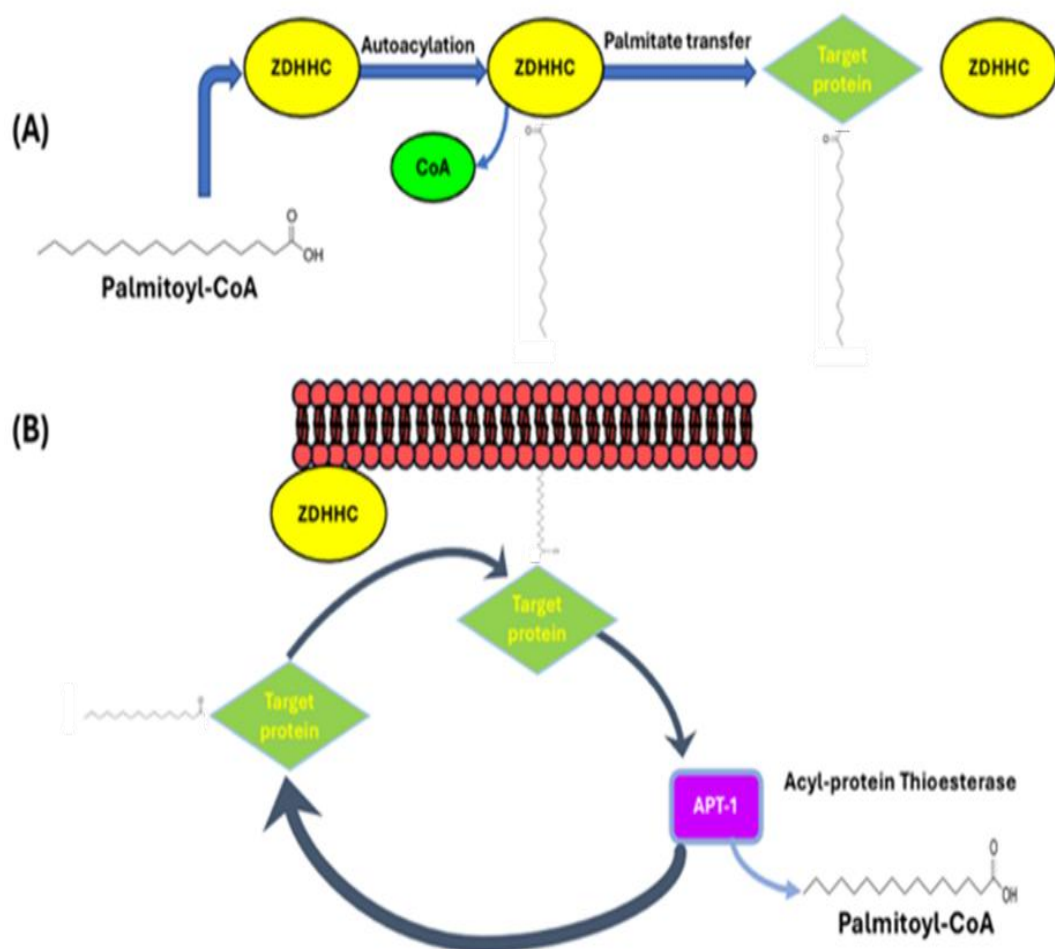


**Figure 1.2 Reversible S-acylation and the enzyme components**

The first step of S-acylation starts with the acyl-CoA reacting with the zDHHC enzyme and forming an autoacylated enzyme intermediate, with the corresponding release of free CoA. In the second step, the acyl chain is transferred to the target protein. The binding of both substrates (acyl-CoA and the protein) to the enzyme causes the enzyme to be at a constant shift between acylated and non-acylated states. (B) The attachment of the acyl chain to the protein might allow the protein to be localised at the cell membrane, whereas the removal of the acyl group, mediated by thioesterases such as APT1, allows the targeted protein to relocate to the cytosol. For

transmembrane protein substrates, the protein would remain associated with the membrane following deacylation.

As discussed above, inhibition of APT2 could be a novel strategy to prevent Scribble mislocalisation and loss of its tumour suppressor activity (Hernandez *et al.*, 2017). There is also interest in targeting H/N-Ras S-acylation as a mechanism to down-regulate their activity in cancer, as acylation-dependent membrane association is key for these proteins' signalling/cell growth activities. With regards to Ras proteins, it might be predicted that blocking S-acylation would inhibit Ras activity and that blocking deacylation would enhance Ras activity (by promoting its membrane association). However, this simplistic view does not appear to hold, as preventing the deacylation of N-Ras led to its mislocalisation to endosomes and, therefore inhibiting deacylation of this protein can also be seen as an approach to inhibit the normal signalling activity of this protein (Rocks *et al.*, 2005). Indeed, Remsberg *et al.* (2021) developed a selective inhibitor of ABHD17, named ABD957, and showed that this compound blocked the deacylation of N-Ras in acute myeloid leukaemia cells and inhibited the growth of NRAS-mutant cells. Therefore, there is clearly scope for both acylation and deacylation inhibitors to be effective at treating elevated Ras signalling in cancer.

Finally, it should be noted that deacylation activity in lysosomes is also critical for normal human health. This has been established for a long time as mutations in the lysosomal PPT1 thioesterase were reported to cause infantile neuronal ceroid lipofuscinosis (INCL) (Vesa *et al.*, 1995). INCL is a neurodegenerative disorder that develops in children, and where the pathogenesis occurs due to the accumulation of S-acylated lysosomal and synaptic proteins. The mutations in PPT1 that cause INCL impact either the location or enzymatic activity of PPT1 (Henderson *et al.*, 2016). In the vein of further understanding the disorder, Gorenberg *et al.* (2022) managed to

identify more than 100 PPT1 substrates at the synapse, drawing a more detailed picture of the disorder's aetiology.

#### **1.4 Subcellular Localisation of Acylation Enzymes**

The subcellular distribution of zDHHC enzymes will likely be crucial in determining their wider substrate networks. Most DHHC enzymes are localized at the Golgi apparatus or the endoplasmic reticulum (ER) (Ohno *et al.*, 2006). However, the specific compartmentalisation of these enzymes observed in different studies can be influenced by various factors, including the cell type used, and enzyme overexpression and epitope-tagging. The first comprehensive analysis of zDHHC enzyme localisation used overexpression of epitope-tagged zDHHC enzymes in yeast and mammalian cells and revealed an enrichment at the Golgi and ER, with some exceptions like zDHHC5, zDHHC20, and zDHHC21, which were found to also stain the plasma membrane (Ohno *et al.*, 2006; Malgapo and Linder, 2021). However, it is important to note that various factors could affect the localisation of these enzymes and potentially make the observations unreliable. These include the use of over-expression, the appendage of epitope tags, and cell-type-specific effects. For example, protein interactions could be saturated by over-expression, affecting pathways that mediate correct zDHHC localization, or immortalised cell lines may lack proteins, lipids, or specific post-translational modification enzymes that are important for the localization of a specific zDHHC enzyme in its native environment and at native expression levels. Indeed, subsequent analyses of individual enzymes have uncovered some discrepancies with the study of Ohno *et al.* (2006). For example, zDHHC2, which was suggested to localise at the Golgi apparatus and ER, was subsequently shown to be present at the plasma membrane and recycling endosomes in PC12 cells and hippocampal neurons (Greaves *et al.*, 2011; Salaün *et al.*, 2017). Furthermore, the localisation of zDHHC2 to these membrane compartments was suggested to be regulated by phosphorylation (Salaün *et al.*,

2017). Additionally, while zDHHC4 was reported by Ohno *et al.* (2006) to localise at the Golgi, this enzyme was later found to be at the ER in hippocampal neurons (Levy *et al.*, 2011), and its ER localisation was determined by a C-terminal dilysine motif that redirected zDHHC3 from the Golgi to the ER when appended to the C-terminus of this enzyme (Gorleku *et al.*, 2011).

Notably, some other reports suggested that accessory proteins can modulate the localisation of zDHHC enzymes, and overexpression of zDHHCs could therefore lose this influence of these accessory factors. A prominent example of this is zDHHC5, which was found to be recruited to the plasma membrane through its accessory protein, Golga7b (Woodley and Collins, 2019). This finding broadens the understanding of the roles of accessory proteins, indicating that they extend beyond the regulation of S-acylation activity (as seen for ERF2/ERF4 and zDHHC9/GCP6) to also impact the specific localisation of zDHHC enzymes.

A detailed understanding of the cellular localisation of zDHHC enzymes will require a potent set of antibody molecules to accurately detect these enzymes in cell and tissue samples. Antibodies against zDHHC enzymes have not been successfully deployed to map their localisation, which likely reflects the very low expression levels of these enzymes. For example, it has been estimated that the *combined* cellular expression levels of all zDHHC enzymes amount to a copy number of only around 43,000-110,000 molecules per cell. As noted by Mesquita *et al.* (2024), this is substantially below the expression level of N-myristoyltransferase I, one of the two enzymes responsible for N-myristoylation, which has been estimated to have approximately 225,000 copies per cell.

As mentioned earlier, APT1 and APT2 are modified by S-acylation, which is important in localising these enzymes to the plasma membrane and intracellular membranes (Kong *et al.*, 2013) and for facilitating access of these enzymes to their S-acylated substrates (Abrami *et al.*, 2021). ABHD enzymes also contain specific membrane-

targeting elements (Holme *et al.*, 2025). For example, ABHD17 is multiply S-acylated at its N-terminus on 4 or 5 cysteine residues. These cysteines are important for targeting to the plasma membrane, but the configuration of the cysteines is also vital for enzyme activity against N-Ras. These S-acylated cysteines are present within an N-terminal helix that lies on one side of the substrate binding pocket. The configuration of S-acylated cysteines is considered necessary for the orientation of this substrate-binding region at the membrane. There is also a loop region on the other side of the binding pocket that interacts with the membrane, which is also essential for optimal positioning of the pocket for efficient substrate deacylation.

## **1.5 Accessory proteins / Co-factors**

### **1.5.1 GCP16 and zDHHC9**

GCP16 undergoes S-acylation at two cysteine residues (Cys-69 and Cys-72) (Ohta *et al.*, 2003), enabling it to associate with Golgi membranes and interact with zDHHC9 (Ohta *et al.*, 2003; Swarthout *et al.*, 2005; Mitchell *et al.*, 2014). The proteins form a stable complex that can be purified from Sf9 insect cells and mammalian cells for functional studies, and zDHHC9 is poorly expressed in the absence of GCP16 (Swarthout *et al.*, 2005). The stabilising effect of GCP16 is evident in its protection of zDHHC9 from aggregation. Size exclusion chromatography analysis showed that zDHHC9 formed high molecular weight complexes/aggregates in HEK293 cell lysates, and that there was an increase in monodispersity when co-expressed with GCP16 (Nguyen *et al.*, 2023). Mutational analysis showed that the removal of the C-terminal 64 amino acids of zDHHC9 did not prevent the stabilising effect of GCP16, whereas the removal of the last 86 amino acids did. This led the authors to focus on the region 279-300 in zDHHC9 as a potential GCP16 interaction site, and they identified a triplet of cysteines in the sequence CCXXXC that was important for the effects of GCP16 on zDHHC9 stabilisation, where Cys-288 was most important. Further analysis by size exclusion chromatography confirmed the importance of the

cysteines for GCP16-zDHHC9 interaction. The effects of GCP16 on protein stability were reported to extend to other enzymes with a C-terminal cysteine motif, including zDHHC14, zDHHC5, zDHHC8, and zDHHC18, but not to enzymes that lack this motif, such as zDHHC3 and zDHHC20 (Nguyen *et al.*, 2023).

Furthermore, the effects of GCP16 on zDHHC14 and zDHHC18 corresponded with an increase in the activity of these enzymes. In contrast, the related Golga7b proteins showed specific stabilisation effects on zDHHC5 and zDHHC8 but not the other zDHHCs. The stabilisation effects of GCP16 on zDHHC9 are consistent with work on the yeast homologues ERF2 and ERF4, which showed that ERF2 undergoes ER-associated degradation in the absence of ERF4 (Mitchell *et al.*, 2012). This study further showed that ERF4 stabilised the autoacylated intermediate of purified ERF2.

### **1.5.2 Golga7b, GCP16 and zDHHC5**

Interestingly, the C-terminal cysteine motif in zDHHC5 was also shown to be necessary for its interaction with Golga7b. The interaction requires the S-acylation of three specific cysteine residues (C236, C237, and C245) located in the C-terminal tail of zDHHC5 (Woodley and Collins, 2019; Collins *et al.*, 2017; Yang *et al.*, 2010). These cysteine residues are essential for effective interaction with Golga7b, thereby promoting its retention at the plasma membrane (Woodley and Collins, 2019). As the C-terminal cysteine motif is important for both the interaction of zDHHC9 with GCP16 and Golga7b with zDHHC5, the general interaction mechanisms of GCP16 and Golga7b with zDHHC enzymes are likely to be conserved.

Although the work of Woodley and Collins (2019) reported an interaction of Golga7b with zDHHC5, other work also reported that GCP16 plays an important role as an accessory protein for this enzyme. Immunoprecipitation assays have demonstrated that GCP16 interacts directly with zDHHC5, and mutations that disrupt the S-acylation sites on either GCP16 or zDHHC5 significantly impair the formation of this complex,

thus compromising its functional roles (Ko *et al.*, 2019). Although initially identified as a Golgi-localised protein (Ohta *et al.*, 2003), recent studies have revealed that GCP16 also co-precipitates with zDHHC5 at the plasma membrane (Solis *et al.*, 2022) and with zDHHC9 at the Golgi, further indicating its ability to regulate these enzymes in different cellular environments.

### **1.5.3 HTT and zDHHC17/13**

Huntington's disease (HD) is a neurodegenerative disorder caused by an expansion of a CAG repeat sequence in the *HTT* gene, leading to a mutant huntingtin (HTT) protein with an extended polyglutamine (polyQ) domain (Tabrizi *et al.*, 2020). Interestingly, polyQ expansion disrupts the interaction between HTT and zDHHC17 and the closely related enzyme zDHHC13 (Singaraja *et al.*, 2002; Fukata *et al.*, 2004; Huang *et al.*, 2004). As these enzymes mediate the S-acylation of HTT at cysteine-214, it has been proposed that a loss of HTT S-acylation could contribute to HD pathogenesis (Huang *et al.*, 2009; Huang *et al.*, 2011).

Remarkably, it was suggested that HTT is not only a substrate of zDHHC17 but also a positive modulator of this enzyme. It was shown that HTT enhanced the ability of zDHHC17 to S-acylate SNAP25 in cell lysates (Huang *et al.*, 2011), and it was suggested that the effects of HTT on zDHHC17 are linked to the stabilisation of the autoacylated enzyme intermediate; for example, zDHHC17 S-acylation was reduced in lysates from HTT heterozygous knockout mice (Huang *et al.*, 2011). However, the exact mechanisms for the effects of HTT on zDHHC17 remain unclear, with evidence suggesting both direct and indirect interactions (Sanders *et al.*, 2014; Butland *et al.*, 2014).

Notably, the disruption of the HTT–zDHHC17 interaction has significant cellular consequences. For example, the loss of S-acylation results in the increased formation of intracellular aggregates of mutant HTT, a hallmark of HD pathology (Yanai *et al.*,

2006). Additionally, mutant HTT negatively affects the activity of zDHH17, as evidenced by reduced S-acylation of key neuronal substrates, including SNAP25 and AMPA receptor subunits in HD models, such as the YAC128 mouse (Singaraja *et al.*, 2011). One particular theory that has been proposed is that zDHH17 activity is decreased in the presence of mutant HTT, leading to the reduced S-acylation of substrates of this enzyme. It has, therefore, been proposed that defective S-acylation could contribute to the pathology of HD. The possible role of zDHH17 (and zDHH13) in HD pathogenesis is supported by analysis of knockout mouse models where the loss of these enzymes leads to HD-like phenotypes (Singaraja *et al.*, 2011; Sutton *et al.*, 2013). These findings show the importance of HTT–zDHH17 interactions in maintaining neuronal health, and highlight the need to produce a comprehensive understanding of the substrates of zDHH17 and how these might link to HD phenotypes.

#### **1.5.4. SelK and zDHH6**

Selenoproteins are a class of proteins that incorporate selenocysteine, a unique amino acid known for its antioxidant and enzymatic properties. SelK, as one such selenoprotein, plays a pivotal role in regulating store-operated  $\text{Ca}^{2+}$  entry (SOCE) in immune cells. SOCE is triggered when ER  $\text{Ca}^{2+}$  stores are depleted, activating a signalling cascade that involves the interaction between inositol trisphosphate (IP3) and the IP3 receptor (Prakriya and Lewis, 2015). SelK is responsible for the regulation of the IP3 receptor, and its absence leads to a disruption in IP3 receptor function. Specifically, in cells lacking SelK, there is a decrease in the protein levels of the IP3 receptor in various immune cells, such as T cells, B cells, and macrophages (Fredericks *et al.*, 2014).

The influence of SelK on the IP3 receptor has been proposed to be linked to S-acylation. Notably, SelK was found to co-immunoprecipitate with zDHH6 and was further suggested to regulate the activity of this enzyme, which mediates the S-



acylation of the IP3 receptor at cysteine residues C56 and C849 (Fredericks *et al.*, 2014). Fredericks *et al.* (2018) also showed that SelK stabilises the autoacylated intermediate of zDHHC6. However, further experiments are needed to directly confirm the mechanisms by which SelK influences zDHHC6 activity, and it will be particularly important to confirm this regulatory role through the analysis of purified SelK and zDHHC6.

## **1.6 S-acylation and disease**

It is notable that nearly 20% of human proteins are susceptible to modification through S-acylation (Blanc *et al.*, 2015), and it is therefore unsurprising that defects in this process are linked to various disorders and diseases. S-acylation has been linked to a variety of conditions, such as cancer, autoimmune diseases, and neurodegenerative and neurological disorders (Zhou *et al.*, 2023; Li *et al.*, 2023; Schirwani *et al.*, 2018).

### **1.6.1 S-acylation and cancer**

There is a well-established and growing body of literature that has highlighted links between S-acylation and cancer. Indeed, over 190 annotated cancer drivers are known to be S-acylated, including H/N-Ras and EGF receptors (Ko and Dixon, 2018). Furthermore, there are links between altered zDHHC enzyme expression and cancer (Li *et al.*, 2023; Yeste-Velasco *et al.*, 2015; Sharma *et al.*, 2017). Sharma *et al.* (2017) reported that zDHHC3 is upregulated in breast cancer and contributes to metastasis and tumorigenesis in this cancer type. Specifically, the researchers employed shRNA to inhibit the expression of zDHHC3, and subsequently found a reduction in tumour metastasis and size in both primary and metastatic tumours. Moreover, a noteworthy event occurred during *in vivo* testing: the increased oxidative stress in zDHHC3-inhibited tumours triggered tumour senescence and facilitated the immune response, leading to the tumour's resolution. According to the researchers, this further cemented

the role of zDHH3 as a tumour driver and/or acting as an oncoprotein in breast cancer.

Indeed, zDHH3 has also been suggested to be a target for chemotherapy in hepatocellular carcinoma (Wu *et al.*, 2024); here, the activities of zDHH3 and ABHD17A were found to modulate both cholesterol synthesis and immune response to the tumour. The researchers suggested that the S-acylation of the SCAP protein by zDHH3, along with the upregulation of zDHH3 by SREBP2, creates a positive feedback loop. This process increases cholesterol concentration in the microenvironment, affecting the immune response.

Despite the described oncogenic activity of zDHH3, previous reports found that through the S-acylation of certain substrates, this enzyme might also have activities linked to tumour suppression, even in the same type of cancer where it was described as an oncoprotein. This was based on the analysis of Tumour necrosis factor-related apoptosis-inducing ligand (TRAIL), also referred to as Death Receptor 4 (DR4), which is a cell surface receptor that plays a crucial role in inducing apoptosis in cancer cells. Research conducted by Oh *et al.* (2012) suggested that zDHH3 S-acylates TRAIL/DR4, thereby mediating its localisation to the cell surface in Hep-3B cells (hepatocellular carcinoma cells), ultimately leading to cell death. This localisation of DR4 receptors supports the notion of a tumour suppressor function for zDHH3. In another study, genomic analysis of cases with squamous cell cervical carcinoma detected the loss of the gene encoding zDHH3, thus suggesting a potential tumour-suppression activity in this cancer type too (Choi *et al.*, 2007). In addition to zDHH3, other enzyme isoforms have also been proposed to have oncogenic activity. This includes work implicating zDHH5 as a possible oncoprotein (Chen *et al.*, 2017; Ko and Dixon, 2018). Chen *et al.* (2017) highlighted this oncogenic potential by demonstrating a significant correlation between zDHH5 overexpression and the presence of p53 mutations, which in turn correlates with increased survival and

metastasis of gliomas in the brain. Additionally, it was found that mutations in the p53 gene lead to a gain of function and interaction with the nuclear transcription factor (NF)-Y, resulting in disrupted transcription of genes that encode oncoproteins. Notably, the promoter region of the zDHHC5 gene contains binding sites for the NF-Y factor, linking p53 mutations to zDHHC5 overexpression. Consequently, the researchers also suggested that the overexpression of zDHHC5 contributes to increased glioma volume, thereby categorising it as a potential oncoprotein.

zDHHC20 has also been implicated as a possible oncoprotein in specific cancer types (Yeste-Velasco *et al.*, 2015). For example, the overexpression of zDHHC20 in breast and ovarian cancers causes cell phenotypic changes and promotes cellular transformation, ultimately increasing tumorigenicity (Draper and Smith, 2010).

In summary, there is a growing body of evidence linking multiple zDHHC enzymes in the pathogenesis of many types of cancer, making these enzymes viable therapeutic targets; however, achieving selective inhibition of the S-acylation activity of certain zDHHC enzymes remains a challenge in the therapeutic field.

On the other hand, as mentioned previously in the case of zDHHC3, some zDHHC enzymes have been suggested to act as tumour suppressors or as proxies through S-acylating specific substrates, which in turn suppress tumour growth. There is evidence that zDHHC2 can suppress several types of cancer. For example, the work of Peng *et al.* (2014) emphasized the tight association between the loss of a genomic region encoding zDHHC2 and significant pathological clinical parameters like the reoccurrence of hepatocellular carcinoma, metastasis, increased tumour size, and the occurrence of portal vein tumour thrombi in patients who underwent liver transplant. This impact of zDHHC2 was also underscored through *in vitro* assays, where over-expression of zDHHC2 inhibited the proliferation and invasion of cancerous cells. This correlation highlights the role of zDHHC2 as a tumour suppressor. Furthermore, in gastric adenocarcinoma, almost the exact correlation

mentioned above was observed, as patients with gastric adenocarcinoma had lower zDHHC2 expression levels as well as the involvement in metastasis to lymph nodes (Yan *et al.*, 2013). These tumour suppression effects of zDHHC2 led to its previous name, before the discovery of the zDHHC family: Reduced Expression Associated with Metastasis (REAM) protein (Oyama *et al.*, 2000).

Another enzyme with possible tumour suppressor activity is zDHHC13. It was suggested that patients with certain characteristics like red hair are more prone to carry mutations in melanocortin-1 receptor (MC1R RHC), which increases the likelihood of melanoma. Chen *et al.* (2017) suggested that the impact of these MC1R RHC variants can be avoided by the S-acylation of MC1R by zDHHC13, thus restoring MC1R signalling and inducing pigmentation, and consequently increasing protection against melanoma.

In summary, understanding the roles of zDHHC enzymes in cancer is complicated since many zDHHC enzymes, like zDHHC3, have been suggested to have a dual role as an oncoprotein and tumour suppressor – this may be linked to differential expression of their substrates in different cell and tissue types. Therefore, further research in this field is pivotal as it can open the door for new cancer therapeutic strategies.

### **1.6.2 S-acylation and inflammasome function**

Recent studies have revealed an important role for S-acylation in the regulation of pro-inflammatory signalling through the recruitment of NLPR3 (NACHT, leucine-rich repeat (LRR) and PYD domain-containing protein-3) to cell membranes (Williams and Peden, 2025). The response of innate immune cells to threat is dependent on a family of pattern recognition receptors (PRRs) (Li and Wu, 2021). An important role for some of these PRRs is to initiate (or "seed") inflammasome formation, and this is where NLPR3 plays a key role. NLPR3 can be activated by a range of stimuli that lead to a decrease in intracellular K<sup>+</sup> levels, including bacterial ionophores. NLPR3 activation

involves structural changes in the protein and exchange of bound ADP for ATP, which leads to the oligomerisation of the protein into a disc structure. Once formed, inflammasomes control the processing and release of specific pro-inflammatory cytokines. Several recent reports have indicated roles for S-acylation in regulating NLRP3. These include studies showing that S-acylation mediates the membrane binding of inflammasomes. Specifically, S-acylation of Cys-130 by zDHHC7 mediates NLRP3 recruitment to the Golgi (Yu *et al.*, 2024; Williams and Peden, 2024; Xu *et al.*, 2024; Nie *et al.*, 2024), which may be important for the activation of inflammasomes through the spatial proximity to relevant binding partners. In addition, S-acylation of NLRP3 at cysteine-844 by zDHHC12 was shown to lead to its degradation, possibly by exposing an amino acid motif that links to Hsc70-dependent chaperone-mediated autophagy, and thereby leads to down-regulation of signalling (Wang *et al.*, 2023; Lv *et al.*, 2023). Conversely, S-acylation at cysteine-837 and cysteine-838 (Zheng *et al.*, 2023) or at cysteine-419 (Hu *et al.*, 2024) was proposed to activate inflammasome signalling by promoting the interaction of NLRP3 with its binding partner NEK7. zDHHC5 and zDHHC17 were implicated as the enzymes involved in the modification of these sites, respectively. Overall, these studies show that the S-acylation of NLRP3 is complex, with several sites and enzymes involved, and that this PTM plays a vital role in regulating the activation status of this key protein through different mechanisms (Williams and Peden, 2025).

### **1.6.3 S-acylation and neurological disorders**

The dynamic nature and diverse functions of S-acylation, regulating the localisation, conformation and function of modified proteins, make it a key factor in brain biology (Liao *et al.*, 2024). This is supported by the fact that it is the most common lipid modification occurring in the brain (Fukata and Fukata, 2010), and by proteomic analysis conducted by Sanders *et al.* (2015), which suggested that 41% of synaptic

genes encode proteins prone to be S-acylated. It is, therefore, not surprising that S-acylation has been linked to different neurological conditions.

The role of zDHHC17 in HD has been discussed in Section 1.5.3, and the role of zDHHC9 in brain physiology and pathophysiology will be described in Section 1.10. Therefore, I only discuss Alzheimer's Disease (AD) in this section. AD is one of the most common neurodegenerative disorders, characterised by slowly progressing clinical complaints like short-term memory loss, mood swings and cognitive impairments (Knopman *et al.*, 2021). The exact causes of AD remain unknown; however, risk factors have been identified, which include age and genetic predisposition (Burns and Iliffe, 2009).

The pathogenesis of AD is hypothesised to be linked to the accumulation of  $\beta$ -amyloid protein, forming  $\beta$ -amyloid plaque, and hyperphosphorylated tau protein, forming Neurofibrillary tangles. Amyloid precursor protein (APP) is cleaved by both  $\beta$ -secretase and  $\gamma$ -secretase, leading to the formation and aggregation of the  $\beta$ -amyloid plaque (Hur, 2022). The body's inability to clear these molecules leads to neurotoxicity and inflammation, subsequently impacting the brain with damage ranging from impaired synaptic connectivity to neural injury and degeneration (Zhang, 2023).

Almost all the key proteins contributing to AD development have been reported to be modulated in one way or another by S-acylation (Liao *et al.*, 2023).

It is suggested that S-acylation of APP results in its embedding into lipid rafts, leading to enhancement of its cleavage by  $\beta$ -secretase, which in turn increases the  $\beta$ -amyloid formation and worsens prognosis (Bhattacharyya *et al.*, 2013). These effects of S-acylation likely reflect a role for lipid rafts in bringing APP and  $\beta$ -secretase together to allow their more effective recognition and interaction. Furthermore, it was found that inhibiting APP S-acylation may lead to a more favourable outcome.

$\beta$ -secretase has also been suggested to be S-acylated, which may mediate the association of this protein with lipid rafts and thus bring it into proximity with raft-associated APP (Andrew *et al.* 2017). It was proposed that inhibiting  $\beta$ -secretase S-acylation may lead to improved cognitive function and the overall status of the disease (Andrew *et al.* 2017).

## **1.7 zDHHHC9**

### **1.7.1 zDHHHC9 structure and function**

zDHHHC9 is a transmembrane protein consisting of 364 amino acids and has a molecular mass of 40,916 Da (www.omim.org). Mouse zDHHHC9 was initially discovered and cloned by Fukata *et al.* (2004), and the following year, human zDHHHC9 and its accessory protein GCP16 were identified as the orthologues of yeast Erf2 and Erf4, respectively (Swarthout *et al.*, 2005).

The cryo-EM structure of zDHHHC9 shows four transmembrane helices (TM1 to TM4) (Figure 1.3) (Yang *et al.*, 2024). The cytoplasmic region falling between the second and third transmembrane helices contains the DHHC domain and the zinc finger motifs. The DHHC motif includes the active site cysteine-169, which was established due to the lack of S-acylation activity when the residue is mutated to serine (Swarthout *et al.*, 2005). On the other hand, the two zinc finger motifs play an essential role in maintaining the first histidine and the catalytic cysteine in the DHHC motif in the proper conformation (the two zinc ions are represented by circles in Figure 1.3). The image shown in Figure 1.3 is of zDHHHC9 in complex with GCP16 (Yang *et al.*, 2024), and this interaction will be discussed further in section 1.8.

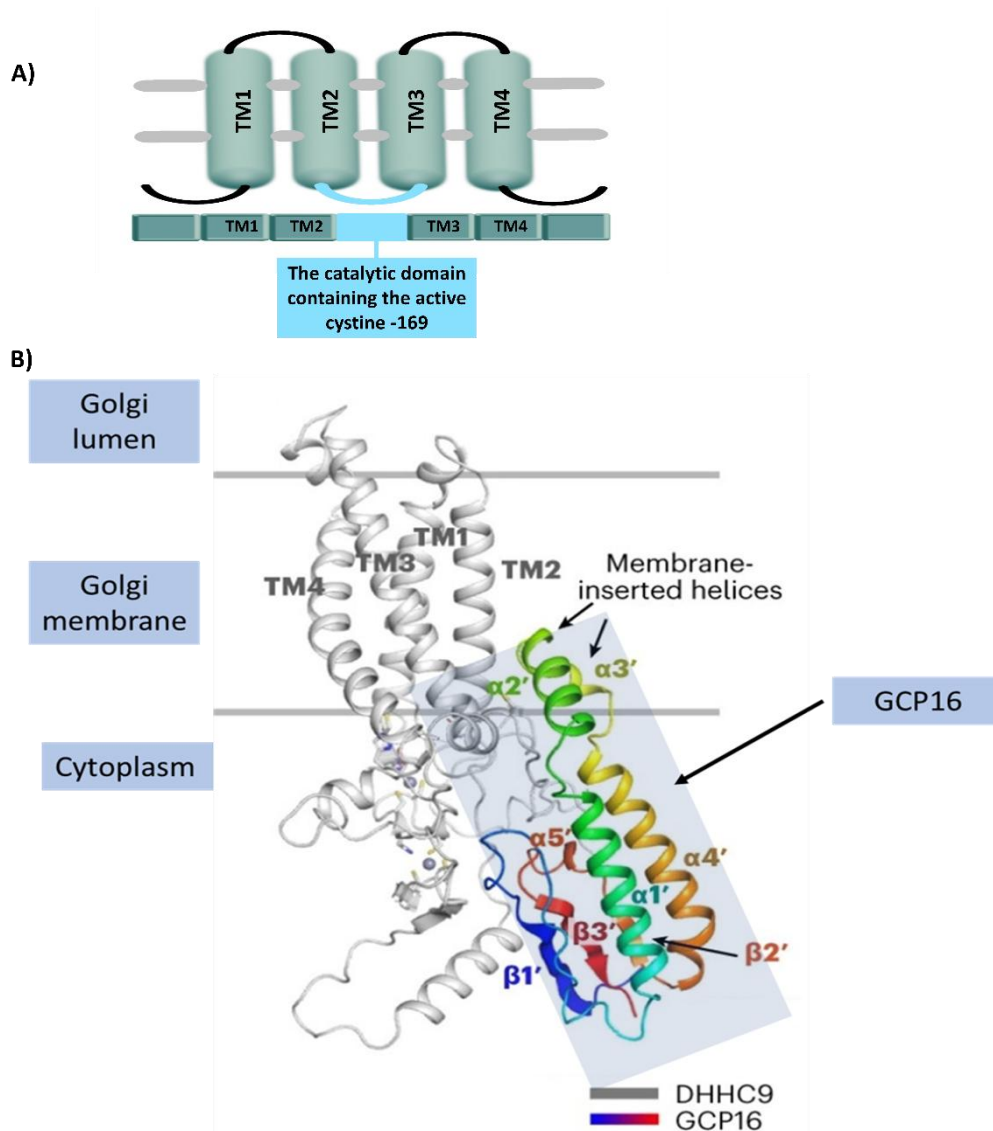


**Figure 1.3 A general diagram of the transmembrane domains of zDHHC9 with Cryo-electron microscopy structure of the human zDHHC9–GCP16 complex.**

**A)** Primary illustration of the consensus zDHHC enzyme domain structure. Most zDHHC (including zDHHC9) enzymes have four transmembrane domains, with the catalytic domain present on an intracellular loop between TMD2 and TMD3. **B)** The structure is taken from Yang *et al.* (2024). The active site of zDHHC9 is present between TMD2 and TMD3. GCP16 (highlighted in faint blue) interacts with zDHHC9 at four interfaces involving both the N- and C-terminal regions, as well as contributions from residues in the central region of GCP16.

S-acylation by zDHHC9 occurs via the two-step mechanism described previously, where the first step is autoacylation leading to the formation of a substrate-enzyme intermediate consisting of an acyl chain from an acyl-CoA donor attached to the cysteine of the DHHC motif through thioester linkage (Mitchell *et al.*, 2010; Jennings



*et al.*, 2012). It is proposed that after the formation of this intermediate that the active cysteine site will be tethered to the membrane *via* the acyl chain. In the second step, the acyl chain is transferred to the cysteine of the protein substrate. In the absence of a protein substrate, hydrolysis of the thioester linkage occurs, producing free fatty acid and the deacylated form of the enzyme (Mitchell *et al.*, 2014).

Swarthout *et al.* (2005) established that zDHHHC9 substrates include N-Ras and H-Ras and that the enzyme is localised to the ER and Golgi apparatus. This localisation was determined using confocal microscopy analysis of GFP and Myc-tagged proteins. However, work in hippocampal neurons has confirmed a Golgi localisation of the endogenous protein (Shimell *et al.*, 2019). In addition to H/N-Ras, other identified substrates include TC10 (Shimell *et al.*, 2019) and BK K<sup>+</sup> channels (Tian *et al.*, 2010).

As mentioned previously, similar to Erf2/Er4 in yeast, zDHHHC9 requires an accessory protein to initiate its acyltransferase activity. Attempts to identify this co-factor by aligning *S. cerevisiae* Erf4 against the genetic database failed to identify a mammalian homologue of this protein. However, further analysis identified an *Aspergillus* Erf4 homologue, which subsequently led (through multiple alignments) to the identification of GCP16 (Golgi-complex associated protein of 16 kDa), which was validated to be the mammalian counterpart of Erf4 (Swarthout *et al.*, 2005). Subsequent enzymatic assays confirmed that GCP16 is indeed a critical protein required for zDHHHC9 activity against purified Ras proteins (Swarthout *et al.*, 2005).

### **1.7.2 The *ZDHHHC9* gene and its transcripts**

The *ZDHHHC9* gene is located on the human X chromosome, specifically at the long arm q26.1 region, and it covers 40.86 Kb, according to the NCBI genetic database ([www.ncbi.nlm.nih.gov](http://www.ncbi.nlm.nih.gov)). *ZDHHHC9* undergoes alternative splicing, producing multiple transcript variants that ultimately encode the same enzyme. According to the NCBI

genetic database ([www.ncbi.nlm.nih.gov](http://www.ncbi.nlm.nih.gov)), this enzyme is widely expressed and highly expressed in the brain, kidney, and prostate. This expression profile is supported by the work of Swarthout *et al.* (2005), who used northern blot analysis to identify a major 2.3 kb human *ZDHHC9* transcript with high expression detected in the brain, kidney, lung, liver and skeletal muscle; moreover, the work of Zeisel *et al.* (2018) found that *zDHHC9* is strongly expressed in the central nervous system (CNS), particularly within oligodendrocytes.

### **1.7.3 Regulation of *ZDHHC9* transcription**

It has been reported that specific microRNAs (miRNA) play a significant role in the transcriptional regulation of *ZDHHC9* (Chai *et al.*, 2013). miRNA are non-coding transcripts of approximately 21 nucleotides that regulate gene expression (Carrel *et al.*, 2009). In neurons, miRNA are implicated in local protein translation, thus regulating dendritic growth, spine formation, growth cone guidance, and neuronal plasticity (Chai *et al.*, 2013). A study by Schratt *et al.* (2006) showed that miRNA-134 (mi-134) in the brain plays a role in the regulation of dendritic spine morphogenesis by affecting Lim-domain-containing protein kinase 1 (Limk1). Chai *et al.* (2013) used the RNA-Induced Silencing Complex (RISC)-Trap method, designed to identify miRNA-mRNA interactions, to identify *ZDHHC9* as a target for miR-134. They further showed that in somatostatin-positive interneurons, *zDHHC9* is down-regulated through neuronal activity by a pathway involving miR-134. The impact of this reduction in *zDHHC9* expression was the disruption of H-Ras localisation and membrane targeting, thus affecting cell signalling.

Notably, recent studies have also identified other miRNAs that interfere with *zDHHC9* expression; for instance, microRNA-7 was suggested to regulate *zDHHC9* expression in beta endocrine cells, as overexpression of miR-7 resulted in decreased expression of *zDHHC9* (Latreille *et al.*, 2014). In addition, miR-145 and miR-203a were also

suggested to play a regulatory role in zDHHC9 expression in pathways associated with hepatocellular carcinoma (HCC) (Qiu *et al.*, 2019).

## **1.8 GCP16 (Golgi Complex-Associated Protein of 16kDa)**

### **1.8.1 Expression and localisation**

As discussed, previous studies on the yeast protein complex Erf2/Erf4 suggested that zDHHC9 activity may require an accessory protein. This led to the identification of GCP16 (Golgi-complex associated protein of 16 kDa), also known as Golga7 (Golgin subfamily A member 7) (Swarthout *et al.*, 2005). The mRNA encoding this protein was detected in all human tissues except the colon and thymus.

The initial discovery of the GCP16 protein came through the analysis of GCP170, a Golgin protein associated with the cytoplasmic face of the Golgi apparatus. A recombinant domain of GCP170 was used as a bait to identify interacting proteins, one of which was GCP16, a 137-amino acid protein with a molecular mass of 16 kDa (Ohta *et al.*, 2003). GCP16 was found to be co-localized with GCP170 and giantin in the Golgi region of cells. Moreover, it was associated with membranes and behaved like an integral membrane protein, and this was shown to be due to the S-acylation of GCP16. Specifically, labelling experiments with [<sup>3</sup>H] palmitic acid revealed that GCP16 is S-acylated at two cysteine sites (amino acid positions 69 and 72), promoting its membrane association; furthermore, removal of these sites by their mutation caused GCP16 to delocalise from the Golgi region (Ohta *et al.*, 2003).

Interestingly, it was found that the overexpression of GCP16 led to a defect in the transfer of newly synthesised proteins from the Golgi to the membrane surface, suggesting a role for the protein in mediating Golgi transport. S-acylation of GCP16 is an essential requirement for both its localisation and function (Ohta *et al.*, 2003).

### 1.8.2 The zDHHHC9-GCP16 complex

The finding that GCP16 is an accessory protein for zDHHHC9 began with the identification of both Erf2/Erf4 in the *S. cerevisiae* (Bartels *et al.*, 1999; Zhao *et al.*, 2002) and subsequent work showing that Erf4 is essential for Erf2 activity (Lobo *et al.*, 2002) and stability (Mitchell *et al.*, 2012). The rapid degradation of Erf2 that was seen in the absence of Erf4 was proposed to be due to ubiquitination-dependent degradation; thus, Erf4 prevents the degradation of Erf2 through this pathway (Mitchell *et al.*, 2012). The stabilizing effect of Erf4 was not limited to the Erf2 protein itself but also to the autoacylated state of the enzyme. Mitchell *et al.* (2012) found that autoacylated Erf2 was significantly decreased in the absence of Erf4 and that this was due to the role of Erf4 in protecting the autoacylated form of the enzyme from hydrolysis by water molecules.

In the mammalian zDHHHC9-GCP16 complex, Swarthout *et al.* (2005) established the essential role of GCP16 for S-acylation activity of zDHHHC9. This was concluded through the purification of a GCP16 and zDHHHC9 complex from SF9 insect cells infected with recombinant zDHHHC9 and GCP16 baculovirus. The purified zDHHHC9-GCP16 complex showed activity towards N-Ras and H-Ras *in vitro*, and activity was abolished in the absence of GCP16. More recent work has provided additional insights into the exact role and effect of GCP16 as a co-factor; the first study by Nguyen *et al.* (2023) found that zDHHHC9 expression is decreased, and the protein aggregated in the absence of GCP16 and that there was a four-fold increase in zDHHHC9 expression when GCP16 was co-expressed in HEK293 cells. To evaluate the role of S-acylation activity in complex stabilization, the researchers mutated the coding sequence of the cysteine in the catalytic domain (CRD) to serine. Despite this change, the same improvements in protein expression and folding were seen, indicating that this is independent of S-acylation activity. As discussed previously (Section 1.5.1), Nguyen *et al.* (2023) identified the C-terminal cysteine motif (CCM) in

zDHHC9 as important for GCP16 interaction, with cysteine 288 recognised as the most crucial residue.

More insight into the zDHHC9-GCP16 complex came from the work of Yang *et al.* (2024), who used cryo-electron microscopy to analyze the complex (see Figure 1.3). This study found that GCP16 binds with zDHHC9 at four interfaces, allowing the complex to be catalytically active, and these interfaces are as follows: (i) the zDHHC9 TM2 and TM3 form hydrogen bonds with the GCP16  $\alpha 3'$  helix, with Tyr-76 of GCP16 and Arg-85 and Tyr-183 of zDHHC9 playing key roles in the interaction; (ii) Pro-290 and Pro-293 in the polyproline II (PPII) helix of zDHHC9 dock into grooves of GCP16, and Pro-292 forms a hydrogen bond with Tyr-86 of GCP16; (iii) residues in the zinc finger motifs of zDHHC9 (including Phe-129, Pro-150, and Glu-163) interact with GCP16 N-terminal amino acids, including Arg-16 and Tyr-18; and (iv) Asp-100 and Glu-101 form interactions with Lys-11, Phe-13, Arg-118 and Arg-121 of GCP16 (Yang *et al.*, 2024).

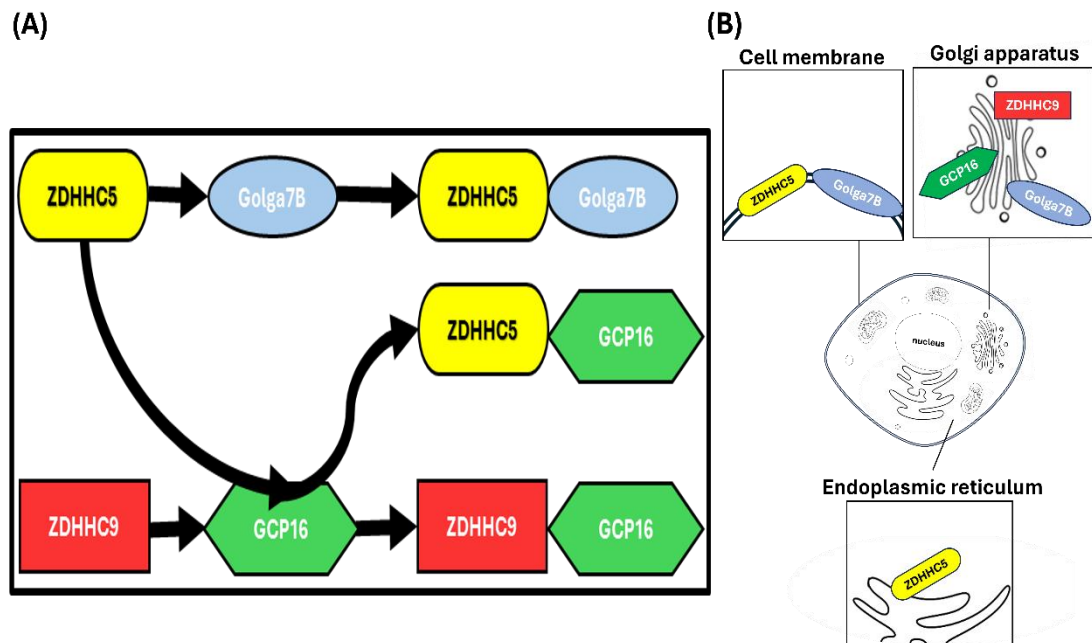


**Figure 1.4 GCP16 and Golga7b interaction with zDHHC5 and zDHHC9 enzymes and the localization of each enzyme.**

**(A)** zDHHC5 has been reported to interact with Golga7b and GCP16, whereas zDHHC9 is reported to interact with GCP16. **(B)** The zDHHC5-Golga7b complex is localized at the plasma membrane, whereas zDHHC9 complexes are at the Golgi complex.

The cryo-EM structure of the zDHHC9-GCP16 complex also confirmed that GCP16 has no transmembrane regions and only inserts  $\alpha$ -helices into the cytosolic face of the membrane, which subsequently stabilizes the zDHHC9-GCP16 structure. Moreover, the zinc motifs in the CRD of zDHHC9 were found to be organised in a manner that allows the complex to be in the correct catalytic conformation, thus facilitating its S-acylation activity (Yang *et al.*, 2024).

### **1.8.3 Golga7 interactions with zDHHC5 and other zDHC enzymes**

It was initially thought that GCP16/Golga7 protein interactions were specific to zDHHC9. However, subsequent work reported that the Golga7b isoform interacts with and stabilises zDHHC5 (Woodley and Collins, 2019), and Ko *et al.* (2019) also reported an interaction of zDHHC5 with GCP16. Regarding the Golga7b interaction, this was reported to stabilise zDHHC5 at the plasma membrane (Figure 1.4) and prevent its internalisation through clathrin-mediated endocytosis; and siRNA-mediated depletion of Golga7b led to reduced surface expression of zDHHC5 (Woodley and Collins, 2019). Indeed, the stabilisation effect was reciprocal as zDHHC5 S-acylated Golga7b, which was essential for the expression of this accessory protein, as non-acylated mutants were degraded by the proteasome (Woodley and Collins, 2019). Ko *et al.* (2019) reported an interaction between zDHHC5 and GCP16 (Figure 1.4) and, interestingly, found that the accessory protein was present at the plasma membrane in HT-1080 cells. It is not clear at this stage why the plasma membrane localisation of GCP16 has not been previously reported. Therefore, it could suggest that the localisation of this accessory protein might be cell-type dependent. Ko *et al.* (2019) were able to show co-immunoprecipitation of GCP16 with both zDHHC9 and zDHHC5, implying the presence of spatially distinct pools of

these zDHHC complexes (zDHHC9-GCP16 at the Golgi and zDHHC5-GCP16 at the plasma membrane). Interestingly, one study showed that zDHHC5-GCP16 and zDHHC5-Golga7b might be functionally distinct, as only the latter was able to S-acylate a peptide substrate from G $\alpha$ o (Solis *et al.*, 2022).

In addition to zDHHC5, GCP16 has also been reported to interact with other zDHHC enzymes, including zDHHC8 (Ko *et al.*, 2019), and zDHHC14, and zDHHC18 (Yang *et al.*, 2024). Indeed, zDHHC14 and zDHHC18 complexed with GCP16 were shown to mediate the S-acylation of purified N-Ras (Yang *et al.*, 2024). It will be interesting to explore in more detail the interactions between the zDHHC family and GCP16/Golga7b to determine if the accessory proteins interact with less conserved zDHHC isoforms.

### 1.9 zDHHC9 Substrates

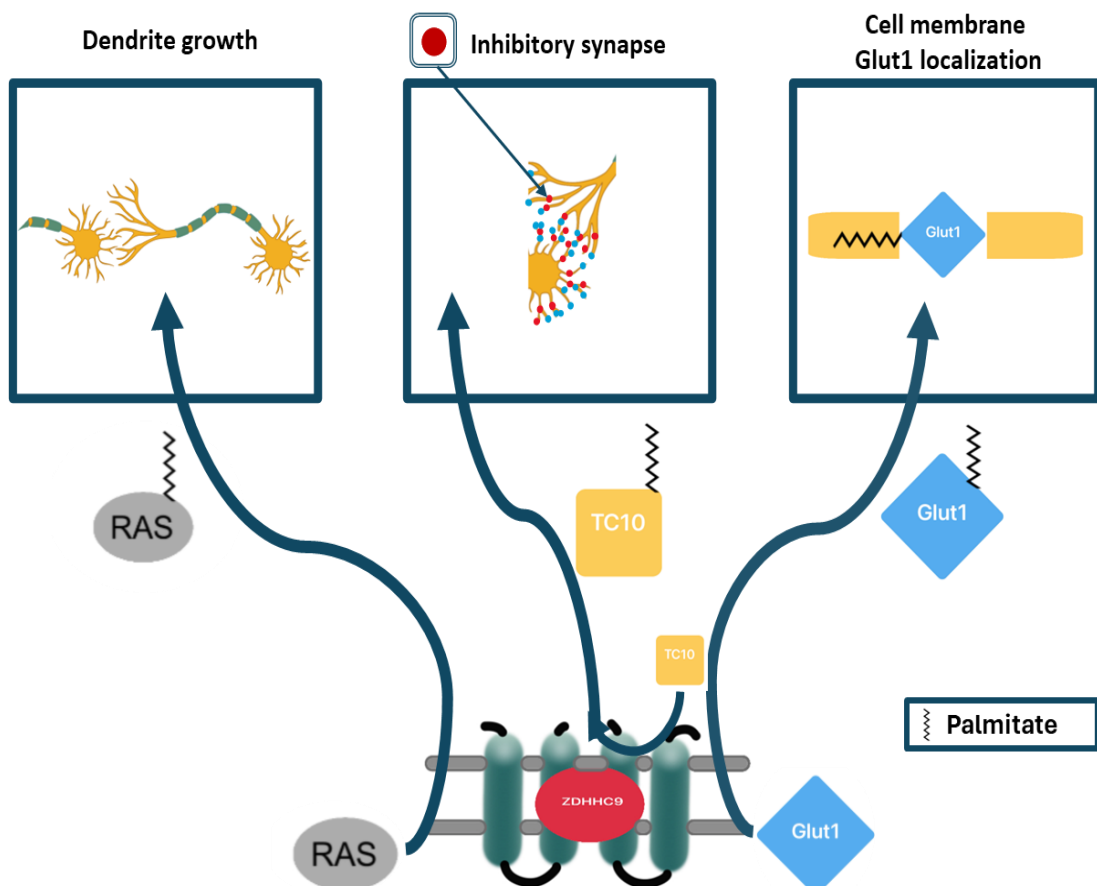


Figure 1.5 zDHHC9 substrates and their functions.

The figure highlights some of the proteins that have been reported to be S-acylated by zDHHC9. These include H/N-Ras, which requires S-acylation by zDHHC9 to mediate dendrite growth and branching, and TC10, which requires S-acylation to promote the formation of inhibitory synapses. In addition, the S-acylation of the glucose transporter GLUT1 by zDHHC9 is vital for its localisation at the plasma membrane.

### **H- and N-Ras**

Ras proteins are critical signalling molecules which act as an on/off switch for a variety of essential cellular functions, such as cell proliferation, differentiation, and survival, and their dysregulation is linked to the pathogenesis of many disorders, including cancer and psychiatric disorders (Wennerberg *et al.*, 2005; Simanshu *et al.*, 2017).

The RAS superfamily are small guanosine triphosphatases (GTPases) that cycle between a GTP-bound active state and a GDP-bound inactive state. This allows Ras proteins to act as on/off switches based on whether they are bound to GTP or GDP (Wennerberg *et al.*, 2005). The nucleotide-bound state of Ras proteins is coordinated by different GTPase-Activating Proteins (which inactivate Ras proteins) and GTP Exchange Factors (which activate Ras) (Wennerberg *et al.*, 2005).

There are three major RAS isoforms (H, N, and K) that share almost 90% amino acid identity. Despite this, these isoforms can have distinct functions that are thought to arise due to their unique localisation patterns, which are influenced by post-translational modification profiles (Prior and Hancock, 2012). After their biosynthesis, all Ras proteins undergo farnesylation in the cytosol, mediated by the farnesyltransferase enzyme. This farnesyl group is added, via a thioether linkage, to the cysteine of a CAAX motif (A = aliphatic amino acid, X = any amino acid) present at the extreme C-terminus of these proteins. This is followed by -AAX cleavage and carboxymethylation of the farnesylated cysteine (Prior and Hancock, 2012). The farnesylation provides a weak membrane affinity that permits the transient association of the proteins with endomembranes. For H/N-Ras, this allows spatial proximity to zDHHC9-GCP16 that mediates S-acylation of Ras, and the double lipid



modification (farnesyl and S-acyl) promotes a strong membrane affinity that traps Ras at the Golgi. This then facilitates the movement of Ras into budding vesicles, which mediate their delivery to the plasma membrane (Rocks *et al.*, 2005; Rocks *et al.*, 2010). However, H- and N-Ras have S-acylation half-lives of only a few minutes, and subsequent deacylation releases the proteins from the membrane and is followed by cytosolic diffusion and reacylation at the Golgi (Rocks *et al.*, 2005; Rocks *et al.*, 2010). The situation with K-Ras is different – following the farnesylation of this isoform, the farnesyl chain and an adjacent polybasic domain provide a strong membrane affinity that promotes targeting to the plasma membrane. In this case, phosphorylation of residues in proximity to the polybasic domain (introducing negative charge) can release K-Ras from membranes (Nair and Saha, 2023).

A study by Shimell *et al.* (2019) showed that N-Ras is a key substrate that underlies the effects of zDHHHC9 in brain physiology. Specifically, they showed that shRNA-mediated depletion of zDHHHC9 in hippocampal neurons led to reduced dendrite growth and branching. This effect was linked to a loss of zDHHHC9 S-acylation activity, as it could be rescued by shRNA-resistant zDHHHC9 WT but not by a catalytically inactive mutant. The study showed that depletion of zDHHHC9 led to a reduction in N-Ras S-acylation and demonstrated that shRNA depletion of N-Ras phenocopied the effect of zDHHHC9 depletion on dendrite growth and branching. Furthermore, N-Ras knockdown could not be rescued by an S-acylation-deficient mutant of N-Ras. Collectively, these data are consistent with a model in which zDHHHC9-mediated S-acylation of N-Ras is important for the function of this signalling molecule in dendritic growth pathways.

The S-acylation of Ras proteins by zDHHHC9 is also relevant outside of the brain – and, indeed, has been linked to cancer development. A study by Liu *et al.* (2016) showed that depletion of zDHHHC9 reduced the ability of oncogenic N-Ras to drive the development of leukaemia. The researchers undertook viral transduction of

oncogenic N-Ras (G12D) into bone marrow cells from either WT or *Zdhhc9* knockout mice and showed that the number of colony-forming units was significantly lower in the knockout cells, highlighting a reduced oncogenic transformation ability of the mutant N-Ras protein in cells lacking zDHHC9. Further analysis showed that the plasma membrane targeting of N-Ras was also reduced in the mutant cells, consistent with a loss of N-Ras S-acylation. The ability of zDHHC9 to modify Ras proteins has garnered much interest in the potential of targeting this enzyme as a means to inhibit Ras-dependent tumour growth and development.

## **GLUT1**

Glucose is the only source of energy for the brain. Because glucose is a polar molecule that cannot diffuse through cell membranes, it requires a particular transporter to mediate the movement from blood to the brain. GLUT1 is a key transporter needed for glucose entry to the brain (Zhang *et al.*, 2025) and is expressed abundantly at the blood-brain barrier (Zhang *et al.*, 2025). GLUT1 deficiency syndrome, which is associated with mutations in the gene encoding this transporter, leads to a range of neurological phenotypes, including intellectual delay and seizures (Zhang *et al.*, 2025). Intriguingly, many of the phenotypes of GLUT1 deficiency syndrome are similar to those seen in patients with *ZDHHC9* mutations (Baker *et al.*, 2015), and this is an area that will be explored in Chapter 5 of this thesis.

It has been known since 1995 that GLUT1 is modified by S-acylation (Pouliot and Béliveau, 1995). The modification site in GLUT1 is Cys-207, and it was shown that S-acylation at this site is essential for plasma membrane localisation, as cysteine mutants had reduced plasma membrane staining when observed by confocal microscopy (Zhang *et al.*, 2021). CRISPR-mediated knockdown of zDHHC9 identified this enzyme as necessary for GLUT S-acylation and plasma membrane targeting (Zhang *et al.*, 2021). Furthermore, the knockdown of zDHHC9 reduced glucose uptake, and the expression of wild-type enzyme could rescue this, whereas a

catalytically inactive zDHHHC9 could not. The knockdown of zDHHHC9 also reduced the growth of glioblastoma and inhibited tumorigenesis, showing that blocking glucose uptake into glioblastoma can be achieved by targeting this enzyme (Zhang *et al.*, 2021). As expected, zDHHHC9 activity against GLUT1 required GCP16, as shown using purified recombinant proteins (Zhang *et al.*, 2021).

## **TC10**

In addition to identifying N-Ras as a key target of zDHHHC9 for neuronal growth, the study of Shimell *et al.* (2019) also identified the small GTPase TC10 as another important substrate of this enzyme. They showed that in addition to reducing dendritic growth, zDHHHC9 depletion also led to a reduced number of inhibitory synapses, which they argued might underlie the epilepsy phenotype seen in patients with *ZDHHHC9* mutations (Baker *et al.*, 2015). Similar to the defect in dendrite growth caused by zDHHHC9 depletion, the decrease in inhibitory synapse formation was also linked to a loss of zDHHHC9 S-acylation activity. Notably, N-Ras depletion did not phenocopy the effects of zDHHHC9 depletion on inhibitory synapse numbers. Instead, the researchers identified TC10 as a novel substrate of zDHHHC9. Further, they showed that depletion of this protein led to a reduced number of inhibitory synapses and that this was not rescued by a TC10 S-acylation-deficient mutant. Collectively, this work suggests that TC10 and N-Ras are two key substrates of zDHHHC9 in the brain and that their S-acylation is required for inhibitory synapse formation and dendritic growth, respectively (Shimell *et al.*, 2019).

### **1.10 *ZDHHHC9* mutations in humans linked to brain abnormalities**

S-acylation is considered the most common lipid modification in the brain (Shimell *et al.*, 2019). This idea was supported by proteomic analysis conducted by Sanders *et al.* (2015), who showed that 41% of synaptic genes encode proteins that are predicted

to be S-acylated. Indeed, previous work has shown important roles for S-acylation of many of these synaptic proteins, such as AMPAR and NMDAR subunits, which require S-acylation for trafficking from the Golgi to dendrites and for clustering at synapses (Hubalkova *et al.*, 2021). Furthermore, the importance of S-acylation in synapse function was also shown by studies that identified regulatory roles for this modification in dendrite outgrowth and spine formation (George *et al.*, 2015). Aligning with the importance of S-acylation in synapse function, mutations in the *ZDHHC9* gene have been shown to cause major human disorders and symptoms, including X-linked intellectual disorders, epilepsy, speech problems, and attention deficits (Raymond *et al.*, 2007; Baker *et al.*, 2015). Rolandic epilepsy (RE), also known as Benign Childhood Epilepsy with Centro-Temporal Spikes, is the most common type of epilepsy in childhood (Kramer *et al.*, 2008) and was found to be associated with loss-of-function mutations in *ZDHHC9*. Patients with mutations in *ZDHHC9* were observed to be more susceptible to focal seizures (Baker *et al.*, 2015).

#### **1.10.1 *ZDHHC9* mutations and their effect on the nervous system**

The first study to describe the *ZDHHC9* mutations linked to XLID was conducted by Raymond *et al.* (2007). The approach of the study was to perform a screen of mutations in genes on the X chromosome in a sample of 250 families with at least two males exhibiting intellectual disability without having a molecular-based diagnosis, and this led to the identification of mutations in *ZDHHC9* in 4 of the 250 families. In three of these families, the intellectual disability clinical phenotype was associated with Marfanoid habitus; however, it is worth mentioning that none of the subjects fit the Ghent criteria for Marfan syndrome. The mutations detected in the *ZDHHC9* gene in this study were one splice site mutation, one frameshift mutation, and two missense mutations. All mutations affected the highly conserved catalytic DHHC domain of *ZDHHC9*. The splice site and frameshift mutations resulted in the

loss of the DHHC catalytic domain, and the two missense mutations resulted in single amino acid changes in this domain (R148W and P150S) (Figure 1.6).

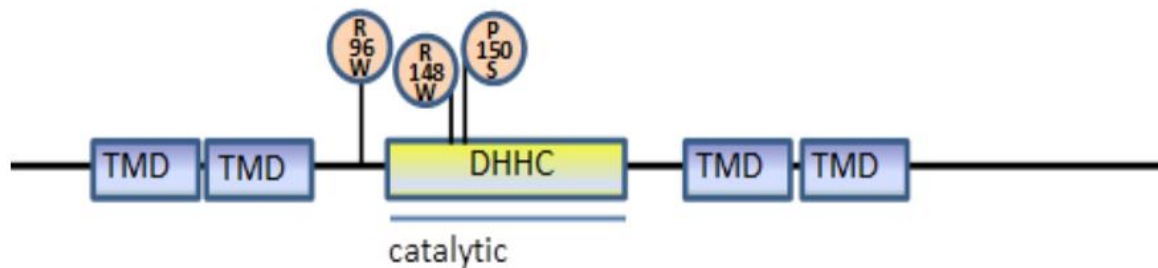


**Figure 1.6 Depiction of the zDHHC9 protein amino acid substitutions.**

The location of P150S and R148W amino acid substitutions falls within the catalytic DHHC- cysteine-rich domain of the enzyme. The other known point mutation linked to intellectual disability causes an R96W substitution, which falls outside of this domain.

These two point mutations were subsequently investigated by Mitchell *et al.* (2014), who demonstrated that the amino acid changes caused instability in the S-acylation process. Specifically, the R148W substitution caused rapid hydrolysis of the zDHHC9 autoacylated intermediate, and the P150S decreased the initiation of autoacylation; both mutations, therefore, compromised the integrity of autoacylated zDHHC9, presumably impacting the S-acylation of various proteins required for intellectual development. Interestingly, Tzschach *et al.* (2015) reported a different point mutation in patients with X-linked intellectual disability, which leads to an R96W substitution in the enzyme, and this mutation is a focus of Chapter 4 of this thesis. The exact mechanism by which this change affects zDHHC9 is not clear, and is particularly interesting to investigate as it falls outside the DHHC catalytic domain in a region of unknown function (Figure 1.6).

The study of Shimell *et al.* (2019), discussed above, clearly showed that N-Ras and TC10 are important substrates of zDHHC9 that may be linked to the intellectual disability and epilepsy phenotypes seen in patients with *ZDHHC9* mutations.

However, another prominent feature of people with *ZDHHC9* mutations, which is also seen in knockout mouse models, is a thinning of the corpus callosum (Baker *et al.*, 2015; Kouskou *et al.*, 2018), which has been linked to the strong expression of zDHHHC9 in oligodendrocytes (Zeisel *et al.*, 2018). Indeed, a more recent study showed that zDHHHC9 is the most highly expressed zDHHHC enzyme in myelinating oligodendrocytes (Jeong *et al.*, 2024). In addition, GCP16 was expressed at far higher levels than any other Golgi protein (including Golgi7b) in these cells. Interestingly, the three mutants described above (R96W, R148W, and P150S) were suggested to have an altered localisation in oligodendrocytes and did not localise to processes in these cells as seen for wild-type zDHHHC9. Although this study did not detect any gross changes in myelination or oligodendrocyte development in *Zdhhc9* knockout mice, it did uncover abnormal patterns of myelination, with some axons lacking myelination and others being hypermyelinated. The study of Jeong *et al.* (2024) also identified a reduced S-acylation of myelin basic protein (MBP) in knockout mice and suggested that impairment of MBP S-acylation-dependent targeting to the myelin membrane might underlie the observed structural abnormalities.

Interestingly, a relationship was established between hypoplasia in the corpus callosum and expressive language deficits by Halgren *et al.* (2012), suggesting that these changes might be linked to the speech and language deficits seen in people with *ZDHHC9* mutations.

### **1.11 Aims**

This thesis aims to shed new light on the interactions and function of zDHHHC9 and to provide new insight into how *ZDHHC9* mutations might lead to the variety of phenotypes seen in patients with these mutations. The specific aims of each results chapter are outlined below.

Chapter 3 – To explore the specificity of interaction between GCP16/Golga7b and zDHHC enzymes and to determine how the interaction of GCP16/Golga7b with zDHHC9 and zDHHC5 impacts protein stability and S-acylation.

Chapter 4 – To understand how the R96W amino acid substitution affects zDHHC9 by comparing its effects to those of R148W on GCP16 interaction and stability and S-acylation of the zDHHC9-GCP16 complex.

Chapter 5 – To shine new light on the phenotypes associated with *ZDHHC9* mutations by examining how the loss of zDHHC9 function affects GLUT1 S-acylation, gene expression profiles, and liver clinical profile (as a measure of possible changes in glucose metabolism linked to GLUT1 deficiency).

## **CHAPTER 2**

# **MATERIALS AND METHODS**



## Chapter 2

### Materials and Methods

#### 2.1 *Zdhhc9* knock-out mice

All animal procedures were conducted, after passing all the modules required to obtain a Personal License (PIL), in the Biological Procedures Unit (BPU) of the University of Strathclyde. The work was conducted under a Program License held by Professor Luke Chamberlain: PPL PP3807835 Investigating the (Patho) Physiological Importance of S-Acylation.

The *Zdhhc9* knock-out (KO) mouse model was originally purchased from the Mutant Mouse Regional Resource Centers (USA). Knock-out was achieved by deleting the first coding exon of *Zdhhc9*. Mice were back-crossed onto the C57BL/6 genetic background, as described in Kouskou *et al.* (2018).

##### 2.1.1 Breeding, genotyping, and analysis of mutant mice

For breeding, male WT mice were caged with *Zdhhc9*<sup>+/-</sup> females. As the *Zdhhc9* gene is on the X chromosome, the resulting male offspring were either WT or KO genotypes. A small part of ear tissue was taken from mice post-weaning and was sent to Transnetyx, Inc. (Cordova, USA) for genotyping analysis.

A total of 10 male mice (5 WT and 5 KO) at 2-3 days of age were used for RNA-Seq analysis. The brains were extracted by Dr Christine Salaün (University of Strathclyde) and immediately added to RNA-Later solution (Thermo Fisher, Loughborough, UK) to preserve RNA content. For serology analysis, 16 male mice (8 WT and 8 KO) were used, aged between 4 to 6 months and weighing 25-35g.

### 2.1.2 Diet protocol for liver stress and ketosis analysis

The mice were maintained in optimal environmental conditions in the Strathclyde BPU. The analysis was based on my hypothesis that loss of zDHHC9 function would lead to Glucose Transporter 1 (GLUT1) mislocalisation and thereby mimic GLUT1 deficiency syndrome (DS). This idea was based on the report by Zhang *et al.* (2021) showing that zDHHC9 S-acylates GLUT1 and that this modification is important for its localisation at the cell surface. A ketogenic diet is the primary treatment for patients with GLUT1 DS. This diet has been reported to induce an elevation in liver enzymes in normal subjects (Anekwe *et al.*, 2020), but interestingly, patients with GLUT1 DS under ketogenic diet conditions had normal liver enzymes with permanent ketosis (Chenouard *et al.*, 2015). Therefore, we assumed that changing to a ketogenic diet would result in a lower level of liver enzymes in the KO mice compared to WT and with a case of ketosis. After consulting with the BPU designated veterinarian, the closest resemblance for a balanced diet with ketogenic effect was breeding diet RM3 (P) (Special Diet Services, Rosenberg Germany) due to its higher fat and protein content in comparison with maintenance diet CRM (P) as shown in (Table 2.1). It should be noted that we opted for the breeding diet for its fulfilling nutrients, thus

NUTRITIONAL COMPOSITION	Maintenance Diet RM3 (P)	Breeding Diet CRM (P)
Nitrogen Free Extract	57,8 %	50,9 %
of which Starch	42,4 %	33,9 %
of which Sugars	3,9 %	4,4 %
Crude Protein	18,4 %	22,5 %
Crude Fat	3,4 %	4,2 %
Crude Ash	6,3 %	8,1 %
Crude Fiber	4,2 %	4,4 %
Moisture	10,0 %	10,0 %

**Table 2.1** The Nutritional Composition of the used Breeding Diet compared to the Maintenance Diet (taken from the product sheet, Special Diet Services, Rosenberg Germany)

eliminating any deficiencies that might affect the results, but prolonged the experiment for six months to induce the ketogenic metabolic stress and observe any effect of the metabolic process by observing liver enzymes, metabolites, and the overall clinical picture revealed through hematology study of both WT and KO.

### **2.1.3 Cardiac Puncture**

A cardiac puncture was performed by a trained animal technician in the BPU to collect blood for serology testing. The mice were put in an anesthesia chamber, and the agent isoflurane was applied. Once the mice lost consciousness, a 25-gauge needle was used with a 5-ml syringe (BD Vacutainer®, Vaud. Switzerland) to collect blood directly from the heart. Approximately 1 ml was collected from each animal and placed into evacuated blood collection tubes. For the Complete blood count (CBC) analysis, 3-ml EDTA Blood Collection Tubes (BD Vacutainer®, Vaud. Switzerland) were used to prevent blood clotting for optimal hematological results, and for blood chemistry analysis, 4-ml LH Lithium Heparin tubes (BD Vacutainer®, Vaud. Switzerland) were used to prevent activation of thrombin and Factor X, thus preventing clotting for optimal results.

### **2.1.4 Blood Preparation for Chemistry and Hematology Tests**

After collecting blood in the appropriate tubes for each test, the samples for blood chemistry analysis were centrifuged at 4500  $\times g$  at room temperature for 10 minutes. After centrifugation, a layer consisting of platelets was formed on top of the blood surface; this was removed using a pipette tip, and the plasma component was aspirated using a P1000 pipette and moved to a fresh 1.5 ml Eppendorf tube and sealed with paraffin. Samples were sent to the University of Glasgow Veterinary Diagnostic Services. The Full Biochemistry profile provided by this service included the following: alkaline phosphatase (AlkPhos), alanine transaminase (ALT), urea,

Creatinine, Albumin, Total Protein (TP), Globulin, Albumin / Globulin ratio, Aspartate Aminotransferase (AST), Gamma-glutamyl Transferase (GGT), bilirubin, electrolytes, calcium, phosphate, cholesterol & triglyceride, and glucose. The Complete Blood Count (CBC) test consists of Red Blood Cells (RBC), Hemoglobin (Hb), Hematocrit (Hct), Mean Corpuscular Volume (MCV), Mean Corpuscular Hemoglobin (MCH), Mean Corpuscular Hemoglobin Concentration (MCHC), Red Cell Distribution Width (RDW), Platelets, White Blood Count (WBC) & Differential Cell Count, Film Comment (microscopic examination of the morphology of the WBC, RBC, and Platelets).

## **2.2 Cellular Biology**

### **2.2.1 Mammalian Cell Culture**

For cell culture, the following materials were used: T75 flasks (Corning®), HEK293T cells (ATCC, Middlesex UK), Poly-D-Lysine coated 24-well plates (Corning® Sigma-Aldrich, Dorset UK), Dulbecco's Modified Eagle Medium (DMEM; Life Technologies, Paisley UK), 0.05 % Trypsin-EDTA (Thermo Fisher Scientific, Loughborough UK), heat-inactivated fetal bovine serum (FBS; Life Technologies, Paisley UK). All steps were performed in a cell culture hood, and all pipettes and surfaces were cleaned using 70% ethanol before use. HEK293T cells were grown in 10% FBS in DMEM in T75 flasks and maintained in a humidified atmosphere of 37 °C/ 5% CO<sub>2</sub>. Cells were split every week, which involved removing the media from the flask, washing cells with 10 ml of sterile PBS, and then incubating in 2.5 ml of Trypsin at 37°C for 3 min to detach cells. Next, 7.5 ml of 10% FBS DMEM media was added to the flask, and the cells were mixed with pipetting. After that, 3 ml of the suspended cells were added to a 15-ml Falcon tube containing 12 ml of 10% FBS DMEM. The cell suspension was gently mixed by inversion, and 500 µl was added to each well of a 24-well plate. In addition, 1/20<sup>th</sup> of the trypsinised cells were added to 12 ml of DMEM-FBS in a T75 flask to provide a stock of cells for the following week.

## 2.2.2 Plasmids

Details of all plasmids used in this thesis are provided in Table 2.1 below.

Plasmid	Source
Human WT zDHHC9 (Uniprot ID: Q9Y397) and mutants (R148W and R96W) in pEF-BOS-HA plasmid (N-terminal 3xHA tag)	Generated by (Genscript Biotech, New Jersey USA) in the pcDNA3.1 plasmid backbone and subsequently subcloned into pEF-BOS-HA vector (Fukata <i>et al.</i> , 2004) using <i>Bam</i> H1 restriction sites
Human zDHHC3 (ID: Q9NYG2), zDHHC5 (ID: Q9C0B5), zDHHC7 (ID: Q9NXF8), zDHHC13 (ID: Q8IUH4), zDHHC17 (ID: Q8IUH5) in pEF-BOS-HA plasmid (N-terminal 3xHA tag)	Provided by Dr. Christine Salaün (University of Strathclyde). Salaün <i>et al.</i> (2022).
Human GCP16 (ID: Q7Z5G4) in pcDNA3.1-GFP (N-terminal GFP tag), and pEF-BOS-HA (N-terminal 3xHA tag) plasmids	pcDNA3.1-GFP construct synthesised by Genscript Biotech (New Jersey, USA) and subsequently cloned into the pEF-BOS-HA plasmid
Human EGFP-GCP16 (C69A,C72A), EGFP-GCP16 (C69A,C72A,C24A), EGFP-GCP16 (C69A,C72A,C81A) in pcDNA3.1 plasmid backbone (N-terminal GFP tag)	Genscript Biotech (New Jersey, USA)
Mouse EGFP-GCP16 (ID: Q91W53) (R118E,R121E) generated from mouse EGFP-GCP16 CS2 construct in pEGFP-C2 plasmid (N-terminal GFP tag)	WT construct was synthesised by Dr. Christine Salaün (University of Strathclyde). R118E, R121E mutant was generated in this study by site-directed mutagenesis (section 2.3.2)
EGFP-GOLGA7B (Human; ID Q2TAP0) in pcDNA3.1-GFP construct (N-terminal GFP tag)	Genscript Biotech (New Jersey, USA)
Human GLUT1-EGFP (ID: P11166) in pEGFP-N plasmid (C-terminal GFP tag)	Professor Gwyn Gould (University of Strathclyde)
Human EGFP-H-Ras (ID: P01112) in pcDNA3.1-GFP construct (N-terminal GFP tag)	Genscript Biotech (New Jersey, USA)

**Table 2.2** Details of plasmids used in this thesis, alongside the origin of these plasmids.

### **2.2.3 Transfection of HEK293T cells**

Twenty-four hours after plating, cells were transfected using a mixture of polyethyleneimine (PEI) at a ratio to DNA plasmid of 2  $\mu$ l:1  $\mu$ g in serum-free DMEM media. For double transfections, 0.33  $\mu$ g of GCP16 plasmid was co-transfected with 0.66  $\mu$ g of zDHHC plasmid. The DNA for each transfection was added to serum-free media (final volume of 100  $\mu$ l) together with 2  $\mu$ l of PEI. The mixtures were then vortexed and incubated at RT for 20 minutes, and then 100  $\mu$ l of the plasmid/PEI mixture was added to each well of the 24-well plate and returned to the incubator to use the following day (20-24 hours post-transfection).

### **2.2.4 Cycloheximide chase experiments to assess protein stability**

Protein stability in eukaryotic cells can be examined following the addition of cycloheximide, which inhibits the biosynthesis of new proteins by preventing the translation process. This approach is commonly used to determine the half-life of specific proteins of interest in different cell lines (Kao *et al.*, 2015)

Twenty-four hours post-transfection, a cycloheximide working solution with a concentration of 50  $\mu$ g/ml was prepared from a cycloheximide stock solution of 50 mg/ml by adding 15  $\mu$ l of the stock solution to 15 ml of serum-free DMEM media. The media was then aspirated from the cells, and 250  $\mu$ l of the cycloheximide solution was added (the control "0-hour" cell samples were immediately lysed and collected at this time). The plate with the cycloheximide-treated cells was returned to the incubator for 8 hours. After this time, the cycloheximide solution was aspirated from the samples, and 100  $\mu$ l of Laemmli sample buffer (supplemented with 25 mM dithiothreitol (DTT)) was added. The resulting cell lysates were then transferred to 1.5 ml Eppendorf tubes, and all samples were stored at -20  $^{\circ}$ C until further use.

## **2.3 Molecular biology**

### **2.3.1 mRNA extraction from mouse brain tissue**

Brains were collected from age-matched WT and *Zdhhc9* knock-out mouse littermates (age 2-3 days) by Dr Christine Salaün (University of Strathclyde), and stored at -80°C in RNA-Later solution (Thermo Fisher, Loughborough, UK). Five brains were obtained from each group, and each was divided into three samples, which were then stored in sterile 1.5 ml Eppendorf tubes. Each sample was weighed and labelled as follows:

New tube ID	Genotype	Tube weight before /g	Tube weight after /g	Tissue weight /g
MA_RNA1_Seq_A1	WT	0.9987	1.0228	0.0241
MA_RNA2_Seq_A1		1.0002	1.028	0.0278
MA_RNA3_Seq_A1		0.9975	1.023	0.0255
MA_RNA1_Seq_A2	KO	0.9987	1.0219	0.0232
MA_RNA2_Seq_A2		0.997	1.0264	0.0294
MA_RNA3_Seq_A2		0.9916	1.0281	0.0365
MA_RNA1_Seq_B1	WT	1.0019	1.0245	0.0226
MA_RNA2_Seq_B1		0.9919	1.0232	0.0313
MA_RNA3_Seq_B1		1.0025	1.0185	0.016
MA_RNA1_Seq_B2	KO	1.0011	1.0337	0.0326
MA_RNA2_Seq_B2		1.0023	1.0317	0.0294
MA_RNA3_Seq_B2		0.9932	1.0283	0.0351
MA_RNA1_Seq_C1	WT	0.9939	1.019	0.0251
MA_RNA2_Seq_C1		1.0021	1.0213	0.0192
MA_RNA3_Seq_C1		1.0005	1.0191	0.0186
MA_RNA1_Seq_C2	KO	1.0023	1.0304	0.0281
MA_RNA2_Seq_C2		0.9969	1.0311	0.0342
MA_RNA3_Seq_C2		0.9931	1.0334	0.0403
MA_RNA1_Seq_D1	WT	0.9934	1.0124	0.019
MA_RNA2_Seq_D1		0.9976	1.0285	0.0309
MA_RNA3_Seq_D1		1.0025	1.0231	0.0206
MA_RNA1_Seq_D2	KO	0.997	1.0247	0.0277
MA_RNA2_Seq_D2		0.9957	1.0231	0.0274
MA_RNA3_Seq_D2		0.9919	1.0174	0.0255
MA_RNA1_Seq_E1	WT	0.9914	1.0187	0.0273
MA_RNA2_Seq_E1		0.9956	1.0218	0.0262
MA_RNA3_Seq_E1		0.994	1.0189	0.0249
MA_RNA1_Seq_E2	KO	0.993	1.0153	0.0223
MA_RNA2_Seq_E2		0.9945	1.0289	0.0344
MA_RNA3_Seq_E2		1.0025	1.0317	0.0292



**Table 2.3** Details of the brain samples used for the total mRNA analysis

For the RNA extraction, two brain samples from each mouse were used with the RNeasy Mini Kit (Qiagen, East Sussex, UK), and the extraction was performed according to supplier instructions (all buffers described in this methodology were provided with the RNeasy kit). First, all surfaces and pipettes were cleaned using RNase Zap (Sigma Aldrich, Dorset, UK). The brain samples were then ground into a fine powder using a pestle and mortar on dry ice, and the recovered powdered brain tissue was placed into 1.5 mL Eppendorf tubes. To prevent cross-contamination, the pestle and mortar were cleaned with 70% ethanol and distilled water while processing each brain sample. Each brain powder was then resuspended in 600  $\mu$ l of RLT lysis buffer (RNeasy mini kit), transferred to a Dounce homogeniser, and subjected to 30 passes to ensure sample homogeneity and to prevent cross-contamination, the homogeniser was cleaned with 70% ethanol and then distilled water between each homogenisation. The homogenised samples were then added to QIAshredder columns (Qiagen, East Sussex, UK) and centrifuged at 16,100  $xg$  for 3 min. The supernatants in the collection tubes were transferred to fresh 1.5 ml tubes, and 550  $\mu$ l of 70% EtOH was added to each lysate sample and pipetted up and down using a P1000 pipette to ensure proper mixing. The mixtures were then transferred to individual RNeasy collection columns, and the columns were centrifuged at 8,000  $xg$  for 15 sec (20 °C). The lysate material was discarded, and 350  $\mu$ l of buffer RW1 was added to each of the columns, which were then centrifuged at 8,000  $xg$  for 15 sec (20 °C), and the flowthrough was discarded. To remove any genomic DNA contamination, 10 $\mu$ l of DNase I solution was mixed with 70  $\mu$ l of RDD buffer. Subsequently, this mixture (80  $\mu$ l per column) was added onto the column membranes and incubated at RT for 15 min. 350  $\mu$ l of buffer RW1 was then added to the columns and centrifuged at 8,000  $xg$  for 15 sec (20 °C), and the flowthrough was discarded. The membranes were then washed with 500  $\mu$ l of buffer RPE, which was added to each column and

centrifuged for 15 sec (20 °C), with the flowthrough being discarded. 500 µl of the same buffer RPE was added to each column and centrifuged at 8,000 xg for 2 min (20 °C) to remove any residual ethanol that could be carried over during the RNA extraction, and then the flowthrough was discarded. Lastly, the columns were placed in clean 1.5 ml sample collection tubes, and 40 µl of RNase-free water was added to each column and left to incubate for 15 min at RT. Next, the columns were centrifuged at 8,000 xg for 1 min (20 °C) to elute RNA, which was stored at -80°C after determining its concentration.

### **2.3.2 Site-directed mutagenesis**

Site-directed mutagenesis is a common tool used to generate mutations at specific sites in plasmid DNA using a PCR reaction. This method was used to generate defined point mutants of GCP16 to experimentally test the 3D protein interaction prediction model generated by the AI protein prediction system Alphafold (refer to section 2.4.1). Alphafold predicted that mutations in the coding sequences for Arginine-118 and Arginine-121 should disrupt the interaction with zDHH9.

#### **2.3.2.1 Primer design**

Oligonucleotide primers for the site-directed PCR reaction were designed using the online NCBI-primer blast tool <https://www.ncbi.nlm.nih.gov/tools/primer-blast/> to introduce mutations in the mouse EGFP-GCP16 plasmid. The nucleotide changes in the primer sequences were designed to replace amino acid R118 (codon sequence AGA) with an alanine residue (the codon used to encode alanine was GCA) and R121 (codon sequence CGA), which was also replaced by GCA. The forward and reverse primer sequences used for PCR mutagenesis, which were synthesised by Merck (Middlesex UK), are shown below in the 5' to 3' orientation.

Primer name	Primer Sequence
<b>GCP16 (R118A,R121A) F</b>	GATTTCAATAACTGCAAGTCCTGCCTCAATGGGGTCT
<b>GCP16 (R118A,R121A) R</b>	AGACCCCATTTGAGGCAGGACTTGCAGTTATTGAAATC

**Table 2.4** The sequences of the primers used in the site-directed mutagenesis of the GCP16 plasmid to introduce R118A and R121A amino acid substitutions.

### 2.3.2.2 PCR amplification to generate mutant GCP16 (R118A, R121A) plasmid

PCR was used to generate the EGFP-GCP16 plasmid containing a codon change of R118A and R121A. Each reaction mixture was prepared by mixing 5 µl of 10x PCR reaction buffer, 1 µl dNTPs (stock at 10 mM each), 1.5 µl of GCP16 plasmid (stock at 50 ng/µl), 1 µl of each forward and reverse primer (stock at 10 µM), 1 µl PFU DNA polymerase (Promega, Southampton UK) and 39.5 µl dH<sub>2</sub>O to give a final volume of 50 µl. The Veriti 96-well thermal cycler (Applied Biosystems, Loughborough, UK) was loaded with the samples, and the PCR reaction started at 95 °C for 2 min to activate the polymerase, followed by 25 cycles at 95 °C for 1 min for denaturation, an annealing step at 54 °C for 1 min and an extension step at 72 °C for 16 min for DNA synthesis.

### 2.3.2.3 Agarose gel electrophoresis

For the analysis of the PCR reaction, agarose gel electrophoresis was used. The principle of this method is to apply an electrical field through the gel, allowing the negatively charged DNA fragments to migrate through the gel matrix. The distance moved by the fragment in the gel is determined by its length, as shorter fragments move faster through the gel pores. Agarose (Bio-Rad, Herts, UK) gel was prepared at a concentration of 1% (w/v) in TAE buffer (25 mM Tris, 1 mM EDTA, acetic acid to pH 8), and SybrSafe® (Life Technologies, Paisley, UK) was added at a 1:10,000 dilution to the gel. The cast gel was submerged in TAE buffer in an electrophoresis tank supplied by Thermo Fisher Scientific (Loughborough UK). 10 µl of the PCR samples were mixed with 10 µl of distilled H<sub>2</sub>O and 4 µl of 6X DNA Gel Loading Dye

(Thermo Fisher Scientific), after which the samples were loaded onto the agarose gel together with HyperLadder 100 bp (Bioline, London, UK) to indicate DNA size. The gel was run at 70 V for 40 min and visualised under UV illumination.

#### 2.3.2.4 Dpn1 treatment

Dpn1 is a restriction enzyme that cleaves only methylated DNA. As DNA methylation only occurs on plasmids amplified in a bacterial host, but not during PCR amplification *in vitro*, this provides an approach to specifically degrade parental DNA. After confirmation of successful PCR amplification by agarose gel electrophoresis, 1 µl of Dpn1 enzyme was added to 10 µl of the PCR mixture and then incubated in a water bath for 1 hour at 37 °C. The samples were then transformed into an *E. coli* host, as described in section 2.3.4.

#### 2.3.3 Subcloning

Expression of zDHC9 WT and the R148W, R96W mutants from the pcDNA3.1 vector used by Genscript Biotech (New Jersey, USA) was found to be very low and often undetectable. Therefore, these coding sequences were moved into the pEF-BOS-HA plasmid backbone. To do this, PCR amplification was performed using designed primers that incorporated restriction sites at either end of the amplified zDHC9 coding sequence.

##### 2.3.3.1 Primer design

Using the online tool Primer3Plus (<https://www.primer3plus.com/index.html>), forward and reverse primers were designed and modified by adding *Bam*H1 restriction sites (GGATCC). An additional three nucleotides were added at the 5' end of the restriction

Primer name	Primer Sequence
zDHC9 PCR F	GCTGGATCCATGTCTGTGATGGTGGT
zDHC9 PCR R	ACCGGATCCCTACTTCTCAGCTTCAGC

**Table 2.5** Sequences of the primers used in subcloning zDHC9 R148W and R96W mutants from the pcDNA3.1 vector into pEF-BOS-HA.

site to facilitate the restriction reaction. Primers were generated by Merck (Middlesex, UK) and resuspended in dH<sub>2</sub>O for a stock concentration of 100 µM.

#### **2.3.3.3 Polymerase Chain Reaction (PCR) to Amplify zDHC9 Coding Sequences**

PCR mixtures were prepared using the designed primers as follows; each mixture consisted of 2 µl of 10 µM forward and reverse primers with 1.5 µl of 50 ng/µl plasmid DNA (zDHC9 in pcDNA3.1 vector) and 1 µl of 10 mM dNTPs, 5 µl of 10X Pfu buffer (Promega, WI, USA) and 1 µl Pfu enzyme (Promega, WI, USA), topped up to a final volume of 50 µl with dH<sub>2</sub>O. The Veriti 96-well thermal cycler (Applied Biosystems, Loughborough, UK) was loaded with the samples and programmed in the following order: an initial denaturation step at 95 °C for 2 minutes, then 35 cycles consisting of a denaturation step at 95 °C for 1 min, then an annealing step at 54 °C for 0.5 min, and finally an elongation step at 72 °C for 2 min per kb of DNA being amplified. Subsequently, the samples were incubated for a final 5 minutes at 72 °C and then held at 4 °C until further analysis. The success of the PCR amplification was confirmed by the visualisation of DNA products of the correct size on agarose gels.

#### **2.3.3.4 Digestion and Ligation of zDHC9 Sequences and pEF-BOS-HA**

For this step, two mixtures were prepared; the first one consisted of 45 µl of the PCR amplified product (insert) and 4 µl of BamH1 digestion enzyme (Thermo Scientific), 6 µl 10X fast digestion green buffer (Thermo Scientific, Loughborough, UK) topped to a final volume of 60 µl with dH<sub>2</sub>O. The second mixture consisted of 1 µL of 1.5 µg/µl of pEF-BOS-HA vector with 1 µl of the same digestion enzyme (*BamH1*), 2 µl 10X digestion buffer, topped up to 20 µl with dH<sub>2</sub>O. The samples were incubated for 4 hours at 37 °C. Afterwards, the plasmid mixture was dephosphorylated for 10 minutes at 37°C using 1 µl phosphatase enzyme (calf intestinal phosphatase, NEB) to prevent the digested plasmid from self-annealing.

The digested DNA products were visualised using agarose gel electrophoresis under UV illumination (Stratagene transilluminator 4000). The relevant DNA bands were excised from the gel using a scalpel and placed in clean 1.5 ml Eppendorf tubes. The scalpel blade was cleaned with 70% ethanol between excising each band. The DNA was then extracted from the excised gel slices using the Invitrogen PureLink® Quick Gel Extraction Kit (Thermofisher Scientific), as per the manufacturer's instructions, with DNA eluted into a final volume of 30 µl of  $dH_2O$ .

For ligation of the purified and digested zDHHC9 and pEF-BOS-HA, 10 µl of zDHHC9 DNA was mixed with 2 µl pEF-BOS-HA plasmid, 1 µl T4 Ligase enzyme (Promega, WI, USA) and 1.4 µl 10X Ligation buffer (Promega, WI, USA). The ligation mixtures were then incubated overnight at RT.

#### **2.3.4 Transformation of *E. coli***

DNA from ligation mixes or site-directed mutagenesis PCR were mixed with 50 µl of TOP10 Chemically Competent *E. Coli* cells and incubated on ice for 20 minutes, after which the mixtures were subjected to "heat shock" by placing in a 42 °C water bath for 90 seconds and thus inducing the bacteria to take up the plasmid by destabilising their membranes. After heat shock, the bacteria were returned to the ice for 2 minutes, and then 200 µL of sterile LB (Lysogeny Broth; 10 g/l NaCl, 10 g/l tryptone, 5 g/l yeast extract) was added under sterile conditions (near a flame), and the mixtures incubated on a shaker (200 rpm) at 37 °C for 1 hour. The bacteria were then plated under sterile conditions on LB agar (15 g/l agar in LB) plates containing either ampicillin (100 µg/ml) or kanamycin (50 µg/ml) according to the antibiotic resistance marker encoded by the vector; the selective antibiotic for the pEF-BOS-HA vector is ampicillin and for the pEGFP vector is kanamycin. Afterwards, the plates were placed in an incubator overnight at 37 °C to allow the growth of bacterial colonies.

### 2.3.5 Isolation of Plasmid DNA

After bacterial colony growth was observed on LB agar plates, small-scale DNA plasmid purifications ("minipreps") were started by placing a single bacterial colony into 5 ml of LB medium containing the appropriate antibiotic at a concentration of 100  $\mu\text{g/ml}$  (ampicillin) or 50  $\mu\text{g/ml}$  (kanamycin) under sterile conditions (near a flame). These liquid cultures were then incubated overnight at 37 °C with shaking at 200 rpm. The following day, the plasmid DNA extraction was conducted using NucleoBond Xtra Mini plasmid DNA purification kit (Macherey-Nagel, Duren, Germany) following the supplier's instructions. Briefly, 1.5 ml of the bacterial culture was pelleted by centrifugation at 13,000  $\times g$  for 2 minutes. The remainder of the bacterial cultures were stored at 4 °C as a starter culture for larger plasmid preparations if appropriate. Cell pellets were then resuspended in 250  $\mu\text{l}$  of Resuspension Buffer R3 containing 100  $\text{mg/ml}$  RNAase, and then 250  $\mu\text{l}$  of L7 Lysis Buffer was added, and the samples were mixed by inversion (5 times) and incubated at RT for 5 minutes. Following this, 350  $\mu\text{l}$  of N4 Precipitation Buffer was added, and the samples were mixed and then centrifuged at 13,000  $\times g$  for 1 minute at RT. The resulting supernatant was added onto a Spin Column and centrifuged at 13,000  $\times g$  for 1 minute. The column was then washed with 700  $\mu\text{l}$  of W9 Wash Buffer, and following centrifugation at 13,000  $\times g$  for 2 minutes, the column was placed in a clean Eppendorf tube, and the DNA was eluted in 50  $\mu\text{l}$  of  $\text{dH}_2\text{O}$  by spinning at 13,000  $\times g$  for 1 minute. After purification of the plasmids, they were sent for sequencing verification (section 2.3.6).

Once sequencing results were obtained and the intended sequences were verified, preparation for a large-scale plasmid purification ("midiprep") was commenced by adding the remaining miniprep cultures into 150 ml LB medium with appropriate antibiotics and incubating overnight with shaking at 200 rpm and 37 °C. The following day, NucleoBond Xtra Midi plasmid DNA purification kit (Macherey-Nagel, Duren, Germany) was used for the DNA extraction following the supplier's instructions.

Briefly, cells were recovered by centrifugation at 4,000 xg for 20 minutes. The pellet of cells was then resuspended in 8 ml of Resuspension Buffer, 8 ml of Lysis Buffer was added, the samples were mixed by inversion (5 times), and incubated for 5 minutes at RT. During this time, a Nucleobond Xtra Column Filter was equilibrated by the addition of 12 ml of Equilibration Buffer. The cell lysate was then neutralised by the addition of 12 ml of Neutralisation Buffer and loaded onto the equilibrated Nucleobond Xtra Column Filter. After the neutralised cell lysate had passed through the filter, the filter was washed with an additional 5 ml of Equilibration Buffer to remove any excess lysate. The filter was then discarded from the column, and the column was washed with 8 ml of Wash Buffer. The DNA bound by the column was then eluted in 5 ml of Elution Buffer and mixed with 3.5 ml of isopropanol to precipitate the DNA, which was pelleted by centrifugation at 4,000 xg for 45 minutes. The DNA pellets were resuspended in 500 µl  $\text{dH}_2\text{O}$  and quantified at A260 nm using a NanoDrop 2000/2000c (Thermo Scientific) and subsequently stored at -20 °C.

### **2.3.6 DNA sequencing**

All DNA plasmids were submitted to Eurofins Genomics UK (Wolverhampton, UK) for sequence analysis in compliance with their instructions, and the results were analysed using Vector NTI software (Invitrogen) or the online NCBI- BLAST tool.

## **2.4 Protein Biochemistry**

### **2.4.1 Click Chemistry**

Click chemistry is a simple and efficient chemical reaction that can be used to incorporate a small molecular probe onto proteins through a copper-catalysed Azide-Alkyne reaction, facilitating the detection, identification, and characterisation of these proteins.



In the S-acylation field, alkyne or azide palmitic acid probes are used to label cells as they are incorporated into S-acylated proteins. Click chemistry can then be used to label these S-acylated proteins with a reporter molecule (such as a fluorescent dye, biotin, or polyethylene glycol (PEG) group), providing a highly efficient and sensitive method for detecting S-acylation (Zhan *et al.*, 2020).

Twenty-four hours post-transfection, HEK293 cells in 24-well plates were labelled. For this, the media was aspirated and cells washed with 500  $\mu$ L of warm PBS, followed by the addition of 500  $\mu$ L per well of labelling mixture consisting of warm serum-free DMEM containing 1 mg/mL Bovine Serum Albumin (fatty acid-free) (Sigma, UK) and 100  $\mu$ M palmitic acid azide (C16-azide; DMSO Stock 50 mM; synthesised by Professor Nicholas Tomkinson, University of Strathclyde). Cells were incubated in this labelling mixture for 4 hours at 37°C. The labelled cells were then washed twice with 1 ml PBS per well and lysed on ice in 100  $\mu$ L lysis buffer (50 mM Tris pH 8, 0.5% SDS) containing a protease inhibitor cocktail (Sigma, UK). The lysates were collected in 1.5 ml Eppendorf tubes at this point and subjected to click reactions with either 5K alkyne-mPEG or alkyne dye-IR800, as outlined below.

**5K Alk-mPEG experiments:** 80  $\mu$ L of click reaction mix consisting of 2 mM CuSO<sub>4</sub>, 0.2 mM TBTA (Tris[(1-benzyl-1H-1,2,3-triazole-4-yl) methyl]), and 200  $\mu$ M Alk-mPEG was added together with 20  $\mu$ L of 40 mM ascorbic acid (Alfa Aesar, UK) to start the reaction.

**Alkyne dye-IR800 experiment:** 80  $\mu$ L of a click mix consisting of 2.5  $\mu$ M of alkyne dye-IR800, 2 mM of CuSO<sub>4</sub>, and 0.2 mM of TBTA was added together with 20  $\mu$ L of 40 mM ascorbic acid to start the reaction.

Following the preparation of the click reaction mixtures above, the procedure for both mPEG and dye labelling was the same. Briefly, the samples were vortexed and incubated with end-over-end rotation for one hour at room temperature. Following the

incubation, 67  $\mu$ l of 4X Laemmli sample buffer with 100 mM DTT was added to each sample and heated at 95 °C for 5 minutes before being resolved by SDS-PAGE.

#### **2.4.2 Co-Immunoprecipitation Assay (Co-IP)**

Co-immunoprecipitation is a widely used method to study protein-protein interactions. Here, GFP Trap® agarose (ChromoTek, Panegg Germany), consisting of a GFP nanobody attached to agarose beads, was used for all immunoprecipitation experiments. The lysis buffer used (PBS supplemented with 0.5% Triton X-100) preserves protein interactions and allows the capture of protein complexes (co-IP). This approach was used to study the interaction of EGFP-GCP16 with HA-tagged zDHHC enzymes.

HEK293T cells expressing EGFP and HA-tagged proteins were treated as follows: the media was aspirated, and each well was washed with 500  $\mu$ l cold PBS, and 200  $\mu$ l lysis buffer (PBS, 0.5 % Triton X-100) with protease inhibitor cocktail (Sigma Aldrich) was added to each well and incubated for 30 minutes on ice. Following this, cell lysates from 3 identical wells were scraped from the well surface using a P200 pipette tip and combined in a single 1.5 ml Eppendorf tube and centrifuged at 14,000 x g for 10 min at 4 °C. 45  $\mu$ L of each cleared cell lysate was retained as "input", and the remainder of the lysate was incubated with 10  $\mu$ l of pre-washed GFP Trap® agarose beads, and incubated for 1 hour at 4 °C with end-over-end rotation.

After the end of the one-hour incubation, the beads were centrifuged at 14,000 x g at 4 °C, and the supernatant was discarded via aspiration with a fine needle to avoid disrupting the bead pellet. The pellet containing the beads was washed with 1 ml cold PBS twice, and for each wash, samples were briefly vortexed and centrifuged at 10,000 x g (4 °C), and PBS was aspirated with a fine needle. 50  $\mu$ L 2X Laemmli sample buffer with 25 mM DTT was added to the beads and heated for 10 minutes at 95 °C, and the samples were then centrifuged at 5,000 x g, and the supernatant

(containing the immunoprecipitated proteins) was collected in fresh tubes for subsequent analysis by SDS-PAGE and Immunoblotting.

#### **2.4.3 Sodium dodecyl sulphate (SDS) polyacrylamide gel electrophoresis (PAGE)**

SDS-PAGE is an analytical method used to separate proteins based on their molecular weight. This is achieved by using SDS, which is an anionic detergent that disrupts the proteins' tertiary structure, unfolding it to a linear structure, binding to it non-covalently, and coating it with a negative charge, and thus neutralising the effect of the charge and the structure of the protein on their rate of migration in the polyacrylamide gel electrophoresis towards the anode.

SDS gels were composed of two different gels: one was the upper stacking gel with 4.5% polyacrylamide concentration, and the lower gel was a 12% polyacrylamide resolving gel. The gels were poured between glass plates in a cassette held by a stand and frame supplied by Bio-Rad (Watford, UK). The 12% polyacrylamide resolving gel was made by mixing 4 ml 30% acrylamide (Sigma Aldrich) with 0.8 ml dH<sub>2</sub>O, 5 ml of 2x resolving buffer (0.2% (w/v) SDS, 4 mM EDTA, 750 mM Tris, pH 8.9), 8 µl TEMED (Tetramethylethylenediamine) (Sigma Aldrich), and 200 µl of 10% ammonium persulfate (APS; Sigma Aldrich), which was then mixed and poured directly between the glass plates with consideration to the space required for subsequent addition of the stacking gel. The gel mix was then covered with a layer of isopropanol to remove air bubbles and speed up the polymerisation reaction. After the gels solidified, the isopropanol was washed away with distilled water. The 4.5% polyacrylamide stacking gel was then made by mixing 0.9 ml 30 % acrylamide with 1.8 ml dH<sub>2</sub>O, 3 ml of 2x stacking buffer (0.2 % (w/v) SDS, 4 mM EDTA, 250 mM Tris, pH 6.8), 8 µl TEMED, and 200 µl 10 % APS. Immediately after pouring the stacking gel, a comb was inserted to create wells for loading the samples, and this was subsequently removed when the solidified gel was submerged in a running buffer.

All samples (in SDS loading buffer) were heated at 95 °C for 10 minutes before being loaded onto gels. 15 µl of each sample was loaded into the gel wells in the buffer tank (Bio-Rad) filled with Running buffer (25 mM Tris, 192 mM Glycine (Fisher Scientific) and 0.1 % SDS (w/v)), and 1 µl EZ-Run pre-stained protein marker (Fisher Scientific) was also loaded in a well as a molecular weight marker. Samples were run at 85 V through the stacking gel and then at 150 V through the resolving gel.

#### **2.4.4 Immunoblotting**

Following SDS-PAGE, the stacking gel was gently removed, and the resolving gel was washed briefly with Transfer buffer (48 mM Tris, 39 mM Glycine, 1.3 mM SDS, 20 % methanol). Two sheets of Whatman filter paper and a piece of nitrocellulose (0.45 µm pore size, Bio-Rad) were then soaked in Transfer buffer. The gels were then overlaid with a sheet of nitrocellulose and filter paper placed at either side, taking care to remove any air bubbles. This was then placed into a Bio-Rad Trans-Blot Cell filled with Transfer buffer, considering the orientation as the gels were on the cathode side to allow the proteins to transfer towards the nitrocellulose. A current of 120 mA was applied overnight. The following day, the membranes were washed briefly in water and then stained with a total protein stain (LI-COR, Cambridge, UK) and scanned on a LI-COR Odyssey infrared Imaging System using the 700 nm channel. The total protein stain was then removed with reversal solution (LICOR), and the nitrocellulose was washed with PBS-T (PBS with 0.02 % (v/v) Tween 20) for 1 min with shaking and then incubated in 5 % (w/v) non-fat milk in PBS-T for 1 hour to block any free protein-binding sites on the nitrocellulose. Afterwards, the membranes were washed briefly in PBS-T and incubated with rat anti-HA (3F10, Roche) at a dilution of 1:1000 and mouse anti-GFP (JL8; 1:4,000) antibodies (Takara, CA, USA) overnight at 4 °C with constant agitation.

The following day, the membranes were washed three times with PBS-T with shaking and incubated for 1 hour at RT with the secondary antibodies, anti-rat IRDye 680RD and anti-mouse IRDye 800CW (LI-COR), both at a dilution of 1:20,000.

After secondary antibody incubation, the membranes were washed with PBS-T three times for 5 minutes each with shaking and scanned using an LI-COR® Odyssey Infrared Imaging System (LI-COR® Biosciences)

## **2.5 Bioinformatic Tools**

### **2.5.1 AlphaFold2 CoLab**

AlphaFold2 CoLab is an artificial intelligence program used to predict protein 3D structures using the amino acid sequence of the target protein; the program was developed by DeepMind Technologies (London, UK), and it relies on running the physical and biological properties of the protein through a machine learning algorithm which in turn predict the 3D structure at the atomic level (Jumper *et al.*, 2021). This tool was implemented to predict the zDHHc9-GCP16 and zDHHc5-GCP16 complex structure using the *Mus musculus* amino acid sequences. We then sought to verify the predictions *via* wet lab experiments. To explore the effects of specific human mutations, we used the *Homo sapiens* amino acid sequence encoding zDHHc9 and the altered sequence encoding zDHHc9(R148W) variant. The predictions were viewed on the platform website and saved in PDB file format. URL: <https://colab.research.google.com/>.

### **2.5.2 mRNA-Seq analysis**

After mRNA extraction from WT. and *Zdhc9* KO. mouse brains, the samples were sent to BGI Genomics (Shenzhen, China) for complete mRNA sequencing; According to the service provider BGI, they employ a proprietary method of sequencing called DNBseq SE50; which stands for DNA Nano Ball sequencing for Single End 50 base

pairs. The main principle of this method is based on converting RNA into cDNA, then circularising the linear DNA into a DNA Nano Ball, hence the name DNB.

Afterwards, the DNA nano balls are loaded onto a customised chip, in which each ball is localised at a location specified for each sequencing cluster. These positions allow for a more accurate and uniform distribution of sequencing templates.

For the sequencing process, this method utilises both fluorescent nucleotide labelling and anchor sequences, thereby identifying nucleotides and achieving highly accurate RNA fragments. Afterwards, these fragments are aligned to the reference genome of C57BL/6 mice to initiate the filtration process, which involves removing rRNA reads, low-quality and high N-content reads, and finally, adaptor-polluted reads; subsequently providing an accurate read count average for each sample.

At this stage, we employed the platform's software (Dr.Tom ) to conduct analysis and compare the WT. with the KO. specimens. The tool has been employed by other researchers (Ye *et al.*, 2019) and received positive feedback on its efficiency and sophisticated analysis. The tool is a web-based solution for the analysis, visualisation, and interpretation of genomic data, and it allows access to both free and licensed KEGG databases, which enables the search for statistically significant results in RNA-Seq data (<https://www.bgi.com/us/dr-tom>).

## **2.6 Data analysis**

Quantitative densitometry of proteins on immunoblots was conducted using Image Studio™ Lite V5.2 (LI-COR Biosciences) by visualising images obtained by the Odyssey ® infrared imaging system (LI-COR) and quantifying protein bands and the background on the same gel, then subtracting it to measure protein expression level. Statistical analysis and graphs were generated using GraphPad Prism V9 software.

All immunoblotting experiments also involved a total protein stain to ensure consistency in experimental samples. The total protein stain was also included in the

quantitative analyses of cycloheximide and steady-state protein expression experiments.

For these cycloheximide experiments, the protein intensity signals at  $t = 0$  and  $t = 8$  hours were normalised to the total protein signal before calculating the % percentage of protein remaining after 8 hours. For this, a box of the same dimensions as that used for the quantification of zDHHC5/zDHHC9/GCP16 bands was placed on the total protein stain image (at the same position for each analysed sample), and the zDHHC5/zDHHC9/GCP16 intensity signal was expressed relative to this total protein intensity signal. These experiments were run two times, with a mean value and SEM calculated using the four 8 hr data points (i.e.  $n = 4$  from two separate experiments). For IP experiments, data were quantified by calculating HA/EGFP for each IP sample. Each experiment was then normalised by setting the highest HA/EGFP value to 100. These experiments were run three times, either from three or two independent experiments as noted in figure legends.

For click chemistry S-acylation experiments, the % S-acylation in each sample was calculated by measuring the band intensities of the non-acylated band and each visible S-acylated band. The % S-acylation was then estimated by:  $[\text{sum of S-acylated bands} / (\text{sum of S-acylated bands} + \text{non-acylated band})] * 100$ . These experiments were run two times, each with an  $n$  of 2, and therefore data quantification used  $n = 4$  from two separate experiments.

Lastly, for the steady-state expression experiments, the protein intensity was quantified and normalised against total protein stain (TPS) in the same manner mentioned in the cycloheximide assay.

Data presentation methods were chosen based on the type of experimental measurement. For cycloheximide experiments, the data were quantified and presented as a % of protein remaining after 8 hours (relative to the corresponding 0-hour sample). S-acylation experiments reported the % S-acylated immunoreactive bands (relative to all immunoreactive signal) in click chemistry assays. In contrast,

co-immunoprecipitation and steady-state expression analyses provided absolute density measurements instead of fractional data. As a result, these values went through normalization procedures (as shown in the y-axis labels of the figures), where the highest value in each experimental repeat was set to 100 and all other data normalised relative to this.

## **2.7 Illustrations tools**

All Illustrations in this thesis were made using Microsoft Office 365: PowerPoint version (2507).



**CHAPTER 3**  
**GENERAL ANALYSIS OF GCP16**  
**INTERACTIONS WITH ZDHHC ENZYMES**

## Chapter 3

### General analysis of GCP16 interactions with zDHHC enzymes

#### 3.1 Introduction

GCP16 was first identified by Ohta *et al.* (2003) from a yeast 2-hybrid screen that used an N-terminal Golgi localisation sequence (amino acids 137-237) of the Golgi family protein GCP170 as the bait. GCP16 was shown to be associated with the cytoplasmic surface of the Golgi apparatus and co-localised with GCP170 and Giantin in this region of HeLa cells. The researchers further found that GCP16 lacks a predicted transmembrane domain but showed, using [<sup>3</sup>H] palmitate labelling experiments, that it is S-acylated at two sites (Cys-69 and Cys-72). Alanine substitutions of these cysteine residues led to reduced Golgi localisation and an increased presence in cytoplasmic fractions isolated by cell fractionation. GCP16 was suggested to play a role in protein sorting through the secretory pathway as its overexpression disrupted the trafficking and secretion of proteins. This was assessed by expressing the G glycoprotein of Vesicular Stomatitis Virus (VSV-G) and showing that GCP16 over-expression led to the accumulation of this protein in the Golgi and blocked its delivery to the cell surface. Similarly, GCP16 overexpression also blocked the secretion of secreted Dipeptidyl Peptidase IV. These effects of GCP16 overexpression were not seen with the cysteine-to-alanine mutant, showing the importance of S-acylation and Golgi localisation for the functional properties of the protein (Ohta *et al.*, 2003).

The role of GCP16 in protein S-acylation was first reported by Swarthout *et al.* (2005). This study followed previous work that had reported a key role for the accessory protein Erf4 in S-acylation mediated by the acyltransferase Erf2 in the yeast *Saccharomyces cerevisiae* (Lobo *et al.*, 2002). The Erf2/Er4 complex in yeast was shown to mediate the S-acylation of Ras2, and Swarthout *et al.* (2005) identified

zDHHC9 and GCP16 as the mammalian proteins sharing the highest identity with Erf2 and Erf4, respectively. They further showed that zDHHC9 co-localises with GCP16 at the Golgi and that the two proteins could be isolated in a complex from cells using immunoprecipitation. Furthermore, the purified complex was shown to mediate the incorporation of [ $^3\text{H}$ ] palmitate into H-Ras and N-Ras, but not GAP43 and G $\alpha$ i. S-acylation was minimal in the absence of GCP16, suggesting it acts as an obligatory co-factor for zDHHC9, analogous to the role of Erf4 as a co-factor for Erf2. In *S. cerevisiae*, Erf4 was shown to stabilize Erf2 by protecting it from ubiquitination-dependent degradation, and it also stabilized the autoacylated intermediate form of Erf2 by acting as a shield, preventing the hydrolysis of the DHHC active site (Mitchell *et al.*, 2012). These effects of Erf4 were shown through the analysis of Erf4 mutant yeast strains (Mitchell *et al.*, 2012). Assuming that the roles of Erf4 and GCP16 are conserved, then the likely role of GCP16 is to stabilise the zDHHC9 enzyme and its ability to catalyze substrate S-acylation. However, this hypothesis has yet to be explored.

In addition to GCP16, more recent work showed that Golga7b, which shares 61% amino acid identity with GCP16, interacts with zDHHC5 (Woodley and Collins, 2019). It was further shown that zDHHC5 S-acylates Golga7b and that this S-acylation stabilizes the zDHHC5-Golga7b complex at the plasma membrane. Moreover, another study reported an interaction of GCP16 with zDHHC5 (Ko *et al.*, 2019).

Despite the observed interaction between zDHHC9 and GCP16 and the importance of this protein complex for the S-acylation of H-Ras and N-Ras (Swarthout *et al.*, 2005), the exact role of GCP16 has not been defined. In addition, whether Golga7b can play a similar role to GCP16 in the S-acylation process is also unclear. Therefore, in this chapter, we sought to understand better the molecular importance of GCP16 and Golga7b for the regulation of zDHHC9 and zDHHC5 and to make use of new advancements in artificial intelligence (AI) applications in the field of molecular

biology, using AI 3D protein prediction software (AlphaFold Colab) to provide models and insight into zDHHC9-GCP16 and zDHHC5-GCP16 complexes that could subsequently be pursued and validated through wet lab work.

In summary, this chapter sought to answer the following questions:

1. Does GCP16 interact with other Golgi zDHHC enzymes, or is the interaction specific to zDHHC9?
2. Does GCP16 have similar effects on zDHHC9 and zDHHC5?
3. Do GCP16 and Golga7b have similar effects on zDHHC5 and zDHHC9?
4. Does perturbing GCP16 S-acylation impact the stability and activity of zDHHC9 and zDHHC5?

## **3.2 Results**

### **3.2.1 Analysis of the effects of GCP16-zDHHC5/zDHHC9 interactions on protein stability**

Although the interaction of Erf4 with Erf2 in *S. cerevisiae* has been shown to impact both the stability and activity of the Erf2 S-acyltransferase (Mitchell *et al.*, 2012), there have not been similar analyses of the effects of GCP16 on zDHHC9. At present, we know that GCP16 can regulate the oligomeric state of zDHHC9 in cell lysates (Nguyen *et al.*, 2023) and the autoacylation of the purified enzyme (Mitchell *et al.*, 2014). However, the importance of this interaction in cells is not well defined. Therefore, I first examined whether the interaction of EGFP-GCP16 with HA-zDHHC9 and HA-zDHHC5 (Ko *et al.*, 2019) affected the stability of the interacting proteins. To do this, the protein synthesis inhibitor cycloheximide was used. Transfected HEK293 cells were treated for 8 hours with 50 µg/ml cycloheximide to block new protein synthesis, and expression levels of EGFP-GCP16 and HA-zDHHC enzymes were

examined relative to parallel untreated samples that were lysed at t=0 (i.e. before cycloheximide treatment). Protein levels were detected by immunoblotting, and protein stability was determined by the loss of immunoreactivity in the cycloheximide-treated samples compared to the untreated (t=0) samples.

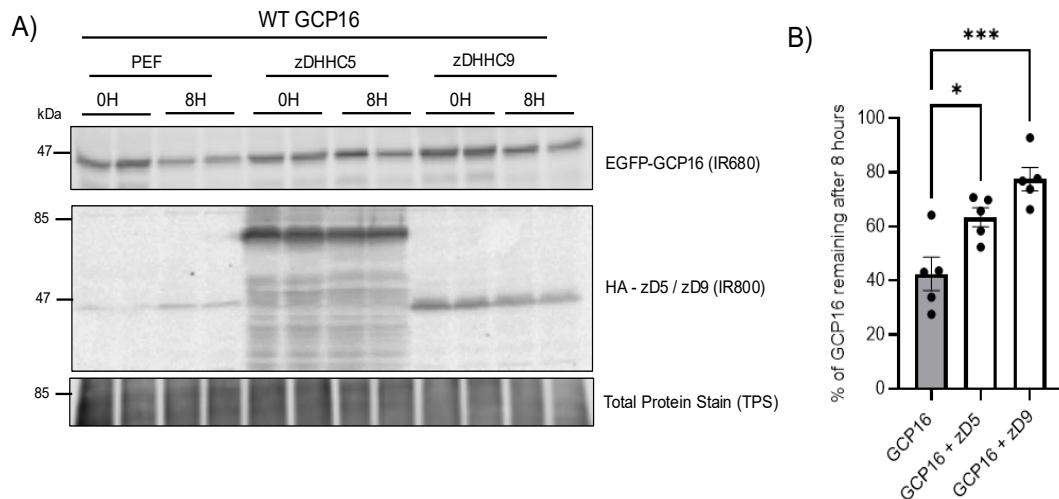


**Figure 3.1 Cycloheximide assay to assess the stability of GCP16 in the absence or presence of zDHC5/zDHC9.**

HEK293 cells were transfected with plasmids encoding EGFP-GCP16 together with HA-tagged zDHC5 or zDHC9, or PEF (empty plasmid) as a negative control. After overnight incubation, samples were either lysed immediately (0 H) or treated with 50 µg/ml cycloheximide for 8 hours (8 H) and then lysed. Samples were then analysed by immunoblotting. A) Representative experiment showing expression levels of EGFP-GCP16 (IR680; top) HA-tagged zDHC5 and zDHC9 (IR800; middle), and the total protein stain (IR680). The molecular weight marker position is shown on the left side of all blots. B) Quantified data showing the mean + SEM of the percentage of the remaining GCP16 after 8 hours; filled circles represent individual samples (n=5 from three separate experiments). Statistical significance was determined using a one-way ANOVA with a Tukey post-test (\* denotes P < 0.05 and \*\*\* for P < 0.001).

The results in Figure 3.1A show that the immunoreactivity of EGFP-GCP16 was reduced at the 8-hour time point compared with the t=0 time point, whereas loss of immunoreactivity appeared less pronounced at the 8-hour time point when EGFP-GCP16 was co-expressed with HA-zDHC5 or HA-zDHC9. Quantification of data from different experiments confirmed that both HA-zDHC5 and HA-zDHC9 co-expression significantly increased the stability of EGFP-GCP16 (Figure 3.1B).

The reciprocal analysis was also undertaken to determine if EGFP-GCP16 affected the stability of HA-zDHHC5 and HA-zDHHC9. This analysis, shown in Figure 3.2, revealed that the stability of both HA-zDHHC5 and HA-zDHHC9 was significantly increased by EGFP-GCP16 co-expression, compared with EGFP.

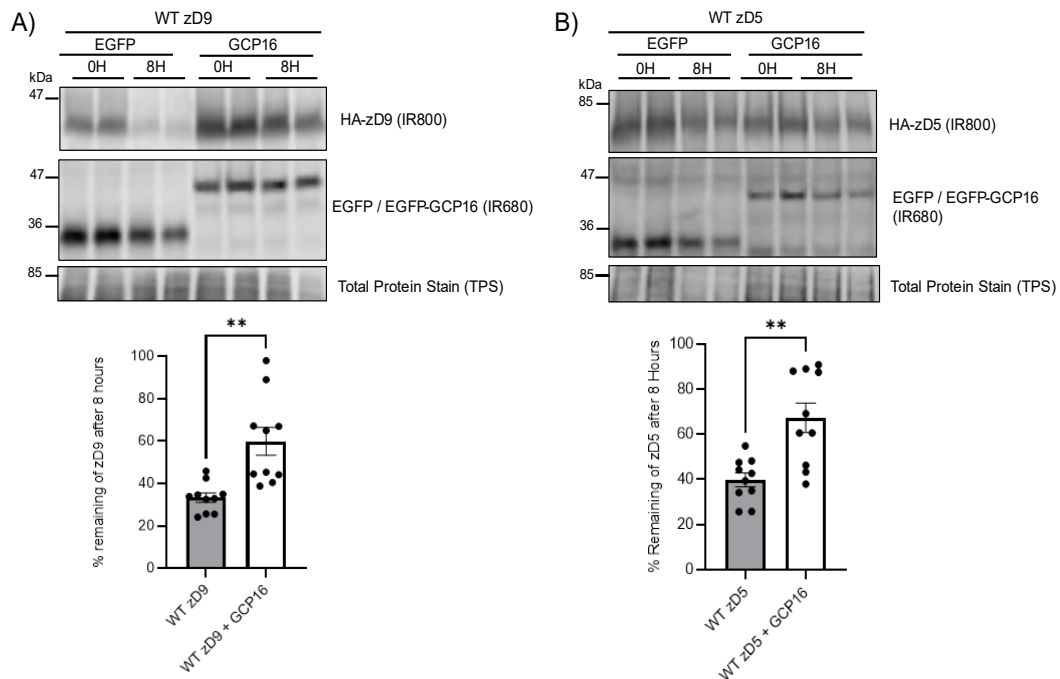


**Figure 3.2 Cycloheximide chase assay to assess the stability of zDHHC5 and zDHHC9 in the absence and presence of GCP16.**

Twenty-four hours after transfecting HEK293 cells with plasmids encoding EGFP or EGFP-GCP16 together with HA-tagged zDHHC9 or zDHHC5, samples were either lysed immediately (0 H) or treated with 50 µg/ml cycloheximide for 8 hours (8 H) before lysis. Samples were then analysed by immunoblotting. A) The level of HA-zDHHC9 (IR800; top) in the presence of EGFP or EGFP-GCP16 (IR680; middle) is shown together with the total protein stain (IR680). The molecular weight marker position is shown on the left side of all blots. The graph shows the mean +SEM percentage of the zDHHC9 remaining after 8 hours; filled circles represent individual samples (n=10 from five separate experiments). An unpaired T-test was used to compare zDHHC9 expression with EGFP or EGFP-GCP16 (\*\*denotes P <0.005). B) The same configuration as (A) was used except with HA-zDHHC5, which was detected at the (IR800) channel and EGFP/EGFP-GCP16 was detected in the (IR680) channel (n=10 from five separate experiments).

In addition to the cycloheximide experiments in Figure 3.2 showing that co-expression of EGFP-GCP16 had a significant effect on the stability of both HA-zDHHC5 and HA-zDHHC9, it was also noted that the steady-state levels of these enzymes in the

presence of GCP16 appeared to be increased in several experiments and indeed quantification of multiple samples confirmed this (Figure 3.3).

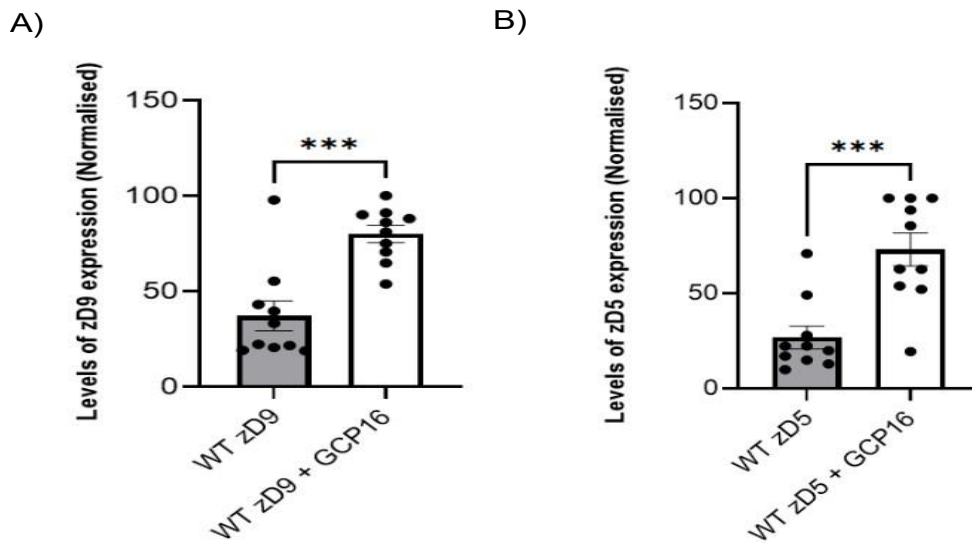


**Figure 3.3 Analysis of the steady-state levels of zDHC9 and zDHC5 in the absence and presence of GCP16.**

HEK293 cells were transfected with plasmids encoding EGFP or EGFP-GCP16 together with HA-tagged zDHC9 (A) or zDHC5 (B). After 24 hours, samples were lysed and analysed by immunoblotting. Quantified data show the level of zDHC9 (A) and zDHC5 (B) expression with and without EGFP-GCP16 co-expression (n=10 from five separate experiments). An unpaired T-Test was used to test statistical significance (\*\*\*) denotes  $p < 0.001$ .

### 3.2.2 Analysis of the interaction of GCP16 with other (Golgi) zDHC enzymes

GCP16 has been described as an interacting partner of both zDHC9 (Swarthout *et al.*, 2005) and zDHC5 (Ko *et al.*, 2019). However, an important question is whether this accessory protein is specific to these two enzymes or has wider interactions with the zDHC family. To assess the interaction of EGFP-GCP16 with a wider set of HA-zDHC enzymes, we employed co-immunoprecipitation (Co-IP) assays. For this, HEK293 cells were transfected with plasmids encoding HA-tagged zDHC3, zDHC5, zDHC7, and zDHC9 together with EGFP-GCP16 or EGFP as a negative control. HA-zDHC3 and HA-zDHC7 were selected for this analysis because they are Golgi enzymes that localize on the same membrane compartment as zDHC9 in

HEK293 cells (Greaves *et al.*, 2008). The cells were lysed approximately 24 hours post-transfection, and the lysates were incubated with GFP-trap beads; these agarose beads are conjugated to GFP nanobodies, which capture any protein with a GFP tag (and associated proteins). Bound proteins were released from the GFP-trap beads using SDS sample buffer, and protein content was assessed by immunoblotting to observe any complex formation between the EGFP-GCP16 and the HA-tagged zDHHC enzymes.

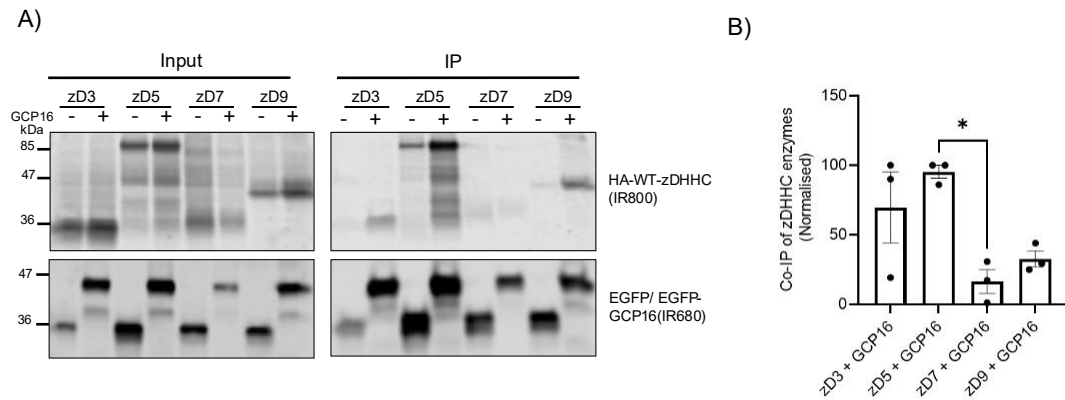


**Figure 3.4 Co-immunoprecipitation analysis of EGFP-GCP16 interaction with zDHHC enzymes.**

HEK293 cells were transfected with plasmids encoding EGFP or EGFP-GCP16 together with plasmids encoding either zDHHC3, zDHHC5, zDHHC7, or zDHHC9. After 24 hours, cells were lysed and incubated with GFP-trap beads to capture EGFP-tagged proteins alongside any HA-tagged zDHHC proteins bound to EGFP-GCP16 or EGFP. A) Representative immunoblots probed with anti-HA (IR800; top) and anti-GFP (IR680; bottom), showing protein levels in the input and IP samples. The molecular weight marker position is shown on the left side of all blots. B) Quantified data (n=3 from two separate experiments) showing normalised HA/GFP signal in the IP samples and statistical analysis using a one-way ANOVA with Tukey post-test (\*\* P<0.01, \*\*\*P <0.001).



Figure 3.4A shows that HA-tagged zDHHC3, zDHHC5, and zDHHC9 binding to EGFP-GCP16 was higher than observed with the negative control (EGFP). In contrast, HA-zDHHC7 showed similar levels in the IP samples with EGFP and EGFP-GCP16. Quantitative analysis of the HA signal/EGFP signal in immunoprecipitated samples showed that the binding of EGFP-GCP16 to HA-zDHHC5 was significantly higher than HA-zDHHC7 and it was also higher than HA-zDHHC3 and HA-zDHHC9 but not with statistical significance. To expand the analysis of GCP16-zDHHC interaction specificity, co-IP assays were also undertaken to compare the interaction of EGFP-GCP16 with the Golgi-localised enzymes, zDHHC13 and zDHHC17. The representative experiment in Figure 3.5A shows that all proteins tested, HA-zDHHC-5, -9, -13, and -17, showed detectable binding to EGFP-GCP16 and greater than that seen with the EGFP controls. Quantification of the HA signal/EGFP signal in immunoprecipitated samples showed that the average amount of capture of HA-zDHHC5 and HA-zDHHC9 appeared to be higher than for HA-zDHHC13 and HA-zDHHC17 (Figure 3.5B). However, the results from these experiments had high variability, and there were no statistically significant differences between the different zDHHC enzymes.

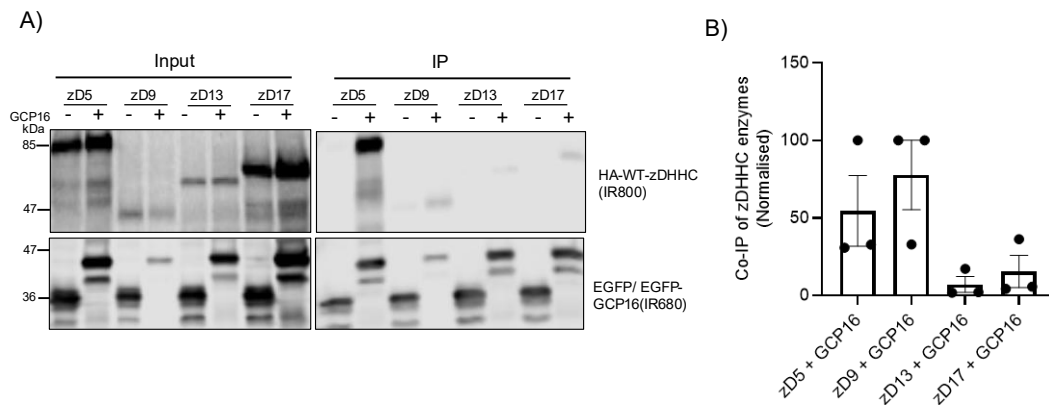


**Figure 3.5 Co-immunoprecipitation analysis of EGFP-GCP16 interaction with HA-zDHHC13 and HA-zDHHC17.**

HEK293 cells were transfected with plasmids encoding EGFP or EGFP-GCP16 together with plasmids encoding either HA-zDHHC5, HA-zDHHC9, HA-zDHHC13, or HA-zDHHC17. After 24 hours, cells were lysed and incubated with GFP-trap beads to capture EGFP-tagged proteins alongside any HA-tagged proteins bound to EGFP-GCP16 or EGFP. A) Representative immunoblots probed with anti-HA (IR800; top) and anti-GFP (IR680; bottom), showing protein levels in the input and IP samples. The molecular weight marker position is

shown on the left side of all blots. B) Quantified data (HA/EGFP) showing the mean  $\pm$  SEM of the amount of zDHHC enzyme co-immunoprecipitated by EGFP-GCP16 (n = 3 from two separate experiments).

Overall, the results presented in Figures 3.4 and 3.5 suggest that EGFP-GCP16 does show some interaction specificity for HA-zDHHC5 and HA-zDHHC9, but there may also be a lower level of interaction with other enzymes, such as HA-zDHHC3; this is consistent with the results of a recent study by Yang *et al.* (2024), which also reported interactions of GCP16 with other zDHHC enzymes.

To extend this analysis further, the S-acylation of EGFP-GCP16 by these zDHHC enzymes was examined. S-acylation is essential for the correct localisation of GCP16 at the Golgi, with cysteine residues at positions 69 and 72 suggested to be particularly important (Ohta *et al.*, 2003). As the strength of binding of substrate proteins to zDHHC enzymes and their subsequent S-acylation is not always directly correlated (Lemonidis *et al.*, 2014), I tested the ability of the enzymes examined in Figures 3.4 and 3.5 to S-acylate EGFP-GCP16. For this, EGFP-GCP16 was co-expressed in HEK293 cells together with the Golgi enzymes HA-zDHHC3, -7, -9, -13, and -17 (an empty HA-pEFBOS plasmid was used as a negative control). S-acylation of GCP16 was then assessed using a click chemistry assay. This involved incubating the cells for 4 hours with palmitic acid-azide, which is incorporated into S-acylated proteins (Greaves *et al.*, 2017). The cells were then lysed and incubated with a click reaction mixture containing Alkyne-mPEG; the reaction of Alk-mPEG with palmitic acid-azide results in a 5 kDa band-shift for each S-acylated cysteine (Salaün *et al.*, 2020). The samples were then resolved by SDS-PAGE and analyzed by immunoblotting.

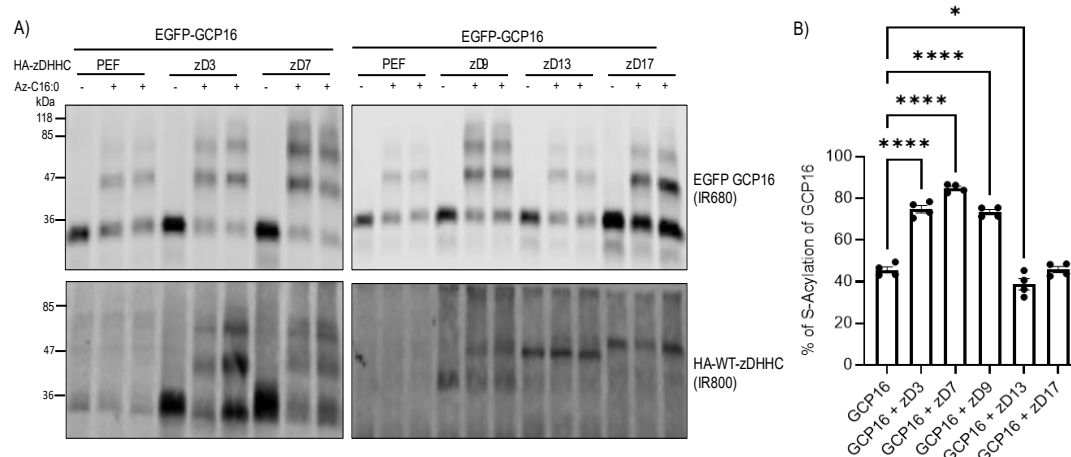


**Figure 3.6 S-acylation of EGFP-GCP16 by Golgi-localised zDHHC enzymes.**

HEK293 cells were co-transfected with plasmids encoding EGFP-GCP16 together with HA-zDHHC3, HA-zDHHC7, HA-zDHHC9, HA-zDHHC13, or HA-zDHHC17 or PEF (empty plasmid) as a (negative control). Twenty-four hours post-transfection, the cells were metabolically labelled with palmitic acid-azide (Az-C16:0) for 4 hours (+); palmitic acid was added as a negative control (-). Cells were then lysed, and a click mixture containing Alk-mPEG was added. The reaction of alkyne and azide groups results in a 5 kDa band-shift in proteins for every S-acylated cysteine. (A) Representative images showing EGFP-GCP16 (IR680; top) and the HA-tagged zDHHC enzymes (IR800; bottom). The molecular weight marker position is shown on the left side of all blots. (B) Quantified data showing EGFP-GCP16 S-acylation by zDHHC3, zDHHC7, zDHHC9, zDHHC13, and zDHHC17 (quantified as the S-acylated immunoreactive bands/total immunoreactive bands). Statistical significance was determined using a one-way ANOVA with Tukey post-test (\*\*\*\* denotes  $P < 0.0001$  and \* denotes  $P < 0.05$ ;  $n = 4$  from 2 separate experiments).

The data shown in Figure 3.6A suggests that EGFP-GCP16 can be S-acylated on at least three sites, as in some samples, there were three upward band-shifts detected in the presence of palmitic acid-azide (“+”) compared with the control samples where cells were instead incubated with palmitic acid (“-”). The data in Figure 3.6B further show that the level of EGFP-GCP16 S-acylation was significantly increased by HA-zDHHC3, HA-zDHHC7, and HA-zDHHC9 but not by HA-zDHHC13 or HA-zDHHC17 (indeed, HA-zDHHC13 co-expression resulted in a significant decrease in EGFP-GCP16 S-acylation). The quantification in Figure 3.6B was done by expressing the combined immunoreactive band intensities of S-acylated bands as a percentage of the total immunoreactive bands for EGFP-GCP16. Thus, although HA-zDHHC9 appears to bind preferentially to EGFP-GCP16 (Figures 3.4 and 3.5), other enzymes, such as zDHHC3 and zDHHC7, may also be relevant to the function and/or

localisation of GCP16 by mediating its S-acylation. The observation that HA-zDHHC3 and HA-zDHHC7 can mediate S-acylation of EGFP-GCP16 in the absence of strong interaction (especially for HA-zDHHC7) is consistent with previous work showing that zDHHC3 and zDHHC7 are high-activity enzymes that can mediate substrate S-acylation in the absence of a detectable interaction (Lemonidis *et al.*, 2014).

### 3.2.3 Analysis of the interactions of GCP16 and Golga7b with zDHHC5 and zDHHC9

Golga7b (Golgin Subfamily A Member 7B) is a 167-amino acid protein that shares 61% amino acid identity with GCP16. Figure 3.7 shows an amino acid alignment that highlights the strong amino acid conservation between these proteins (*purple shading*) and the extended N- and C-termini of Golga7b (*grey shading*). Golga7b was identified as a potential binding partner of zDHHC5 in the Bioplex study (Huttlin *et al.*, 2015), and this was confirmed by Woodley and Collins (2019). The interaction was reported to have a reciprocal impact on the stability and localisation of both Golga7b and zDHHC5 (Woodley and Collins, 2019).



Alignment method : TM-align which perform residue to residue alignment based on structural similarity.

TM-score : value for scaling structural similarity ranging from (0.1) no similarity to (1) resembling perfect similarity.

This alignment was generated by aligning sequences for plasmids we used in the lab, using Protein Data Bank (PDB)

<https://www.rcsb.org/alignment>

#### Figure 3.7 Amino acid alignment of Golga7b and GCP16

The sequence alignment provides an insight into the regions of similarity between both proteins; here, Golga7b was used as a template to cross-reference GCP16, resulting in 75% similarity and a high TM-score, indicating high structural similarities.

Given the strong similarity between Golga7b and GCP16 (Figure 3.7) and their known interactions with zDHHC enzymes, it was examined whether these two accessory proteins have interchangeable activity or exhibit some zDHHC specificity. As a starting point, co-IP experiments were undertaken to compare the binding of EGFP-Golga7b and EGFP-GCP16 to HA-zDHHC5 and HA-zDHHC9 and also to examine

the possibility of homo- and hetero-dimerisation of Golga7b/GCP16. HEK293 cells were transfected with either EGFP, EGFP-Golga7b or EGFP-GCP16 together with HA-zDHHHC9, HA-zDHHHC5, or HA-GCP16. After approximately 24 hours, the transfected cells were lysed and incubated with GFP-trap beads to capture the EGFP, EGFP-GCP16, or EGFP-Golga7b. Immunoblotting analyses were then performed to determine the level of Co-IP of both HA-zDHHHC enzymes and HA-GCP16.

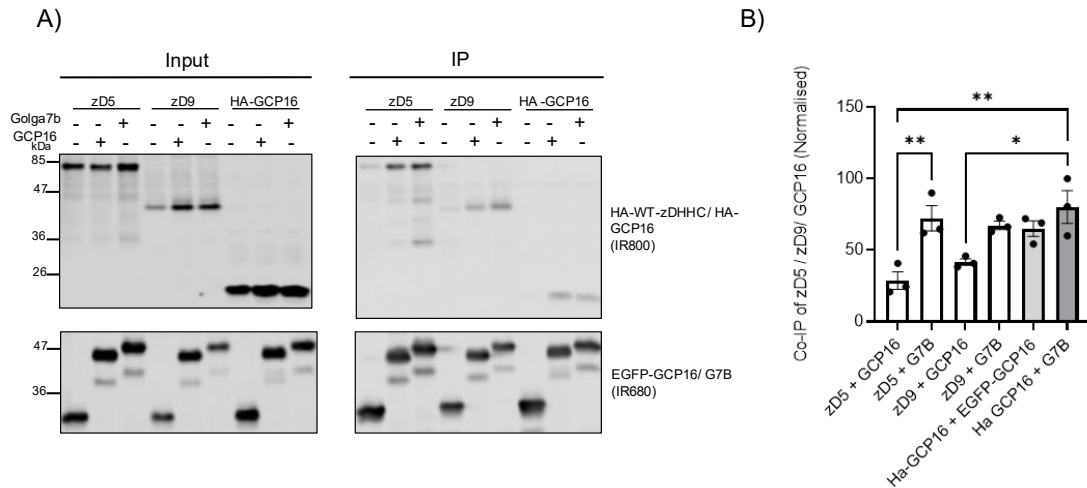


**Figure 3.8 Analysis of the binding of HA-zDHHHC5, HA-zDHHHC9, and HA-GCP16 to EGFP-GCP16 and EGFP-Golga7b.**

HEK293 cells were transfected with EGFP-Golga7b or EGFP-GCP16 together with either HA-tagged zDHHHC9, zDHHHC5, or GCP16. Twenty-four hours later, cell lysates were incubated with GFP-trap beads, and eluted proteins were examined by immunoblotting. A) Representative blot showing co-immunoprecipitation of HA-tagged zDHHHC5, zDHHHC9, or HA-GCP16 (IR800) by either EGFP-Golga7b or EGFP-GCP16 (IR:680); the input blot confirms expression of transfected proteins. The molecular weight marker position is shown on the left side of all blots. B) Quantitative analysis of the binding of HA-zDHHHC9, HA-zDHHHC5, and HA-GCP16 to EGFP-Golga7b and EGFP-GCP16. Statistical analysis was performed using a One-Way ANOVA with Tukey post-test (\*\* denotes  $P < 0.005$ , \* denotes  $P < 0.05$ ;  $n = 3$  from 3 separate experiments).

As shown in Figure 3.8, EGFP-Golga7b and EGFP-GCP16 were found to co-IP both HA-zDHHHC5 and HA-zDHHHC9. Interestingly, the binding of HA-zDHHHC5 to EGFP-Golga7b was significantly higher than its binding to EGFP-GCP16. HA-zDHHHC9 also appeared to have higher binding to EGFP-Golga7b than EGFP-GCP16, but a statistical comparison showed no statistical significance (Figure 3.8B). Interestingly, it was also found that HA-GCP16 interacted with both EGFP-Golga7b and EGFP-GCP16. This is a novel finding, and there was no detectable binding of HA-GCP16 to

the EGFP control (Figure 8A). Having shown that Golga7b and GCP16 both interact with HA-zDHHC5 and HA-zDHHC9, it was next examined if the stability of EGFP-Golga7b was also increased in the presence of HA-zDHHC5 and HA-zDHHC9 as seen for EGFP-GCP16 (see Figure 3.1). To examine this, the steady-state expression levels of EGFP-Golga7b and EGFP-GCP16 in lysates of HEK293 cells that were co-transfected with either HA-zDHHC9, HA-zDHHC5 or the empty pEFBOS-HA plasmid (negative control) were quantified. Consistent with the results shown in Figure 3.1, this analysis showed a significant increase in EGFP-GCP16 expression levels with HA-zDHHC5 and HA-zDHHC9 (Figure 3.9). Similarly, EGFP-Golga7b expression was also significantly higher with HA-zDHHC5, whereas HA-zDHHC9 co-expression had no significant effect on steady-state levels of EGFP-Golga7b (Figure 3.9).

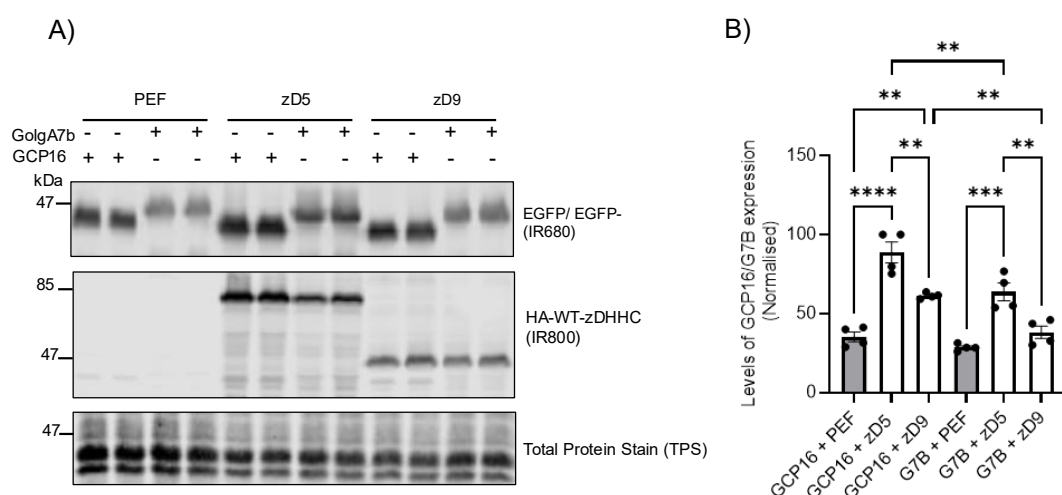


**Figure 3.9 Comparison of the expression levels of EGFP-Golga7b and EGFP-GCP16 when co-expressed with either HA-zDHHC5 or HA-zDHHC9.**

HEK293 cells were transfected with EGFP-Golga7b or EGFP-GCP16 together with either HA-tagged zDHHC9, zDHHC5, or PEF (empty plasmid). Twenty-four hours later, samples were lysed and analysed by immunoblotting. A) Representative blot showing levels of EGFP-Golga7b and EGFP-GCP16 (IR680) when expressed together with HA-zDHHC5 or HA-zDHHC9 compared with the negative control PEF (empty plasmid) (IR800). Total Protein stain (TPS) is also shown. The molecular weight marker position is shown on the left side of all blots. B) Quantitative analysis comparing the effects of HA-zDHHC5 and HA-zDHHC9 co-expression on the levels of EGFP-Golga7b and EGFP-GCP16. The data was analysed using a one-way ANOVA with a Tukey post-test (n=4 from 2 separate experiments). (\*\* denotes  $p < 0.01$  and \*\*\*\* denotes  $P < 0.0005$ ).

To extend the GCP16/Golga7b interaction analysis with zDHHC5 and zDHHC9, click chemistry S-acylation assays were undertaken to examine if both proteins are S-

acylation substrates of these enzymes. HEK293 cells were transfected with EGFP-Golga7b or EGFP-GCP16 together with either HA-zDHHC5, HA-zDHHC9 or pEFBOS-HA as a negative control. Approximately twenty-four hours post-transfection, cells were metabolically labelled with palmitic acid-azide for 4 hours, and the cells were then lysed and reacted with Alk-mPEG. As shown earlier (Figure 3.6), this results in a 5 kDa band-shift for each S-acylated cysteine.

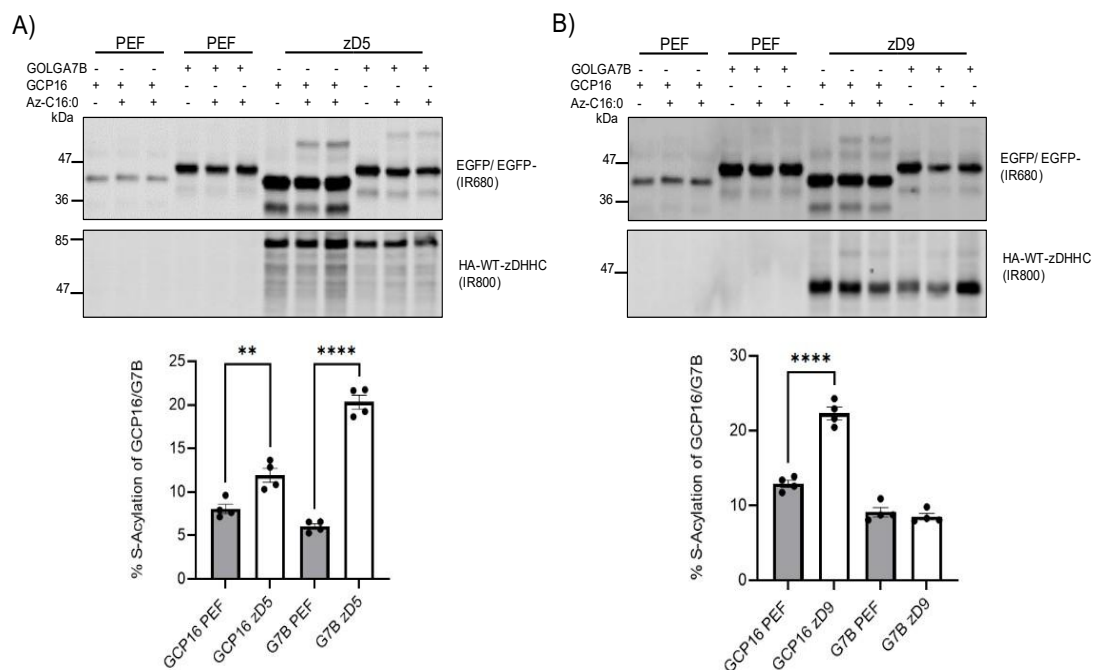


**Figure 3.10 Effect of HA-zDHHC5 and HA-zDHHC9 on the S-Acylation of EGFP-Golga7b and EGFP-GCP16.**

HEK293 cells were transfected with plasmids encoding EGFP-Golga7b or EGFP-GCP16 together with either HA-tagged ZDHHC9, zDHHC5, or PEF (empty plasmid). Twenty-four hours later, cells were incubated with palmitic acid-azide (Az-C16:0; +) or palmitic acid as a control (-) for 4 hours, and cell lysates were reacted with Alk-mPEG. A) Representative immunoblot showing S-acylation of EGFP-Golga7b and EGFP-GCP16 with PEF (empty plasmid) negative control of with HA-zDHHC5. EGFP (IR;680) and HA-zDHHC5 (IR800). The molecular weight marker position is shown on the left side of all blots. The lower panel displays the quantitative analysis of the S-acylation of EGFP-GCP16 and EGFP-Golga7b. B) S-Acylation of EGFP-GCP16 and EGFP-Golga7b in the presence and absence of HA-zDHHC9. All data was analysed by One-way ANOVA with Tukey post-test (\*\*\*\*P<0.0005, \*\*P<0.005; n=4 from 2 separate experiments).

The results in Figure 3.10 reveal that S-acylation of EGFP-GCP16 was significantly increased when co-expressed with either HA-zDHHC5 or HA-zDHHC9 compared to



pEFBOS-HA negative control samples. Interestingly, however, for EGFP-Golga7b, there was an almost three-fold increase in S-acylation with HA-zDHHC5 compared to control, but no significant effect of HA-zDHHC9 co-expression on the S-acylation of this protein.

#### **3.2.4. Implementation of a computational model to predict the 3D structure of zDHHC9 interactions and subsequent experimental validation**

Access to structural data on proteins and protein complexes is important to enhance our understanding of the interactions and functions of cellular proteins; however, the experimental process for determining a single protein structure is both challenging and time-consuming (Thompson *et al.*, 2020). Recent advances in AI and machine learning have proven to be greatly beneficial in the biology field, and I used the online software AlphaFold2 (ColabFold) to explore the 3D structure of zDHHC9 and zDHHC5 and their interaction with GCP16. This software is a machine learning algorithm that uses physical and biological knowledge about a protein to accurately predict its 3D structure using the amino acid sequence. We also attempted to validate these predictions using wet lab work. These analyses are particularly relevant because the functional effects of GCP16/Golga7b appear to be different for zDHHC5 and zDHHC9 (Salaün *et al.*, 2020). It should be noted that the structure of the zDHHC9-GCP16 complex was reported in bioRxiv prior to its publication in 2024 and, therefore, the complex reported by AlphaFold2 was based on the experimentally determined structure of Yang *et al.* (2024).

AlphaFold2 CoLab was used to predict the 3D structure of each protein alongside their interactions and complex formation using the mouse (*mus musculus*) amino acid sequences. The predictions, shown in Figure 3.11, suggested two crucial amino acids in the GCP16 structure for interaction with zDHHC9 and zDHHC5: Arginine-118, which forms 10 Hydrogen bonds with various amino acids in the zDHHC9 and zDHHC5 structures, and Arginine-121, which forms 4 Hydrogen bonds with multiple residues in both zDHHC9 and zDHHC5.

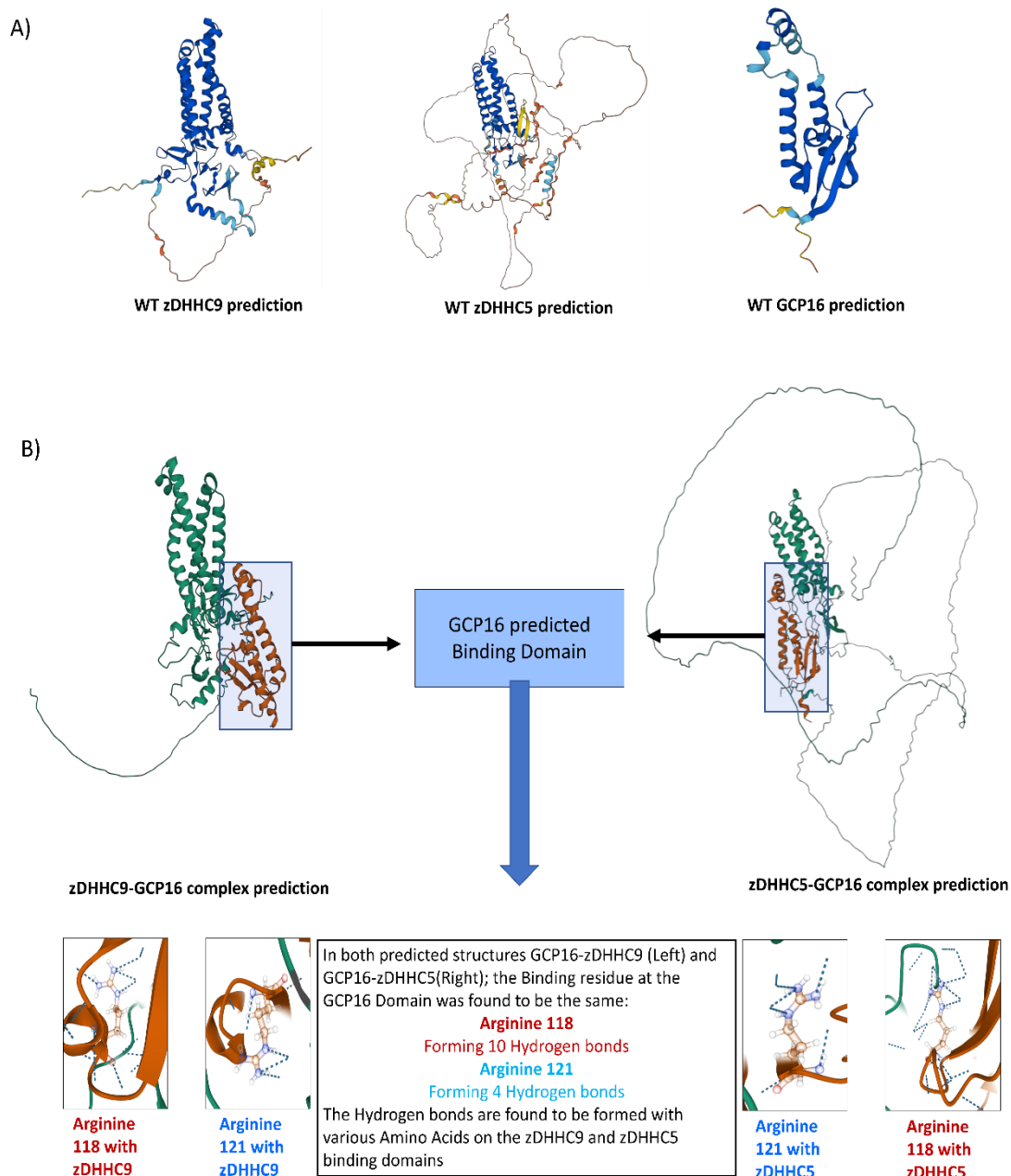


**Figure 3.11 3D protein structure and interaction predictions for GCP16, zDHC5, and zDHC9 using AlphFold2 CoLab software.**

Protein structure predictions are generated using AlphFold2 CoLab, which implements the physical and biological properties of proteins with previously predicted structures in generating 3D structures with accuracy at the atomic level. A) The predicted 3D structures of GCP16, zDHC9 and zDHC5. These predictions were generated based on the amino acid sequence of the mouse protein. B) Predictions of the complex formation of zDHC9-GCP16 (left) and zDHC5-GCP16 (right) with the suggested binding site highlighted in both complexes, in which GCP16 Arginine-118 and Arginine-121 were found to form hydrogen bonds in both complexes with various residues in zDHC9 and zDHC5. An interesting observation was that the catalytic DHHC domain of zDHC9 was found to be within the presumed binding location, but this was not the case for zDHC5, which had the catalytic DHHC domain facing away from the assumed binding location, which might account for the distinct complex formation properties of each protein

GCP16 suggested interacting residues	zDHHHC9 Interacting residues	zDHHHC5 interacting residues
Arginine-118	ASP-79 GLU-80	PRO-95 GLU-101
Arginine-121	PRO-74 GLU-80	LEU-98 LEU-120 ILE-148

**Table 3.1** List of zDHHHC5/zDHHHC9 residues forming bonds with GCP16 Arginine-118/121

In an attempt to validate the AlphaFold protein interaction predictions, a mouse EGFP-GCP16 mutant (R118A, R121A) was generated *via* site-directed mutagenesis using oligonucleotide primers, which were designed to introduce mutations into the coding sequence by amplifying the EGFP-GCP16 plasmid by PCR reaction. The generated mutant EGFP-GCP16 plasmid was validated by sequencing and then transfected into HEK293 cells together with plasmids encoding HA-tagged zDHHHC5 and zDHHHC9. For comparison, similar co-transfections were done with wild-type EGFP-GCP16 (positive control) and EGFP (negative control). After 24 hours, cells were lysed and incubated with GFP-trap beads and bound proteins eluted in SDS sample buffer, resolved by SDS-PAGE, and revealed by immunoblotting.

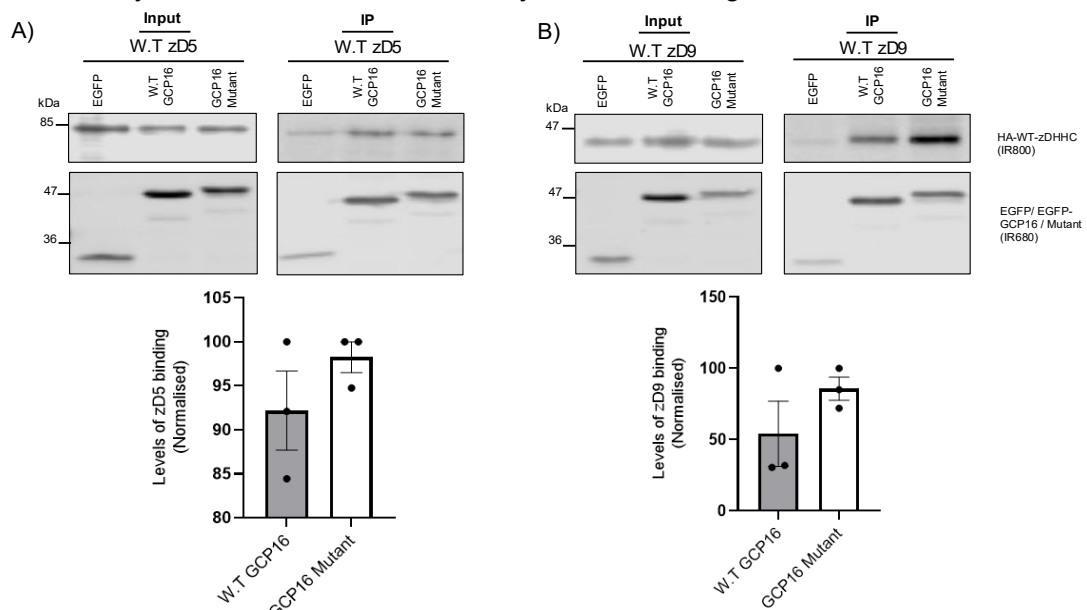


**Figure 3.12** Analysis of EGFP-GCP16 mutant (R118A, R121A) binding to HA-zDHHHC5 and HA-zDHHHC9.

HEK293 cells were transfected with plasmids encoding HA-tagged zDHHC5 or zDHHC9 together with either EGFP, EGFP-GCP16, or EGFP-GCP16 (R118A, R121A) mutant. After 24 hours, cells were lysed and incubated with GFP-trap beads. Immunoprecipitated proteins were then eluted and revealed by immunoblotting. A) Representative experiment with HA-zDHHC5/9 detected at IR800 (top) and the EGFP-GCP16 detected at IR680 (bottom). The molecular weight marker position is shown on the left side of all blots. B) Quantitative analysis of the co-IP of zDHHC5/9 as HA signal/EGFP signal in the immunoprecipitated samples. The data was analysed using an unpaired T-test (n=3 from two separate experiments).

Figure 3.12 shows that the amino acid substitutions introduced in EGFP-GCP16 did not affect the co-IP of either HA-zDHHC5 (panel A) or HA-zDHHC9 (panel B). This shows that residues Arg-118 and Arg-121 are not essential for binding of GCP16 to zDHHC5 and zDHHC9, perhaps suggesting that other crucial sites or factors also govern the formation of the GCP16-zDHHC5 and GCP16-zDHHC9 complexes. This idea is supported by the recent cryo-EM structure of the zDHHC9-GCP16 complex (Yang *et al.*, 2024), which showed that there are four binding interfaces, with Arg-118 and Arg-121 only involved in one of these.

### **3.3 The effect of GCP16 S-acylation on its interactions with zDHHC5 and zDHHC9**

GCP16 is known to associate with the Golgi through S-acylation of Cys-69 and Cys-72 (Ohta *et al.*, 2003). The structure of zDHHC9-GCP16 reported by Yang *et al.* (2024) shows this region of GCP16 embedded in the outer part of the membrane. Thus, GCP16 S-acylation may play an important role in interaction with zDHHC9 and zDHHC5. Indeed, the S-acylation of these zDHHC enzymes has been shown to be important for their interaction with GCP16 (Nguyen *et al.*, 2023; Woodley and Collins, 2019).

In this section, I sought to better understand the relationship between GCP16 S-acylation status and its interaction with zDHHC enzymes. Initially, a co-immunoprecipitation assay was undertaken using HEK293 cells transfected with either wild-type EGFP-GCP16, EGFP-GCP16 (C69,72A), a mutant in which the major S-acylated cystines (69 and 72) are substituted by alanine, or EGFP as a negative

control. These cells were co-transfected with HA-zDHHHC3, HA-zDHHHC5, HA-zDHHHC7, or HA-zDHHHC9 (with empty pEF-BOS-HA plasmid used as a negative control). After 24 hours, cells were lysed and incubated with GFP-trap beads, and bound proteins were revealed by immunoblotting.

Figure 3.13 shows that only zDHHHC5 binding was significantly affected by the introduction of C69A and C72A substitutions in GCP16, whereas the other zDHHHC enzymes showed no significant differences in binding to wild-type *versus* EGFP-GCP16 (C96A, C72A). In this set of experiments, the binding of wild-type EGFP-GCP16 to HA-zDHHHC3 and HA-zDHHHC7 appeared to be higher than observed previously (Figure 3.4).

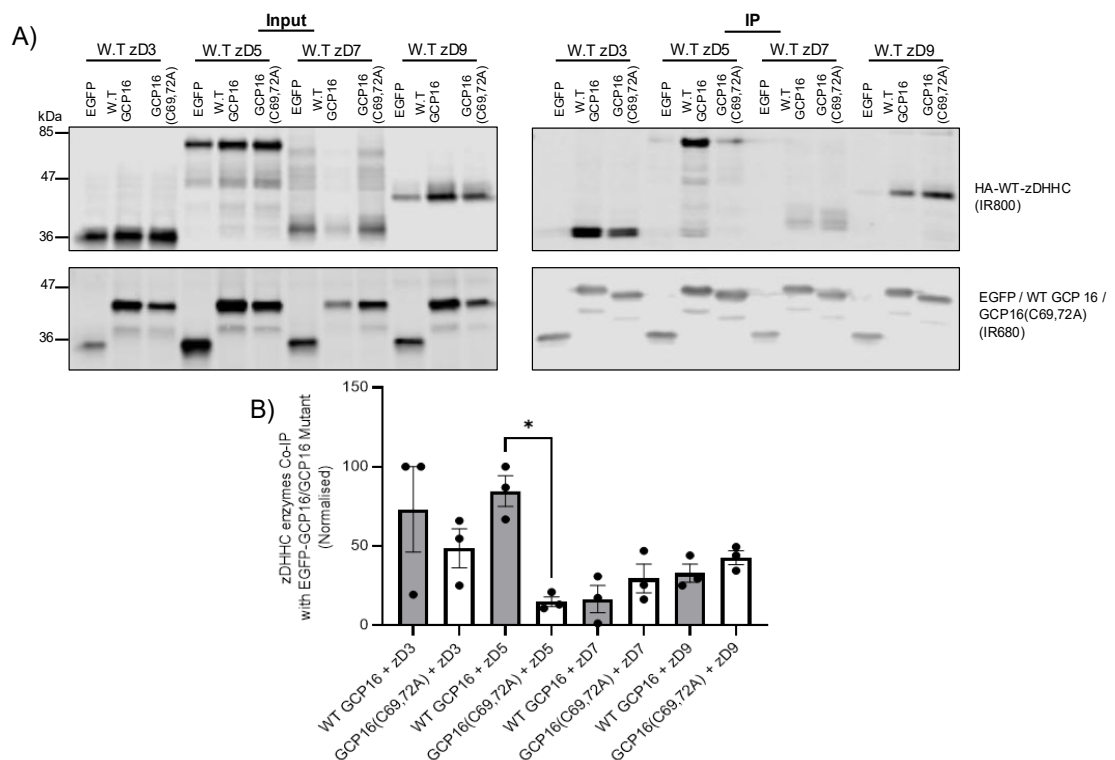


**Figure 3.13 Effect of mutating the major S-acylation sites in GCP16 on zDHHHC interactions.**

HEK293 cells were transfected with either EGFP, EGFP-GCP16, or an EGFP-GCP16 acylation mutant (C69,72A) together with plasmids encoding either HA-zDHHHC3, HA-zDHHHC5, HA-zDHHHC7, or HA-zDHHHC9. After approximately 24 hours, cell lysates were incubated with GFP-trap beads, and bound proteins were eluted. Samples were then resolved by SDS-PAGE and analysed by immunoblotting. A) Representative immunoblot probed with anti-HA (IR800) and anti-GFP (IR680). The molecular weight marker position is shown on the left side of all blots. B) Quantified data showing HA signal in eluted samples (normalised to

the GFP signal); grey bars are with wild-type EGFP-GCP16 while white bars are with the EGFP-GCP16(C69,72A) mutant. Data was analysed using a one-way ANOVA with Tukey (\* $p > 0.05$ ;  $n = 3$  from three separate experiments).

As only HA-zDHHC5 exhibited compromised complex formation with the EGFP-GCP16 S-acylation mutant, it was next examined how HA-zDHHC enzyme stability was affected by wild-type *versus* mutant EGFP-GCP16. In this experiment, HA-zDHHC5 and HA-zDHHC9 were compared as the latter enzyme bound equally well to wild-type and mutant GCP16 (Figure 3.13). To do so, a cycloheximide assay was undertaken in which HEK293 cells were transfected with HA-zDHHC9 or HA-zDHHC5 together with either EGFP, EGFP-GCP16 or the EGFP-GCP16 (C69,72A) mutant. After 24 hours, one set of samples ( $t = 0$ ) were lysed, and another set was treated with 50  $\mu\text{g/ml}$  cycloheximide for 8 hours prior to lysis. The samples were then analysed by immunoblotting (Figure 3.14).

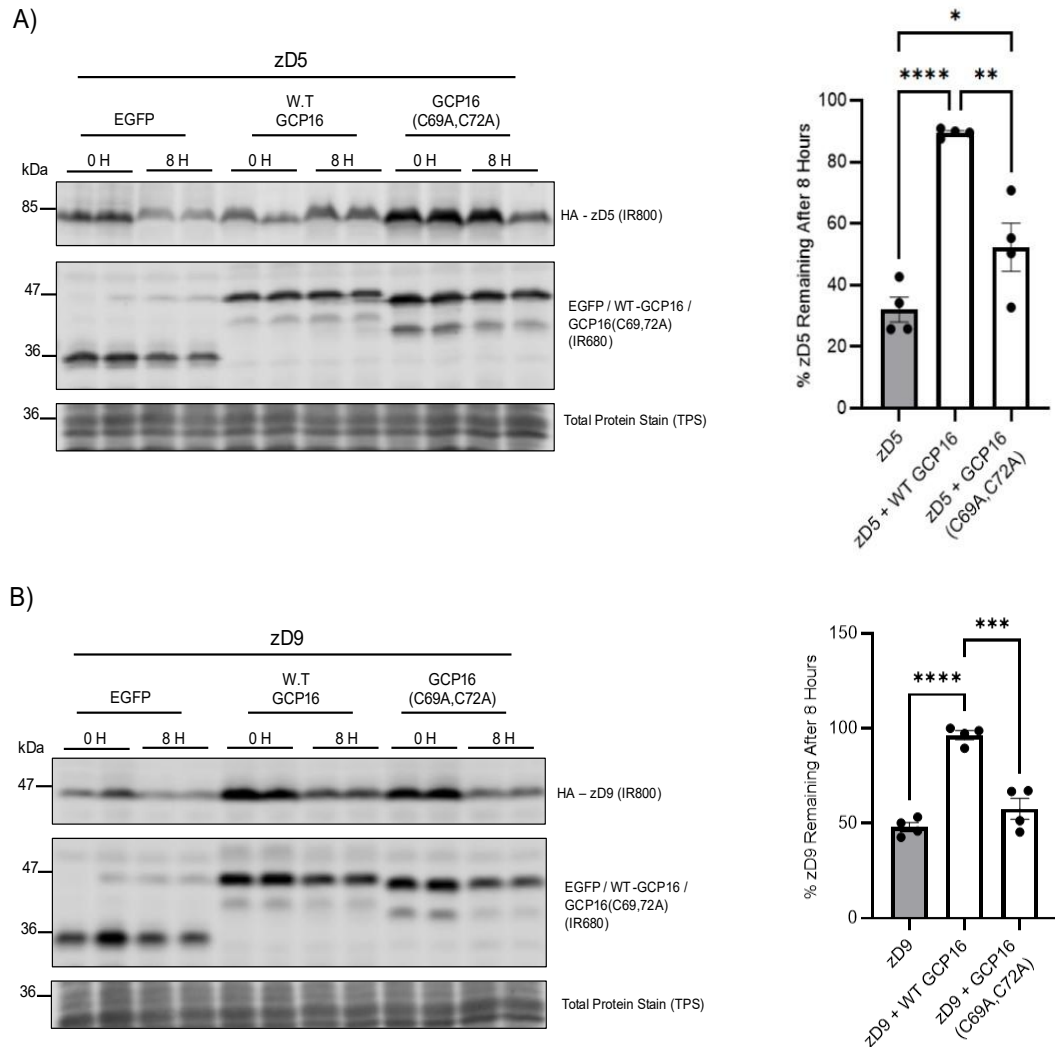


**Figure 3.14 Effect of mutating EGFP-GCP16 S-acylated cysteines on the stability of HA-zDHHC5 and HA-zDHHC9.**

HEK293 cells were transfected for approximately 24 hours with either EGFP, EGFP-GCP16, or EGFP-GCP16 (C69, C72A) together with HA-zDHHC5 or HA-zDHHC9. One set of cell samples was lysed immediately (0 H), whereas another set was lysed after an 8-hour treatment with 50 µg/ml cycloheximide (8 H). **A) Left**, Representative immunoblot showing HA-zDHHC5 (IR800) and EGFP-GCP16 wild type and acylation mutant (IR680). The molecular weight marker position is shown on the left side of all blots. **Right**, Quantified data showing the mean  $\pm$ SEM percentage of the protein remaining after 8 hours; data was analysed using a one-way ANOVA with Tukey post-test (\*\*\*\*P <0.0001, P <0.001; n=4). **B) Left**, Representative immunoblot showing HA-zDHHC9 (IR800) and EGFP-GCP16 wild-type and acylation mutant (IR;680) - same as for A but with zDHHC9. **Right**, Quantified data showing the mean  $\pm$ SEM percentage of the protein remaining after 8 hours; data was analysed using a one-way ANOVA with Tukey post-test (\*\*\*\*P <0.0001, P <0.001; n=4 from two separate experiments).

The data in Figure 3.14A show that HA-zDHHC5 was stabilised by EGFP-GCP16 wild-type; however, this stabilising effect was diminished with the EGFP-GCP16

(C69,72A) mutant. This is consistent with the reduced binding of the mutant GCP16 to zDHHC5 seen in Figure 3.13. Interestingly, the same effect was seen with HA-zDHHC9, where the stability of the protein was increased with wild-type EGFP-GCP16 but not with EGFP-GCP16 (C69,72A) mutant. This is despite the mutant GCP16 having no loss of binding to zDHHC9 (Figure 3.13). Overall, these results suggest that S-acylation is important for the binding of EGFP-GCP16 to zDHHC5 and for the stabilisation effect of GCP16 on both zDHHC5 and zDHHC9.

As the C69,72A substitutions caused a reduction in the stabilisation of both HA-zDHHC5 and HA-zDHHC9 by EGFP-GCP16, we next examined how this mutant affected the S-acylation of the enzymes. For this, a click chemistry assay using 5kDa-PEG was used. HEK293 cells were transfected with either EGFP-GCP16 wild-type, EGFP-GCP16 (C69, 72A), or EGFP, together with HA-tagged zDHHC5 or zDHHC9. After approximately 24 hours, cells were metabolically labelled with palmitic acid-azide for 4 hours, and cell lysates were then reacted with Alk-mPEG. As previously discussed, this procedure results in a five kDa band shift for each S-acylated cysteine. Immunoblotting was then undertaken to visualise the proteins (Figure 3.15).



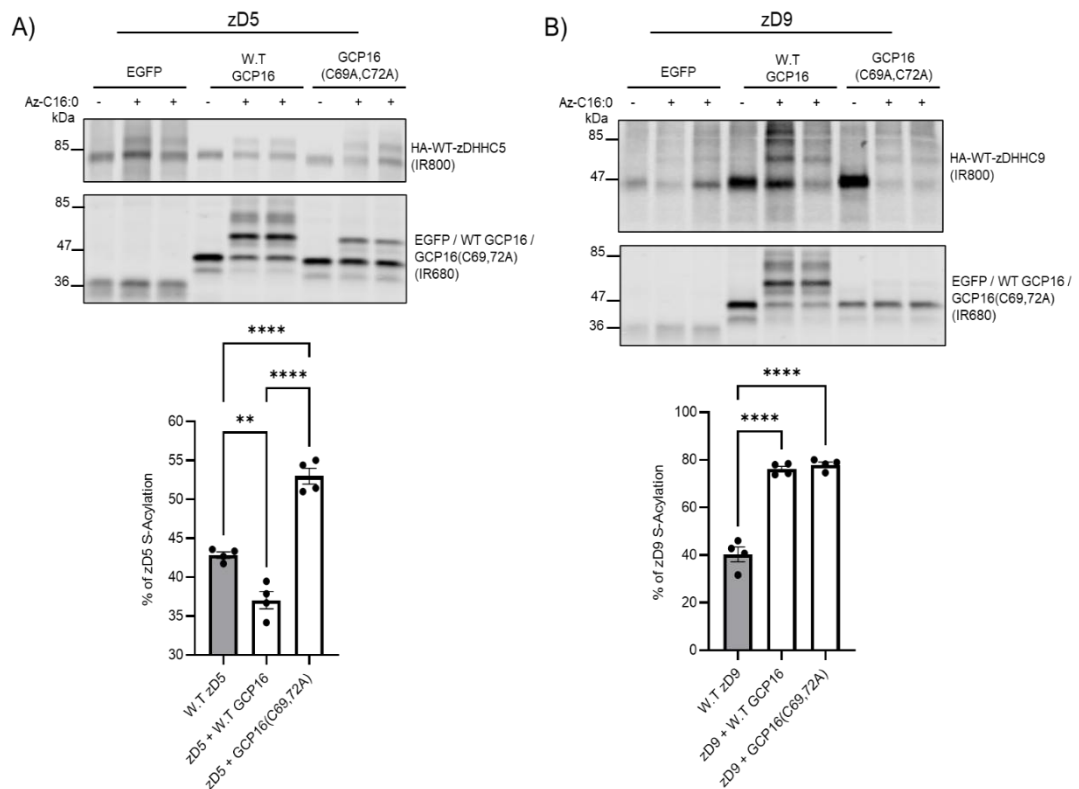


**Figure 3.15 Effect of wild-type and C69,72A mutant GCP16 on S-acylation of zDHC5 and zDHC9.**

HEK293 cells were transfected with plasmids encoding HA-zDHC5 or HA-zDHC9 together with EGFP, EGFP-GCP16 or the EGFP-GCP16 (C69,72A) mutant. After approximately 24 hours, cells were metabolically labelled with palmitic acid-azide (Az-C16:0; +) or palmitic acid as a control (-) for 4 hours and then lysed and a click chemistry S-acylation assay was performed using alk-mPEG, resulting in a 5 kDa band shift for each S-acylated cysteine. **A) Top**, Representative immunoblot showing the S-acylation of the HA-zDHC5 (IR800) in the form of 5kDa shifts in the presence of either EGFP-GCP16 wild-type or the EGFP-GCP16 (C69,72A) mutant (IR680). The molecular weight marker position is shown on the left side of all blots. **Bottom**, Quantified data showing the mean  $\pm$  SEM of zDHC5 S-acylation compared using a one-way ANOVA with Tukey test (\*\*\*\* $P < 0.0001$ , \*\*  $P < 0.005$ ;  $n = 4$ ). **B) Top** immunoblot showing HA-zDHC9 (IR800) S-acylation alone or with either EGFP-GCP16 wild-type or EGFP-GCP16(C69,72A) mutant (IR680). **Bottom**, Quantified data showing mean  $\pm$  SEM levels of zDHC9 S-acylation compared using one-way ANOVA with Tukey (\*\*\*\* $P < 0.0001$ ;  $n = 4$  from two separate experiments).

Surprisingly, it was found that HA-zDHC5 was significantly more S-acylated when co-expressed with the EGFP-GCP16 (C69,72A) mutant compared with wild-type GCP16 (Figure 3.15A). In contrast, HA-zDHC9 was significantly more S-acylated in the presence of both EGFP-GCP16 wild-type and the C69,72A mutant compared with the EGFP control (Figure 3.15B). These results further emphasize the varied behaviour of the wild-type versus cysteine mutant GCP16 when expressed with either

zDHHHC5 or zDHHHC9. Interestingly, we further noted that S-acylation of the EGFP-GCP16(C69,72A) mutant was still detected when co-expressed with zDHHHC5 but not zDHHHC9 (compare the immunoblots in Figure 3.15A/B). This is intriguing as the general assumption is that the major sites for GCP16 S-acylation are located at positions 69 and 72 (Ohta *et al.*, 2004). This suggests that zDHHHC5 (but not zDHHHC9) might modify other cysteines in GCP16, highlighting a unique zDHHHC5-GCP16 relationship.

The potential differential S-acylation of GCP16 (and the C69,72A mutant) by zDHHHC5 and zDHHHC9, might result in distinct effects of these enzymes on the stability of EGFP-GCP16 (C69,72A) *versus* wild-type GCP16. Therefore, this possibility was investigated using a cycloheximide assay in which HEK293 cells were transfected with EGFP-GCP16 wild-type or EGFP-GCP16(C69,72A) together with HA-zDHHHC5, HA-zDHHHC9 or pEF-BOS-HA as a negative control. Approximately 24 hours later, one set of samples was lysed (t=0) and the other set was treated with cycloheximide for eight hours, and then lysed. The samples were then analyzed by immunoblotting.

Figure 3.16A shows a marked increase in EGFP-GCP16 wild-type stability when co-expressed with HA-zDHHHC5; almost the same impact can be seen with HA-zDHHHC9. In contrast, the EGFP-GCP16(C69,72A) mutant showed a significant increase in

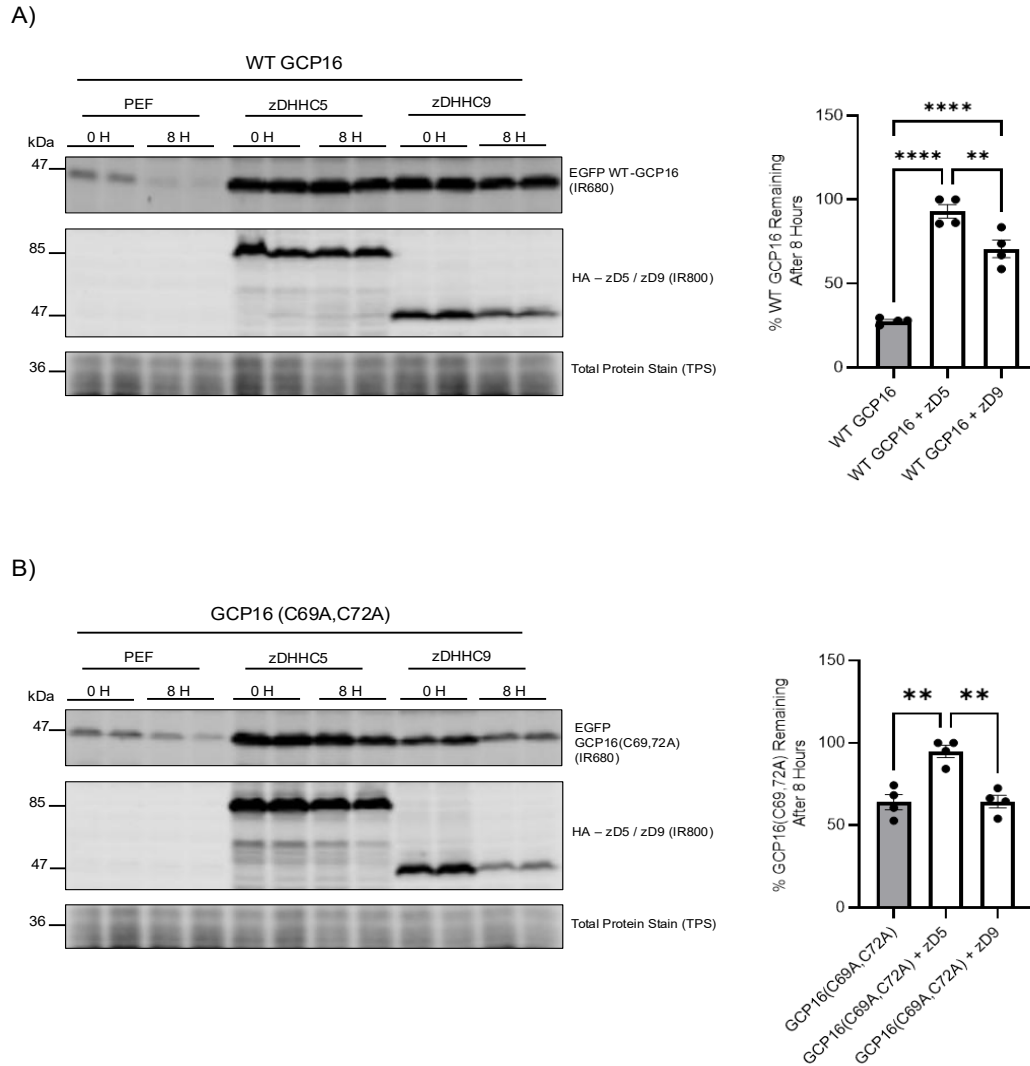


**Figure 3.16 Cycloheximide chase assays to assess the stability of EGFP-GCP16 wild-type and the C69,72A mutant when co-expressed with either HA-zDHC5 or HA-zDHC9.**

HEK293 cells were transfected with plasmids encoding EGFP-GCP16 wild-type or C69,72A mutant together with plasmids encoding either HA-zDHC9, HA-zDHC5, or PEF (empty plasmid) negative control. Twenty-four hours post-transfection (0 H) samples were collected, and cycloheximide was added to the remaining cells for 8 hours (8 H) before lysis and analysis by immunoblotting. **A) Left**, EGFP-GCP16 wild-type was detected at IR680 (top), and the HA-tagged zDHC9 and zDHC5 were detected at IR800 (middle); total protein stain (TPS) visualised at IR680 (bottom). The molecular weight marker position is shown on the left side of all blots. **Right**, quantified data for the percentage of EGFP-GCP16 remaining after 8 hours of cycloheximide treatment in the presence of either PEF (empty plasmid), HA-zDHC5 or HA-zDHC9. Data was analysed using One-way ANOVA with Tukey post-test (\*\*\*\* $P < 0.0001$ , \*\*  $P < 0.005$ ;  $n = 4$ ). **B)** Same as in panel (A) but using the EGFP-GCP16(C69,72A) rather than wild-type GCP16. Data was analysed using One-way ANOVA with Tukey post-test (\*\* $P < 0.005$ ;  $n = 4$  from two separate experiments).

stability only when co-expressed with HA-zDHHC5, and almost no change was seen with HA-zDHHC9 co-expression (Figure 3.16B), highlighting again a different aspect of the GCP16-zDHHC5 interaction. Given that the GCP16 acylation mutant has a loss of binding to zDHHC5 (Figure 3.13), I assume that the increased stability when co-expressed with HA-zDHHC5 reflects S-acylation of another cysteine in the GCP16 mutant.

We next moved towards quantifying the level of S-acylation seen for the EGFP-GCP16(C69,72) mutant when co-expressed with HA-zDHHC5 and HA-zDHHC9; for this, a click chemistry assay was employed using 5 kDa mPEG.

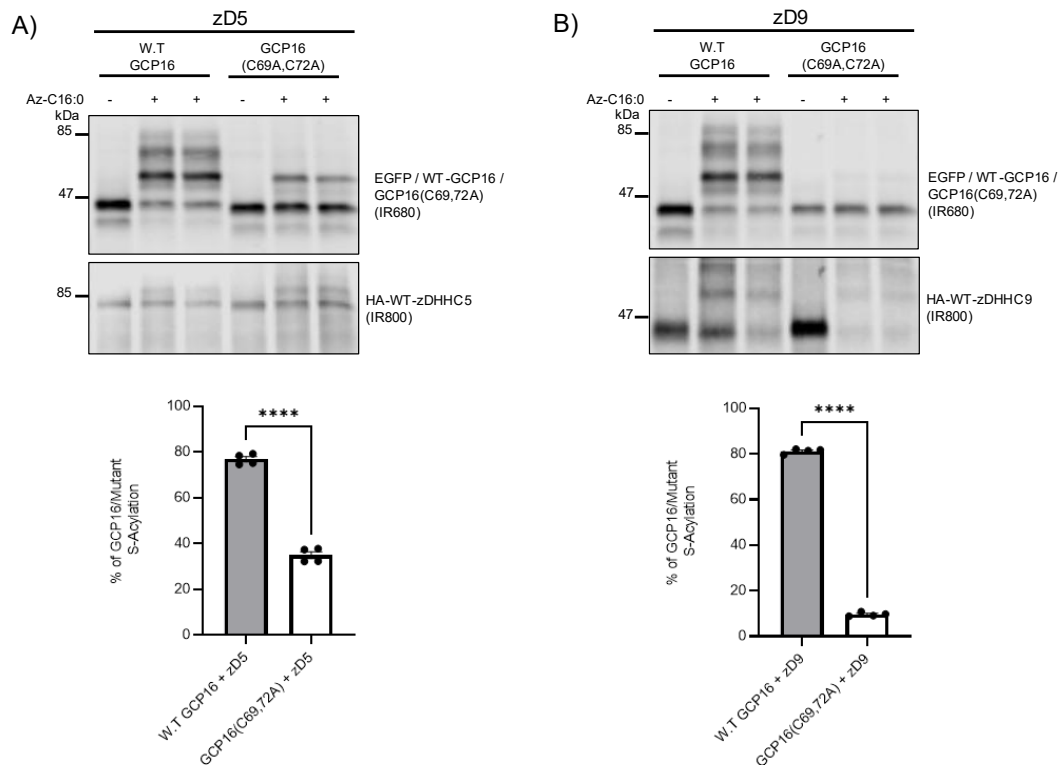


**Figure 3.17 Comparison of the S-acylation of EGFP-GCP16 (C69,72A) mutant when co-expressed with HA-zDHHC5 or HA-zDHHC9.**

HEK293 cells were transfected with plasmids encoding HA-zDHHC5 or HA-zDHHC9 together with EGFP-GCP16 wild-type or the EGFP-GCP16 (C69,72A) mutant. Approximately 24 hours later, cells were metabolically labelled with azide-palmitic acid (Az-C16:0; +) or palmitic acid as a control (-). Cell lysates were then reacted with alk-mPEG, which produces a 5 kDa band shift for every S-acylated cysteine. **A) Top**, Representative immunoblots showing EGFP-GCP16 wild-type and GCP16(C69,72A) mutant detected at (IR680) and the HA-tagged zDHHC5 (IR800). The molecular weight marker position is shown on the left side of all blots. **Bottom**, the quantitative data show mean  $\pm$  SEM of the S-acylation levels of both WT and mutant EGFP-GCP16. Data was analysed using an unpaired T-test (\*\*\*\* P < 0.0001; n=4). **B)** Same as for panel (A) except with HA-zDHHC9 rather than HA-zDHHC5. Data was analysed using an unpaired T-test (\*\*\*\* P < 0.0001; n=4 from two separate experiments).

The results of this experiment revealed a complete loss of S-acylation of the EGFP-GCP16(C69,72A) mutant with zDHHC9 (Figure 3.17B). However, with zDHHC5, there was a significant decrease in S-acylation of the EGFP-GCP16(C69,72A) mutant compared with wild-type GCP16, but still almost 40% S-acylation was retained, with band shifts of the GCP16 mutant clearly visible in the immunoblots when co-expressed with HA-zDHHC5 (Figure 3.17A, top panel). This finding suggests that one of the remaining cysteines (positions 24 or 81) was being S-acylated by HA-zDHHC5.

To pursue the observation that the EGFP-GCP16(C69,72A) mutant was still S-acylated when co-expressed with HA-zDHHC5, GCP16 mutants were designed to have the remaining cysteines at positions 24 or 81 substituted (together with the already mutated C69 and C72 codons). The synthesised mutants were EGFP-GCP16(C24,69,72A) and EGFP-GCP16(C69,72,81A). These mutants were used in a 5 kDa click chemistry assay in which HEK293 cells were transfected with the GCP16 mutants together with either HA-zDHHC5, HA-zDHHC9 or pEF-BOS-HA (negative control) and 24 hours later, the click chemistry assay was performed and samples analysed by immunoblotting.

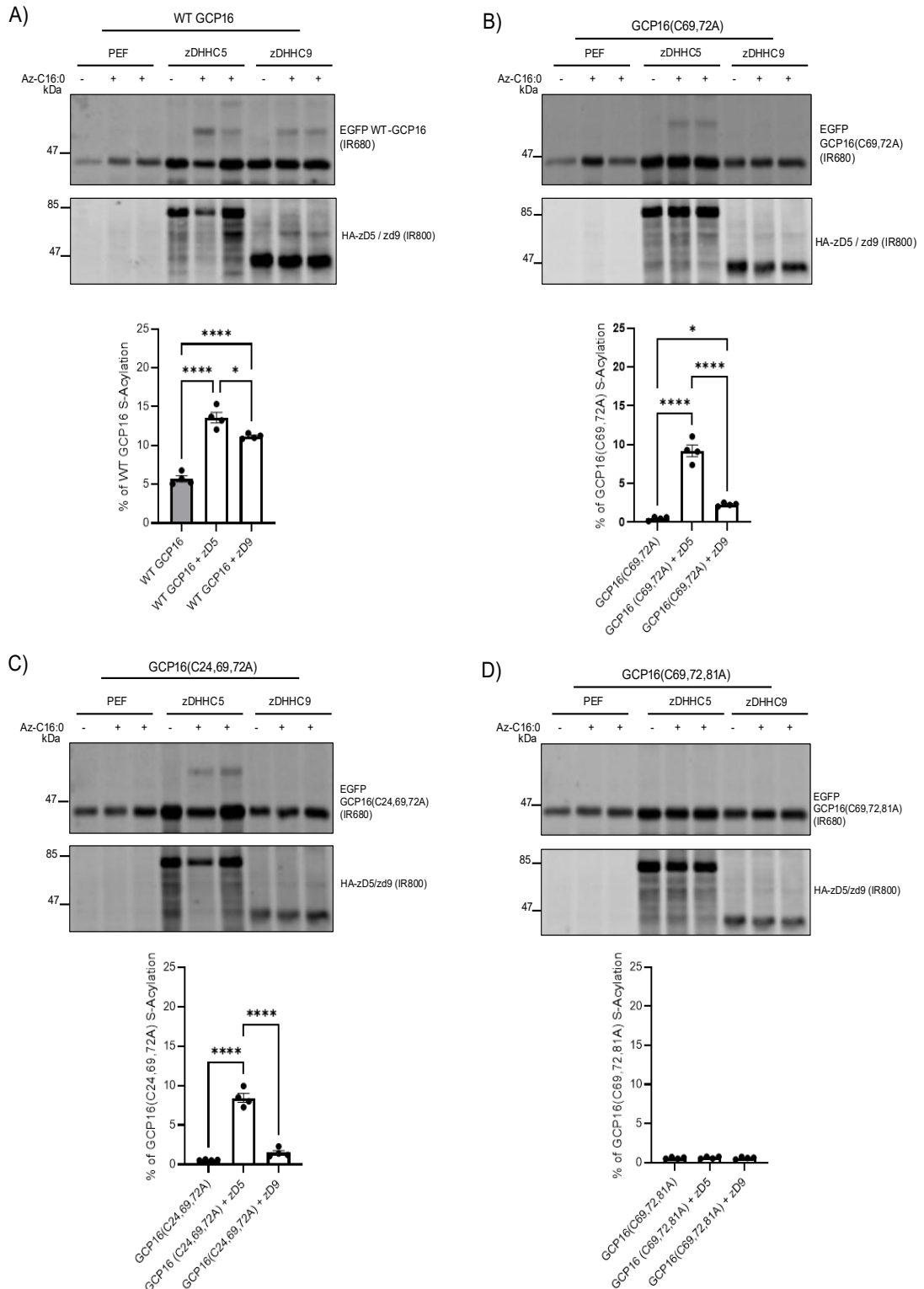


**Figure 3.18 Analysis of S-acylation of EGFP-GCP16 cysteine mutants by HA-zDHHC5 and HA-zDHHC9.**

HEK 293 cells were transfected HA-zDHHC5, HA-zDHHC9 or PEF (empty plasmid) as negative control, together with either EGFP-GCP16 wild-type (**A**), EGFP-GCP16(C69,72A) (**B**), EGFP-GCP16(C24,69,72A) (**C**), or EGFP-GCP16(C69,72,81A) (**D**). After approximately

24 hours, cells were metabolically labelled with palmitic acid Azide (Az-C16:0; +) or palmitic acid (-) for 4 hours, followed by cell lysis and reaction with a click mixture containing Alk-mPEG. Samples were then resolved by SDS-PAGE and analysed by immunoblotting, where any S-acylated bands appear as a 5 kDa band shift. EGFP-GCP16 was detected at IR860, and the HA-zDHHC5/zDHHC9 at IR800. The molecular weight marker position is shown on the left side of all blots. Graphs show mean S-acylation  $\pm$  SEM, and data were analysed using a one-way ANOVA with Tukey post-test (n=4 from two separate experiments). \*\*\*\*P<0.0001, \*P<0.005.

Figure 3.18 shows that S-acylation of EGFP-GCP16 wild-type was significantly increased by both zDHHC5 and zDHHC9. For the EGFP-GCP16(C69,72A) mutant, almost 10% of the protein was S-acylated by HA-zDHHC5 with a clearly visible five kDa band shift, whereas only 1-2% of this mutant was S-acylated by HA-zDHHC9 with almost no visible band shift signal seen in the immunoblots. The triple cysteine mutant EGFP-GCP16(C24,69,72A) showed a similar S-acylation percentage as EGFP-GCP16(C69,72A), indicating that the one remaining cysteine in this mutant (C81) might be modified by HA-zDHHC5. Indeed, this was supported by results with mutant EGFP-GCP16(C69,72,81A), where almost no S-acylation of the mutant was seen with zDHHC5 or zDHHC9, thus supporting that cysteine-81 is exclusively S-acylated by HA-zDHHC5, together with the known acylation sites at cysteines 69 and 72.

### 3.4 Discussion

This first results chapter has described several novel observations that are important for the S-acylation field. The novel findings include: (i) reciprocal stabilisation of GCP16 and zDHHc5/9; (ii) the interaction of GCP16 and Golga7b with both zDHHc5 and zDHHc9; (iii) the specific S-acylation of GCP16, but not Golga7b, by zDHHc9; (iv) homo- and hetero-dimerisation of GCP16 and Golga7b; and (v) different S-acylation patterns of GCP16 mediated by zDHHc5 *versus* zDHHc9. These findings provide new insights into these accessory proteins, which are discussed in more detail below.

#### 3.4.1 GCP16 and zDHHc5/zDHHc9 show reciprocal stabilisation

The intricate mechanisms of enzyme modulation are pivotal for understanding cellular processes and identifying potential therapeutic targets. GCP16 has been largely considered an accessory protein of zDHHc9, but it can also interact with zDHHc5 (Ko *et al.*, 2019). Furthermore, Golga7b has also been reported as a zDHHc5 accessory protein that regulates the localisation of this enzyme (Woodley and Collins, 2019). Given the close amino acid similarity of GCP16 and Golga7b and their localization at the Golgi, it was important to develop a clearer understanding of their relationships with zDHHc9 and zDHHc5 and to identify conserved features and differences in their interactions.

The first step was to compare the reciprocal effect of both zDHHc9 and zDHHc5 on GCP16 stability. Indeed, previous work has suggested a role for the yeast GCP16 orthologue Erf4 in regulating the stability of the acyltransferase Erf2 (Mitchell *et al.*, 2012). To explore the effects on protein stability, we used the protein synthesis inhibitor cycloheximide (Schneider-Poetsch *et al.*, 2010) in a chase assay, allowing the amount of protein remaining after 8 hours of protein synthesis inhibition to be established (Locatelli *et al.*, 2020). Interestingly, the stability of GCP16 was



significantly increased when it was co-expressed with both zDHHC5 and zDHHC9 (Figure 3.1). Furthermore, this effect on stability was reciprocal, as both zDHHC5 and zDHHC9 exhibited increased expression levels when co-expressed with GCP16. The work of Bartels *et al.* (1999) on *Saccharomyces cerevisiae* led to the identification of the Erf2/Erf4 complex, and it was subsequently reported that levels of Erf2 protein (the zDHHC9 counterpart) were reduced in cells lacking Erf4 (GCP16 counterpart) by Lobo *et al.* (2002). Indeed, Mitchell *et al.* (2012) proposed that Erf4 protects Erf2 from ubiquitination-dependent degradation, and this might also apply to the mammalian zDHHC9-GCP16 complex, providing a possible explanation behind the increased stability of zDHHC9 and zDHHC5 with GCP16 co-expression seen in the results of this chapter. This observation is also consistent with the work of Nguyen *et al.* (2023) who showed decreased oligomerisation of zDHHC9 in the presence of GCP16, suggested to represent increased stability of the enzyme. By contrast, the direct stabilisation of zDHHC5 by GCP16 has not previously been reported, although Ko *et al.* (2019) did report that the GCP16-zDHHC5 complex is stabilised by localisation to the plasma membrane of HT-1080 cells. Moreover, Golga7b was also found to stabilise zDHHC5 by localizing it to the plasma membrane (Woodley and Collins, 2019). The reciprocal effects of the zDHHC enzymes on GCP16 stability have not previously been reported, and it will be interesting to explore in future work if the ubiquitination of GCP16 is reduced when in complex with these zDHHC enzymes, or if it is the S-acylation of GCP16 that stabilises this protein.

After establishing these reciprocal stabilising effects between GCP16 and zDHHC5/zDHHC9, the impact of these interactions on S-acylation was examined. Mitchell *et al.* (2012) previously reported that Erf4 (GCP16 counterpart) prevents the hydrolysis of the S-acylated intermediate palmitoyl-Erf2 by shielding the active site from water molecules. The work presented in this chapter also shows that GCP16 can influence the S-acylated state of both zDHHC9 and zDHHC5, consistent with the

work of Mitchell *et al.* (2012) on the Erf2/Erf4 interaction. Thus, GCP16 is likely to be of fundamental importance to the S-acyltransferase activity of zDHHC9 and might also modulate the S-acylation/activity of zDHHC5. It will be interesting to develop a more expansive set of mutant forms of GCP16 and zDHHC5/9 that disrupt their interaction and examine the ability of these mutants to functionally rescue the knockdown of these proteins. For example, siRNA-mediated knockdown of zDHHC9 has been shown to reduce dendrite growth and formation of inhibitory synapses in primary hippocampal cultures (Shimell *et al.*, 2019), and it would be interesting to examine the effects of GCP16-binding mutants of this enzyme on rescue of these neuronal phenotypes.

#### **3.4.2 GCP16 interactions with different zDHHC enzymes**

GCP16 was initially considered to be a specific accessory protein of zDHHC9 (Swarthout *et al.*, 2005), but subsequent studies showed that zDHHC5 is also a target for GCP16 interaction (Ko *et al.*, 2019). Thus, we widened the analysis to include the potential interactions of GCP16 with other Golgi-localised S-acylation enzymes. To limit this analysis, we focused on specific Golgi zDHHC enzymes that are well-established to be active (Chamberlain and Shipston, 2015). Therefore, we included zDHHC3 and zDHHC7, which are highly active enzymes that mediate the S-acylation of a broad array of substrates (Lemonidis *et al.*, 2014). Both of these enzymes displayed significantly lower binding with GCP16 compared to zDHHC5 and zDHHC9 (Figure 3.4). Similarly, zDHHC13 and zDHHC17, related enzymes which interact with the S-acylated proteins SNAP25 and CSP (Lemonidis *et al.*, 2014), also displayed a lower binding capacity with GCP16 compared to zDHHC5 and zDHHC9. These results suggest that GCP16 has some level of specificity and selectivity towards zDHHC5 and zDHHC9; however, binding to the other enzymes was still detected in our assays (above the background binding to EGFP). Very recent work reported that GCP16 forms complexes with zDHHC14 and zDHHC18, which are more highly

related to zDHHC9 than zDHHC3/7/13/17. Furthermore, the complexes of GCP16 with zDHHC14 and zDHHC18 were functional as they mediated Ras S-acylation (Yang *et al.*, 2024). Based on these observations and our own, it is clear that a wider analysis of the interaction of GCP16 (and Golga7b) with the full zDHHC family would be interesting to explore in future work. For example, testing how the depletion of these accessory proteins affects the S-acylation of known substrates of specific zDHHC enzymes would be an interesting first step.

As GCP16 S-acylation is essential for anchoring it onto the Golgi (Ohta *et al.*, 2003), we also examined how these different Golgi enzymes affected GCP16 S-acylation. Previous work (Lemonidis *et al.*, 2014) reported that the strength of interaction of zDHHC enzymes with protein partners does not directly correlate with S-acylation; for example, it was shown that zDHHC3 and zDHHC7 interact much more weakly with CSP and SNAP25 than zDHHC17 does and yet the S-acylation of these substrates by zDHHC3 and zDHHC7 was much higher (Lemonidis *et al.*, 2014). In agreement with these findings, the work presented in this chapter showed that both zDHHC3 and zDHHC7 S-acylate GCP16 more efficiently than either zDHHC9 or zDHHC5 (which interact more strongly with GCP16). Thus, there may be a broader set of enzymes that can S-acylate GCP16, even if the reciprocal effects on stability are more specific to zDHHC5 and zDHHC9.

### **3.4.3 Comparison of the interactions of Golga7b and GCP16 with zDHHC enzymes**

Swarthout *et al.* (2005) established that zDHHC9 and GCP16 are the human orthologues of Erf4 and Erf2, respectively. However, the possible role of GCP16 in S-acylation was widened by the work of Ko *et al.* (2019), who reported the zDHHC5-GCP16 interaction. This study was published around the same time as the work of Woodley and Collins (2019) who reported a regulatory role of Golga7b for zDHHC5. Golga7b was established to be essential for the plasma membrane localisation of

zDHHC5 by preventing its internalisation through clathrin-mediated endocytosis. Furthermore, Golga7b was important for the S-acylation activity of zDHHC5 as it was found to play a fundamental role in the modification of desmoglein-2 and plakophilin-3, substrates of zDHHC5 (Woodley and Collins, 2019). As Golga7b shares 61% amino acid identity with GCP16 and given the reported interactions of both proteins with zDHHC5, we compared the interactions and impacts of these proteins on zDHHC5 and zDHHC9 and whether they have interchangeable effects.

In addition to examining the interaction of GCP16 and Golga7b with zDHHC5 and zDHHC9, we also explored their possible homo- and hetero-dimerisation. This avenue is currently unexplored, but it could allow for a more detailed understanding of the mechanistic properties of these proteins and their possible collaboration in the shuttling and trafficking of zDHHC5 and zDHHC9. Indeed, the results of these analyses were quite interesting (Figure 3.8) as Golga7b exhibited a higher binding than GCP16 to zDHHC5, and this was also seen to a lesser extent with zDHHC9. Furthermore, the formation of a GCP16 homodimer was detected as EGFP-GCP16 co-immunoprecipitated HA-GCP16, and indeed HA-GCP16 also formed a heterodimer with EGFP-Golga7b. The hetero-dimerisation of GCP16-Golga7b is especially interesting as it raises the possibility that these proteins work together in regulating zDHHC enzymes. Indeed, there is also evidence for oligomerisation of zDHHC enzymes (Lai and Linder, 2013), and it will be interesting to explore the potential role of GCP16/Golga7b in this process. Regarding the interactions of Golga7b and GCP16 with zDHHC5/9, knockdown experiments will be a useful approach to explore redundancy in the system, examining the effects of individual and combined knockdown of GCP16 and Golga7b on zDHHC5/9 cell functions. Here, it will be important to study the effects of these knockdowns on different systems and cell types to identify any cell type-specific effects linked to the relative expression profiles of GCP16 and Golga7b.

A comparison of the effects of zDHHc5 and zDHHc9 on GCP16 and Golga7b stability revealed some interesting differences. GCP16 stability was higher in the presence of both zDHHc5 and zDHHc9 (Figure 3.1), whereas stability of Golga7b was only increased with zDHHc5 (Figure 3.9). These changes in stability might be linked to the finding that GCP16 is S-acylated by both zDHHc5 and zDHHc9, whereas only zDHHc5 is active against Golga7b. This reasoning is supported by Woodley and Collins (2019), who reported that a Golga7b S-acylation mutant could not be detected unless MG132 inhibited proteasome activity.

It will be interesting to explore the mechanistic basis for these differences in S-acylation and, in particular, solving the cryoEM structure of both enzymes in complex with GCP16 and Golga7b would be especially revealing (Yang *et al.*, 20124). Given the interaction of zDHHc5 with GCP16 and its ability to S-acylate this accessory protein, it will also be interesting to better understand whether zDHHc5 can compensate for any changes caused by the loss of zDHHc9 function in humans. For example, it would be interesting to explore if brain regions with lower zDHHc5 expression show more overt changes than those with higher zDHHc5 expression in the presence of *zDHHc9* mutations (Baker *et al.*, 2015).

#### **3.4.4 Predicting GCP16 interactions using the Alphafold 3D protein prediction tool**

The 3D protein prediction tool AlphaFold2 provides a unique platform to undertake protein structure (and protein complex) prediction by using machine learning analysis of the protein's amino acid sequence to predict the structure and achieve atomic accuracy (Jumper *et al.*, 2021; Senior *et al.*, 2020). This tool was capable of predicting the zDHHc9-GCP16 and zDHHc5-GCP16 complex structures (Figure 3.10). Navigating the predicted interaction interfaces, two potentially critical amino acids in the GCP16 structure, Arginine-118 and Arginine-121, were identified. These amino acids are predicted to form different hydrogen bonds with zDHHc9 and zDHHc5.

Arg-118 was found to form bonds with Glu-80 and Asp-79, and Arg-121 formed bonds with Glu-80 and Pro-74 in zDHHC9. Whereas for zDHHC5, Arg-118 forms bonds with Pro-95 and Glu-101, and Arg-121 forms bonds with Leu-98, Ile-120. The study of Yang *et al.* (2024) showed that other binding interfaces also contribute to the GCP16-zDHHC9 interaction. Nevertheless, we used site-directed mutagenesis to specifically examine the importance of Arg-118/121 for zDHHC5/zDHHC9 co-immunoprecipitation, and the initial results (Figure 3.11) showed almost no change in zDHHC5 or zDHHC9 binding to this mutant. This presumably reflects remaining interactions with other binding interfaces.

It is important to note that AlphaFold may not accurately predict all protein complex structures. For example, He *et al.* (2022) reported testing the validity of predicted G protein-coupled receptors against verified experimental structures, and although the researchers confirmed the ability of AlphaFold2 to predict the overall backbone of the GPCRs, they noted limitations when it comes to extracellular domains or transmembrane domains. Thus, it is important to proceed cautiously when using predictions collected via AlphaFold. Although the AlphaFold models for GCP16-zDHHC9 are based on an experimentally-verified structure (Yang *et al.* 2024), this is not the case for zDHHC5.

#### **3.4.5 Overall effect of GCP16 S-acylation on its interaction with zDHHC5 and zDHHC9**

To explore the role of GCP16 S-acylation in its interaction with zDHHC enzymes, a mutant with alanine substitutions of the known S-acylated cysteines (69,72) was examined. Co-immunoprecipitation results (Figure 3.13) imply that the zDHHC5-GCP16 interaction may be different from zDHHC9-GCP16, as only zDHHC5 exhibited a significant decrease in binding to the S-acylation mutant. This suggests

that the interaction of zDHHc5 with GCP16 is S-acylation-dependent (or relies on cysteines 69 and 72), in contrast to the interaction of this accessory protein with zDHHc9.

The fact that zDHHc9-GCP16 complex formation appears to be S-acylation independent is interesting because S-acylation was reported to be required for Golgi localisation of GCP16 (Ohta *et al.*, 2003). It will be interesting to confirm that the interaction truly is S-acylation-independent and is not being affected by the over-expression conditions employed. To test this, the codons of the cysteines in GCP16 could be mutated in the GCP16 genes in a cell line (e.g., using CRISPR), allowing the effects of this to be examined at endogenous expression levels. It is not clear why zDHHc5 does not interact with the GCP16 S-acylation mutant, but it could be that GCP16 has an underlying weak affinity for Golgi membranes that brings it into proximity with Golgi-localised zDHHc9 but not plasma membrane-localised zDHHc5 – and that targeting of GCP16 to the plasma membrane requires S-acylation. Indeed, the GCP16 S-acylation mutant was unable to significantly increase the stability of either zDHHc5 or zDHHc9. In the case of zDHHc9, this suggests that complex formation alone is not enough to enhance the stability of the enzyme.

By using click chemistry S-acylation assays, a marked increase in the formation of the zDHHc5 S-acylated intermediate was detected when co-expressed with the GCP16 S-acylation mutant, and surprisingly, a decreased level of S-acylation with wild-type GCP16. zDHHc9, on the other hand, showed a significant increase in S-acylation with both wild-type and cysteine mutant GCP16. The results with zDHHc5 show a clear separation in the effects of GCP16 on the stability of the enzyme versus the S-acylation of the enzyme.

One of the benefits of the five kDa mPEG click chemistry assay that was used to study S-acylation (Salaün *et al.*, 2020) is that it reveals every S-acylated cysteine in the form of a five kDa band-shift. In the previous assay, a band-shift in the EGFP-

GCP16 (C69,72A) mutant was apparent when co-expressed with zDHHC5 but not zDHHC9. This suggests that one of the remaining cysteines in GCP16 is exclusively S-acylated by zDHHC5 but not zDHHC9. This could also indicate a different spatial orientation of GCP16 at the membrane when it is S-acylated by zDHHC5 as a result of the additional S-acylation site becoming membrane-attached. Indeed, we found that only zDHHC5 was capable of stabilising the GCP16 S-acylation mutant, which might reflect the modification of additional cysteines in this mutant by zDHHC5 (but not zDHHC9). This is novel data that can strengthen the argument that GCP16 itself is a dynamic accessory protein, being anchored differently when S-acylated by different partner enzymes, which can also mean a different spatial orientation and perhaps also a different localisation of GCP16 when S-acylated by zDHHC5.

To determine which of the remaining cysteines in GCP16 is S-acylated by zDHHC5, mutants were designed in which three cysteines (including Cys-69 and Cys-72) were mutated into alanine, which resulted in the identification of cysteine-81 as a third cysteine modified by zDHHC5. It will be interesting to examine how the modification of this additional cysteine affects the localisation of GCP16. It would also be interesting to undertake acyl-PEG switch assays (Yokoi *et al.*, 2016) on endogenous GCP16 to determine the number of cysteines that are modified endogenously and how this changes with depletion (or over-expression) of zDHHC5 and zDHHC9.

In conclusion, the data collected in this chapter extend our understanding of the interactions of GCP16/Golga7b accessory proteins with zDHHC enzymes and the functional effect of these interactions, in terms of protein stability and S-acylation. The different cysteines S-acylated in GCP16 by zDHHC5 and zDHHC9 are likely to lead to distinct membrane orientations of the accessory protein that can underpin different structural interactions with zDHHC9 and zDHHC5. A major breakthrough for our understanding here would be to solve the cryoEM structure of the GCP16-zDHHC5 complex. Similarly, insights into the structural differences in complexes containing



GCP16 and Golga7b are likely to shine new light on how these accessory proteins regulate the wider zDHHC family.

**CHAPTER 4**

**MOLECULAR ANALYSIS OF *ZDHH*C9  
MUTANTS (R96W AND R148W) LINKED TO  
PATHOPHYSIOLOGY**

## Chapter 4

### Molecular analysis of *ZDHHC9* mutants (R96W and R148W) linked to pathophysiology

#### 4.1 Introduction

Several studies have identified a link between *ZDHHC9* mutations and X-linked intellectual disability (XLID). The first study on *zDHHC9* was undertaken by Raymond *et al.* (2007), in which four mutations of the *ZDHHC9* gene associated with XLID were described. This study reported one splice site mutation, one frameshift mutation, and two missense mutations, all affecting the highly conserved catalytic DHHC domain of *zDHHC9*. The splice site and frameshift mutations led to the complete loss of the DHHC catalytic domain, while the missense mutations resulted in single amino acid changes within this domain (R148W and P150S).

Subsequent investigations by Mitchell *et al.* (2014) explored the molecular consequences of the R148W and P150S amino acid substitutions. Their findings revealed that these amino acid changes significantly disrupted the S-acylation process. Specifically, the R148W substitution led to rapid hydrolysis of the *zDHHC9* autoacylated state, which is closely coupled to enzyme S-acylation activity (Jennings and Linder, 2012). In contrast, the P150S substitution decreased the initiation of autoacylation, with a similar negative impact on enzyme S-acylation activity (Mitchell *et al.*, 2014). By compromising the integrity of autoacylated *zDHHC9*, these mutations will likely disrupt the S-acylation of various proteins crucial for normal neural development (Chamberlain and Shipston, 2015).

A subsequent study by Tzschach *et al.* (2015) identified another point mutation in patients with XLID, leading to an R96W substitution in the *zDHHC9* enzyme. Unlike the R148W and P150S substitutions within the DHHC catalytic domain, the R96W substitution occurs within an upstream cytosolic region of unknown function. The

exact mechanism by which this amino acid change affects zDHHC9 remains unclear, but it presents an intriguing avenue for further investigation.

Many intellectual disability syndromes have been linked to *ZDHHC9* mutations; Raymond *et al.* (2007) described symptoms of developmental delay and intellectual disability, which are the hallmark of Marfanoid habitus, suggesting Marfan syndromes as a diagnosis for males with *ZDHHC9* mutations. However, none of the study subjects met the Ghent criteria, a tool that aids the diagnosis and management of patients suffering from Marfan syndrome; it detects clinical and cardiac features to diagnose and determine the severity of the cases (Ramlingam and Natarajasundaram, 2015). Baker *et al.* (2015) later identified Rolandic epilepsy (RE) as a feature of people with *ZDHHC9* mutations. RE is the most common type of childhood epilepsy and is also known as Benign Childhood Epilepsy with Centro-Temporal Spikes, characterised by delayed speech and language development with impaired comprehension and variably impaired cognitive function (Stevenson *et al.*, 2012). RE was suggested as a primary diagnosis for seven (out of nine) males with *ZDHHC9* mutations by Baker *et al.* (2015), where loss-of-function of zDHHC9 resulted in increased susceptibility to focal seizures, together with specific cognitive impairments and hypoplasia of the corpus callosum, highlighting anatomical and functional abnormalities accompanying *ZDHHC9* mutations. A clinical report by Schirwani *et al.* (2018) drew a comprehensive clinical picture of the manifestations imposed by *ZDHHC9* mutations, in which symptoms range from mild to severe cognitive impairments.

As discussed previously, several mutations in *ZDHHC9* cause intellectual disability, and while most of these mutations are linked to a loss of enzyme activity, the R96W change occurs outside of the catalytic domain, and it is unclear how this amino acid substitution disrupts zDHHC9 function. In this chapter, I undertook a comparison of the properties of zDHHC9 with either an R96W substitution or a R148W substitution,

to compare how these amino acid changes affect: (i) the zDHHC9-GCP16 interaction; (ii) the stability of zDHHC9 and GCP16; (iii) the S-acylation of zDHHC9 and GCP16; and (iv) zDHHC9 structure.

## **4.2 Results**

### **4.2.1 Sub-cloning of human zDHHC9 and mutants into the pEFBOS-HA vector**

At the early stages of this study, expression of human HA-zDHHC9 and the variants R148W and R96W could not be detected in transfected HEK293 cells using pcDNA3.1 constructs manufactured by Genscript Biotech (New Jersey, USA). The coding sequences were, therefore, sub-cloned into the pEFBOS-HA plasmid, which has been used extensively for the expression of mouse zDHHC proteins by our laboratory. For this, primers were designed to amplify the coding sequences with incorporated *Bam*H1 restriction sites at either end to facilitate cloning (refer to subcloning in section 2.3.3 and see Figure 4.1 for schematic). After confirming the identity of the sub-cloned coding sequences by sequencing, HEK293 cells were transfected with these plasmids and protein expression compared to cells expressing the mouse HA-tagged WT zDHHC9. Figure 4.1 shows that immunoreactive bands were detected for all proteins at the expected molecular weight, and these newly subcloned plasmids were used in all further experiments.

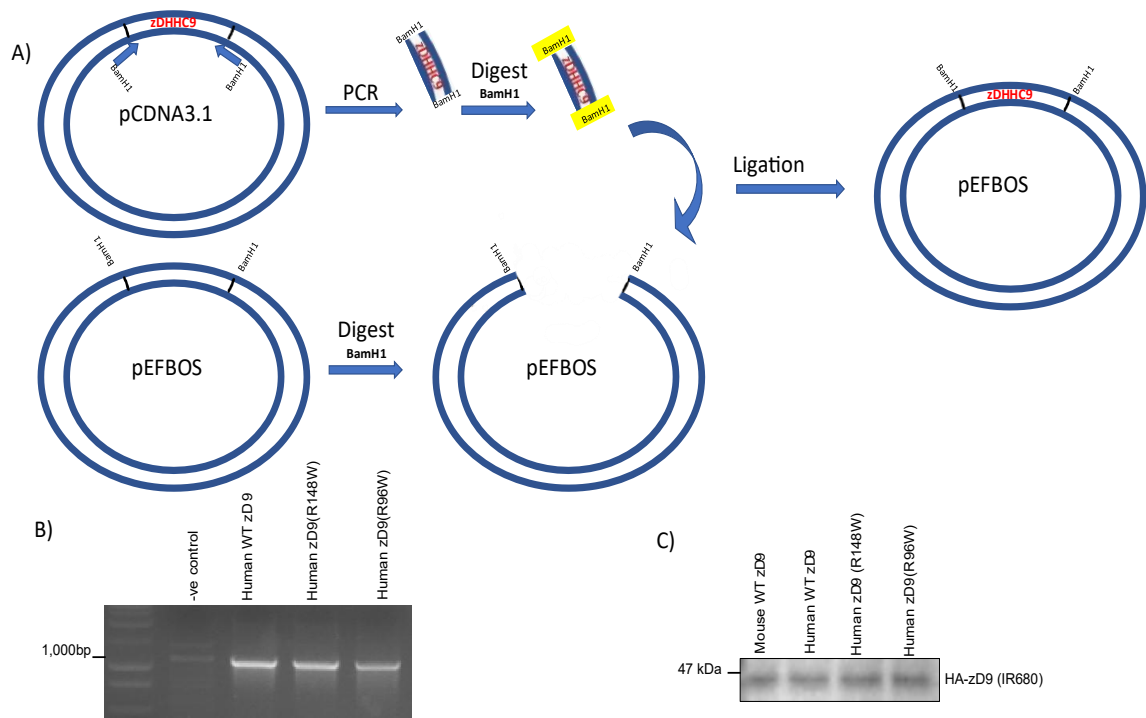


**Figure 4.1 Sub-cloning of zDHHc9 and mutants into the pEFBOS-HA vector**

**A)** Schematic of the sub-cloning process in which oligonucleotide primers containing *Bam*H1 restriction sites were used to amplify zDHHc9 wild-type and R96W/R148W mutant coding sequences from the pcDNA3.1 vector. The amplified products have *Bam*H1 restriction sites at both ends. PCR products (insert) and pEFBOS-HA vector (backbone) were then digested using *Bam*H1 and dephosphorylated with calf intestinal phosphatase enzyme to prevent the digested plasmid from self-annealing. Following this, the digested PCR mixture and digested plasmid were separated using agarose gel electrophoresis, and DNA was excised with the aid of UV illumination. These DNA bands were then purified and incubated with each other overnight in the presence of T4 DNA ligase enzyme. Following this, the ligation mixture was transformed into TOP10 chemically competent *E. coli* for antibiotic selection (kanamycin) and subsequent plasmid production. **B)** Image showing the zDHHc9 DNA after separation using agarose gel electrophoresis, visualized using UV illumination. The position of the 1,000 bp marker is shown on the left. **C)** After confirming the correct identities of sub-cloned zDHHc9 constructs in pEFBOS-HA vector *via* sequencing, HEK293 cells were transfected with these constructs together with mouse zDHHc9 in the same plasmid. After 24 hours, the cells were lysed, and the protein was revealed by immunoblotting. The position of the 47 kDa molecular weight marker is shown on the left.

#### 4.2.2 Analysis of the effects of R96W and R148W substitutions on the reciprocal stabilisation and interaction with EGFP-GCP16

Having confirmed the expression of HA-tagged human zDHHc9 constructs in HEK293 cells (Figure 4.1), the same techniques described in chapter 3 were then used to explore how the mutant zDHHc9 proteins were affected in their interaction with and S-acylation of GCP16. As a first step, the effects of the mutations on the

stability of HA-zDHHc9 and the impact of EGFP-GCP16 on the stability of the mutants were examined. Furthermore, the stability of EGFP-GCP16 when expressed with wild-type and mutant zDHHc9 was also examined. Thus, cycloheximide chase assays were performed in which HEK293 cells were transfected with plasmids encoding either EGFP or EGFP-GCP16 together with either HA-zDHHc9 wild-type, HA-zDHHc9 (R148W), or HA-zDHHc9 (R96W). For analysis of GCP16 stability, an additional transfection was included that had EGFP-GCP16 together with pEFBOS-HA as a negative control. After 24 hours, cells were either lysed directly or incubated in 50 µg/ml cycloheximide for 8 hours before lysis. The samples were then examined by immunoblotting. Figure 4.2A shows, as reported in Chapter 3, that EGFP-GCP16 stabilises HA-zDHHc9 wild-type. In contrast, there was no effect observed of EGFP-GCP16 on the HA-zDHHc9 R148W mutant (Figure 4.2B). The zDHHc9 R96W

mutant showed an increased stability in the presence of EGFP-GCP16, which was not as pronounced as the effect on wild-type HA-zDHHc9 (Figure 4.2C).

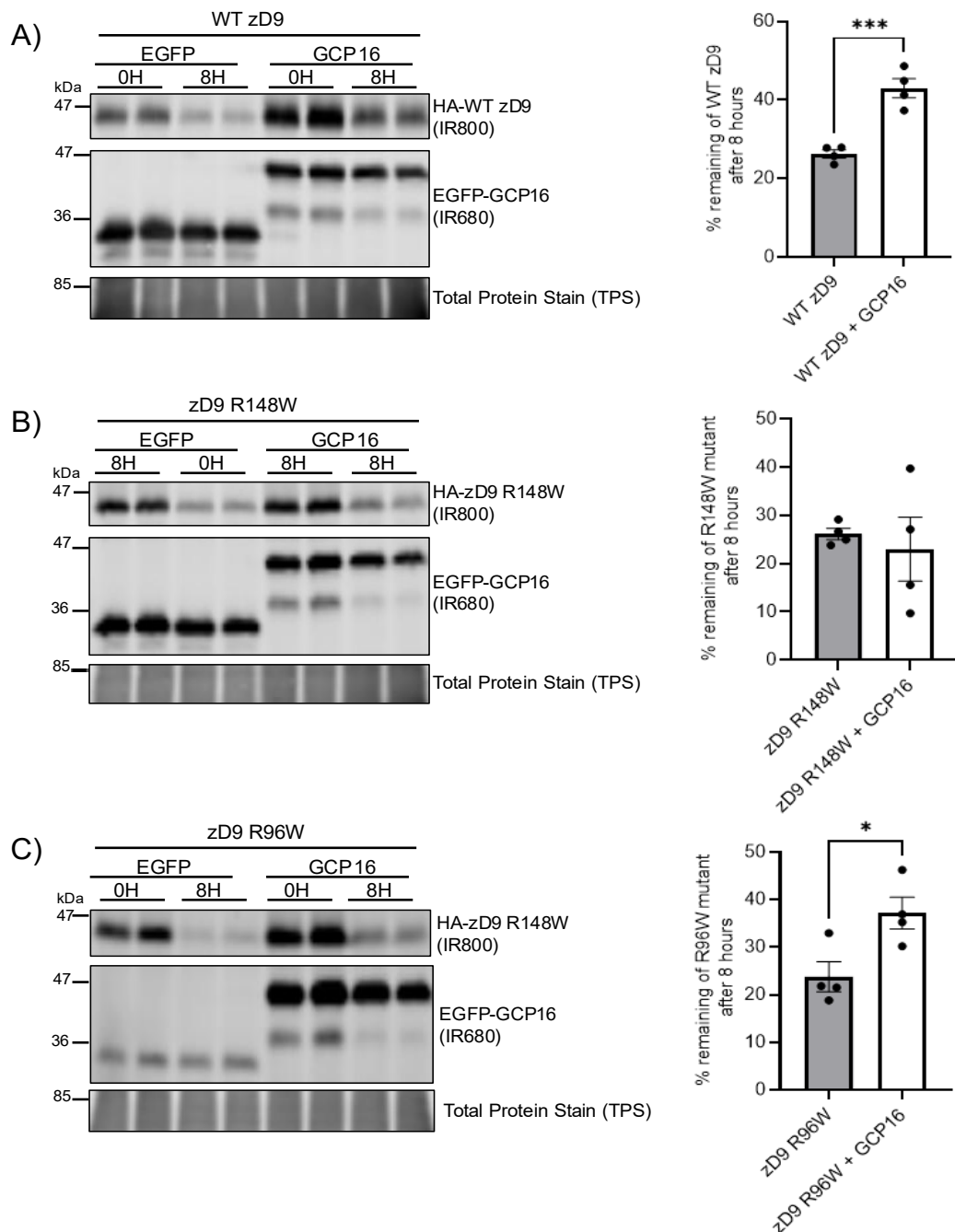


**Figure 4.2 Cycloheximide chase assays to assess the effect of EGFP-GCP16 on the stability of HA-zDHHc9 wild-type and the R96W and R148W mutants**

HEK293 cells were transfected with plasmids encoding HA-zDHHc9 (WT, R96W, or R148W) and EGFP-GCP16. Cells were either lysed immediately (0 H) after overnight transfection or instead incubated with cycloheximide for 8 hours before lysis (8 H). Samples were then examined by immunoblotting. The representative immunoblots show HA-zDHHc9 WT or mutants (IR800; top), EGFP/EGFP-GCP16 (IR680; middle), and the total protein stain (bottom). Representative blots are shown for **A)** HA-zDHHc9 wild-type, **B)** HA-zDHHc9 (R148W), and **C)** HA-zDHHc9 (R96W) in the left panel. Quantified data showing the



percentage of each HA-zDHHHC9 protein remaining after 8 hours of cycloheximide treatment in the absence and presence of EGFP-GCP16 is shown on the right of all panels. The data was compared using an unpaired T-Test (\*P <0.05, \*\*\*P<0.001; n=4 from two separate experiments).

Next, the reciprocal analysis was performed, examining the effect of HA-zDHHHC9 wild-type and mutant proteins on EGFP-GCP16 stability (Figure 4.3). HA-zDHHHC9 wild-type and the HA-zDHHHC9 (R96W) enhanced the stability of EGFP-GCP16 (panels A and C), whereas HA-zDHHHC9 (R148W) (panel B) did not cause a stabilisation of EGFP-GCP16.

Thus, overall, the R96W mutant behaves broadly similarly to wild-type zDHHHC9 in these assays, whereas there is a loss of the reciprocal stabilisation of zDHHHC9 and GCP16 in the presence of the R148W substitution.

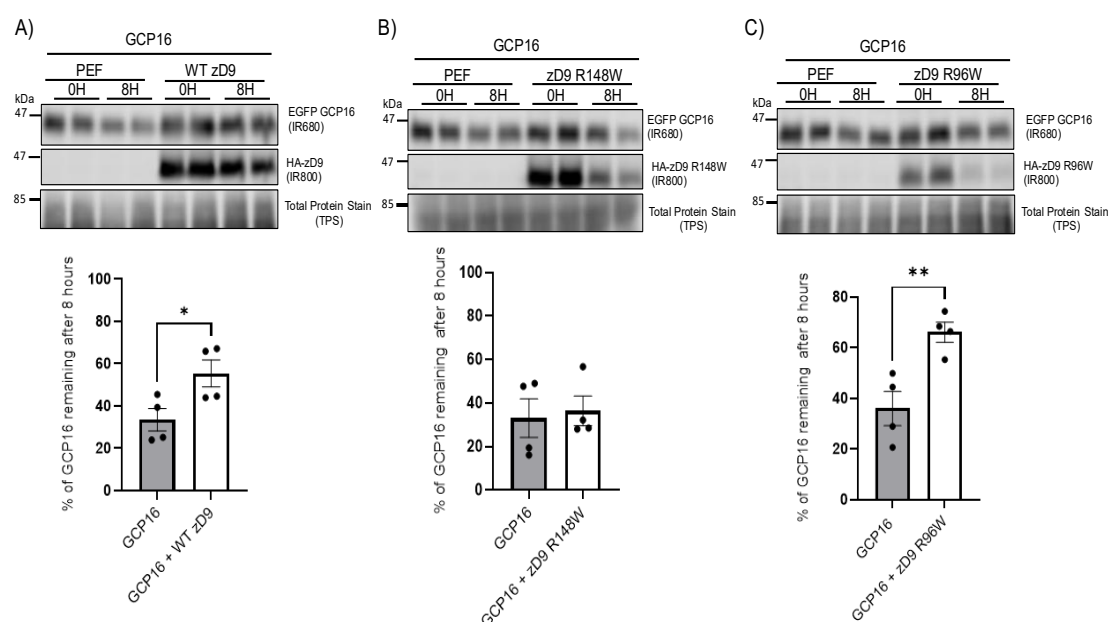


**Figure 4.3 Cycloheximide chase assays to assess the effect of HA-zDHHHC9 wild-type and mutant proteins on the stability of EGFP-GCP16.**

HEK293 cells were transfected with plasmids encoding EGFP-GCP16 together with either HA-zDHHHC9 wild-type (A), or the R148W (B) or R96W (C) mutants; PEF (empty plasmid) was used as a negative control. Approximately twenty-four hours post-transfection, cells were either lysed immediately (0 H) or treated with cycloheximide for 8 hours before lysis (8 H). Lysates were then examined by immunoblotting. In panels A-C, EGFP-GCP16 was detected at IR680 (top), the HA-tagged zDHHHC9 was detected at IR800 (middle), and the total protein stain at IR680 (bottom). The position of molecular weight markers is shown on the left. The bottom panels show quantified data for the percentage of EGFP-GCP16 remaining after 8 hours of cycloheximide treatment. Data was analysed using an unpaired T-test (\*P<0.05, \*\*P<0.01; n=4 from two separate experiments).

Given that the R98W and R148W proteins showed differences in their ability to stabilize EGFP-GCP16, it was next examined whether the mutant HA-zDHHC9 proteins have an altered interaction with EGFP-GCP16. For this, co-immunoprecipitation experiments were performed. HEK293 cells were transfected with either EGFP or EGFP-GCP16 together with HA-zDHHC9 wild-type or R148W and R96W mutants. After 24 hours, cells were lysed and incubated with GFP-trap beads to capture EGFP-GCP16. Immunoblotting analyses were then performed to determine the level of co-IP of the different HA-zDHHC9 proteins with EGFP-GCP16. Figure 4.4 shows a significant decrease in the amount of the R148W mutant captured by EGFP-GCP16, compared to wild-type zDHHC9. In contrast, the R96W mutant had a similar level of capture as the HA-zDHHC9 wild-type. Despite these differences, it should be noted that the R148W mutant still showed a robust binding to GCP16, and the observed decrease in co-IP may be linked to the lower expression levels of the R148W mutant in the input samples (Figure 4.4A, lower panel). This lower expression of R148W is presumably linked, at least in part, to its decreased stabilisation by GCP16 compared to wild-type zDHHC9 and the R96W mutant (Figure 4.2).

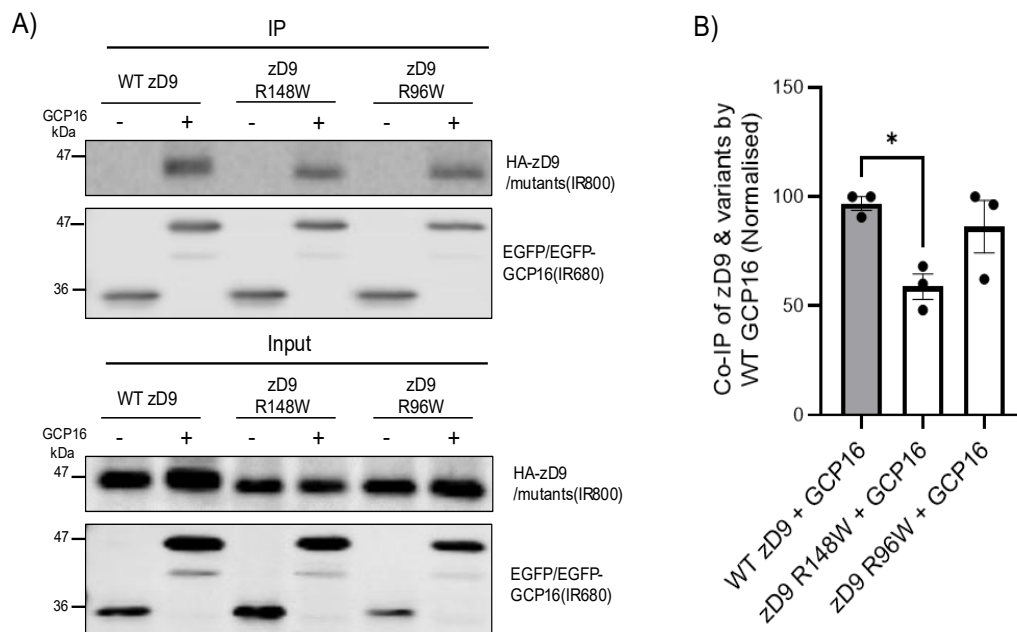


**Figure 4.4 Co-Immunoprecipitation of HA-zDHHC9 wild-type and R148W/R96W mutants with EGFP-GCP16.**

HEK293 cells were transfected with plasmids encoding EGFP or EGFP-GCP16 with one of HA-zDHHHC9 wild-type or R148W/R96W mutants. After approximately 24 hours, cells were lysed and incubated with GFP-trap beads to capture EGFP-tagged proteins alongside any bound HA-zDHHHC9 proteins. Samples were then analysed by immunoblotting. **A)** Representative immunoblots showing the HA-zDHHHC9 wild-type and mutants detected at IR800 (top) and EGFP/EGFP-GCP16 detected at IR680 (bottom) in input and immunoprecipitated (IP) samples. **B)** Quantified data (normalised) showing the co-IP of zDHHHC9 proteins with EGFP-GCP16 and analysed using a one-way ANOVA with Tukey post-test (\* $P < 0.05$ ;  $n = 3$  from three separate experiments).

#### **4.2.3 Analysis of the interaction of R96W and R148W zDHHHC9 mutants with the substrate protein EGFP-H-Ras**

The previous results found that the R148W zDHHHC9 mutant may have a partially reduced interaction with EGFP-GCP16. Furthermore, this mutant also showed a reduced ability to stabilise and to be stabilised by EGFP-GCP16. To explore if the R148W and R96W substitutions impacted their interaction with substrate proteins, their binding to EGFP-H-Ras was also assessed. H-Ras has been identified by many researchers (e.g. Swarthout *et al.*, 2005; Hernandez *et al.*, 2017) to be S-acylated at two sites, cysteine 181 and 184, by zDHHHC9. However, there has been no reported analysis of how zDHHHC9 interacts with or recognises Ras proteins. A co-immunoprecipitation assay was therefore performed to examine the zDHHHC9-H-Ras interaction, in which HEK293 cells were transfected with EGFP or EGFP-H-Ras together with one of the plasmids encoding HA-zDHHHC9 wild-type or variants R148W or R96W; 24 hours later, samples were incubated with GFP-trap beads to capture EGFP-H-Ras, and the recovered samples were analysed by immunoblotting.

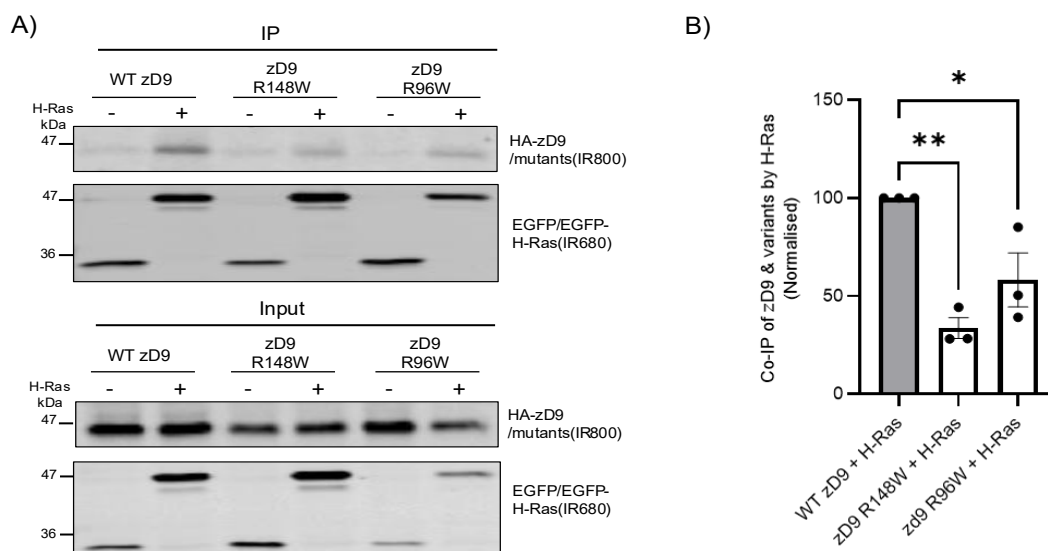


**Figure 4.5 Analysis of the interaction of HA-zDHHc9 wild-type and R148W/R96W mutants with EGFP-H-Ras**

HEK293 cells were transfected with plasmids encoding EGFP or EGFP-H-Ras and HA-zDHHc9 wild-type or R148W/R96W mutants. Approximately 24 hours later, cells were lysed and incubated with GFP-trap beads to capture EGFP-tagged proteins. The samples were then analysed by immunoblotting. **A)** Representative blot showing the HA-zDHHc9 wild-type and R148W/R96W mutants detected at IR800, with the lower blot showing EGFP/EGFP-H-Ras detected at IR680 (top blots show the IP, lower blots show the input). The position of molecular weight markers is shown on the left. **B)** Quantified data (normalised) was tested using a one-way ANOVA with Tukey post-test to compare H-Ras binding with zDHHc9 and mutants. The R148W and R96W mutants had a significant loss of binding compared to WT zDHHc9 (\* denotes  $P < 0.05$  and \*\* for  $P < 0.01$ ;  $n=3$  from three separate experiments).

The results presented in Figure 4.5 show that the binding of both R96W and R148W mutants to EGFP-H-Ras was reduced compared to wild-type zDHHc9.

#### 4.2.4 Analysis of the effects of R96W and R148W substitutions on S-acylation of HA-zDHHc9 and EGFP-GCP16

The experiments to this point have assessed the effects of the R148W and R96W substitutions on interaction of zDHHc9 with GCP16 and effects of this on reciprocal stabilisation, and examined their interaction with the substrate protein H-Ras. EGFP-GCP16 was previously shown in chapter three to be S-acylated by WT zDHHc9, and

therefore I next examined if there were changes in the ability of the R148W and R96W mutants to S-acylate GCP16. To address this, a click chemistry acylation assay was performed. HEK293 cells were transfected with HA-zDHHC9 wild-type or mutants together with EGFP-GCP16. Twenty-four hours post-transfection, cells were metabolically labelled with palmitic acid-azide for 4 hours, and cell lysates were prepared and reacted with Alk-mPEG. As discussed earlier, this process results in a five kDa band-shift for each S-acylated cysteine. The processed samples were examined by immunoblotting.

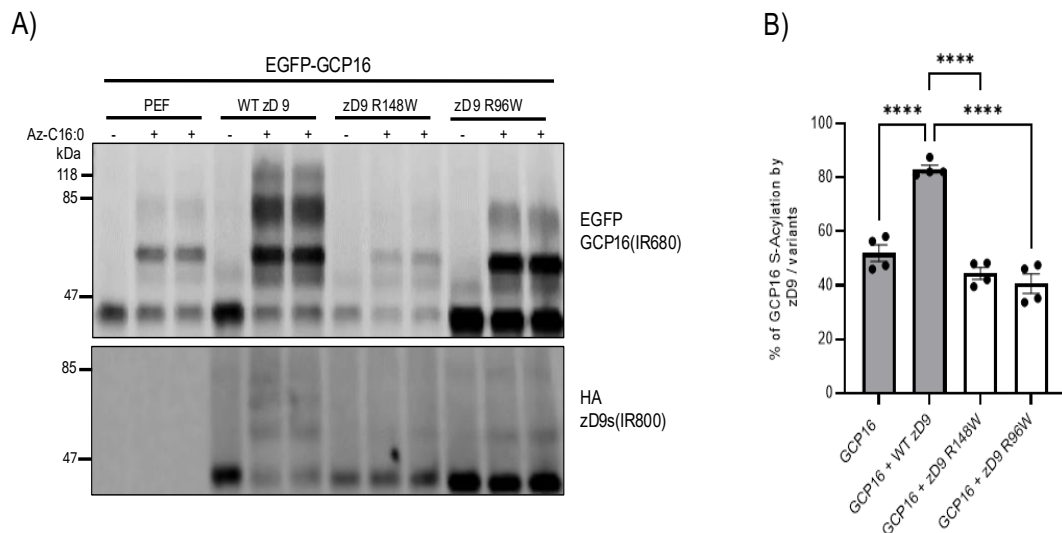


**Figure 4.6 Analysis of S-acylation of EGFP-GCP16 by HA-zDHHC9 wild-type and R148W and R96W mutants.**

HEK293 cells were transfected with plasmids encoding EGFP-GCP16 together with HA-zDHHC9 (wild-type or R148W or R96W mutants). The cells were metabolically labelled with palmitic acid-azide (Az-C16:0; +) for 4 hours. Cells were lysed, and a click mixture containing Alk-mPEG was added and then incubated for 1 hour; when the palmitic acid Azide is clicked with alk-mPEG, any S-acylated cysteine results in a 5 kDa band shift. **A)** Representative immunoblots showing EGFP-GCP16 detected at IR680 (top) and the HA-zDHHC9 proteins detected at IR800 (bottom). Samples indicated with "-" are control samples labelled with palmitic acid. The position of molecular weight markers is shown on the left. **B)** Quantified data showing levels of EGFP-GCP16 S-acylation in the presence of wild-type and mutant HA-zDHHC9, analysed by one-way ANOVA with Tukey post-test (\*\*\*\*P<0.0001, n=4 from two separate experiments).

The results presented in Figure 4.6 show that HA-zDHHC9 wild-type increased the S-acylation of EGFP-GCP16, as previously shown in Chapter 3. In contrast, the R148W and R96W mutants were completely ineffective at S-acylating EGFP-GCP16, and S-acylation levels were similar to those seen in the negative control samples.

As the S-acylation of zDHHC9 is essential for its enzymatic activity (via the autoacylated enzyme intermediate), we next examined the S-acylation status of wild-type and mutant zDHHC9 in the absence and presence of EGFP-GCP16. Results in Chapter 3 previously showed that S-acylation of wild-type HA-zDHHC9 was increased in the presence of EGFP-GCP16.

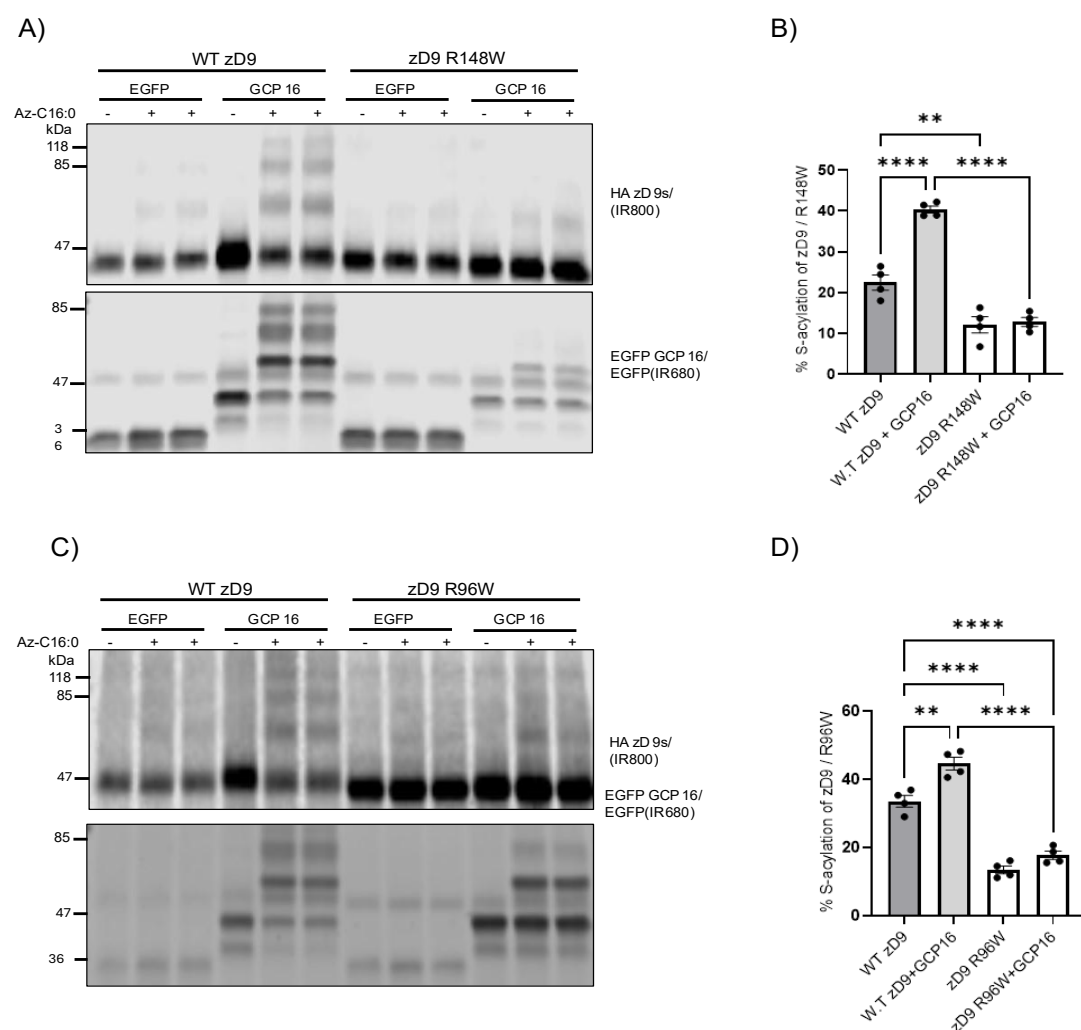


**Figure 4.7 Effect of EGFP-GCP16 on the S-acylation of HA-zDHHC9 (R148W) and zDHHC9 (R96W) mutants**

HEK293 cells were transfected with plasmids encoding HA-zDHHC9 wild-type or R148W or R96W mutants together with either EGFP or EGFP-GCP16. After approximately 24 hours, cells were incubated with palmitic acid-azide (Az-C16:0; +) or palmitic acid as a control (-) for 4 hours and then lysed and a click chemistry S-acylation assay performed using alk-mPEG, resulting in a 5 kDa band shift for each S-acylated cysteine. **A)** Representative immunoblot showing wild-type or R148W HA-zDHHC9 in the presence of EGFP or EGFP-GCP16, where HA-zDHHC9 proteins were detected at IR800 (top) and the EGFP/EGFP-GCP16 at IR680 (bottom). **B)** Quantified data showing the mean  $\pm$  SEM levels of S-acylation of the zDHHC9 (R148W) mutant and the WT zDHHC9 in the presence and absence of GCP16. A one-way ANOVA with Tukey post-test was conducted for statistical significance (\*\*  $P < 0.005$ , \*\*\*  $P < 0.0001$ ;  $n = 4$  from 2 separate experiments). **C)** Representative immunoblot showing levels of S-acylation of the HA-zDHHC9 (R96W) mutant with and without EGFP-GCP16 in comparison to WT HA-zDHHC9. HA-tagged zDHHC9 was detected at IR800 (top) and the EGFP-GCP16 at IR680 (bottom). **D)** Quantified data showing mean  $\pm$  SEM levels of zDHHC9 (R96W) S-acylation compared using one-way ANOVA with Tukey post-test (\*\*  $P < 0.005$ , \*\*\*\*  $P < 0.0001$ ;  $n = 4$  from two separate experiments).

The results presented in Figure 4.7 show that the S-acylation of both the HA-zDHHC9 R148W and R96W mutants was almost completely abolished, and there was no increase in S-acylation of either mutant when co-expressed with EGFP-GCP16 compared with negative control samples.

#### 4.2.5 AlphaFold analysis of wild-type and mutant zDHHC9 proteins

zDHHC9 (R96W) is a loss-of-function mutant despite being outside the protein's catalytic domain. The results so far suggest that this protein has decreased S-acylation and fails to S-acylate EGFP-GCP16. Furthermore, the mutant may also have decreased binding to the substrate protein EGFP-H-Ras. To understand this mutant further and to extend on the results presented in this chapter, the AI protein prediction software AlphaFold Colab was employed to predict the three-dimensional shapes of both WT zDHHC9 and the R96W mutant. Interestingly, the findings suggest the mutant's loss-of-function may be attributed to a conformational change caused by altered hydrogen bond formation between the Tryptophan-96 residue and the Aspartic acid-159 residue, which is only five residues away from the catalytic domain of zDHHC9 (Figure 4.8).

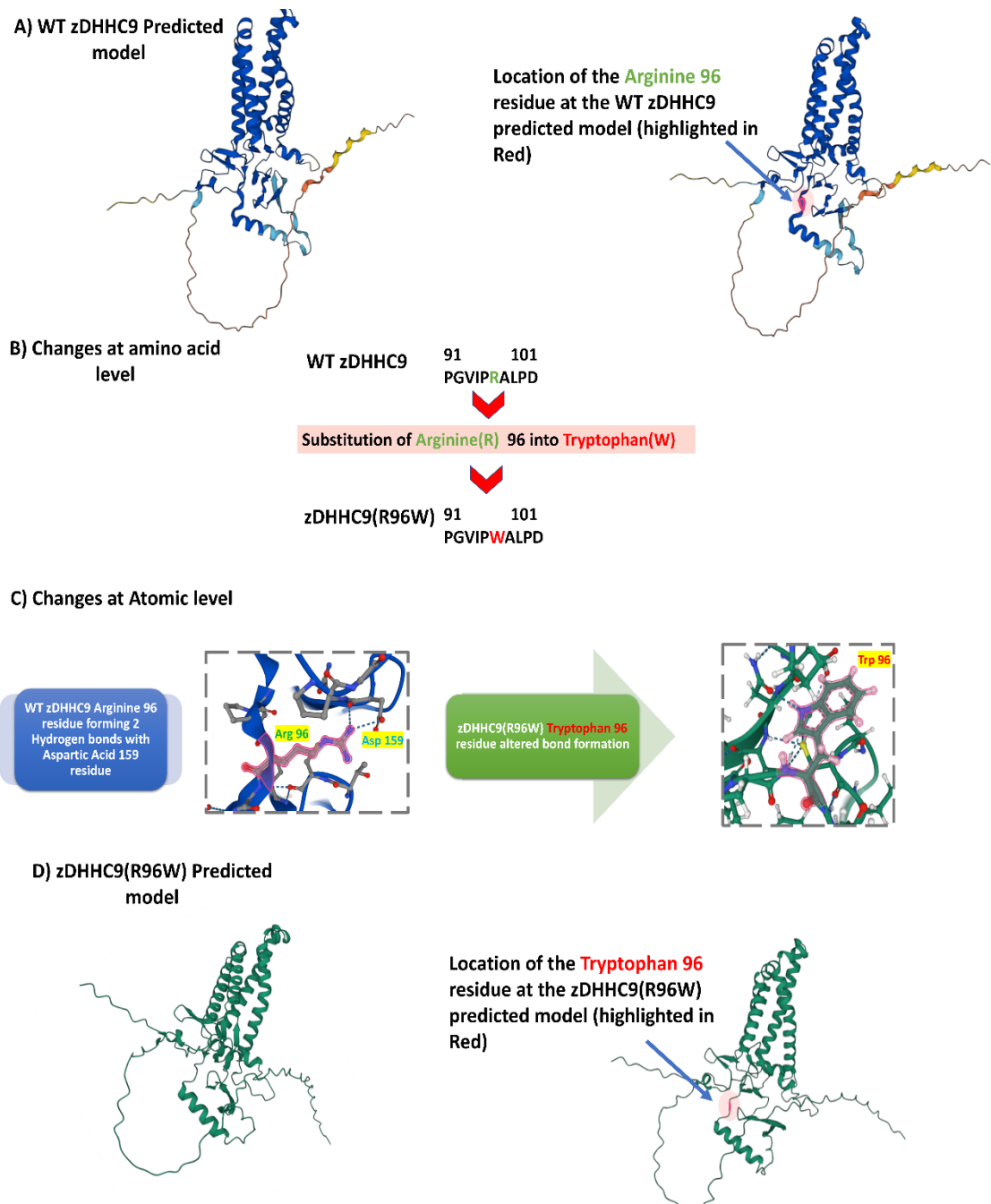


**Figure 4.8 Alphafold analysis of the effects of the R96W substitution in zDHHC9**

Human sequences were used to generate both WT zDHHC9 and the zDHHC9 (R96W) variants in pursuit of understanding the impact of this amino acid substitution. **A)** The WT zDHHC9 structural prediction, with the site of Arginine-96 highlighted. **B)** The location of the amino acid substitution at the level of protein sequence. **C)** Analysis of the change caused by the R96W substitution at the atomic level. The structural prediction suggests that the Arginine-96 residue forms two Hydrogen bonds with the Aspartic acid-159 residue, which is only 5 residues away from the DHHC catalytic domain. Substituting the Arginine-96 into Tryptophan alters Hydrogen bond formation in proximity to the DHHC catalytic domain which might provide a justification for the loss-of-function of the mutant protein. **D)** The zDHHC9 (R96W) mutant's predicted 3D structure with the altered residue location highlighted.



### 4.3 Discussion

In this chapter, we attempted to understand the molecular changes caused by the *ZDHHC9* gene mutations linked to intellectual disability. In particular, there is very little known about the effects of the R96W mutation, whereas the R148W mutation has been shown to disrupt the autoacylation of zDHHHC9 (Mitchell *et al.*, 2014). The R96W mutation is particularly interesting as this change does not affect the sequence of the catalytic DHHC domain. The analyses identified several key novel observations: (i) The R148W substitution (but not the R96W substitution) led to a loss of the reciprocal stabilisation effect on GCP16; (ii) both the R148W and the R96W mutants failed to S-acylate GCP16, and (iii) both mutants showed reduced S-acylation that was not stabilised by GCP16. These findings likely underlie the loss-of-function of R96W. Interestingly, AlphaFold analysis suggested that this loss of R96W S-acylation activity may be a result of a structural change that causes hydrogen bonding between the Tryptophan-96 residue and Aspartic acid-159, which is only five residues away from the catalytic domain. In addition to these key observations, co-immunoprecipitation analyses suggested that the R148W mutant might also have reduced binding to GCP16 and that both R148W and R96W mutants may have reduced interaction with the substrate H-Ras. However, these latter findings might be influenced by differences in mutant zDHHHC9 expression and will therefore require further analysis. As a first step to confirm the co-immunoprecipitation results, it would be useful to purify GCP16 from an *E. coli* expression system and perform pull-down experiments on zDHHHC9 wild-type and mutant enzymes from HEK293 cell lysates (e.g. Lemonidis *et al.*, 2017).

A recent cryo-EM study by Yang *et al.* (2024) suggested that GCP16 binds to zDHHHC9 through four main interfaces. The first interface involves interactions between Arginine-85 and Tyrosine-183 of zDHHHC9 with Tyrosine-76 in GCP16. The second interface involves a polyproline helix in the C-terminus of zDHHHC9, where

Proline-290 and Proline-293 dock into negatively charged pockets of GCP16 with an additional interaction of Proline-292 with Tyrosine-86 in GCP16. The third interface involves interactions between Proline-150 and Phenylalanine-129 of zDHHC9 with Tyrosine-18 of GCP16 and interaction of Glutamate-163 in zDHHC9 with Arginine-16 of GCP16. Finally, the fourth interface involves the interaction of Aspartate-100 of zDHHC9 with Lysine-11 and Phenylalanine-13 of GCP16 and Glutamate-101 in zDHHC9 interaction with Arginine-118 and Arginine-121 of GCP16. Moreover, the authors of this study suggested that substituting R148 with a bulky Tryptophan residue (i.e. R148W) may disrupt the catalytic site, which is consistent with the results of this chapter and also with the study of Mitchell *et al.* (2014), who showed that this amino acid change caused rapid hydrolysis of the autoacylated intermediate. The Alphafold prediction that the R96W substitution results in hydrogen bonding between the tryptophan and a region near the DHHC active site is consistent with the loss of S-acylation and loss of S-acylation activity observed with this mutant. It will be interesting in future work to introduce additional mutations into the region of zDHHC9 that forms hydrogen bonds with W96 to test if this can rescue the S-acylation defects of the R96W mutant (by preventing the tryptophan from interacting with the DHHC domain).

Given that both the R96W and R148W mutants have a loss of S-acylation activity towards GCP16, it is interesting that they had different effects on the reciprocal stabilisation of zDHHC9 and GCP16 in cycloheximide experiments. This observation suggests that S-acylation of GCP16 by zDHHC9 is not strictly required for the increase in protein stability and that the R96W mutant, because of its altered structure, likely has a modified interaction with GCP16 that preserves the stabilising effects in the absence of S-acylation. Our Alphafold analysis supports the idea that the structure of R96W is affected and that this substitution promotes interactions of the tryptophan with the catalytic domain (Figure 4.8). Furthermore, it is also possible

that both R96W and R148W perturb the interaction with GCP16 but in different ways. Indeed, the study of Yang *et al.* (2024) showed that Proline-150 (two residues downstream from R148) interacts with Arginine-18 in GCP16. In addition, there are contacts between Asparatate-100 and Glutamate-101 of zDHHC9 with Lysine-11/Phenylalanine-13 and Arginine-118/Arginine-121, respectively, which could be affected by the R96W substitution in zDHHC9. Neither the R96W nor R148W substitutions had a major effect on the interaction of zDHHC9 with GCP16, although there was a possible reduction in co-immunoprecipitation of the R148W mutant with EGFP-GCP16 (Figure 4.4). However, co-immunoprecipitation experiments likely lack the sensitivity to detect subtle changes in binding, and it will be particularly revealing to study the interaction of the zDHHC9 R96W and R148W mutants with GCP16 using cryo-EM.

The 3D protein prediction software AlphFold2 provided a fascinating potential molecular explanation for the disrupting effects of the R96W substitution. Although this model was compelling, it is important to recognise that these models are not always accurate, as discussed in Chapter 3. Thus, we should proceed cautiously with these predictions, and further experimental work is important to validate this model.

It is also important to reflect on the results of this Chapter compared to those in Chapter 3. Here, the reciprocal stabilisation of the zDHHC9 R96W mutant and GCP16 observed in this chapter is interesting in light of the observation made in Figure 3.14 and Figure 3.16, which showed that alanine substitution of the two main S-acylation sites in GCP16 (C69,72A) led to the reciprocal stabilisation effect being lost. This is interesting because the R96W zDHHC9 mutant failed to promote the S-acylation of GCP16, yet it still stabilised the GCP16 protein. Here, it may be relevant that GCP16 can be S-acylated by other enzymes, such as zDHHC3 and zDHHC7 (Figure 3.6), and indeed, S-acylation of GCP16 is detected in cells lacking zDHHC co-expression (Figure 3.6 and Figure 4.6). Therefore, the S-acylation of GCP16 by endogenous

zDHHHC enzymes may be sufficient to allow this protein to stabilise zDHHHC9 R96W and *vice versa*.

Interestingly, a recent study by Nguyen *et al.* (2023) suggested that the R96W mutant had compromised stability and almost no enhancement when co-expressed with GCP16. However, the approach used in this study was fluorescence-detection size-exclusion chromatography analysis of purified protein from Sf9 insect cells, where protein folding and aggregation were used for the measurement of stability. On the other hand, our approach more directly tested the effects on protein turnover in cells using a cycloheximide protein synthesis block. One potential issue that is worthwhile reflecting on at this stage is the possibility that blocking protein synthesis alters the dynamics of protein degradation and turnover. This could lead to changes in protein half-life that are indirect consequences of cycloheximide action. Therefore, it would be interesting in future work to perform pulse-chase experiments, for example, where cells are incubated with radiolabelled methionine. This is incorporated into newly-synthesised proteins, allowing turnover (as measured by loss of radiation signal in immunoprecipitated protein) to be quantified in cells where protein synthesis is not inhibited (e.g. Greaves *et al.*, 2008).

The effects of the R96W and R148W substitutions on the catalytic activity of these mutants are likely to underpin their loss-of-function effects. To extend these findings, the interaction of the mutant proteins with a substrate H-Ras was also examined. Ras is one of the few confirmed substrates of zDHHHC9, and indeed, S-acylation of N-Ras by this enzyme is important for dendrite growth and branching in hippocampal neurons, and defects in this process could contribute to intellectual disability features (Shimell *et al.*, 2019). Both R96W and R148W showed a reduced co-immunoprecipitation with EGFP-H-Ras compared with wild-type zDHHHC9 (Figure 4.5). Thus, the structural changes associated with these amino acid substitutions may also disrupt substrate recognition. The binding site in H/N-Ras for zDHHHC9 has not

been determined, but as the C-terminal 8 amino acids in Ras are sufficient for S-acylation when expressed in cells (Hancock *et al.*, 1989), zDHHc9 may recognise features in proximity to the S-acylation sites (which are within this 8 amino acid region). As there was reduced expression of the R148W mutant in HEK293 cells, it is possible that this contributed to the reduced level of co-immunoprecipitation and, therefore, direct binding of the zDHHc9 mutants to H-Ras should be explored using pull-down experiments with purified proteins to validate our co-immunoprecipitation results.

The biochemical and molecular properties of R96W and R148W are interesting as a case report by Ramos *et al.* (2023) discussed the various clinical manifestations caused by zDHHc9 gene mutations, where the manifestations associated with R96W mutation were less severe, especially in terms of brain morphology. The differences we observed in R148W and R96W could possibly underpin the reported varied clinical phenotypes ranging from mild intellectual disabilities to severe intellectual disability and, in some cases, changes in the brain morphology and thinning of the corpus callosum (Schirwani *et al.*, 2018). It would be especially interesting to understand how the expression levels of the R96W and R148W mutants compare in clinical cases, as well as how GCP16 (or Golga7b) levels are affected *in vivo* in the presence of these mutants. Indeed, following on from the focus and results of Chapter 3, it is interesting to consider how *ZDHHc9* mutations could indirectly impact zDHHc5. If the R148W substitution impacts the stability of GCP16, then reduced levels of this protein (or of Golga7b) could also impact zDHHc5. This is relevant, as a *Zdhhc5* knockout mouse model exhibited behavioural changes that could link to the clinical features seen in people with *ZDHHc9* mutations. Specifically, the mice displayed a deficit in contextual fear conditioning, a process that is linked to hippocampal-dependent learning (Li *et al.*, 2010). Although zDHHc5 can also stabilise GCP16 (Figure 3.1), in tissues with a high ratio of zDHHc9:zDHHc5, there could be a marked decrease in GCP16 levels,

which could have a corresponding impact on zDHHC5. A more detailed analysis of protein expression levels in samples from people with *ZDHH9* mutations could uncover important changes not only in GCP16/Golga7b levels but also, of course, in the expression and S-acylation of substrate proteins.

Overall, the results in this chapter have successfully identified molecular changes in the R96W zDHHC9 mutant that are likely to contribute to the phenotypes seen in people carrying this mutation. Furthermore, the differences observed in the molecular effects of R96W and R148W could reveal why these mutations can lead to different clinical phenotypes (with R148W generally being more severe). A key area for future work is to map the substrate network of zDHHC9 and then to determine how the R148W substitution impacts the S-acylation of these proteins *versus* the R96W substitution. Specifically, are all substrates equally affected by both R96W and R148W, and is the level of disruption of S-acylation similar for both of these zDHHC9 mutants? These questions could be tested in cultured neurons from *Zdhhc9* knockout mice that have been transfected with wild-type or the R96W/R148W mutant plasmids. Alternatively, wild-type neurons could be treated with siRNA to deplete zDHHC9 and then rescued with siRNA-resistant wild-type, R96W, or R148W mutant plasmids (e.g., Shimell *et al.*, 2019). Ultimately, the development of knockin mice carrying the R96W or R148W mutants would allow a detailed characterisation of the effects of these mutations on the S-acylated substrate network, brain anatomy, and behaviour (Kouskou *et al.*, 2018).

**CHAPTER 5**

**EFFECTS OF *ZDHH*C9 MUTATIONS:  
MOLECULAR, GENOMIC, AND CLINICAL  
PERSPECTIVE**

## Chapter 5

### Effects of *ZDHHHC9* Mutations: Molecular, Genomic, and Clinical Perspective

#### 5.1 Introduction

Reports of *ZDHHHC9* mutation patients have been growing over the past few years. Raymond *et al.* (2007) first reported that mutations in the *ZDHHHC9* gene cause intellectual disability. In the four affected families identified in this study (out of 250 families that were studied), the clinical outcome varied despite having a single identified molecular dysfunction, disruption of *ZDHHHC9*. Intellectual disability was the predominant feature in all patients; however, in some cases, consistent and inconsistent clinical abnormalities were also reported, ranging from epilepsy and brain morphology abnormalities like macrocephaly to changes in body features like short stature and muscular spasticity. The overall description of the cases was developmental delay and the clinical stereotype of Marfanoid Habitus, with none of the patients meeting Ghent criteria for Marfan syndrome. The researchers proposed that these clinical complaints might be attributed to loss of H-Ras and N-Ras S-acylation. Subsequently, Mitchell *et al.* (2014) examined the effect of the two missense point mutations (R148W) and (P150S) identified in the Raymond *et al.* (2007) study. They suggested that although both variants have a similar negative impact on enzyme activity, each has a distinct mechanism, either impacting the formation or stability of the autoacylated intermediate. In 2015, Baker *et al.* published their findings after investigating nine males with *ZDHHHC9* mutations; the researchers provided a comprehensive clinical picture for the subjects, in which eight out of the nine patients exhibited mild or moderate intellectual disabilities (ID), with one case presenting a severe form of ID. Global impairments were present in all patients, and, interestingly, neuroanatomical abnormalities varied, with hypoplasia of the corpus callosum present in seven subjects, global cerebral volume loss observed in five, and



ventricular enlargement seen in six cases, thus establishing the varied clinical phenotype in patients with *ZDHHHC9* gene mutations even if the molecular outcome in all is loss of zDHHHC9 function. An additional *ZDHHHC9* variant R96W, in which the point mutation falls outside the catalytic DHHC domain of the enzyme was reported by Tzschach *et al.* (2015) in a patient suffering from ID; the same variant was also reported by Han *et al.* (2017) in a male suffering from early onset developmental delay but without the other hallmarks of *ZDHHHC9* mutations such as anatomical abnormalities impacting the nervous system or the signs associated with Marfanoid Habitus.

Similar to the clinical findings in patients, mutant zDHHHC9 mice display several phenotypes similar to those reported in humans with *ZDHHHC9* mutations.

Kouskou *et al.* (2018) conducted a series of behavioural tests on the *Zdhhc9* KO mice to determine the impact of *Zdhhc9* loss-of-function. It was observed that mutant mice spent more time in anxiety-provoking areas, such as the aversive open arms of the EPM apparatus (Elevated plus maze) and the central zones of OFT (open field test) during habituation period, indicating lower anxiety levels compared to wild-type littermates. Additionally, mutant mice show a diminished acoustic startle response, further supporting the interpretation of reduced anxiety.

The *Zdhhc9* mutant mice also exhibited reduced muscle tone, as evidenced by their shorter hanging time in the hanging wire test; a phenotype that closely resembles the hypotonia observed in individuals with *ZDHHHC9* mutations. To further examine structural changes, Fast low angle shot magnetic resonance imaging (FLASH MRI) analysis revealed a 35% reduction in corpus callosum volume in mutant mice, paralleling anatomical abnormalities reported in affected individuals. Given that impaired learning is a core feature of intellectual disability, spatial learning and memory were also tested using the Morris Water Maze. Consistently, mutant mice performance demonstrated clear deficits in hippocampal-dependent learning tasks,

with impaired acquisition of the spatial memory task. These findings support the notion that spatial learning impairment extends beyond cognitive dysfunction and may reflect a broader behavioural phenotype. Specifically, when considered alongside the anxiolytic pattern and increased exploratory activity observed in the Elevated Plus Maze and Open Field Test.

It is important to note that both the wild-type and *Zdhhc9* knockout mice used in this study originate from the same colony maintained at the Biological Procedures Unit of University of Strathclyde's. Therefore, the mouse model utilized here is consistent with that used in our research.

The mechanisms underlying the variations in clinical manifestations seen in patients with *ZDHHC9* loss-of-function mutations and the knock-out mouse model remain unclear. However, a recent study by Zhang *et al.* (2021) in glioblastoma cells suggested that zDHHC9 S-acylates the glucose transporter GLUT1 at cysteine-207 and that the loss of S-acylation results in disruption of its plasma membrane localisation. These findings are interesting as there are similarities between GLUT1 deficiency syndrome (DS) and features of patients with *ZDHHC9* mutations, where GLUT1-DS causes a mild to severe array of symptoms like epilepsy, ID, and developmental delays (De Giorgis and Veggiotti, 2013). The implication of GLUT1 S-acylation and its potential link to the features seen in *ZDHHC9* mutation carriers remains unclear. In this chapter, we sought to understand why the clinical symptoms associated with *ZDHHC9* mutations develop. Our approach included a general analysis of changes in mRNA expression levels in *Zdhhc9* knockout mice to identify any other genes or pathways affected. In addition, we also undertook analyses that were more focused on our hypothesis linking zDHHC9 disruption to GLUT1-DS. Here, we explored the interaction of zDHHC9 with GLUT1 and how this is affected by the R148W and R96W amino acid changes, and we also examined the liver clinical profile

in *Zdhhc9* knockout mice to identify signs of GLUT1-DS. The specific questions addressed were:

1. Can GLUT1 binding to zDHHC9 be detected, and does this differ for the two distinct zDHHC9 variants, R148W and R96W?
2. What other S-acylation enzymes interact with GLUT1?
3. What mRNA changes occur when the *Zdhhc9* gene is disrupted?
4. What are the effects of diet on the liver clinical profile in *Zdhhc9* knock-out mice compared to wild-type?

## **5.2 Results**

### **5.2.1 Molecular analysis of GLUT1 interaction with zDHHC9**

GLUT1 is essential for normal brain development, so any disruption to this glucose transporter can result in many neurological symptoms (De Giorgis and Veggiotti, 2013; Tang and Monani, 2021). It is well established that point mutations (R148W and P150S) in the DHHC domain of zDHHC9 lead to a loss of activity and would, therefore, be predicted to disrupt the targeting of GLUT1 to the plasma membrane (Zhang *et al.*, 2021). To further explore how the mutations might affect GLUT1, we employed co-immunoprecipitation experiments, where HEK293 cells were transfected with plasmids encoding EGFP-GLUT1 or EGFP as a negative control, together with either HA-tagged WT zDHHC9 or its variants R148W and R96W. Approximately 24 hours later, cell lysates were incubated with GFP-trap beads to capture EGFP-tagged GLUT1 and any interacting HA-tagged proteins (Figure 5.1)

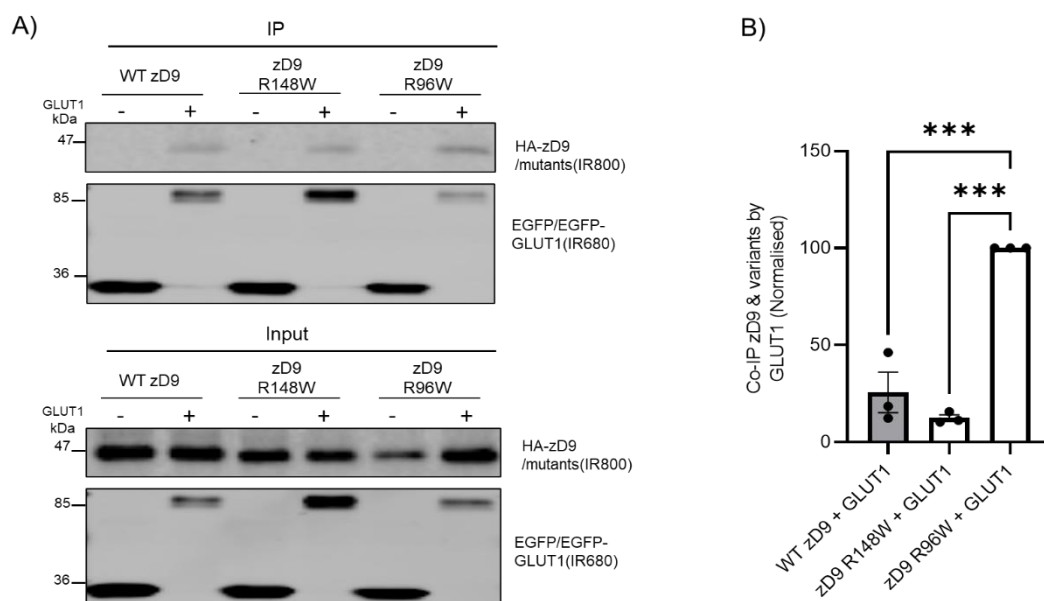


**Figure 5.1 Analysis of GLUT1 binding to zDHC9 Wild-Type, and R148W and R96W variants**

Approximately 24 hours after transfecting HEK293 cells with plasmids encoding EGFP-GLUT1 or EGFP together with one of the HA-tagged zDHC9 WT, R148W, or R96W variants, cell lysates were prepared and EGFP-tagged proteins captured using GFP-trap beads and examined by immunoblotting. **A)** Representative immunoblots showing HA-tagged wild-type zDHC9 and the R148W and R96W mutants, which were detected in the IR800 channel, and EGFP-GLUT1, which was detected in the IR680 channel. **B)** Quantitative analysis of the data (HA/EGFP signal) show a significant increase in binding of the R96W mutant with EGFP-GLUT1 compared to WT or R148W mutant. One-way ANOVA with Tukey was performed (n=3 from three separate experiments, \*\*\* denotes  $P < 0.001$ ).

The results presented in Figure 5.1A show that the binding of HA-zDHC9 to EGFP-GLUT1 could be detected by co-IP. Interestingly, the quantified data suggest that the R96W mutant has a significantly greater interaction with EGFP-GLUT1 than either wild-type zDHC9 or the R148W mutant (Figure 5.1B). However, this aspect needs to be cautiously interpreted as the quantified signal was affected greatly by the low level of EGFP-GLUT1 that was immunoprecipitated (data is quantified using HA/EGFP signal).

Subsequently, it was examined if (i) the interaction with zDHHC9 was selective to this zDHHC isoform and (ii) if there was any interaction of GLUT1 with the accessory protein GCP16. The enzymes that were compared were zDHHC5 because of similarities with zDHHC9 in the use of the GCP16/Golga7 accessory protein (Salaün *et al.*, 2020) and zDHHC7, as this enzyme is known to S-acylate the related glucose transporter GLUT4 (Du *et al.*, 2017). As before, the interaction of EGFP-GLUT1 with HA-tagged versions of these enzymes and accessory proteins was examined by co-IP (Figure 5.2).

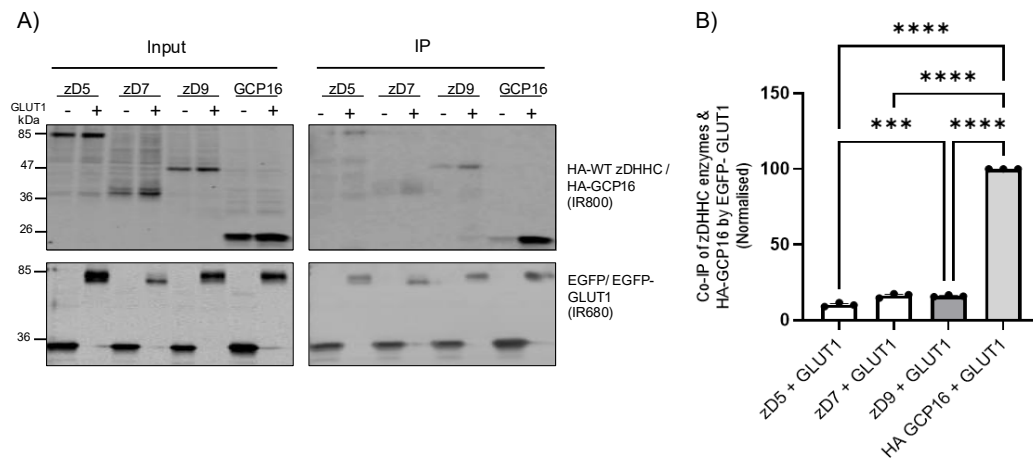


**Figure 5.2 Co-immunoprecipitation analysis of the interaction of EGFP-GLUT1 with different zDHHC enzymes and GCP16**

Approximately 24 hours after transfecting HEK293 cells with plasmids encoding EGFP-GLUT1 or EGFP together with HA-tagged zDHHC9, zDHHC5, zDHHC7, or GCP16, cell lysates were prepared, and EGFP-tagged proteins were captured using GFP-trap beads and examined by immunoblotting. **A)** Representative immunoblots showing HA-tagged proteins detected in the IR800 channel and EGFP-GLUT1/EGFP detected in the IR680 channel. **B)** Quantitative analysis of the data (HA/EGFP signal) showing a significant increase in binding of the GCP16 to EGFP-GLUT1 compared with any of the zDHHC enzymes. Data was compared using One-Way ANOVA with Tukey post-test; the binding of GLUT1 was higher with HA-GCP16 than any of HA-zDHHC enzymes (n=3 from three separate experiments, \* denotes  $P < 0.05$ , \*\*\*\* denotes  $P < 0.0001$ ).

The results in Figure 5.2 show that binding to all zDHHC enzymes was detectable and at a level above that in the EGFP control. Surprisingly, the co-IP of HA-tagged GCP16 by EGFP-GLUT1 was greater than for all the zDHHC enzymes. This suggests that GCP16 may play an additional role in the S-acylation process by interacting with substrate proteins, in this case, GLUT1. The higher levels of HA-GCP16 expression

compared to the HA-zDHHC enzymes might contribute to the higher observed co-IP for GCP16, but the data clearly show a robust interaction between GCP16 and EGFP-GLUT1.

To extend the findings of the co-IP experiments, we next examined whether the presence of HA-GCP16 enhanced S-acylation of EGFP-GLUT1 by HA-zDHHC9. To do this, cells were transfected with EGFP-GLUT1 in the presence of HA-GCP16, HA-zDHHC9, or both proteins. Approximately 24 hours later, cells were labelled with either palmitic acid azide or palmitic acid for 4 hours, and cell lysates were prepared and subjected to click chemistry using 5 kDa PEG-alkyne (which results in a 5 kDa band-shift for each S-acylated cysteine). Using this assay, there was no noticeable change in the profile of EGFP-GLUT1 immunoreactivity when cells were labelled with palmitic acid azide (+) compared to palmitic acid (-) (Figure 5.3A). Therefore, S-acylation was also investigated using an alkyne infrared dye (IR800) rather than alkyne-PEG (Figure 5.3B). Using this assay, an S-acylation signal was obtained with both zDHHC9 and zDHHC9/GCP16 co-expression. The signal appeared of similar intensity in both the presence of zDHHC9 and zDHHC9/GCP16, implying that the presence of the GCP16 accessory protein did not lead to an additional enhancement of S-acylation above that seen with zDHHC9 alone. A further point to note from the results of Figure 5.3B is that there was a shift in the immunoreactive bands for EGFP-GLUT1 when HA-zDHHC9 was present, suggesting that S-acylation might alter the glycosylation pattern of the glucose transporter, presumably by affecting its trafficking and localisation.

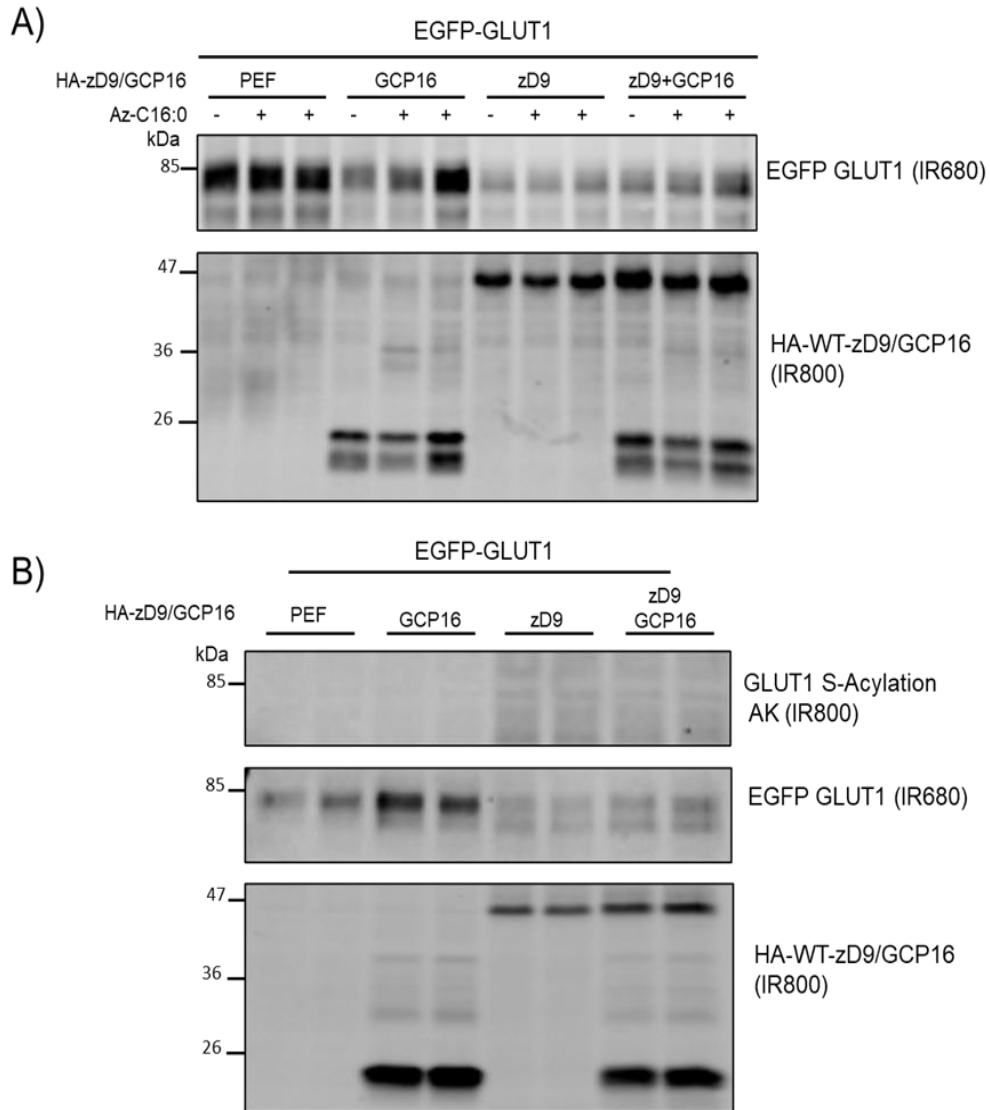


**Figure 5.3 Analysis of EGFP-GLUT1 S-acylation by HA-zDHH9 and HA-GCP16**

HEK293 cells were transfected with EGFP-GLUT1 together with either HA-zDHH9, HA-GCP16, or both, PEF (empty plasmid) was used as a negative control. **A)** Cells were labelled with palmitic acid-Azide (+) or palmitic acid for 4 hours (-), and then a click mixture was added to cell lysates that contained 5 kDa Alk-mPEG; S-acylation in this assay is detected by a 5 kDa band-shift for each cysteine. **B)** Transfected cells were labelled with palmitic acid azide, and cell lysates were then incubated with a click chemistry reaction mixture containing alkyne (AK) IRdye-800 nm. EGFP-GLUT1 and HA-tagged proteins were detected in the IR680 channel. The position of molecular weight markers is shown on the left side of all immunoblots.

### 5.2.2 Analysis of changes in mRNA expression in *Zdhhc9* knockout mouse brain

The data in section 5.2.1 suggest that zDHHHC9-GCP16 interacts with GLUT1 and that binding does not seem disrupted by the R148W and R96W amino acid changes. However, despite binding to GLUT1, the R148W mutant (and possibly also R96W) is not expected to S-acylate this protein. To explore if any brain expression changes occur when zDHHHC9 is non-functional that might link to GLUT1-DS, total RNA was extracted from ten frozen brain samples (five wild-type and five knock-out). The concentration of the RNA samples were quantified and sent to BGI Genomics Inc. (Beijing, China) for RNA-Seq analysis (refer to section 2.5.2 mRNA-Seq analysis). After a lengthy process of sequencing and filtering the results from low quality reads, adaptor polluted reads, and so on, the end result samples had an average of 25.19 million reads per sample. Afterwards, knock-out samples were compared against the wild-type samples to pin point genes with a significant change in read count. This resulted in 5 hits (including *Zdhhc9*) in the knock-out group, which all displayed a decrease in read count compared to the wild-type samples (including *Zdhhc9*) (Table 5.1).

Importantly, this analysis identified zDHHHC9 mRNA expression as reduced in the KO mice, providing confidence in the reliability of the data. The genes that were additionally identified included *Cfd* (Complement factor D), *Gm14434* (predicted gene 14434), *Hapln2* (Hyaluronan and proteoglycan link protein 2), and *Ddit4* (DNA



damage-inducible transcript 4); interestingly, none of these genes encoded proteins that are known to be S-acylated according to SwissPalm.org.

Gene Symbol	Description	Related Diseases
<b>CFD</b>	complement factor D ( <del>adipsin</del> )	Alternative complement pathway component defects
<b>zDHHC9</b>	zinc finger, DHHC domain containing 9	Syndromic X-linked mental retardation
<b>Gm14434</b>	predicted gene 14434	Non-syndromic X-linked mental retardation, Postaxial polydactyly, Transient neonatal diabetes mellitus (TNDM)
<b>Hapln2</b>	hyaluronan and proteoglycan link protein 2	unknown
<b>Ddit4</b>	DNA-damage-inducible transcript 4	unknown

**Table 5.1** Differentially expressed genes in *Zdhhc9* knockout mice.

Differentially expressed genes were identified as those with significantly lower read count in knockout samples compared to the WT wild-type, samples were statistically analysed using unpaired T-test (P value <.05%, n=5 WT and 5 KO mice samples).

### **5.2.3 Inducing liver stress in knockout mice using a high-calorie diet to assess physiological adaptation that has been associated with GLUT1 deficiency syndrome**

GLUT1 deficiency syndrome is a rare neurological disorder resulting from mutations in the *SLC2A1* gene. The subsequent clinical outcome manifests in neurological symptoms that can vary in severity and characterisation (De Giorgis and Veggiotti, 2013), yet they encompass almost all of the symptoms resulting from *ZDHHC9* mutations. This, combined with reports indicating that GLUT1 is modified by zDHHHC9 (Zhang *et al.*, 2021), prompted me to explore the idea that zDHHHC9-related disorders might be a mimic of a mild case of GLUT1 deficiency. In this case, the deficiency would be caused not by reduced expression of GLUT1 but by failure to localise correctly to the plasma membrane due to a lack of zDHHHC9-mediated S-acylation. The scarcity of reports providing a complete clinical picture of the metabolic aspects of patients with *ZDHHC9* mutations limited our ability to explore this idea through the literature. Instead, we examined the effects of long-term exposure to a high protein and fat diet that was expected to trigger liver stress in wild-type mice, as this type of diet is the closest resemblance to a ketogenic diet, which can be associated with elevated liver enzymes (Purkins *et al.*, 2004). A report by Chenouard *et al.* (2015) presented a case diagnosed with GLUT1 DS that showed spontaneous permanent ketosis yet exhibited cerebral metabolic adaptation. No further data on other physiological adaptation features reflected by permanent ketosis were provided. We hypothesized that if GLUT1 deficiency was contributing to the phenotypic effects of zDHHHC9 mutations, the knock-out mice would exhibit some metabolic adaptation reflected in liver enzyme readings, with increased Beta-Hydroxybutyrate (BHB) corresponding with the GLUT1 DS case report (Chenouard *et al.*, 2015).

Twelve mice, six wild-type and six *Zdhhc9* knockout, were placed on a breeding diet for six months; this diet was composed of 50% nitrogen-free extracts with 22.5% crude protein and 4.2% crude fat. Afterwards, the mice were euthanised, and blood

samples were collected and sent for analysis at Glasgow University Veterinary Services. The results of these analyses are shown in Figure 5.4. Liver enzymes ALT (alanine transaminase), AST (aspartate aminotransferase), and GGT (gamma-glutamyl transferase) serve as biomarkers for liver function and stress. The data show significantly higher GGT in the wild-type mice compared to the knockout group, with ALT and AST also showing a non-significant trend towards higher levels in knockout animals. The knockouts had a higher ketone body concentration (BHB), suggesting some sort of liver resiliency towards prolonged exposure to the breeding diet. Although only GGT levels were significantly different between the wild-type and knockout mice, the findings can be reasonable grounds for future work investigating metabolic aspects of zDHHc9 mutations.

Sample size	6 Wild –Type 6 Knock-out	Special conditions	High protein diet 4 Hours fasting
Sex	Males	Age	6 Months

Name of analysis	Knock-Out mean value ± SEM	Wild-Type mean value ± SEM	Normal Range*
AST (U/L)	184.8 ± 59.11	299.2 ± 71.81	40–60 (U/L)
ALT (U/L)	38.67 ± 3.57	42.83 ± 6.33	24–40 (U/L)
GGT (U/L)	7 ± 0.68	10 ± 0.96	3–8 (U/L)
BHB (mmol/L)	0.47 ± 0.13	0.17 ± 0.09	Below 0.5 (mmol/L)

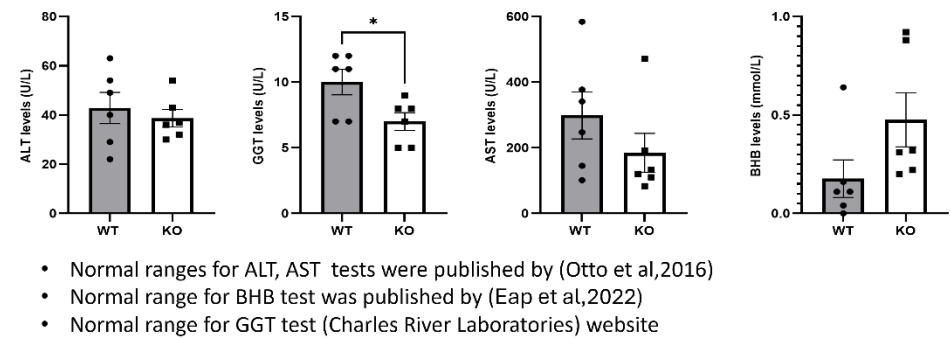


**Figure 5.4 Liver function biomarkers and BHB levels in wild-type and *Zdhhc9* knock-out mice after six months of a high-calorie diet**

After six months of exposure to a high-calorie diet, blood samples were collected and sent for analysis to measure the AST, ALT, GGT, and BHB levels in wild-type and knockout mice (n=6). The data was analysed by unpaired T-test (\*indicates p<0.05).

### 5.3 Discussion

The first study that showed an association between *ZDHHHC9* mutations and XLID (Raymond *et al.*, 2007) identified four disease-causing variants: two truncation and two missense mutations. Intriguingly, all the mutations led to consistent and inconsistent clinical phenotypes; even in patients with the same mutation, the clinical manifestations varied. For instance, siblings with the same truncation mutation showed different intellectual disabilities and global developmental delay progression rates and severity. Furthermore, some anomalies like hypotonia, cowlick, and high forehead made FG syndrome a possible diagnosis, but the absence of some major symptoms like macrocephaly made it unlikely. These variations in symptoms, even among siblings with the same mutation, were also observed with a splice-site mutation in the *ZDHHHC9* gene, where both siblings had intellectual disability and developmental delays, yet the eldest developed schizophrenia during adulthood (Raymond *et al.*, 2007). Lastly, the two frameshift mutations, R148W and P150S, had similar clinical phenotypes but varied in severity. It is also worth noting that some patients exhibited skeletal symptoms of Marfan syndrome but did not meet the diagnostic criteria.

This pattern of similarities and variations in the clinical complaints was observed across most reported variants. Schirwani *et al.* (2017) examined two brothers and the maternal uncle from one family and a fourth patient previously mentioned by Wright *et al.* (2015). All patients suffered from *ZDHHHC9* loss-of-function in the form of two *ZDHHHC9* mutations; the three patients from one family had a 2 kb deletion mutation, and the fourth patient had the R148W variant; interestingly, on top of intellectual disability and developmental delays, the fourth patient - despite suffering from same molecular outcome (loss of *ZDHHHC9* function) - had significantly varied clinical complaints in the form of obsessive-compulsive disorder (OCD), autism and the brain MRI revealed structural abnormalities such as thinning of corpus callosum.

The R96W variant causes loss of zDHHC9 function despite falling outside the catalytic domain (Tzscharch *et al.*, 2015; Han *et al.*, 2017). The overall presentation in both case reports is intellectual disabilities, and Han *et al.* (2017) provided a more detailed clinical picture with the same pattern of similar symptoms yet varied severity; most interestingly, facial dysmorphism, marfanoid symptoms, and brain structural abnormalities were absent.

These variations in symptoms, severity, and even bodily structure raise the question of how the loss of zDHHC9 S-acylation activity might lead to such variations. So, we shifted our attention toward zDHHC9 substrates, specifically GLUT1, which was our main focus in this chapter for the following reasons:

1. GLUT1 is essential for supplying glucose to the brain. Found in erythrocytes and capillaries of the blood-brain barrier, GLUT1 facilitates glucose uptake and utilisation in different brain regions (Vivo *et al.*, 1991). GLUT1 dysfunction has severe consequences for brain development and leads to global developmental delays and epilepsy (Ang *et al.*, 2021).
2. GLUT1 deficiency is a well-documented syndrome with a spectrum of symptoms (Braakman *et al.*, 2017), intriguingly covering almost all symptoms seen in *ZDHHC9* mutation patients.
3. The discrepancies and inconsistencies in the clinical manifestations in patients with GLUT1 deficiency and those with *ZDHHC9* mutations are closely related. This could suggest that GLUT1 dysfunction is a major contributor to pathogenesis in patients with *ZDHHC9* mutations, where symptoms are linked to glucose starvation in various brain regions.
4. The varied symptoms seen in patients with GLUT1 deficiency or *ZDHHC9* mutations might be attributed to their diet, as a ketogenic diet is considered a main component of GLUT1 deficiency management.

5. Recent reports highlighted the importance of S-acylation for stable plasma membrane localization of GLUT1. Furthermore, Zhang *et al.* (2021) demonstrated an important role for zDHH9 in S-acylating GLUT1 at Cys-207 in glioblastoma cells, suggesting therapeutic approaches involving the inhibition of zDHH9 activity for a better prognosis.

In conclusion, based on the above, I proposed that GLUT1 dysfunction (alongside disrupted S-acylation of other substrates of zDHH9) may play a significant role in the clinical outcome of patients with *ZDHH9* mutations. If this is true, then management of GLUT1 DS could be implemented in the case of zDHH9 loss-of-function.

### **5.3.1 Molecular and mRNA expression analyses**

Our molecular analysis started by testing the binding capacity of GLUT1 to zDHH9 and its variants. The observation of co-immunoprecipitation of zDHH9 by EGFP-GLUT1 but not EGFP is the first demonstration that these proteins can form a stable complex. The R148W and R96W variants also displayed co-immunoprecipitation with EGFP-GLUT1. The quantified data for R96W suggested that this variant has a substantially increased level of association with GLUT1, and R96W binding was almost three fold higher than the WT zDHH9. These results might be attributed to the conformational changes occurring in the mutant by replacing Arginine at position 96 with Tryptophan; this was discussed in the previous chapter; the AlphaFold 3D protein predictions software (Figure 4.8) suggested the loss of five hydrogen bonds in this mutant resulting in a slight unwinding of the structure, which might result in exposing more sites for binding to GLUT1. Although this difference in binding is potentially interesting and should be followed up in future work, it should be noted that this difference could also reflect the quantification approach used. Here, the HA-zDHH9 signal in the immunoprecipitated samples is expressed as a fraction of the EGFP-GLUT1 signal. This is to account for any differences in expression or

immunoprecipitation of EGFP-GLUT1 between samples. As the level of EGFP-GLUT1 in R96W transfections was consistently lower than in WT zDHHC9 transfections, it will be important to try to normalise expression levels in these experiments (e.g., through transfection with different plasmid amounts) to compare WT and R96W zDHHC9 co-immunoprecipitation levels when EGFP-GLUT1 is present at similar levels.

After observing zDHHC9 co-immunoprecipitation with GLUT1, two questions arose: (i) How selective is GLUT1 to zDHHC9 compared to other DHHC enzymes, specifically zDHHC5, which also uses a GCP16/Golga7 accessory protein, or the Golgi-localized zDHHC7 enzyme that S-acylates the glucose transporters like GLUT4 (Du *et al.*, 2017)? (ii) Does GCP16 play a further role in the overall process of S-acylation of GLUT1 by zDHHC9? Analysing our results revealed little specificity in zDHHC9/5/7 binding to GLUT1, but remarkably, a robust interaction with GCP16 was identified. Indeed, this observation relates to acyl biotin exchange assays performed by Zhang *et al.* (2021) measuring levels of GLUT1 S-acylation, where GLUT1 was found to be modified at Cys-207 only when both WT zDHHC9 and GCP16 were present. Thereby breaking down the zDHHC9/GCP16-GLUT1 interaction, one can speculate that in addition to GCP16's roles in enhancing zDHHC9 S-acylation activity, it may also contribute to substrate binding/specificity by recruiting GLUT1 to the zDHHC9-GCP16 complex, subsequently facilitating its S-acylation. These results add a layer of complexity to the dynamic multi-functions of GCP16, where there may be some unique functions in specific settings, depending on several variables, one of which is the target substrate itself.

After establishing the role of GCP16 in binding with GLUT1, we attempted to observe, verify, and quantify the S-acylation of GLUT1 using different click chemistry detection approaches. As shown in Figure 5.3, we were able to detect possible S-acylation of GLUT1 using an alkyne infrared dye (IR800) but not using alkyne-PEG. However, we

could not consistently detect the S-acylation of GLUT1 using this assay and, therefore, could not examine how the R148W and R96W variants affected GLUT1 S-acylation. We suspect that the R148W mutant would disrupt GLUT1 S-acylation as it interferes with zDHHC9 autoacylation (Mitchell *et al.*, 2014), but it would be especially interesting to see the effects of R96W, which we suspect would also disrupt GLUT1 S-acylation based on the findings presented in Chapter 4. In follow-up work, an acyl RAC (resin-assisted capture) assay could be used to study the S-acylation of GLUT1, which may offer more sensitivity to detect the modification of this transporter.

Although the focus of Chapter 5 was centred on the hypothesis that *ZDHHC9* variants might lead to a condition mimicking GLUT1 DS through defects in GLUT1 S-acylation, we were also interested in exploring the wider impacts of zDHHC9 loss-of-function. For this, we purified RNA from WT and *Zdhhc9* knockout brain samples and sent these for RNA sequencing analysis. The brains were from mouse pups (post-natal days 2-3), as intellectual disability is considered a neurodevelopmental disorder. This analysis returned a very restricted set of significant changes in mRNA expression between WT and knockout mice, with only five genes significantly down-regulated in the knockout samples. Confidence in this data was enhanced by the fact that one of these down-regulated mRNAs was for zDHHC9. The exact mechanism behind the down-regulation of the four genes is unclear, and it might be attributed to an adaptive response in the *Zdhhc9* knock-out model. Nevertheless, it is interesting to discuss the known functions of the genes identified in the RNA sequencing analysis.

Ddit4 contributes to multiple biological processes, including the phosphatidylinositol 3-kinase (PI3K)-Akt signalling pathway, which regulates crucial cellular functions such as translation, proliferation, growth, and survival. Hers *et al.* (2011) discussed the role of Akt in cell survival, and its dysregulation is known to be a significant causative factor for major medical conditions such as cancer, diabetes, and neurological disorders, where it mediates the maintenance and survival of dopamine



neurons of the substantia nigra and prevent their decay, which leads to Parkinson's disease. Furthermore, Skaper (2012) reported the role of Akt in activating neurotrophins, which are a group of proteins responsible for the survival and development of sympathetic and sensory neurons in both the central and peripheral nervous systems.

Another gene identified in the RNA sequencing analysis was Hapln4, which encodes hyaluronan and proteoglycan link protein 2, an essential player in the formation and control of hyaluronan-based condensed perineuronal nets, which are crucial for neuronal plasticity (Oohashi *et al.*, 2015). It was recently found that Hapln4 plays a vital role in transmitting signals from the cerebral cortex to the deep cerebellar nuclei through Purkinje cells by selectively regulating the formation and transmission of GABAergic synapses, as Hapln4/Bral2 knock-out mice exhibited decreased inhibitory synaptic strengths (Edamatsu *et al.*, 2018) striking an excitatory: inhibitory imbalance, and mimicking results observed in loss-of-function *Zdhhc9* mutations (Shimell *et al.*, 2019). These observations make the Hapln4 protein an intriguing candidate for further analysis, as its deficit manifests similarly to zDHHC9 loss-of-function.

The third downregulated gene was GM14434, which encodes a protein called Novel KRAB box and zinc finger, C2H2 type domain-containing protein, which belongs to the KRAB-zinc finger protein family; KRAB refers to the Kruppel-associated box domain, which possesses the ability to repress genes binding to it through recruitment of various transcriptional factors (Yang *et al.*, 2017). The function of GM14434 is poorly understood, but some of the KRAB-zinc finger family encode proteins that have been reported to play a role in erythroid cell differentiation, regulating hematopoietic differentiation and the suppression of some oncogenic genes like ZNF382 protein, which plays a pro-apoptotic role and inhibit the proliferation of tumour cells (Cheng *et al.*, 2010). However, on the other hand, this protein has been reported to have a role in suppressing anti-apoptotic genes involved in leukaemia development (Lupo *et al.*,

2013). Furthermore, some members of the KRAB-zinc finger family have been related to non-syndromic intellectual disability; two ZNF41 mutations were identified: a proline-to-leucine amino acid mutation and a splice-site mutation, and both of these mutations resulted in intellectual disability, and further investigation is needed to understand the role of ZNF41 in brain development (Shoichet, 2003).

The final gene identified by our analysis was CFD encoding complement factor D protein, a member of the chymotrypsin family that has a pivotal role in the immune system response, specifically in the alternative pathway, a cascade of the complement system responsible for innate immunity. The initiation of the CFD function depends on conformational changes, as this allows binding to factor B, which is then cleaved into Bb and Ba subunits, ultimately leading to the common final pathway and forming the membrane attack complex (MAC) (Ruiz-Ojeda *et al.*, 2018). CFD deficiency has been described to occur due to a mutation changing the TCG codon for serine 42 into a TAG stop codon, leading to impaired expression, which manifests as low CFD serum levels; interestingly, patients having no CFD activity and subsequently, no alternative pathway activity, exhibit high susceptibility to infections (Biesma *et al.*, 2001). Overall, we believe that further analysis of this small set of genes could uncover other pathways within which *zDhhc9* functions.

### **5.3.2 Inducing liver stress to assess adaptive responses in *Zdhhc9* knockout mice**

GLUT1 dysfunction can lead to brain starvation due to its abundance in brain capillaries (Weiler-Güttler *et al.*, 1989). This can lead to neurological symptoms such as seizures and developmental delays, and it can also drive the brain to use ketone bodies as a source of energy (Vivo *et al.*, 1991). Considering the critical importance of GLUT1, we hypothesized that a lack of GLUT1 S-acylation and subsequent defect in delivery to the plasma membrane could provide a general explanation for the

majority of the zDHHC9 clinical implications and perhaps pave the way for a management guideline.

To test this hypothesis, our final focus was a 6-month trial designed based on the following: (i) We assumed patients with zDHHC9 loss-of-function mutations have mild to moderate intellectual disability mimicking GLUT1 deficiency syndrome stemming from a lack of S-acylation of GLUT1. (ii) A ketogenic diet (high fat/ moderate protein) is the first treatment of choice for GLUT1 deficiency syndrome (Sandu *et al.*, 2019); however, in normal subjects, a ketogenic diet induces elevated liver enzymes significantly beyond normal levels (Anekwe *et al.*, 2020). (iii) Case reports of patients with GLUT1 deficiency syndrome undergoing a permanent ketogenic diet developed cerebral metabolic adaptation relying on ketone bodies as an energy source with surprisingly normal liver enzymes, permanent Ketosis, and improved neurological symptoms (Chenouard *et al.*, 2015).

After six months of exposing WT. and *Zdhhc9* knockout mice to a breeding diet resembling a ketogenic diet with relatively high fat, moderate protein, and sufficient nutrients, the results were quite striking. Liver enzyme ALT was slightly higher in the WT, AST was almost twofold higher in the WT, and GGT was significantly higher in the WT; on the other hand, the ketone body BHB was almost threefold higher in the KO, suggesting Ketosis. These results support the hypothesis that loss of GLUT1 S-acylation by zDHHC9 could lead to its mislocalisation and, subsequently, the development of a case that mimics GLUT1 deficiency. Although these results are interesting, it will be essential to repeat the analysis on a larger number of animals. If this is validated, then we recommend neurological testing of the knockout mice to monitor any improvements. For example, Kouskou *et al.* (2018) showed that the knockout mice have deficits in learning and memory assessed using the Morris water maze, and Shimell *et al.* (2019) showed changes in the ratio of excitatory: inhibitory synapses and dendrite growth in knockout mice. Thus, it will be interesting to examine

how these phenotypes are affected by diet. It is also worth considering modifying the maternal diet of mice during pregnancy, as ketone bodies cross the blood-placental barrier and might prevent these neurological changes, which could offer a major insight into the development of symptoms in patients with *ZDHHC9* mutations.

## **CHAPTER 6**

### **GENERAL DISCUSSION**

## Chapter six

### General Discussion

S-acylation is the only reversible lipid modification occurring on proteins after their synthesis, controlling their location and stability and, by extension, their function. However, understanding the full impact of S-acylation on modified proteins has been challenging; this is due to the number of factors that come into play for each protein, like the number of cysteines modified, the dynamics of acyl chain turnover, and the enzyme(s) modifying the protein and their localisation. Therefore, each of these factors should be studied to develop a comprehensive understanding of this process. The overarching goal of this thesis was to provide a new understanding of the zDHHC9 enzyme and how mutations in the gene encoding this enzyme might cause neurological dysfunction. To do so, I explored how the accessory protein GCP16 regulates zDHHC9 and compared this to the effects of this protein on zDHHC5. In addition, I investigated how the uncharacterised R96W variant might disrupt zDHHC9 function (including through altered GCP16 interaction) and compared this to the better-characterised R148W variant. Lastly, I focused on undertaking an analysis of *Zdhhc9* knockout mouse samples, which sought to define gene expression changes brought about by the loss of zDHHC9 function and to test a novel hypothesis that neurological changes that occur with *ZDHHC9* mutations might be linked to GLUT1 deficiency. The final question has the potential to open up possible treatment of zDHHC9 loss-of-function through dietary intervention.

GCP16 appears to have functions beyond zDHHC9 (Salaün *et al.*, 2020), and GCP16 or its close homologue Golga7b can also influence zDHHC5 localisation and function (Woodley and Collins, 2019; Ko *et al.*, 2019; Solis *et al.*, 2022). In addition, GCP16 can influence the S-acylation activity of enzymes closely related to zDHHC9, such as zDHHC14 and zDHHC18 (Yang *et al.*, 2024). Furthermore, GCP16 is also a substrate for some of these enzymes, as shown for zDHHC5 (Solis *et al.*, 2022). Thus, there

may be three possible relationships between GCP16 and S-acylation enzymes: (i) as a substrate, for example, when GCP16 is S-acylated by zDHHC5 (Solis *et al.*, 2022); (ii) as an accessory protein forming a functional complex with a zDHHC enzyme and regulating S-acylation activity (Swarthout *et al.*, 2005; Yang *et al.*, 2024), or (iii) as an accessory protein facilitating substrate recruitment to a zDHHC enzyme, for example, the possible recruitment of GLUT1 to zDHHC9 (Chapter 5).

The results presented in Chapter 3 confirmed the interaction of GCP16 with both zDHHC5 and zDHHC9, but also highlighted a weaker interaction with zDHHC3 (Figures 3.5 and 3.5). These results are consistent with recent work showing that GCP16 can modulate the activity of zDHHC14 and zDHHC18 (Yang *et al.*, 2024), and extend these findings by showing that GCP16 also interacts with more distantly related enzymes such as zDHHC3. It will be interesting to understand what effect GCP16 has on zDHHC3, which is one of the most active enzymes in the zDHHC family with no requirement for a co-factor for activity (Jennings and Linder, 2012; Lemonidis *et al.*, 2014). Here, it would be interesting to explore if GCP16 regulates zDHHC3 stability or localisation at the Golgi, for example. It is also interesting to speculate how zDHHC3 might interact with GCP16 as the only clear conservation between this enzyme and zDHHC9 is in the DHHC domain, together with a few other conserved regions (Mitchell *et al.*, 2006). One of the four binding interfaces between GCP16 and zDHHC9 does involve the zinc finger domain (Yang *et al.*, 2024) and, therefore, this region of zDHHC3 could be central to its interaction with GCP16.

Focusing on the more robust interaction of GCP16 with zDHHC9 and zDHHC5, Figures 3.1-3.3 uncovered a reciprocal relationship linked to protein stability and expression, with GCP16 stabilising zDHHC9/5 and the enzymes stabilising GCP16. This observation is interesting as previous work on the yeast homologues of zDHHC9 and GCP16, ERF2 and ERF4, showed that ERF4 was important to prevent ubiquitination and degradation of ERF2 (Mitchell *et al.*, 2012). It would, therefore, be

interesting to examine the ubiquitination status of zDHHc9/5 when GCP16 is absent (and *vice versa*) and if inhibiting proteasome or lysosome activity prevents enzyme degradation. Our observation of increased enzyme stability is also consistent with the work of Nguyen *et al.* (2023), who showed that zDHHc9 formed higher molecular weight aggregates in the absence of GCP16, consistent with reduced stability/folding. In addition to the effects of GCP16 on zDHHc5/9 stability, we also observed GCP16 acting as a substrate, where it was S-acylated by the Golgi enzymes zDHHc-3,-7, and -9, and also by zDHHc5 (Figure 3.7 and Figure 3.18). It will be interesting to explore further how GCP16 S-acylation is linked to its regulatory effects. The cryo-EM study of Yang *et al.* (2024) suggested that S-acylation is important for the correct positioning of GCP16 to facilitate zDHHc9 interaction, and it will be interesting to determine if GCP16 S-acylation in cells is primarily mediated by the enzymes it regulates or if other enzymes (such as zDHHc3/7) mediate S-acylation of GCP16, bringing it to the Golgi and thereby facilitating interaction with Golgi-localised zDHHc9.

Another avenue I explored was a related GCP16 isoform sharing almost 61% amino acid similarity (Salaün *et al.*, 2020) named Golga7b, which was identified as an accessory protein for zDHHc5 (Woodley and Collins, 2019). Interestingly, the results in Figure 3.8 showed that zDHHc5 had a higher complex formation capacity with Golga7b than the other enzymes that were tested, but Golga7b also interacted robustly with zDHHc9. Intriguingly, however, zDHHc9 did not stabilise Golga7b and also did not increase its S-acylation status (Figures 3.9 and 3.10), perhaps suggesting that GCP16 (rather than Golga7b) might be the most physiologically relevant accessory factor for this enzyme. Another interesting observation was the co-immunoprecipitation of GCP16 with itself and with Golga7b, highlighting potential homo- and hetero-dimerisation between these related accessory proteins. The significance of GCP16/Golga7b dimerisation is not clear, and has not been previously



reported. Here, it will be interesting to identify the regions of these proteins that mediate self-association and how they relate to the binding interfaces involved in zDHHC9 interaction (Yang *et al.*, 2024). By introducing mutations that block dimerisation, the importance of homo- and hetero-dimerization of GCP16/Golga7b on the activity and stability of zDHHC9/5 can be explored in more detail.

Despite zDHHC9 and zDHHC5 interacting with GCP16 and showing similar reciprocal stabilisation and S-acylation, the interaction of these enzymes showed distinct dependencies on GCP16 S-acylation. This was revealed from co-immunoprecipitation experiments comparing wild-type GCP16 with a mutant in which the two major S-acylated cysteines (Cys-69 and Cys-72; Ohta *et al.*, 2003) were replaced by alanine residues. These cysteine substitutions did not affect the interaction of GCP16 with zDHHC9 but did block the interaction with zDHHC5 (Figure 3.13). Furthermore, despite interacting with zDHHC9 as well as the wild-type GCP16 did, the cysteine mutant was not able to enhance the stability of zDHHC9 (Figure 3.14). This observation with zDHHC9 discriminates a *physical* interaction of zDHHC9 with GCP16 (detected by co-immunoprecipitation) from a *functional* interaction (changes in stability or S-acylation).

Interestingly, despite Cys-69 and Cys-72 being identified as the major S-acylation sites in GCP16 by Ohta *et al.* (2003), S-acylation of the GCP16 mutant lacking these sites was still detected when co-expressed with zDHHC5 (Figure 3.17), and further analysis identified that this enzyme also had activity towards an additional cysteine residue, Cys-81 (Figure 3.18). This might suggest that zDHHC5 produces a distinct form of GCP16 that interacts with membranes in a different manner from GCP16 that is S-acylated by zDHHC9 (because Cys-81 would be membrane-embedded with zDHHC5, but not with zDHHC9). These S-acylation differences between GCP16 with zDHHC5 and zDHHC9, combined with the observed homo- and hetero-interactions

between GCP16 and Golga7b, indicate that many aspects to these interactions that require further investigation.

In Chapter 4, I focused on the R96W mutation in zDHHC9, which is linked to neurological dysfunction and intellectual disability (Tzschach *et al.*, 2015). Unlike R148W and P150S mutations, the effects of the R96W amino acid substitution have not been explored and are particularly interesting due to the presence of this amino acid outside of the catalytic domain of zDHHC9. Raymond *et al.* (2007) first described the R148W mutation and provided a clinical picture that varied in symptoms and manifestations, which even led to the consideration of Marfanoid syndrome. Some patients suffered from severe to moderate intellectual disability, with some exhibiting changes in body morphology, such as facial dysmorphism and thinning of the corpus callosum (Schirwani *et al.*, 2018; Ramos *et al.*, 2023). The R96W mutation described by Tzschach *et al.* (2015) had almost the same manifestations as the R148W mutation, except that no changes in the brain morphology were detected.

The reports of Ramos *et al.* (2023) and Tzschach *et al.* (2015) highlight a compelling correlation between various mutations and a diverse range of clinical symptoms in patients despite the uniform outcome of zDHHC9 function loss. The symptomatic manifestations observed in the cohort included autism, developmental delays, epilepsy, dysmorphic features, intellectual disability, and abnormalities on brain MRI. This suggests that while the underlying genetic mutation may differ, the resultant functional impairment of zDHHC9 leads to a common pathological outcome, underscoring the complexity of genotype-phenotype relationships in neurodevelopmental disorders.

Initially, I wanted to confirm the loss-of-function of both R96W and R148W mutants, and Figure 4.6 showed that S-acylation of GCP16 was not seen with either of the mutants. Thus, even though R96W occurs outside the catalytic domain, it nevertheless leads to a loss of zDHHC9 activity towards GCP16. Subsequently, I also

tested the S-acylation of the R96W and R148W mutants; Figure 4.7 shows that the S-acylation of both of these zDHHc9 mutants was decreased and that there was no increase in the presence of GCP16. So, both the activity and the S-acylation of the R148W and R96W mutants are decreased compared to wild-type zDHHc9. I used the prediction software AlphaFold Colab to predict the shape of the mutant, as shown in Figure 4.8. The structure predicts that the R96W substitution affects hydrogen bonding around the active site, changing its conformation and thus possibly providing a reason for the decreased activity of this mutant against GCP16.

Interestingly, however, I did uncover a difference between the R148W and R96W mutants concerning their stability. Figure 4.2 shows almost no effect of GCP16 on the stability of the R148W mutant. This is in agreement with Yang *et al.* (2024), who argued that the replacement of arginine-148 with a bulky tryptophan residue is likely to disrupt zinc binding to this region of zDHHc9, thus disrupting the stability of the enzyme. In contrast, I found that GCP16 was able to stabilise the R96W mutant, which is in contrast to the work of Nguyen *et al.* (2023), who argued that GCP16 did not affect the stability of the R96W mutant, assessed through size exclusion chromatography analysis showing that GCP16 did not rescue the aggregation of R96W. It will be important to understand why cycloheximide chase experiments give different conclusions from size exclusion chromatography, but we would argue that the latter approach does not directly measure effects on protein half-life, while the cycloheximide approach does. Indeed, we also found that the R148W mutant had a reduced binding to GCP16 compared to wild-type zDHHc9, whereas the R96W mutant showed similar binding as wild-type enzyme. In addition to this, the R148W mutant also displayed reduced binding to the substrate protein H-Ras.

Interestingly, the clinical reports of these zDHHc9 variants showed many varied symptoms, from almost normal with slight mental delay to severe forms of autism and intellectual disability; even some patients from the same family with the same variant

had different developmental delays and learning disabilities (Schirwani *et al.*, 2018). Overall, this is consistent with the observed varied molecular behaviour of the R96W and R148W mutants seen in chapter four.

The final chapter of the thesis focused on one substrate of zDHHc9 that was of specific interest: GLUT1. It was reported by Zhang *et al.* (2021) that GLUT1 is S-acylated by zDHHc9 in Glioblastoma cells, and this substrate was of particular interest because GLUT1 deficiency syndrome shares many common features with zDHHc9 loss-of-function. Therefore, we examined the binding of GLUT1 to the zDHHc9 mutants and other zDHHc enzymes that might mediate the S-acylation of this glucose transporter. Interestingly, GLUT1 appeared to bind almost four-fold better to the R96W mutant than to wild-type zDHHc9, assessed using co-immunoprecipitation experiments (Figure 5.1). Furthermore, GLUT1 was found to bind to GCP16, and more GLUT1 protein was co-precipitated with GCP16 than with any zDHHc enzyme (Figure 5.2).

Unfortunately, efforts to study the S-acylation of GLUT1 and how this was affected by the zDHHc9 mutants were unsuccessful, and the assay was not sensitive enough to detect the S-acylation of this substrate. Our group has previously found that transmembrane protein S-acylation can be challenging to detect using click chemistry approaches, and therefore, it will be interesting also to explore this question using other S-acylation detection methods such as acyl resin-assisted capture (Acyl-RAC) or acyl-biotin exchange (Chamberlain and Shipston, 2015).

Due to the scarcity of clinical data, I designed a long-term *in vivo* experiment to test whether loss of GLUT1 function might be present in the *Zdhhc9* knockout mouse model. Based on the assumption that these mice have a non-syndromic case mimicking a mild GLUT1 deficiency, I devised a protocol based on the treatment of GLUT1 deficiency syndrome and the haematology findings that correspond with this rare syndrome.

As this syndrome can vary in severity (De Giorgis and Veggiotti, 2013), I changed the diet of the mice (with controls kept on a regular diet) into a breeding diet with a higher fat and protein content, mimicking a ketogenic diet, for six months. This was done as the ketogenic diet is considered the first treatment line for GLUT1 deficiency (Sandu *et al.*, 2019); however, this comes with a package of elevated liver enzymes for the normal subjects (Anekwe *et al.*, 2020) and normal liver and metabolic adaptation in the form of ketoacidosis in patients with GLUT1 deficiency (Chenouard *et al.*, 2015).

Chemistry and haematology analysis on the mice, which assessed the function of the liver through its enzymes and the presence of the BHB (ketone) body, were performed after six months. Intriguingly, the results almost completely correlated with patients with GLUT1 deficiency syndrome, and the liver enzymes in normal subjects were higher than the knockouts, suggesting metabolic adaptation (Chenouard *et al.*, 2015). Whilst this is only preliminary data that needs to be repeated on a larger cohort of animals and explored further through access to medical reports, I believe it may open the door for new possibilities for the treatment of patients with *ZDHHC9* mutations or at least for symptom management.

Finally, it is important to reflect on some of the limitations of the work reported in this thesis. The cell biochemistry experiments all used HEK293 cells and involved the overexpression of tagged forms of the proteins of interest. It will be important in future work to validate the key findings in more physiological settings, such as primary neurons, and also to use systems that allow more control of protein expression levels (e.g. induction by the addition of doxycycline). It is likely that the expression levels achieved in this study are substantially higher than those observed for endogenous *zDHHC9* and *GCP16*. Indeed, a recent review by Mesquita *et al.*, (2024) highlighted the very low endogenous expression levels of *zDHHC* enzymes. The results of two proteomics studies in HeLa cells, one by Hein *et al.* (2015), which analyzed 9 *zDHHC* enzymes, and the other by Bekker-Jensen *et al.* (2017), analyzing 17 of the *zDHHC*

enzymes, highlighted that enzyme expression (copy number) ranges from hundreds to several thousands, with an overall (combined) copy number for all zDHHC enzymes in the range of 43,000–110,000. Mesquita *et al.* (2024) noted that this combined copy number for all zDHHC enzymes was lower than the copy number of a single N-myristoyl transferase enzyme. This observation clearly highlights the importance of future work studying zDHHC enzymes at the lowest possible level of over-expression, which still allows reasonable detection.

It should be noted that the S-acylation field suffers from a lack of antibodies that are sensitive enough to detect endogenously expressed zDHHC enzymes. Therefore, enzyme over-expression has been widely used to study the localization and function of the enzymes (e.g. Ohno *et al.*, 2006). Enzyme over-expression could be associated with saturation of cell pathways, mis-localisation, and could also lead to S-acylation of proteins that are not usually (at endogenous expression levels) targets of that enzyme. The discovery of antibodies that detect endogenous zDHHC enzymes, will therefore represent an important step forward for the field. Interestingly, a commercial antibody is able to detect zDHHC9 albeit with low sensitivity (Kouskou *et al.*, 2018). It might therefore be possible to generate mutations in endogenous proteins and study the functional consequences of this. For example, specific mutations (R96W and R148W) could be introduced into endogenous zDHHC9 using techniques such as CRISPR to study effects on stability and localisation. In addition, such manipulation of endogenous proteins will also remove issues associated with protein tagging. Here, the appendage of tags to the N- or C-terminus of proteins can interfere with normal protein interactions, including with factors that regulate the normal cellular distribution or targeting of the proteins of interest.

Finally, it will be important to repeat some of the experiments in this thesis where replicates were low, and to increase biological replicates to validate some of the results reported here.

# **CHAPTER 7**

## **REFERENCES**

## References

- Abrami, L, Kunz B, Iacovache I, van der Goot FG. Palmitoylation and ubiquitination regulate exit of the Wnt signaling protein LRP6 from the endoplasmic reticulum. *Proceedings of the National Academy of Sciences*. 2008;105(14):5384-89.
- Abrami, L, Dallavilla T, Sandoz PA, Demir M, Kunz B, Savoglidis G, Hatzimanikatis V, van der Goot FG. Identification and dynamics of the human ZDHHC16-ZDHHC6 palmitoylation cascade. *Elife*. 2017;6:e27826.
- Abrami, L, Audagnotto M, Ho S, Marcaida MJ, Mesquita FS, Anwar MU, Sandoz PA, Fonti G, Pojer F, Dal Peraro M, van der Goot FG. Palmitoylated acyl protein thioesterase APT2 deforms membranes to extract substrate acyl chains. *Nat Chem Biol*. 2021;17(4):438-47.
- Adachi, N, Hess DT, McLaughlin P, Stamler JS. S-Palmitoylation of a Novel Site in the  $\beta$ 2-Adrenergic Receptor Associated with a Novel Intracellular Itinerary. *J Biol Chem*. 2016;291(38):20232-46.
- Adams, MN, Christensen ME, He Y, Waterhouse NJ, Hooper JD. The Role of Palmitoylation in Signalling, Cellular Trafficking and Plasma Membrane Localization of Protease-Activated Receptor-2. *PLoS One*. 2011;6(11):e28018.
- Aitken, A, Cohen P, Santikarn S, Williams DH, Calder AG, Smith A, Klee CB. Identification of the NH<sub>2</sub>-terminal blocking group of calcineurin B as myristic acid. *FEBS Lett*. 1982;150(2):314-8.
- Alfaphold2 Colab for 3D protein prediction (<https://colab.research.google.com/>)
- Amara, N, Foe IT, Onguka O, Garland M, Bogyo M. Synthetic Fluorogenic Peptides Reveal Dynamic Substrate Specificity of Depalmitoylases. *Cell Chem Biol*. 2019;26(1):35-47.e7.



Andrew, RJ, Fernandez CG, Stanley M, Jiang H, Nguyen P, Rice RC, Buggia-Prévo V, De Rossi P, Vetrivel KS, Lamb R, Argemi A, Allaert ES, Rathbun EM, Krause SV, Wagner SL, Parent AT, Holtzman DM, Thinakaran G. Lack of BACE1 S-palmitoylation reduces amyloid burden and mitigates memory deficits in transgenic mouse models of Alzheimer's disease. *Proc Natl Acad Sci U S A*. 2017;114(45):E9665-e74.

Anekwe, CV, Chandrasekaran P, Stanford FC. Ketogenic Diet-induced Elevated Cholesterol, Elevated Liver Enzymes and Potential Non-alcoholic Fatty Liver Disease. *Cureus*. 2020;12(1):e6605.

Anwar, MU, van der Goot FG. Refining S-acylation: Structure, regulation, dynamics, and therapeutic implications. *J Cell Biol*. 2023; 222(11):e202307103.

Baker, K, Astle DE, Scerif G, Barnes J, Smith J, Moffat G, Gillard J, Baldeweg T, Raymond FL. Epilepsy, cognitive deficits and neuroanatomy in males with ZDHHC9 mutations. *Annals of clinical and translational neurology*. 2015;2(5):559-69.

Bartels, DJ, Mitchell DA, Dong X, Deschenes RJ. Erf2, a Novel Gene Product That Affects the Localization and Palmitoylation of Ras2 in *Saccharomyces cerevisiae*. *Molecular and Cellular Biology*. 1999;19(10):6775-87.

Bhattacharyya, R, Barren C, Kovacs DM. Palmitoylation of Amyloid Precursor Protein Regulates Amyloidogenic Processing in Lipid Rafts. *The Journal of Neuroscience*. 2013;33(27):11169-83.

Bekker-Jensen, DB, Kelstrup CD, Batth TS, Larsen SC, Haldrup C, Bramsen JB, Sørensen KD, Høyer S, Ørntoft TF, Andersen CL, Nielsen ML, Olsen JV. An Optimized Shotgun Strategy for the Rapid Generation of Comprehensive Human Proteomes. *Cell Syst*. 2017;4(6):587-99.e4.

Biesma, DH, Hannema AJ, van Velzen-Blad H, Mulder L, van Zwieten R, Kluijdt I, Roos D. A family with complement factor D deficiency. *The Journal of Clinical Investigation*. 2001;108(2):233-40.

Blanc, M, David FPA, van der Goot FG. SwissPalm 2: Protein S-Palmitoylation Database. *Methods Mol Biol*. 2019;2009:203-14.

Blanc, M, David F, Abrami L, Migliozi D, Armand F, Bürgi J, van der Goot FG. SwissPalm: Protein Palmitoylation database. *F1000Res*. 2015; 16(4):261.

Blanpain, C, Wittamer V, Vanderwinden JM, Boom A, Renneboog B, Lee B, Le Poul E, El Asmar L, Govaerts C, Vassart G, Doms RW, Parmentier M. Palmitoylation of CCR5 is critical for receptor trafficking and efficient activation of intracellular signaling pathways. *J Biol Chem*. 2001;276(26):23795-804.

Braakman, HMH, Nicolai J, Willemsen MAAP. Stroke-like episodes add to the phenotypic spectrum of GLUT1 deficiency syndrome. *European Journal of Paediatric Neurology*. 2017;21:e176.

Burns, A, Iliffe S. Alzheimer's disease. *BMJ*. 2009;338:b158.

Busquets-Hernández, C, Ribó S, Gratacós-Batlle E, Carbajo D, Tsiotsia A, Blanco-Canosa JB, Chamberlain LH, Triola G. Quantitative analysis of protein lipidation and acyl-CoAs reveals substrate preferences of the S-acylation machinery. *Chem Sci*. 2024;15(32):12845-55.

Butland, SL, Sanders SS, Schmidt ME, Riechers SP, Lin DT, Martin DD, Vaid K, Graham RK, Singaraja RR, Wanker EE, Conibear E, Hayden MR. The palmitoyl acyltransferase HIP14 shares a high proportion of interactors with huntingtin: implications for a role in the pathogenesis of Huntington's disease. *Hum Mol Genet*. 2014;23(15):4142-60.

Camp, LA, Verkruyse LA, Afendis SJ, Slaughter CA, Hofmann SL. Molecular cloning and expression of palmitoyl-protein thioesterase. *J Biol Chem.* 1994;269(37):23212-9.

Carrel, D, Firestein BL. MicroRNA-mediated regulation of synaptic palmitoylation: shrinking fat spines. *Nature Cell Biology.* 2009;11(6):681-82.

Castro-Cruz, M, Lembo F, Borg J-P, Travé G, Vincentelli R, Zimmermann P. The Human PDZome 2.0: Characterization of a New Resource to Test for PDZ Interactions by Yeast Two-Hybrid. *Membranes.* 2023;13(8):737.

Chai, S, Cambronne XA, Eichhorn SW, Goodman RH. MicroRNA-134 activity in somatostatin interneurons regulates H-Ras localization by repressing the palmitoylation enzyme, DHHC9. *Proceedings of the National Academy of Sciences.* 2013;110(44):17898-903.

Chamberlain, LH, Shipston MJ. The physiology of protein S-acylation. *Physiol Rev.* 2015;95(2):341-76.

Chen, X, Ma H, Wang Z, Zhang S, Yang H, Fang Z. EZH2 Palmitoylation Mediated by ZDHHC5 in p53-Mutant Glioma Drives Malignant Development and Progression. *Cancer Res.* 2017;77(18):4998-5010.

Cheng, X, Wang K, Zhao Y, Wang K. Research progress on post-translational modification of proteins and cardiovascular diseases. *Cell Death Discovery.* 2023;9(1):275.

Cheng, Y, Geng H, Cheng SH, Liang P, Bai Y, Li J, Srivastava G, Ng MH, Fukagawa T, Wu X, Chan AT, Tao Q. KRAB zinc finger protein ZNF382 is a proapoptotic tumor suppressor that represses multiple oncogenes and is commonly silenced in multiple carcinomas. *Cancer Res.* 2010;70(16):6516-26.

Chenouard, A, Vuillaumier-Barrot S, Seta N, Kuster A. A Cause of Permanent Ketosis: GLUT-1 Deficiency. *JIMD Rep.* 2015;18:79-83.

Cherezov, V, Rosenbaum DM, Hanson MA, Rasmussen SGF, Thian FS, Kobilka TS, Choi H-J, Kuhn P, Weis WI, Kobilka BK, Stevens RC. High-Resolution Crystal Structure of an Engineered Human Adrenergic G Protein-Coupled Receptor. *Science.* 2007;318(5854):1258-65.

Choi, YW, Bae SM, Kim YW, Lee HN, Kim YW, Park TC, Ro DY, Shin JC, Shin SJ, Seo JS, Ahn WS. Gene expression profiles in squamous cell cervical carcinoma using array-based comparative genomic hybridization analysis. *Int J Gynecol Cancer.* 2007;17(3):687-96.

Collins, MO, Woodley KT, Choudhary JS. Global, site-specific analysis of neuronal protein S-acylation. *Sci Rep.* 2017;7(1):4683.

Cori, GT. THE EFFECT OF STIMULATION AND RECOVERY ON THE PHOSPHORYLASE a CONTENT OF MUSCLE. *Journal of Biological Chemistry.* 1945;158(2):333-39.

De Giorgis, V, Veggiotti P. GLUT1 deficiency syndrome 2013: Current state of the art. *Seizure.* 2013;22(10):803-11.

Desai, S, Juncker M, Kim C. Regulation of mitophagy by the ubiquitin pathway in neurodegenerative diseases. *Exp Biol Med (Maywood).* 2018;243(6):554-62.

Draper, JM, Smith CD. DHHC20: a human palmitoyl acyltransferase that causes cellular transformation. *Molecular Membrane Biology.* 2010;27(2-3):123-36.

Du, Z, Zheng H, Huang B, Ma R, Wu J, Zhang X, He J, Xiang Y, Wang Q, Li Y, Ma J, Zhang X, Zhang K, Wang Y, Zhang MQ, Gao J, Dixon JR, Wang X, Zeng J, Xie W. Allelic reprogramming of 3D chromatin architecture during early mammalian development. *Nature.* 2017;547(7662):232-35.

Duncan, JA, Gilman AG. A Cytoplasmic Acyl-Protein Thioesterase That Removes Palmitate from G Protein  $\alpha$  Subunits and p21RAS. *Journal of Biological Chemistry*. 1998;273(25):15830-37.

Ebersole, B, Petko J, Woll M, Murakami S, Sokolina K, Wong V, Stagljar I, Lüscher B, Levenson R. Effect of C-Terminal S-Palmitoylation on D2 Dopamine Receptor Trafficking and Stability. *PLoS One*. 2015;10(11):e0140661.

Edamatsu, M, Miyano R, Fujikawa A, Fujii F, Hori T, Sakaba T, Oohashi T. Hapln4/Bral2 is a selective regulator for formation and transmission of GABAergic synapses between Purkinje and deep cerebellar nuclei neurons. *J Neurochem*. 2018;147(6):748-63.

Ernst, AM, Syed SA, Zaki O, Bottanelli F, Zheng H, Hacke M, Xi Z, Rivera-Molina F, Graham M, Rebane AA, Björkholm P, Baddeley D, Toomre D, Pincet F, Rothman JE. S-Palmitoylation Sorts Membrane Cargo for Anterograde Transport in the Golgi. *Dev Cell*. 2018;47(4):479-93.e7.

F, SM, Abrami L, Linder ME, Bamji SX, Dickinson BC, van der Goot FG. Mechanisms and functions of protein S-acylation. *Nat Rev Mol Cell Biol*. 2024;25(6):488-509.

Fredericks, GJ, Hoffmann FW, Hondal RJ, Rozovsky S, Urschitz J, Hoffmann PR. Selenoprotein K Increases Efficiency of DHHC6 Catalyzed Protein Palmitoylation by Stabilizing the Acyl-DHHC6 Intermediate. *Antioxidants*. 2018;7(1):4.

Fredericks, GJ, Hoffmann FW, Rose AH, Osterheld HJ, Hess FM, Mercier F, Hoffmann PR. Stable expression and function of the inositol 1,4,5-triphosphate receptor requires palmitoylation by a DHHC6/selenoprotein K complex. *Proc Natl Acad Sci U S A*. 2014;111(46):16478-83.

Fukata, M, Fukata Y, Adesnik H, Nicoll RA, Brecht DS. Identification of PSD-95 Palmitoylating Enzymes. *Neuron*. 2004;44(6):987-96.

Fukata, Y, Fukata M. Protein palmitoylation in neuronal development and synaptic plasticity. *Nat Rev Neurosci*. 2010;11(3):161-75.

George, J, Soares C, Montersino A, Beique JC, Thomas GM. Palmitoylation of LIM Kinase-1 ensures spine-specific actin polymerization and morphological plasticity. *Elife*. 2015;4:e06327.

Goodwin, JS, Drake KR, Rogers C, Wright L, Lippincott-Schwartz J, Philips MR, Kenworthy AK. Depalmitoylated Ras traffics to and from the Golgi complex via a nonvesicular pathway. *The Journal of cell biology*. 2005;170(2):261-72.

Gorenberg, EL, Massaro Tieze S, Yücel B, Zhao HR, Chou V, Wirak GS, Tomita S, Lam TT, Chandra SS. Identification of substrates of palmitoyl protein thioesterase 1 highlights roles of depalmitoylation in disulfide bond formation and synaptic function. *PLOS Biology*. 2022;20(3):e3001590.

Gorleku, OA, Barns AM, Prescott GR, Greaves J, Chamberlain LH. Endoplasmic reticulum localization of DHHC palmitoyltransferases mediated by lysine-based sorting signals. *J Biol Chem*. 2011;286(45):39573-84.

Greaves, J, Chamberlain LH. Differential palmitoylation regulates intracellular patterning of SNAP25. *J Cell Sci*. 2011;124(Pt 8):1351-60.

Greaves, J, Chamberlain LH. DHHC palmitoyl transferases: substrate interactions and (patho)physiology. *Trends Biochem Sci*. 2011;36(5):245-53.

Greaves, J, Gorleku OA, Salaün C, Chamberlain LH. Palmitoylation of the SNAP25 protein family: specificity and regulation by DHHC palmitoyl transferases. *J Biol Chem*. 2010;285(32):24629-38.

Greaves, J, Munro KR, Davidson SC, Riviere M, Wojno J, Smith TK, Tomkinson NCO, Chamberlain LH. Molecular basis of fatty acid selectivity in the zDHHC family of S-acyltransferases revealed by click chemistry. *Proceedings of the National Academy of Sciences*. 2017;114(8):E1365-E74.

Guan, X, Fierke CA. Understanding Protein Palmitoylation: Biological Significance and Enzymology. *Sci China Chem*. 2011;54(12):1888-97.

Halgren, C, Kjaergaard S, Bak M, Hansen C, El-Schich Z, Anderson C, Henriksen K, Hjalgrim H, Kirchhoff M, Bijlsma E, Nielsen M, den Hollander N, Ruivenkamp C, Isidor B, Le Caignec C, Zannolli R, Mucciolo M, Renieri A, Mari F, Anderlid B-M, Andrieux J, Dieux A, Tommerup N, Bache I. Corpus callosum abnormalities, intellectual disability, speech impairment, and autism in patients with haploinsufficiency of ARID1B. *Clinical Genetics*. 2012;82(3):248-55.

Han, JY, Lee IG, Shin S, Kim M, Jang JH, Park J. The first patient with sporadic X-linked intellectual disability with de novo ZDHHC9 mutation identified by targeted next-generation sequencing. *European journal of medical genetics*. 2017;60(10):499-503.

Hancock, JF, Magee AI, Childs JE, Marshall CJ. All ras proteins are polyisoprenylated but only some are palmitoylated. *Cell*. 1989;57(7):1167-77.

He, X, You C, Jiang H-I, Jiang Y, Xu E, Cheng X. AlphaFold2 versus experimental structures: evaluation on G protein-coupled receptors. *Acta Pharmacologica Sinica*. 2022;10.1038/s41401-022-00938-y:1-7.

Hein, MY, Hubner NC, Poser I, Cox J, Nagaraj N, Toyoda Y, Gak IA, Weisswange I, Mansfeld J, Buchholz F, Hyman AA, Mann M. A human interactome in three quantitative dimensions organized by stoichiometries and abundances. *Cell*. 2015;163(3):712-23.

Henderson, MX, Wirak GS, Zhang YQ, Dai F, Ginsberg SD, Dolzhanskaya N, Staropoli JF, Nijssen PC, Lam TT, Roth AF, Davis NG, Dawson G, Velinov M, Chandra SS. Neuronal ceroid lipofuscinosis with DNAJC5/CSP $\alpha$  mutation has PPT1 pathology and exhibit aberrant protein palmitoylation. *Acta Neuropathol.* 2016;131(4):621-37.

Hermann, J, Schurgers L, Jankowski V. Identification and characterization of post-translational modifications: Clinical implications. *Molecular Aspects of Medicine.* 2022;86:101066.

Hernandez, JL, Davda D, Cheung See Kit M, Majmudar JD, Won SJ, Gang M, Pasupuleti SC, Choi AI, Bartkowiak CM, Martin BR. APT2 Inhibition Restores Scribble Localization and S-Palmitoylation in Snail-Transformed Cells. *Cell Chem Biol.* 2017;24(1):87-97.

Hers, I, Vincent EE, Tavaré JM. Akt signalling in health and disease. *Cellular Signalling.* 2011;23(10):1515-27.

Hu, D, Li Y, Wang X, Zou H, Li Z, Chen W, Meng Y, Wang Y, Li Q, Liao F, Wu K, Wu J, Li G, Wang W. Palmitoylation of NLRP3 Modulates Inflammasome Activation and Inflammatory Bowel Disease Development. *J Immunol.* 2024;213(4):481-93.

Huang, K, Sanders S, Singaraja R, Orban P, Cijssouw T, Arstikaitis P, Yanai A, Hayden MR, El-Husseini A. Neuronal palmitoyl acyl transferases exhibit distinct substrate specificity. *Faseb j.* 2009;23(8):2605-15.

Huang, K, Yanai A, Kang R, Arstikaitis P, Singaraja RR, Metzler M, Mullard A, Haigh B, Gauthier-Campbell C, Gutekunst CA, Hayden MR, El-Husseini A. Huntingtin-interacting protein HIP14 is a palmitoyl transferase involved in palmitoylation and trafficking of multiple neuronal proteins. *Neuron.* 2004;44(6):977-86.



Hubalkova, P, Ladislav M, Vyklicky V, Smejkalova T, Hrcka Krausova B, Kysilov B, Krusek J, Naimová Z, Korinek M, Chodounska H, Kudova E, Cerny J, Vyklicky L. Palmitoylation Controls NMDA Receptor Function and Steroid Sensitivity. *The Journal of Neuroscience*. 2021;41(10):2119-34.

Hur, J-Y.  $\gamma$ -Secretase in Alzheimer's disease. *Experimental & Molecular Medicine*. 2022;54(4):433-46.

Huttlin, EL, Ting L, Bruckner RJ, Gebreab F, Gygi MP, Szpyt J, Tam S, Zarraga G, Colby G, Baltier K, Dong R, Guarani V, Vaites LP, Ordureau A, Rad R, Erickson BK, Wühr M, Chick J, Zhai B, Kolippakkam D, Mintseris J, Obar RA, Harris T, Artavanis-Tsakonas S, Sowa ME, De Camilli P, Paulo JA, Harper JW, Gygi SP. The BioPlex Network: A Systematic Exploration of the Human Interactome. *Cell*. 2015;162(2):425-40.

Jennings, BC, Linder ME. DHHC protein S-acyltransferases use similar ping-pong kinetic mechanisms but display different acyl-CoA specificities. *J Biol Chem*. 2012;287(10):7236-45.

Jeong, H-K, Gonzalez-Fernandez E, Crawley I, Hwang J, Martin DDO, Bamji SX, Kim J-I, Kang SH, Thomas GM. Micro-Scale Control of Oligodendrocyte Morphology and Myelination by the Intellectual Disability-Linked Protein Acyltransferase ZDHHC9. *eLife* 2024;13:RP97151.

Jumper, J, Evans R, Pritzel A, Green T, Figurnov M, Ronneberger O, Tunyasuvunakool K, Bates R, Žídek A, Potapenko A, Bridgland A, Meyer C, Kohl SAA, Ballard AJ, Cowie A, Romera-Paredes B, Nikolov S, Jain R, Adler J, Back T, Petersen S, Reiman D, Clancy E, Zielinski M, Steinegger M, Pacholska M, Berghammer T, Bodenstein S, Silver D, Vinyals O, Senior AW, Kavukcuoglu K, Kohli P, Hassabis D. Highly accurate protein structure prediction with AlphaFold. *Nature*. 2021;596(7873):583-89.

Kao, SH, Wang WL, Chen CY, Chang YL, Wu YY, Wang YT, Wang SP, Nesvizhskii AI, Chen YJ, Hong TM, Yang PC. Analysis of Protein Stability by the Cycloheximide Chase Assay. *Bio Protoc.* 2015;5(1):e1374.

Kawate, N, Menon KM. Palmitoylation of luteinizing hormone/human choriogonadotropin receptors in transfected cells. Abolition of palmitoylation by mutation of Cys-621 and Cys-622 residues in the cytoplasmic tail increases ligand-induced internalization of the receptor. *J Biol Chem.* 1994;269(48):30651-8.

Knopman, DS, Amieva H, Petersen RC, Chételat G, Holtzman DM, Hyman BT, Nixon RA, Jones DT. Alzheimer disease. *Nat Rev Dis Primers.* 2021;7(1):33.

Ko, P-J, Woodrow C, Dubreuil MM, Martin BR, Skouta R, Bassik MC, Dixon SJ. A ZDHHC5-GOLGA7 Protein Acyltransferase Complex Promotes Nonapoptotic Cell Death. *Cell Chemical Biology.* 2019;26(12):1716-24.

Ko, PJ, Dixon SJ. Protein palmitoylation and cancer. *EMBO Rep.* 2018;19(10):e46666.

Ko, PJ, Woodrow C, Dubreuil MM, Martin BR, Skouta R, Bassik MC, Dixon SJ. A ZDHHC5-GOLGA7 Protein Acyltransferase Complex Promotes Nonapoptotic Cell Death. *Cell Chem Biol.* 2019;26(12):1716-24.

Kohl, A, Binz HK, Forrer P, Stumpp MT, Plückthun A, Grütter MG. Designed to be stable: Crystal structure of a consensus ankyrin repeat protein. *Proceedings of the National Academy of Sciences.* 2003;100(4):1700-05.

Kong, E, Peng S, Chandra G, Sarkar C, Zhang Z, Bagh MB, Mukherjee AB. Dynamic palmitoylation links cytosol-membrane shuttling of acyl-protein thioesterase-1 and acyl-protein thioesterase-2 with that of proto-oncogene H-ras product and growth-associated protein-43. *J Biol Chem.* 2013;288(13):9112-25.

Kouskou, M, Thomson DM, Brett RR, Wheeler L, Tate RJ, Pratt JA, Chamberlain LH. Disruption of the *Zdhhc9* intellectual disability gene leads to behavioural abnormalities in a mouse model. *Exp Neurol*. 2018;308:35-46.

Kramer, U. Atypical Presentations of Benign Childhood Epilepsy With Centrotemporal Spikes: A Review. *Journal of Child Neurology*. 2008;23(7):785-90.

Lai, J, Linder ME. Oligomerization of DHHC protein S-acyltransferases. *J Biol Chem*. 2013;288(31):22862-70.

Latreille, M, Hausser J, Stützer I, Zhang Q, Hastoy B, Gargani S, Kerr-Conte J, Pattou F, Zavolan M, Esguerra JL, Eliasson L, Rülcke T, Rorsman P, Stoffel M. MicroRNA-7a regulates pancreatic  $\beta$  cell function. *J Clin Invest*. 2014;124(6):2722-35.

Lemonidis, K, Sanchez-Perez MC, Chamberlain LH. Identification of a Novel Sequence Motif Recognized by the Ankyrin Repeat Domain of zDHHC17/13 S-Acyltransferases. *J Biol Chem*. 2015;290(36):21939-50.

Lemonidis, K, MacLeod R, Baillie GS, Chamberlain LH. Peptide array-based screening reveals a large number of proteins interacting with the ankyrin-repeat domain of the zDHHC17 S-acyltransferase. *J Biol Chem*. 2017;292(42):17190-202.

Lemonidis, K, Gorleku OA, Sanchez-Perez MC, Grefen C, Chamberlain LH. The Golgi S-acylation machinery comprises zDHHC enzymes with major differences in substrate affinity and S-acylation activity. *Mol Biol Cell*. 2014;25(24):3870-83.

Lemonidis, K, Gorleku OA, Sanchez-Perez MC, Grefen C, Chamberlain LH. The Golgi S-acylation machinery comprises zDHHC enzymes with major differences in substrate affinity and S-acylation activity. *Molecular Biology of the Cell*. 2014;25(24):3870-83.

Lemonidis, K, Werno Martin W, Greaves J, Diez-Ardanuy C, Sanchez-Perez Maria C, Salaün C, Thomson David M, Chamberlain Luke H. The zDHHC family of S-acyltransferases. *Biochemical Society Transactions*. 2015;43(2):217-21.

Levy, AD, Devignot V, Fukata Y, Fukata M, Sobel A, Chauvin S. Subcellular Golgi localization of stathmin family proteins is promoted by a specific set of DHHC palmitoyl transferases. *Mol Biol Cell*. 2011;22(11):1930-42.

Li, D, Wu M. Pattern recognition receptors in health and diseases. *Signal Transduction and Targeted Therapy*. 2021;6(1):291.

Li, N, Hamor C, An Y, Zhu L, Gong Y, Toh Y, Guo Y. Biological functions and therapeutic potential of acylation by histone acetyltransferases. *Acta Materia Medica*. 2023;2(2):228-254.

Liao, D, Huang Y, Liu D, Zhang H, Shi X, Li X, Luo P. The role of s-palmitoylation in neurological diseases: implication for zDHHC family. *Front Pharmacol*. 2023;14:1342830.

Liao, D, Huang Y, Liu D, Zhang H, Shi X, Li X, Luo P. The role of s-palmitoylation in neurological diseases: implication for zDHHC family. *Frontiers in Pharmacology*. 2024;14:1342830.

Lin, DTS, Conibear E. ABHD17 proteins are novel protein depalmitoylases that regulate N-Ras palmitate turnover and subcellular localization. *Elife*. 2015;4:e11306.

Liu, P, Jiao B, Zhang R, Zhao H, Zhang C, Wu M, Li D, Zhao X, Qiu Q, Li J, Ren R. Palmitoylacyltransferase Zdhhc9 inactivation mitigates leukemogenic potential of oncogenic Nras. *Leukemia*. 2016;30(5):1225-28.

Lobo, S, Greentree WK, Linder ME, Deschenes RJ. Identification of a Ras Palmitoyltransferase in *Saccharomyces cerevisiae*. *Journal of Biological Chemistry*. 2002;277(43):41268-73.

Locatelli, C, Lemonidis K, Salaün C, Tomkinson NCO, Chamberlain LH. Identification of key features required for efficient S-acylation and plasma membrane targeting of sprouty-2. *J Cell Sci*. 2020;133(21):jcs249664.

Lupo, A, Cesaro E, Montano G, Zurlo D, Izzo P, Costanzo P. KRAB-Zinc Finger Proteins: A Repressor Family Displaying Multiple Biological Functions. *Current genomics*. 2013;14(4):268-78.

Lv, D, Cao X, Zhong L, Dong Y, Xu Z, Rong Y, Xu H, Wang Z, Yang H, Yin R, Chen M, Ke C, Hu Z, Deng W, Tang B. Targeting phenylpyruvate restrains excessive NLRP3 inflammasome activation and pathological inflammation in diabetic wound healing. *Cell Rep Med*. 2023;4(8):101129.

Magee, AI, Gutierrez L, McKay IA, Marshall CJ, Hall A. Dynamic fatty acylation of p21N-ras. *Embo J*. 1987;6(11):3353-7.

Malgapo, MIP, Linder ME. Substrate recruitment by zDHHC protein acyltransferases. *Open Biol*. 2021;11(4):210026.

Mesquita, FS, Abrami L, Sergeeva O, Turelli P, Qing E, Kunz B, Raclot C, Paz Montoya J, Abriata LA, Gallagher T, Dal Peraro M, Trono D, D'Angelo G, van der Goot FG. S-acylation controls SARS-CoV-2 membrane lipid organization and enhances infectivity. *Dev Cell*. 2021;56(20):2790-807.

Milligan, G, Parenti M, Magee AI. The dynamic role of palmitoylation in signal transduction. *Trends in Biochemical Sciences*. 1995;20(5):181-86.

Mitchell, DA, Mitchell G, Ling Y, Budde C, Deschenes RJ. Mutational analysis of *Saccharomyces cerevisiae* Erf2 reveals a two-step reaction mechanism for protein palmitoylation by DHHC enzymes. *J Biol Chem*. 2010;285(49):38104-14.

Mitchell, DA, Hamel LD, Ishizuka K, Mitchell G, Schaefer LM, Deschenes RJ. The Erf4 subunit of the yeast Ras palmitoyl acyltransferase is required for stability of the Acyl-Erf2 intermediate and palmitoyl transfer to a Ras2 substrate. *J Biol Chem*. 2012;287(41):34337-48.

Mitchell, DA, Hamel LD, Reddy KD, Farh L, Rettew LM, Sanchez PR, Deschenes RJ. Mutations in the X-linked Intellectual Disability Gene, *zDHHC9*, Alter Autopalmitoylation Activity by Distinct Mechanisms\*. *Journal of Biological Chemistry*. 2014;289(26):18582-92.

Nadolski, MJ, Linder ME. Protein lipidation. *The FEBS Journal*. 2007;274(20):5202-10.

Nair, A, Saha B. Regulation of Ras-GTPase Signaling and Localization by Post-Translational Modifications. *Kinases and Phosphatases*. 2023;1(2):97-116.

NCBI-primer blast tool (<https://www.ncbi.nlm.nih.gov/tools/primer-blast>)

Nguyen, PL, Greentree WK, Kawate T, Linder ME. GCP16 stabilizes the DHHC9 subfamily of protein acyltransferases through a conserved C-terminal cysteine motif. *Front Physiol*. 2023;14:1167094.

Nie, L, Fei C, Fan Y, Dang F, Zhao Z, Zhu T, Wu X, Dai T, Balasubramanian A, Pan J, Hu Y, Luo HR, Wei W, Chen J. Consecutive palmitoylation and phosphorylation orchestrates NLRP3 membrane trafficking and inflammasome activation. *Mol Cell*. 2024;84(17):3336-53.

Nomura, M., Murad, N. F., Madhavan, S. S., Eap, B., Garcia, T. Y., Aguirre, C. G., Verdin, E., Ellerby, L., Furman, D., & Newman, J. C. (2023). A ketogenic diet

reduces age-induced chronic neuroinflammation in mice Running title: ketogenic diet and brain inflammaging. *bioRxiv : the preprint server for biology*, 2023;12(1):569598.

Oh, Y, Jeon YJ, Hong GS, Kim I, Woo HN, Jung YK. Regulation in the targeting of TRAIL receptor 1 to cell surface via GODZ for TRAIL sensitivity in tumor cells. *Cell Death & Differentiation*. 2012;19(7):1196-207.

Ohno, Y, Kihara A, Sano T, Igarashi Y. Intracellular localization and tissue-specific distribution of human and yeast DHHC cysteine-rich domain-containing proteins. *Biochimica et Biophysica Acta (BBA) - Molecular and Cell Biology of Lipids*. 2006;1761(4):474-83.

Ohta, E, Misumi Y, Sohda M, Fujiwara T, Yano A, Ikehara Y. Identification and Characterization of GCP16, a Novel Acylated Golgi Protein That Interacts with GCP170. *Journal of Biological Chemistry*. 2003;278(51):51957-67.

Oohashi, T, Edamatsu M, Bekku Y, Carulli D. The hyaluronan and proteoglycan link proteins: Organizers of the brain extracellular matrix and key molecules for neuronal function and plasticity. *Exp Neurol*. 2015;274(Pt B):134-44.

Otto, G. P., Rathkolb, B., Oestereich, M. A., Lengger, C. J., Moerth, C., Micklich, K., Fuchs, H., Gailus-Durner, V., Wolf, E., & Hrabě de Angelis, M. (2016). Clinical Chemistry Reference Intervals for C57BL/6J, C57BL/6N, and C3HeB/FeJ Mice (Mus musculus). *Journal of the American Association for Laboratory Animal Science : JAALAS*, 55(4), 375–386.

Oyama, T, Miyoshi Y, Koyama K, Nakagawa H, Yamori T, Ito T, Matsuda H, Arakawa H, Nakamura Y. Isolation of a novel gene on 8p21.3-22 whose expression is reduced significantly in human colorectal cancers with liver metastasis. *Genes Chromosomes Cancer*. 2000;29(1):9-15.

- Patwardhan, A, Cheng N, Trejo J. Post-Translational Modifications of G Protein-Coupled Receptors Control Cellular Signaling Dynamics in Space and Time. *Pharmacol Rev.* 2021;73(1):120-51.
- Peng, C, Zhang Z, Wu J, Lv Z, Tang J, Xie H, Zhou L, Zheng S. A critical role for ZDHHC2 in metastasis and recurrence in human hepatocellular carcinoma. *Biomed Res Int.* 2014;2014:832712.
- Politis, EG, Roth AF, Davis NG. Transmembrane topology of the protein palmitoyl transferase Akr1. *J Biol Chem.* 2005;280(11):10156-63.
- Pouliot, JF, Béliveau R. Palmitoylation of the glucose transporter in blood-brain barrier capillaries. *Biochim Biophys Acta.* 1995;1234(2):191-6.
- Prakriya, M, Lewis RS. Store-Operated Calcium Channels. *Physiol Rev.* 2015;95(4):1383-436.
- Prior, IA, Hancock JF. Ras trafficking, localization and compartmentalized signalling. *Semin Cell Dev Biol.* 2012;23(2):145-53.
- Purkins, L, Love ER, Eve MD, Wooldridge CL, Cowan C, Smart TS, Johnson PJ, Rapeport WG. The influence of diet upon liver function tests and serum lipids in healthy male volunteers resident in a Phase I unit. *Br J Clin Pharmacol.* 2004;57(2):199-208.
- Qiu, L, Wang T, Ge Q, Xu H, Wu Y, Tang Q, Chen K. Circular RNA Signature in Hepatocellular Carcinoma. *J Cancer.* 2019;10(15):3361-72.
- Ramazi, S, Zahiri J. Posttranslational modifications in proteins: resources, tools and prediction methods. *Database (Oxford).* 2021:baab012.
- Ramlingam, G, Natarajasundaram UM. Ghent Criteria an Aid to Diagnose Latent Systemic Diseases in Marfan Syndrome. *J Clin Diagn Res.* 2015;9(5):Zj01-2.



Ramos, AKS, Caldas-Rosa ECC, Ferreira BM, Versiani BR, Moretti PN, de Oliveira SF, Pic-Taylor A, Mazzeu JF. ZDHHC9 X-linked intellectual disability: Clinical and molecular characterization. *Am J Med Genet A*. 2023;191(2):599-604.

Rana, MS, Kumar P, Lee CJ, Verardi R, Rajashankar KR, Banerjee A. Fatty acyl recognition and transfer by an integral membrane S-acyltransferase. *Science*. 2018;359(6372):eaao6326.

Raymond, FL, Tarpey PS, Edkins S, Tofts C, O'Meara S, Teague J, Butler A, Stevens C, Barthorpe S, Buck G, Cole J, Dicks E, Gray K, Halliday K, Hills K, Hinton J, Jones D, Menzies A, Perry J, Raine K, Shepherd R, Small A, Varian J, Widaa S, Mallya U, Moon J, Luo Y, Shaw M, Boyle J, Kerr B, Turner G, Quarrell O, Cole T, Easton DF, Wooster R, Bobrow M, Schwartz CE, Gecz J, Stratton MR, Futreal PA. Mutations in ZDHHC9, Which Encodes a Palmitoyltransferase of NRAS and HRAS, Cause X-Linked Mental Retardation Associated with a Marfanoid Habitus. *The American Journal of Human Genetics*. 2007;80(5):982-87

RCSB-PDB Pairwise Structure Alignment (<https://www.rcsb.org/alignment>)

Remsberg, JR, Suciu RM, Zambetti NA, Hanigan TW, Firestone AJ, Inguva A, Long A, Ngo N, Lum KM, Henry CL, Richardson SK, Predovic M, Huang B, Dix MM, Howell AR, Niphakis MJ, Shannon K, Cravatt BF. ABHD17 regulation of plasma membrane palmitoylation and N-Ras-dependent cancer growth. *Nature Chemical Biology*. 2021;17(8):856-64.

Rocks, O, Peyker A, Kahms M, Verveer PJ, Koerner C, Lumbierres M, Kuhlmann J, Waldmann H, Wittinghofer A, Bastiaens PI. An acylation cycle regulates localization and activity of palmitoylated Ras isoforms. *Science*. 2005;307(5716):1746-52.

Rocks, O, Gerauer M, Vartak N, Koch S, Huang ZP, Pechlivanis M, Kuhlmann J, Brunsveld L, Chandra A, Ellinger B, Waldmann H, Bastiaens PI. The palmitoylation

machinery is a spatially organizing system for peripheral membrane proteins. *Cell*. 2010;141(3):458-71.

Rodenburg, RNP, Snijder J, van de Waterbeemd M, Schouten A, Granneman J, Heck AJR, Gros P. Stochastic palmitoylation of accessible cysteines in membrane proteins revealed by native mass spectrometry. *Nature Communications*. 2017;8(1):1280.

Roth, AF, Feng Y, Chen L, Davis NG. The yeast DHHC cysteine-rich domain protein Akr1p is a palmitoyl transferase. *J Cell Biol*. 2002;159(1):23-8.

Ruiz-Ojeda, FJ, Olza J, Gil Á, Aguilera CM. Chapter 1 - Oxidative Stress and Inflammation in Obesity and Metabolic Syndrome. In: del Moral AM, Aguilera García CM, editors. *Obesity Academic Press*; 2018. p. 1-15.

Salaün, C, Ritchie L, Greaves J, Bushell TJ, Chamberlain LH. The C-terminal domain of zDHHC2 contains distinct sorting signals that regulate intracellular localisation in neurons and neuroendocrine cells. *Mol Cell Neurosci*. 2017;85:235-46.

Salaün, C, Locatelli C, Zmuda F, Cabrera González J, Chamberlain LH. Accessory proteins of the zDHHC family of S-acylation enzymes. *J Cell Sci*. 2020;133(22):jcs251819.

Salaün, C, Gould GW, Chamberlain LH. The SNARE Proteins SNAP-25 and SNAP-23 Display Different Affinities for Lipid Rafts in PC12 Cells: REGULATION BY DISTINCT CYSTEINE-RICH DOMAINS. *Journal of Biological Chemistry*. 2005;280(2):1236-40.

Sanders, SS, Mui KKN, Sutton LM, Hayden MR. Identification of Binding Sites in Huntingtin for the Huntingtin Interacting Proteins HIP14 and HIP14L. *PLoS One*. 2014;9(2):e90669.

Sanders, SS, Martin DD, Butland SL, Lavallée-Adam M, Calzolari D, Kay C, Yates JR, 3rd, Hayden MR. Curation of the Mammalian Palmitoylome Indicates a Pivotal Role for Palmitoylation in Diseases and Disorders of the Nervous System and Cancers. *PLoS Comput Biol*. 2015;11(8):e1004405.

Sandu, C, Burloiu CM, Barca DG, Magureanu SA, Craiu DC. Ketogenic Diet in Patients with GLUT1 Deficiency Syndrome. *Maedica (Bucur)*. 2019;14(2):93-97.

Schirwani, S, Wakeling E, Smith K, Balasubramanian M. Expanding the molecular basis and phenotypic spectrum of ZDHHC9-associated X-linked intellectual disability. *Am J Med Genet A*. 2018;176(5):1238-44.

Schmidt, MFG, Schlesinger MJ. Fatty acid binding to vesicular stomatitis virus glycoprotein: a new type of post-translational modification of the viral glycoprotein. *Cell*. 1979;17(4):813-19.

Schneider-Poetsch, T, Ju J, Eyler DE, Dang Y, Bhat S, Merrick WC, Green R, Shen B, Liu JO. Inhibition of eukaryotic translation elongation by cycloheximide and lactimidomycin. *Nat Chem Biol*. 2010;6(3):209-17.

Schratt, GM, Tuebing F, Nigh EA, Kane CG, Sabatini ME, Kiebler M, Greenberg ME. A brain-specific microRNA regulates dendritic spine development. *Nature*. 2006;439(7074):283-89.

Senior, AW, Evans R, Jumper J, Kirkpatrick J, Sifre L, Green T, Qin C, Žídek A, Nelson AWR, Bridgland A, Penedones H, Petersen S, Simonyan K, Crossan S, Kohli P, Jones DT, Silver D, Kavukcuoglu K, Hassabis D. Improved protein structure prediction using potentials from deep learning. *Nature*. 2020;577(7792):706-10.

Shahinian, S, Silvius JR. Doubly-lipid-modified protein sequence motifs exhibit long-lived anchorage to lipid bilayer membranes. *Biochemistry*. 1995;34(11):3813-22.

Sharma, C, Wang HX, Li Q, Knoblich K, Reisenbichler ES, Richardson AL, Hemler ME. Protein Acyltransferase DHHC3 Regulates Breast Tumour Growth, Oxidative Stress, and Senescence. *Cancer Res*. 2017;77(24):6880-90.

Shimell, JJ, Shah BS, Cain SM, Thouta S, Kuhlmann N, Tatarnikov I, Jovellar DB, Brigidi GS, Kass J, Milnerwood AJ, Snutch TP, Bamji SX. The X-Linked Intellectual Disability Gene *Zdhhc9* Is Essential for Dendrite Outgrowth and Inhibitory Synapse Formation. *Cell Rep*. 2019;29(8):2422-37.

Shoichet, SA, Hoffmann K, Menzel C, Trautmann U, Moser B, Hoeltzenbein M, Echenne B, Partington M, Van Bokhoven H, Moraine C, Fryns JP, Chelly J, Rott HD, Ropers HH, Kalscheuer VM. Mutations in the *ZNF41* gene are associated with cognitive deficits: identification of a new candidate for X-linked mental retardation. *Am J Hum Genet*. 2003;73(6):1341-54.

Siegel, G, Obernosterer G, Fiore R, Oehmen M, Bicker S, Christensen M, Khudayberdiev S, Leuschner PF, Busch CJL, Kane C, Hübel K, Dekker F, Hedberg C, Rengarajan B, Drepper C, Waldmann H, Kauppinen S, Greenberg ME, Draguhn A, Rehmsmeier M, Martinez J, Schratt GM. A functional screen implicates microRNA-138-dependent regulation of the depalmitoylation enzyme APT1 in dendritic spine morphogenesis. *Nature Cell Biology*. 2009;11(6):705-16.

Simanshu, DK, Nissley DV, McCormick F. RAS Proteins and Their Regulators in Human Disease. *Cell*. 2017;170(1):17-33.

Singaraja, RR, Hadano S, Metzler M, Givan S, Wellington CL, Warby S, Yanai A, Gutekunst CA, Leavitt BR, Yi H, Fichter K, Gan L, McCutcheon K, Chopra V, Michel J, Hersch SM, Ikeda JE, Hayden MR. HIP14, a novel ankyrin domain-containing

protein, links huntingtin to intracellular trafficking and endocytosis. *Hum Mol Genet.* 2002;11(23):2815-28.

Singaraja, RR, Huang K, Sanders SS, Milnerwood AJ, Hines R, Lerch JP, Franciosi S, Drisdell RC, Vaid K, Young FB, Doty C, Wan J, Bissada N, Henkelman RM, Green WN, Davis NG, Raymond LA, Hayden MR. Altered palmitoylation and neuropathological deficits in mice lacking HIP14. *Human Molecular Genetics.* 2011;20(20):3899-909.

Skaper, SD. The neurotrophin family of neurotrophic factors: an overview. *Methods Mol Biol.* 2012;846:1-12.

Solis, GP, Kazemzadeh A, Abrami L, Valnohova J, Alvarez C, van der Goot FG, Katanaev VL. Local and substrate-specific S-palmitoylation determines subcellular localization of Gao. *Nature Communications.* 2022;13(1):2072.

Stevenson, RE, Holden KR, Rogers RC, Schwartz CE. Seizures and X-linked intellectual disability. *Eur J Med Genet.* 2012;55(5):307-12.

Suskiewicz, MJ. The logic of protein post-translational modifications (PTMs): Chemistry, mechanisms and evolution of protein regulation through covalent attachments. *BioEssays.* 2024;46(3):2300178.

Sutton, LM, Sanders SS, Butland SL, Singaraja RR, Franciosi S, Southwell AL, Doty CN, Schmidt ME, Mui KKN, Kovalik V, Young FB, Zhang W, Hayden MR. Hip14I-deficient mice develop neuropathological and behavioural features of Huntington disease. *Human Molecular Genetics.* 2012;22(3):452-65.

Swarthout, JT, Lobo S, Farh L, Croke MR, Greentree WK, Deschenes RJ, Linder ME. DHHC9 and GCP16 Constitute a Human Protein Fatty Acyltransferase with Specificity for H- and N-Ras. *Journal of Biological Chemistry.* 2005;280(35):31141-48.

Tabrizi, SJ, Flower MD, Ross CA, Wild EJ. Huntington disease: new insights into molecular pathogenesis and therapeutic opportunities. *Nat Rev Neurol*. 2020;16(10):529-46.

Tang, M, Monani UR. Glut1 deficiency syndrome: New and emerging insights into a prototypical brain energy failure disorder. *Neurosci Insights*. 2021;16:26331055211011507.

Thomas, GM, Hayashi T, Chiu SL, Chen CM, Huganir RL. Palmitoylation by DHHC5/8 targets GRIP1 to dendritic endosomes to regulate AMPA-R trafficking. *Neuron*. 2012;73(3):482-96.

Tian, L, McClafferty H, Jeffries O, Shipston MJ. Multiple Palmitoyltransferases Are Required for Palmitoylation-dependent Regulation of Large Conductance Calcium- and Voltage-activated Potassium Channels. *Journal of Biological Chemistry*. 2010;285(31):23954-62.

Tomatis, VM, Trenchi A, Gomez GA, Daniotti JL. Acyl-protein thioesterase 2 catalyzes the deacylation of peripheral membrane-associated GAP-43. *PLoS One*. 2010;5(11):e15045.

Toyoda, T, Sugimoto H, Yamashita S. Sequence, expression in *Escherichia coli*, and characterization of lysophospholipase II. *Biochim Biophys Acta*. 1999;1437(2):182-93.

Tzschach, A, Grasshoff U, Beck-Woedl S, Dufke C, Bauer C, Kehrer M, Evers C, Moog U, Oehl-Jaschkowitz B, Di Donato N, Maiwald R, Jung C, Kuechler A, Schulz S, Meinecke P, Spranger S, Kohlhase J, Seidel J, Reif S, Rieger M, Riess A, Sturm M, Bickmann J, Schroeder C, Dufke A, Riess O, Bauer P. Next-generation sequencing in X-linked intellectual disability. *European Journal of Human Genetics*. 2015;23(11):1513-18.

Tzschach, A, Grasshoff U, Beck-Woedl S, Dufke C, Bauer C, Kehrer M, Evers C, Moog U, Oehl-Jaschkowitz B, Di Donato N, Maiwald R, Jung C, Kuechler A, Schulz S, Meinecke P, Spranger S, Kohlhase J, Seidel J, Reif S, Rieger M, Riess A, Sturm M, Bickmann J, Schroeder C, Dufke A, Riess O, Bauer P. Next-generation sequencing in X-linked intellectual disability. *Eur J Hum Genet.* 2015;23(11):1513-8.

Udenwobele, DI, Su R-C, Good SV, Ball TB, Varma Shrivastav S, Shrivastav A. Myristoylation: An Important Protein Modification in the Immune Response. *Frontiers in Immunology.* 2017;8:751.

Valdez-Taubas, J, Pelham H. Swf1-dependent palmitoylation of the SNARE Tlg1 prevents its ubiquitination and degradation. *Embo J.* 2005;24(14):2524-32.

Verkruyse, LA, Hofmann SL. Lysosomal targeting of palmitoyl-protein thioesterase. *J Biol Chem.* 1996;271(26):15831-6.

Vesa, J, Hellsten E, Verkruyse LA, Camp LA, Rapola J, Santavuori P, Hofmann SL, Peltonen L. Mutations in the palmitoyl protein thioesterase gene causing infantile neuronal ceroid lipofuscinosis. *Nature.* 1995;376(6541):584-7.

Vivo, DCD, Trifiletti RR, Jacobson RI, Ronen GM, Behmand RA, Harik SI. Defective Glucose Transport across the Blood-Brain Barrier as a Cause of Persistent Hypoglycorrhachia, Seizures, and Developmental Delay. *New England Journal of Medicine.* 1991;325(10):703-09.

Vogel, K, Roche PA. SNAP-23 and SNAP-25 Are Palmitoylated in Vivo. *Biochemical and Biophysical Research Communications.* 1999;258(2):407-10.

Wang, L, Cai J, Zhao X, Ma L, Zeng P, Zhou L, Liu Y, Yang S, Cai Z, Zhang S, Zhou L, Yang J, Liu T, Jin S, Cui J. Palmitoylation prevents sustained inflammation by limiting NLRP3 inflammasome activation through chaperone-mediated autophagy. *Molecular Cell.* 2023;83(2):281-97.

Weiler-Güttler, H, Zinke H, Möckel B, Frey A, Gassen HG. cDNA cloning and sequence analysis of the glucose transporter from porcine blood-brain barrier. *Biol Chem Hoppe Seyler*. 1989;370(5):467-73.

Wennerberg, K, Rossman KL, Der CJ. The Ras superfamily at a glance. *Journal of Cell Science*. 2005;118(5):843-46.

Williams, DM, Peden AA. S-acylation of NLRP3 provides a nigericin sensitive gating mechanism that controls access to the Golgi. *eLife* 2024;13:RP94302

Williams, DM, Peden AA. Greasing the wheels of inflammasome formation: regulation of NLRP3 function by S-linked fatty acids. *Biochem Soc Trans*. 2025;10.1042/bst20241738.

Woodley, KT, Collins MO. S-acylated Golga7b stabilises DHHC5 at the plasma membrane to regulate cell adhesion. *EMBO Rep*. 2019;20(10):e47472.

Wright, CF, Fitzgerald TW, Jones WD, Clayton S, McRae JF, van Kogelenberg M, King DA, Ambridge K, Barrett DM, Bayzetinova T, Bevan AP, Bragin E, Chatzimichali EA, Gribble S, Jones P, Krishnappa N, Mason LE, Miller R, Morley KI, Parthiban V, Prigmore E, Rajan D, Sifrim A, Swaminathan GJ, Tivey AR, Middleton A, Parker M, Carter NP, Barrett JC, Hurles ME, FitzPatrick DR, Firth HV. Genetic diagnosis of developmental disorders in the DDD study: a scalable analysis of genome-wide research data. *Lancet*. 2015;385(9975):1305-14.

Wu, M, Zhou X, Zhou X, Wang G, Zeng Y, Li J, Prochownik EV, Wang F, Li Y. ZDHHC3-mediated SCAP S-acylation promotes cholesterol biosynthesis and tumor immune escape in hepatocellular carcinoma. *Cell Reports*. 2024;43(11):114962.

Xu, J, Pickard JM, Núñez G. FDA-approved disulfiram inhibits the NLRP3 inflammasome by regulating NLRP3 palmitoylation. *Cell Rep*. 2024;43(8):114609.



Yan, SM, Tang JJ, Huang CY, Xi SY, Huang MY, Liang JZ, Jiang YX, Li YH, Zhou ZW, Ernberg I, Wu QL, Du ZM. Reduced expression of ZDHHC2 is associated with lymph node metastasis and poor prognosis in gastric adenocarcinoma. *PLoS One*. 2013;8(2):e56366.

Yanai, A, Huang K, Kang R, Singaraja RR, Arstikaitis P, Gan L, Orban PC, Mullard A, Cowan CM, Raymond LA, Drisdell RC, Green WN, Ravikumar B, Rubinsztein DC, El-Husseini A, Hayden MR. Palmitoylation of huntingtin by HIP14 is essential for its trafficking and function. *Nat Neurosci*. 2006;9(6):824-31.

Yang, A, Liu S, Zhang Y, Chen J, Fan Y, Wang F, Zou Y, Feng S, Wu J, Hu Q. Regulation of RAS palmitoyltransferases by accessory proteins and palmitoylation. *Nature Structural & Molecular Biology*. 2024;31(3):436-46.

Yang, P, Wang Y, Macfarlan TS. The Role of KRAB-ZFPs in Transposable Element Repression and Mammalian Evolution. *Trends in Genetics*. 2017;33(11):871-81.

Yang, W, Di Vizio D, Kirchner M, Steen H, Freeman MR. Proteome scale characterization of human S-acylated proteins in lipid raft-enriched and non-raft membranes. *Mol Cell Proteomics*. 2010;9(1):54-70.

Ye, J, Zha J, Shi Y, Li Y, Yuan D, Chen Q, Lin F, Fang Z, Yu Y, Dai Y, Xu B. Co-inhibition of HDAC and MLL-menin interaction targets MLL-rearranged acute myeloid leukemia cells via disruption of DNA damage checkpoint and DNA repair. *Clinical Epigenetics*. 2019;11(1):137.

Yeste-Velasco, M, Linder ME, Lu YJ. Protein S-palmitoylation and cancer. *Biochim Biophys Acta*. 2015;1856(1):107-20.

Yokoi, N, Fukata Y, Sekiya A, Murakami T, Kobayashi K, Fukata M. Identification of PSD-95 Depalmitoylating Enzymes. *J Neurosci*. 2016;36(24):6431-44.

Yu, T, Hou D, Zhao J, Lu X, Greentree WK, Zhao Q, Yang M, Conde DG, Linder ME, Lin H. NLRP3 Cys126 palmitoylation by ZDHHC7 promotes inflammasome activation. *Cell Rep.* 2024;43(4):114070.

Zeisel, A, Hochgerner H, Lönnerberg P, Johnsson A, Memic F, van der Zwan J, Häring M, Braun E, Borm LE, La Manno G, Codeluppi S, Furlan A, Lee K, Skene N, Harris KD, Hjerling-Leffler J, Arenas E, Ernfors P, Marklund U, Linnarsson S. Molecular Architecture of the Mouse Nervous System. *Cell.* 2018;174(4):999-1014.e22.

Zhan, F-L, Gao S-Y, Xie Y-D, Zhang J-M, Li Y, Liu N. Applications of Click Chemistry Reaction for Proteomics Analysis. *Chinese Journal of Analytical Chemistry.* 2020;48(4):431-38.

Zhang, C. Etiology of Alzheimer's Disease. *Discovery medicine.* 2023;35(178):757-76.

Zhang, M-J, Wu D, Yu L-F, Li H, Sun D, Liang J-M, Lu X-P, Luo R, Guo Q-H, Jin R-F, Zhang H-W, Lei G-F, Sun R-P, Wang M, Zhou Y-F, Wang Y-Y, Tang J-H, Hua Y, Shi X-L, Liu X-M, Shi X-Y, Yang G, Wang H, Gao F, Jia T-M, Wang J-W, Liao J-X, Bao X-H. Diagnosis and treatment recommendations for glucose transporter 1 deficiency syndrome. *World Journal of Pediatrics.* 2025;21(2):149-58.

Zhang, Z, Li X, Yang F, Chen C, Liu P, Ren Y, Sun P, Wang Z, You Y, Zeng YX, Li X. DHHC9-mediated GLUT1 S-palmitoylation promotes glioblastoma glycolysis and tumorigenesis. *Nat Commun.* 2021;12(1):5872.

Zhao, L, Lobo S, Dong X, Ault AD, Deschenes RJ. Erf4p and Erf2p Form an Endoplasmic Reticulum-associated Complex Involved in the Plasma Membrane Localization of Yeast Ras Proteins. *Journal of Biological Chemistry.* 2002;277(51):49352-59.

Zheng, S, Que X, Wang S, Zhou Q, Xing X, Chen L, Hou C, Ma J, An P, Peng Y, Yao Y, Song Q, Li J, Zhang P, Pei H. ZDHHC5-mediated NLRP3 palmitoylation promotes NLRP3-NEK7 interaction and inflammasome activation. *Mol Cell*. 2023;83(24):4570-85.

Zhou, B, Hao Q, Liang Y, Kong E. Protein palmitoylation in cancer: molecular functions and therapeutic potential. *Mol Oncol*. 2023;17(1):3-26.